JACOBS
UNIVERSITY

Authorized for Publication

Bremen, Thursday, July 19, 2007

_____

Dr. Antje Boetius, Professor of Microbiology,
Chair of Doctoral Examination Committee

JACOBS UNIVERSITY

Function and diversity of marine and hypersaline mat forming microbial communities

by

Enoma Osasuyi Omoregie

A thesis submitted in partial fulfillment of the requirements for the degree of

Doctor of Philosophy

in Marine Microbiology

Approved, Thesis Committee:

Dr. Antje Boetius, Professor of Microbiology, Chair

Dr. Matthias Ullrich, Professor of Microbiology

Dr. Friedrich Widdel, Professor of Microbiology

Defense date: Thursday, July 5, 2007

School of Engineering and Science

Table of contents

Acknowledgments	Page 4
Summary	Pages 5 - 7
Chapter I: Introduction to marine and hypersaline microbial mats	Pages 8 - 33
Part 1: The role of microbial mats in the ecosystem	Pages 8 - 9
Part 2: Photosynthetic mats	Pages 9 - 15
Part 3: Anaerobic methanotrophic mats	Pages 15 - 18
Part 4: Sulfide-oxidizing mats	Pages 18 - 21
Part 5: Iron-cycling microbial mats	Pages 21 - 24
Part 6: General questions addressed in chapters II-V and author contributions	Pages 31 - 33
Chapter II: Diversity and function of Chloroflexus-like bacteria in a hypersaline microbial mat: phylogenetic characterization and impact on aerobic respiration	Pages 34 - 73
Chapter III: Microbial methane turnover at mud volcanoes of the Gulf of Cadiz	Pages 74 - 136
Chapter IV: Anaerobic oxidation of methane and sulfate reduction at cold seeps in the Eastern Mediterranean sea	Pages 137 - 178
Chapter V: Biogeochemistry and community composition of iron- and sulfide-oxidizing microbial mats at the Chefren mud volcano	Pages 179 - 232
Chapter VI: General conclusions	Pages 233 - 234
List of Publications	Page 235 - 236
List of Presentations	Pages 237 - 238
List of activities in the MARMIC program	Page 239

Acknowledgments

I would like to thank my advisor Antje Boetius for providing this opportunity to me, as well as all the support she given me over the last 3 years.

I would like to thank my thesis committee members Matthias Ullrich, Victoria Orphan, and Friedrich Widdel for their helpful discussions, as well as their review of my dissertation.

I would like to thank all the participants of the MEDIFLUX, and the Chiprana project for their help and support.

I would like to thank the members of the Departments of Biogeochemistry, Microbiology and Molecular Ecology for their help.

Special thanks to my “BEKANNTE” within the Habitat group, Gunter, Simone, and Jan, and of course all the many other friends I have gotten to know at the MPI.

Summary

Archaeal and bacterial communities exert a huge influence over biogeochemical processes on Earth. Microbial mats are the earliest known forms of biological communities, and can offer significant insight into the functioning of past and present element cycling and microbial population interaction. To gain a better understanding of the diversity of microbial processes in marine and hypersaline mats and sediments, the activities and diversity of microbes in several types of ecosystems were examined: (1) Chloroflexus-like bacteria from a hypersaline cyanobacterial mat. (2 - 3) Methane-oxidizing and sulfate-reducing sediment communities from cold seeps in the Gulf of Cadiz and the Eastern Mediterranean. (4) Sulfide- and iron-oxidizing mats from cold seeps in the Eastern Mediterranean. Non-mat-forming sediment communities were included in this work, because they often support mat communities and share similar processes and organisms, especially with regard to anaerobic oxidation of methane. The major themes addressed within this dissertation: (a) Which microbial populations are responsible for the dominant biogeochemical processes in the investigated habitat? (b) How abundant are these key microbes within the microbial community and which other microorganisms are associated with them? (c) How active are the microbes within these communities, and what are their main environmental signatures?

1. Chloroflexus-like bacteria (CLB) are filamentous anoxygenic phototrophs. They are often abundant in cyanobacterial mats, however their role within these mat communities remains largely unknown. The affect of CLB on carbon and oxygen dynamics within a cyanobacterial mat from the hypersaline lake, La Salada de Chiprana, was investigated. Pigment analysis and microscopy indicated that CLB as well as cyanobacteria were abundant within the surface of these mats. 16S rRNA gene analysis indicated the presence of several distinct CLB phylotypes within these mats. Exposure of the mat to visible light (400 - 700 nm) using a Light emitting diode (LED) resulted in oxygen concentrations of up 190 µM. Supplementation with near-infrared (710 – 770 nm) light using a LED resulted in oxygen concentrations of up to 230 µM. This 25 % increase in oxygen concentrations was attributed to decreased respiration by CLB. They were able to switch from aerobic respiration to non-oxygenic photosynthesis in response to infrared illumination. These results suggest that CLB may play a significant role in carbon and oxygen dynamics in cyanobacterial mats.

2. The Gulf of Cadiz is characterized by an abundance of fluid and gas emitting structures along its seabed, such as mud volcanoes, diapirs, and pockmarks. These types of structures have been shown to emit methane through the seabed in several environments. However, methanotrophic microbial communities within these sediments often attenuate this flux. Several cold seep structures within the Gulf of Cadiz were investigated. The abundance of ^{13}C-depleted biomarkers recovered from seeps within the Gulf of Cadiz, indicated microbial communities involved in the anaerobic oxidation of methane (AOM) and sulfate reduction (SR) were important at these seeps. Typical populations of anaerobic methanotrophs and their partners were found to occupy a small sediment horizon in the methane-sulfate transition zone. The rates of AOM and SR were in general very low, due to the low fluid flow at the investigated sites (37 - 708 mmol m^{-2} year). SR exceeded AOM by several-fold at most sites, indicating that other hydrocarbons fueled SR. This activity, however, was sufficient to halt methane emission to the bottom waters of these seeps.

3. The Eastern Mediterranean, similar to the Gulf of Cadiz, is characterized by an abundance of fluid and gas emitting structures along its seabed. Previous work on such structures at the Central Mediterranean Ridge has shown that AOM coupled to SR was an important process in shaping geological and biological processes at these seeps. Here we investigated for the first time, the activity and microbial community structure in relation to AOM and SR at novel seeps of the Nile Deep Sea Fan. AOM and SR rates were in general higher than those encountered in the Gulf of Cadiz, but moderate compared to other seep settings. SR activity exceeded that of AOM, indicating the preferential use of other hydrocarbons in fueling SR. Fluorescence in situ hybridization and 16S rRNA gene analysis revealed the presence of all known groups of methane oxidizing archaea, as well as their bacterial partners at these seeps. However, unlike the Gulf of Cadiz AOM and SR activity were not high enough to completely control the emission of hydrocarbons to the hydrosphere.

4. Along the steep slope of the Chefren Mud volcano in the Eastern Mediterranean, we discovered novel white and orange bacterial mats, which were linked to local biogeochemical processes. Microscopy and 16S rRNA gene analysis indicated these mats were composed of elemental sulfur- and iron-oxidizing microbial communities. Sulfide was produced via the oxidation of higher hydrocarbons by sulfate reducing bacteria in the underlying sediments. It was consumed by the activities of the ε-proteobacterium "*Candidatus* Arcobacter sulfidicus", which produced elemental sulfur precipitates. The iron precipitates consisted of mostly of

Fe(III)-hydroxide encrusted sheaths similar to those produced by the neutrophilic Fe-oxidizing β-proteobacterium *Leptothrix*. Fe(II) was supplied by the activities of Fe(III)-reducing bacteria in the sediments underlying the iron mats, using unidentified substrates.

Chapter I: Introduction to marine and hypersaline microbial mats

Part 1: The role of microbial mats in the ecosystem

Microbes, particularly archaea and bacteria are the most pervasive and enigmatic forms of life on the planet. They are found all over the Earth, from the subsurface through the entire ocean and atmosphere. They are the earliest known forms of life, and their activities, most of which have not been elucidated, have had a profound effect on the biosphere of early Earth (Nisbet and Fowler, 1999; Nisbet and Sleep, 2001 and references therein). Today microbes continue to exert a profound influence over the cycling of elements. The contribution of prokaryotes to the Earth extends far beyond what will be covered within this dissertation. This introduction will cover general aspects of different types of microbial mat communities, such as their significance, selected key processes and microbes involved in their viability.

"Microbial mats are planar microbial communities". This definition is broad, and encompasses everything from oral plaques, hydrothermal vent surface mats to highly laminated microbial communities observed within hypersaline ponds and lakes. This definition also includes, thin microbial films, or biofilms which lack a clear visible lamination. Microbial mats can consist of a single clonal organism (Entcheva-Dimitrov and Spormann, 2004) or very diverse microbial populations (Ley et al., 2006). Consequently the microbial processes hosted in mats can be quite broad and encompass many different types of microbial metabolisms. Mats can often be recognized due to the pigments produced by certain populations in the mat community, or by microbe induced mineral or elemental precipitation (Jannasch et al., 1989; Canfield and Des Marais, 1993; Emerson and Revsbech, 1994; Paerl et al., 2001). Their distribution is very broad and they persist where environmental conditions permit, especially where grazing pressure is limited as in many extreme environments.

Within the medical field, microbial mats are a major concern because they can form biofilms on the surfaces of medical equipment serving as a platform for subsequent microbial infection (Raad, 1998). Furthermore, microbial mats are associated with may different diseases, such as Cystic fibrosis, Pneumonia, Otitis media, and Periodontitis, where microorganisms accumulate on tissues and internal organs ((Davey and O'Toole, 2000), and references therein). A typical characteristic of such microbial biofilms is decreased

susceptibility to antibiotics. A considerable amount of research has thus been devoted to understanding the interactions between the microorganisms in these communities ((Davey and O'Toole, 2000), and references therein), in order to prevent their formation.

Microbial mats in the environment are of immense interest for several reasons, their similarity to ancient microbial communities (Stolz, 1985), their role in elemental transformations (Canfield and Des Marais, 1993), and their use as indicators for biogeochemical processes, such as high sulfide fluxes from underlying methanotrophic communities (Treude et al., 2003; Joye et al., 2004). This introduction will cover several well-known types of marine and hypersaline microbial mats systems which are pertinent to the topic of this dissertation. The relevance of these mat systems, key processes, and major organisms involved in these processes will be discussed. The types of microbial mats that will be covered within this introduction are photosynthetic, methanotrophic, sulfide-oxidizing and iron-oxidizing microbial mats.

Part 2: Photosynthetic mats

Photosynthetic mats are microbial mats that are dominated by photosynthetic organisms, such as cyanobacteria, diatoms, and anoxygenic photoautotrophs (Canfield et al., 2005). Cyanobacterial mats are thought to be among the earliest known forms of microbial communities (Tice and Lowe, 2004). They can be loosely associated biofilms, gelatinous or even well laminated microbial structures, such as the famous stromatolites (Reid et al., 2000). The most well known photosynthetic mats are those that are formed by filamentous cyanobacteria, which excrete exopolysaccharides that hold the mat together (Stal and Caumette, 1994). Cyanobacterial mats can be highly productive, almost self-sustaining microbial ecosystems, capable of their own C and N fixation (Stal and Caumette, 1994). They are excellent food sources for higher organisms, i.e. worms, fish and crabs, therefore, mats thrive in environments where grazing by higher organisms is excluded by environmental conditions, such as high temperatures at hydrothermal springs, and high salinities in hypersaline ponds and lakes. Examples are the cyanobacterial mats of Guerrero Negro, Mexico (Omoregie et al., 2004a), Sharks bay, Australia (Papineau et al., 2005), Saragossa, Spain (Jonkers et al., 2003), and thermal springs in Yellowstone, USA (Ward et al., 2006).

Figure 1. (A) Hypersaline pond in Guerrero Negro, Mexico, with submerged *Microcoleus chthonoplastes* cyanobacterial mats.

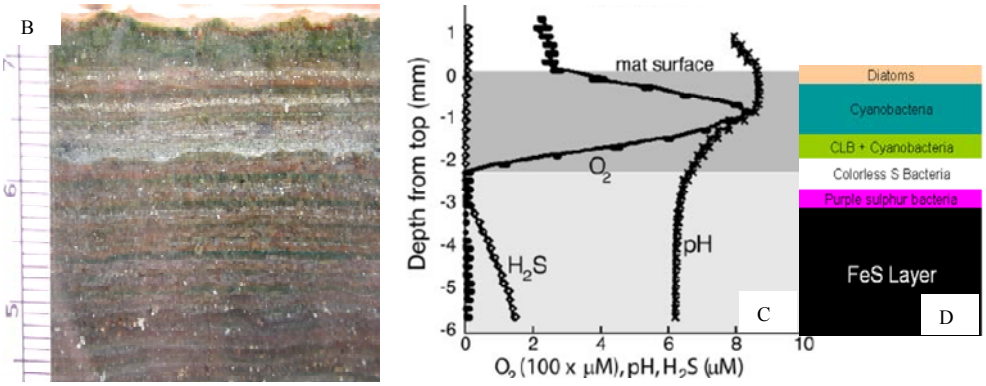

Figure 1. (B) Cross section of a cyanobacterial mat from the pond pictured above. (C) Profiles of O_2, H_2S, and pH from a *Microcoleus chthonoplastes* mat (modified from Ley, *et al*. 2006). Oxygen production is a result of oxygenic photosynthesis. Sulfide is produced as a result of sulfate reduction from the oxidation of photosynthetic products. (D) Schematic of vertical distribution of bacterial communities in a cyanobacterial mat (Courtesy of Ami I. Bachar). CLB are Chloroflexus-like bacteria, and the FeS layer is a sulfidic layer produced by the precipitation of sulfide and iron.

Lamination in a cyanobacterial mat typically follows a vertical distribution of microbial processes (Figure 1). The top layer is the oxic zone, which consists of oxygen producing cyanobacteria and diatoms, as well as oxygen consuming microorganisms. This layer is followed by anoxic zone that consists of anoxygenic photoautotrophs, such as green and purple bacteria. They are followed by other anaerobic organisms, such as sulfate reducing bacteria and methanogens. This description is nominal, as many microorganisms are also found outside their idealized layer (Teske et al., 1998; Minz et al., 1999a; Minz et al., 1999b).

Cyanobacterial mats are of immense interest due to their implications for early life on Earth (Hoehler et al., 2001), their close coupling of various microbial processes in the carbon, nitrogen and sulfur cycle (Canfield and Des Marais, 1993), as well as their contribution to local ecosystems (Webb et al., 1975; Wiebe et al., 1975) They are among the earliest

examples of microbial communities, which existed billions of years ago (Tice and Lowe, 2004). Some cyanobacterial communities have been preserved as fossils, the oldest ones possibly dating back to ~ 3.5 bya (Buick et al., 1981). Extant microbial mats are our best examples of these ancient ecosystems, as they carry out many of the same microbial processes that these ancient microbial communities performed. Therefore, investigating modern microbial mats can help to elucidate the activities of past microbial ecosystems, and their possible interaction with the early Earth's biosphere, especially with regard to Earth's oxygenation (Hoehler et al., 2001).

The contribution of cyanobacterial mats to global productivity is not well-defined, but is believed to be low, as most cyanobacterial mats are restricted to very small environments. However, on local scales, such as coral reefs, cyanobacterial mats can contribute significantly to local productivity, as they are a source of nutrients in otherwise nutrient depleted environments (Webb et al., 1975; Wiebe et al., 1975).

Photosynthesis in cyanobacterial mats

Due to the high diversity of organisms within cyanobacterial mats (Ley et al., 2006), there are literally thousands of different processes that occur within them. The most important function of cyanobacteria is their photolithoautotrophy. Photosynthesis and nitrogen fixation are major processes for the entry of fixed carbon and nitrogen into the mat (Canfield and Des Marais, 1993; Omoregie et al., 2004b), as well as a major mode of life for the cyanobacteria, which are responsible for constructing the mat. Other autotrophic and heterotrophic processes such as sulfide oxidation, and sulfate reduction are also very important for the recycling of energy and elements in cyanobacterial mats (Canfield and Des Marais, 1993).

Photosynthesis is the use of light energy for the generation of organic matter:

$$CO_2 + 2\ H_2O^* + light \rightarrow (CH_2O) + H_2O + O_2^* \quad (1)$$

$$CO_2 + 2\ H_2S^* + light \rightarrow (CH_2O) + H_2O + 2S^* \quad (2)$$

It generally falls into two categories, oxygenic (eq. 1) and anoxygenic photosynthesis (eq. 2). Oxygenic photosynthesis is used by diatoms, cyanobacteria and green plants, where H_2O is used as an electron donor resulting in the production of oxygen. In anoxygenic photosynthesis, no oxygen is generated; instead other electron donors (H_2S, Fe^{2+} and others) can be used that do not result in the production of oxygen.

Photosynthesis can be further subdivided into two types of reactions, reactions that require light (typically the generation of energy and reducing power), and those that are light independent (typically carbon fixation). In the light reactions, light is absorbed by antenna pigments, and the energy is transferred to the photosynthetic reaction centers (series of proteins, and electron transporting molecules), Photosystem I or II. Cyanobacteria have two photosystems, whereas anoxygenic photoautotrophs have either a Photosystem I or II.

Energy is generated by photosynthesis, when photons from sunlight excite chlorophyll molecules; these excited molecules release electrons, which flow through a series of electron carriers, ultimately resulting in the generation of ATP. Electrons can also be returned to the chlorophyll molecules, such that there is no net change in electrons. In this cyclic electron flow, no external electron donor is needed. In some organisms reductive power (NADPH) is generated via a reverse electron flow (i.e. electrons flowing from a source ultimately reducing NADP). Electrons are injected from an external source (i.e. H_2S, Fe and H_2O), this results in the generation of S, O and Fe-oxides. In cyanobacteria, Photosystem II removes electrons from water. These electrons move through an electron transport chain and are ultimately passed to Photosystem I. From there, these electrons flow into NADP generating NADPH. Alternatively the electrons can flow back to Photosystem II resulting in the generation of ATP.

The dark reactions in photosynthesis can differ significantly depending on the organisms. But typically these reactions involve the generation of organic matter with the enzyme ribulose bisphosphate carboxylase (RUBISCO). This enzyme adds CO_2 to ribulose bisphosphate, creating two molecules of phosphoglyceric acid (PGA). PGA is converted to sugars for biological synthesis. This method of organic matter generation is used by most bacteria, including cyanobacteria. However, green sulfur bacteria, and green bacteria such as *Chlorobium* and *Chloroflexus* use alternative pathways, the reverse citric acid cycle (rTCA) and the 3-hydroxypropionate pathway for carbon fixation, respectively (Madigan et al., 2003).

Major photosynthesizing organisms in cyanobacterial mats

There are many types of photosynthesizing organisms that have been identified within cyanobacterial mats. They range from cyanobacteria, to members of the α-, γ-Proteobacteria, as well as the Chloroflexi. Various types of cyanobacteria are prevalent within these types of mats. Cyanobacteria include filamentous, major mat building genera such as *Microcoleus*

chthonoplastes (Figure 2), *Lyngbya* (Stal et al., 1994), and the heterocystous cyanobacterium *Calothrix* (Canfield et al., 2005). Unicellular cyanobacteria such as *Aphanothece halophytica* (Canfield et al., 2005) are also prevalent in cyanobacterial mats. All other known photosynthesizing bacteria in cyanobacterial mats are anoxygenic photoautotrophs. The full metabolic flexibility of these groups of organisms is still poorly understood, but most contain species that can grow photoautrophically, photoheterotrophically, as well as heterotrophically. Anoxygenic phototrophs include the green and purple bacteria. The green sulfur bacteria, such as *Chlorobium,* are in the phylum Chlorobi. They can utilize inorganic compounds, but most notably H_2S as electron donor for photosynthesis (Madigan et al., 2003). The "green non-sulfur bacteria", commonly referred to as "filamentous anoxygenic photoautotrophs" belong to the phylum Chloroflexi (Figure 2). Members of this phylum include *Chloroflexus*, *Heliothrix* and *Oscillochloris*. They can utilize sulfide, H_2 and even organic compounds for photosynthesis (Hanada and Pierson, 2006). The purple sulfur bacteria, such as *Chromatium* and *Thiocapsa* are α- and γ-Proteobacteria, respectively. They can utilize sulfide and H_2 as electron donors for photosynthesis (Hanada and Pierson, 2006). The purple non-sulfur bacteria are within the α-Proteobacteria, such as *Rhodobacter,* and *Rhodospirillum,* these organisms primarily use H_2 or other molecules as electron donors, but can also use sulfide (Hanada and Pierson, 2006).

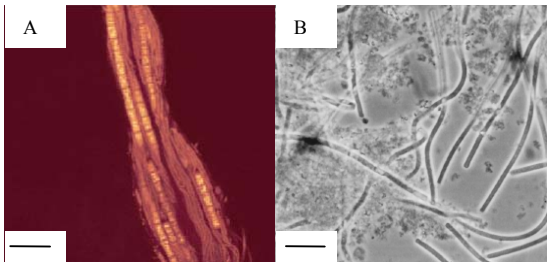

Figure 2. (A) *Microcoleus chthonoplastes* filaments (thick) intertwined with Chloroflexi filaments (thin), in a *Microcoleus chthonoplastes* mat (modified from Ley*, et al.* 2006). (B) *Desulfonema* spp. filaments from a cyanobacterial mat (Modified from Teske *et al.* 1998). Scale bars indicate 10 µm.

Dissimilatory sulfate reduction in cyanobacterial mats

Next to oxygen, sulfate is the most important electron acceptor in the marine environment (Kasten and Jørgensen, 2000). Oxygen penetration in cyanobacterial mats can be quite shallow, just a few millimeters (Teske et al., 1998). After this zone, sulfate reduction becomes one of the most important respiratory processes responsible for carbon re-mineralization (Figure 1) (Canfield and Des Marais, 1993). The availability of sulfate in marine ecosystems, and especially in hypersaline environments, make it an important

electron acceptor. In cyanobacterial mats its importance is revealed by very high rates of sulfate reduction (Teske et al., 1998).

Dissimilatory sulfate reduction is typically the oxidation of organic matter with sulfate as an electron accepter, as described by the equation below (eq. 3):

$$CH_3COO^- + SO_4^{2-} \rightarrow 2HCO_3^- + HS^- \quad (3)$$

Sulfate-reducing bacteria can use a variety of typically low weight molecular substrates for their metabolism, e.g. acetate, fumarate and pyruvate, as well as inorganic compounds such as H_2, which result from anaerobic fermentative processes in the degradation of organic matter. Another fermentative product fueling sulfate reduction in cyanobacterial mats is glycolate, which is produced by cyanobacteria (Teske et al., 1998).

Sulfate reduction is a multistage process where electrons are abstracted from the metabolism of organic compounds, or hydrogen and ultimately transferred to sulfate, producing sulfide. In the first stage, sulfate is activated by the transfer of an ADP (adenosine diphosphate) group to sulfate, by ATP sulfurylase, producing adenosine phosphosulfate (APS). APS is then reduced by APS reductase, producing sulfite (SO_3^{2-}). Sulfite is then reduced to sulfide via the addition of two electrons from sulfite reductase. The resulting sulfide is then excreted by the cell.

Major sulfate-reducing organisms in cyanobacterial mats

Sulfate-reducing bacteria encompass many different bacterial and archaeal lineages, however, most are found within the delta proteobacteria. The most well-known sulfate reducing bacteria in cyanobacterial mats are the filamentous δ-Proteobacteria, which belong to *Desulfonema* (Figure 2). They can be up to 30% of the total mat rRNA content in certain mat sections (Minz et al., 1999a). Other δ-Proteobacteria identified in cyanobacterial mats include relatives of *Desulfococcus*, *Desulfobulbus* and *Desulfobacter* (Minz et al., 1999b). Although there are several known species of sulfate reducing archaea (Canfield et al., 2005), none have been identified in cyanobacterial mats.

Major areas of research on cyanobacterial mats

Cyanobacterial mats continue to be a very important object of scientific investigation, because of what these microbial communities can tell us about past and current interactions

between microorganisms. Several major areas of research that focus on cyanobacterial mats are mentioned below.

- The role of cyanobacterial mats in the oxygenation of the atmosphere by the release of O_2 and H_2 gases over 2 billion years ago (Hoehler et al., 2001).
- The diversity of microbes and processes that contribute to the viability and self-sustainability of cyanobacterial mat communities (Jungblut et al., 2005; Ley et al., 2006).
- Specific research on the diversity of microbes that contribute to the N (Michotey and Bonin, 1997; Omoregie et al., 2004b; Goregues et al., 2005; Bonin and Michotey, 2006), C (Jonkers et al., 2003; van der Meer et al., 2005), S (Teske et al., 1998; Wieland et al., 2005) (Minz et al., 1999a) and O (Jonkers et al., 2003; Wieland and Kuhl, 2006) cycles in cyanobacterial mats.

Part 3: Anaerobic methanotrophic mats

Methane is one of the most potent green house gases known, it is about 25 times more effective than carbon dioxide at trapping heat in our atmosphere (Manne and Richels, 2001). It can be produced through a number of ways. Microbial production of methane includes methanogenesis in landfills, rice paddies, ruminants and termite guts, limnic systems, terrestrial soils and marine sediments. Geologically it is produced by thermogenic degradation of organic matter buried deeply in the seafloor, or through high temperature seawater-rock interactions (serpentinization) (Kelley et al., 2001). There are large reservoirs of methane stored in the form of gas hydrate within marine sediments from which methane is continuously released (Reeburgh, 2007). Very little of this methane reaches the atmosphere as it is oxidized already within the seafloor, primarily through microbial anaerobic oxidation of methane (AOM) (Hinrichs and Boetius, 2002; Reeburgh, 2007).

The analyses of 16S rRNA gene sequences and stable isotope signatures of specific biomarkers identified several phylogenetic clusters of archaea related to Methanosarcinales as the dominant anaerobic methanotrophs (ANME) (Boetius et al., 2000; Orphan et al., 2001). In most AOM habitats studied so far, the archaea live in consortia with sulfate-reducing

bacteria (SRB) of the *Desulfosarcina/Desulfococcus* or *Desulfobulbus* groups (DSS, DBB) (Hinrichs et al., 1999; Boetius et al., 2000; Orphan et al., 2001; Michaelis et al., 2002; Niemann et al., 2006). This association is commonly explained as obligate syntrophy in which the archaeal partner activates and metabolizes methane, providing an intermediate, which is scavenged by the sulfate-reducing partner (Valentine and Reeburgh, 2000). Earlier work has shown that hotspot sediment horizons of AOM are dominated by methane oxidizing archaea and sulfate reducing bacteria which often make up more than 90% of the total microbial community biomass (Boetius et al., 2000; Knittel et al., 2003; Knittel et al., 2005). In 2002, conspicuous microbial structures forming reef-like systems were found in the permanently anoxic Black Sea (Michaelis et al., 2002). It was found that these reefs are formed by methanotrophic microbial mats consisting of the same type of microorganisms as found in sedimentary AOM hotspots, i.e. methane-sulfate transition zones (Hinrichs et al. 2002). Today, at least two examples of these methanotrophic mats are known, those that form carbonate encrusted microbial reefs extending vertically along gas ebullition pathways into the anoxic water column of the Black Sea (Michaelis et al., 2002; Treude et al., 2007), and those that form horizontally growing subsurface calcifying mats ca. 20-30 cm below the seafloor of the Black Sea (Stadnitskaia et al., 2005; Treude et al., 2005a).

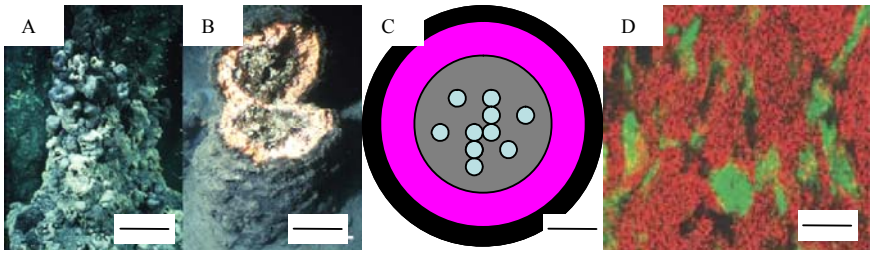

Figure 3. (A) Carbonate reef from the Black Sea (modified from Michaelis *et al.* 2002). (B) Broken carbonate reef from the black sea (modified from Michaelis *et al.* 2002). (C) Cross section of a carbonate reef. Outer ring is composed of microbial mat dominated by ANME-1. Inner pink ring is composed of microbial mat dominated by ANME-1 and -2. Inner grey ring is composed of calcified porous material through which fluids and gases flow. (C) Fluorescence in situ hybridization image of a carbonate section from a reef. ANME-1 archaea are red and sulfate reducers are green (modified from Michaelis *et al*. 2002). Scale bars indicate 20 cm (A-B), 10 cm (C), and 10 μm (D).

Anaerobic oxidation of methane in methanotrophic mats

The major process responsible for the growth of these mats is the anaerobic oxidation of methane (Michaelis et al., 2002).

$$CH_4 + SO_4^{2-} \rightarrow HCO^-_3 + HS^- + H_2O \quad (4)$$

The mats are fueled by sulfate that diffuses in from the seawater and by methane that seeps upwards from reservoirs deep below the reefs (Treude et al., 2005b; Treude et al., 2007). AOM is a process that has not been clearly elucidated. It is thought to be a two-stage process that is carried out by a consortium of methane oxidizing archaea and sulfate reducing bacteria (Hoehler and Alperin, 1996; Hinrichs and Boetius, 2002; Nauhaus et al., 2002). Methane is oxidized by an archaeon and then a metabolite is transferred to the sulfate reducing bacterium, ultimately producing H_2S. The methane oxidation part of this reaction is thought to involve similar enzymes as in methanogenesis, which would operate in reverse. Indeed, methane oxidizing archaea have been shown to possess most of the genes necessary for methanogenesis (Hallam et al., 2004). The last step in methanogenesis would be the reduction of methyl-co-enzyme M, by methyl-coenzyme M reductase (MCR). This enzyme adds an H to a methyl group on methyl Co-enzyme, forming methane. It is thought to catalyze the first step in AOM. Recent evidence has shown that this enzyme is present in high concentrations in active methanotrophic mats from the Black Sea (Krüger et al., 2003).

The nature of the metabolite transferred between the archaea and bacteria is to date unknown. Several substrates have been tested (hydrogen, acetate, formate and methanol), but none have been shown to be a viable transfer metabolite between both partners of the AOM consortia (Nauhaus et al., 2002). Sulfate reduction within the bacteria would be similar to the process described in the previous section. There is, however, some debate as to whether this process could be carried out by the archaea alone. The archaea are often found without directly attached bacterial partners (Orphan et al., 2002; Knittel et al., 2005), suggesting that they may be able to carry out AOM on their own. In this case they would have to possess the functional genes in sulfate reduction, which has not yet been shown.

Major organisms involved in the anaerobic oxidation of methane in methanotrophic mats

There are currently four clades of anaerobic methane oxidizing archaea known. The first three that were discovered are termed ANME-1 through 3 and the last is undesignated. ANME-1 archaea are distantly related to the Methanosarcinales and Methanomicrobiales (Michaelis et al., 2002), ANME-2 belong to the Methanosarcinales (Boetius et al., 2000), and ANME-3 *Methanococcoides* (Lösekann et al., 2007). The fourth clade of ANME organisms was recently discovered and is most closely related to Methanosarcinales (Raghoebarsing et al., 2006). Not only phylogenetically distinct from the other three ANME clades, it is thought to perform AOM with a nitrate reducer as opposed to a sulfate reducing bacterium

(Raghoebarsing et al., 2006). Multiple groups of ANME are present in methane rich environments, but typically just one group dominates (Knittel et al., 2005). ANME-1 and ANME-2 are the dominant groups within the mats located in Black Sea (Knittel et al., 2005; Stadnitskaia et al., 2005).

Sulfate reducing bacteria associated with the ANME belong to the δ-Proteobacteria. Members of the *Desulfococcus*/*Desulfosarcina* cluster form consortia with ANME-1 and -2 (Knittel et al., 2005), and the *Desulfobulbus* cluster with ANME-3 (Lösekann et al., 2007). The methanotrophic mats of the Black Sea are dominated by members of the *Desulfococcus*/*Desulfosarcina* cluster (Knittel et al., 2005; Treude et al., 2007).

Major areas of research on anaerobic marine methanotrophic mats

The methanotrophic mats in the Black Sea continue to be of great scientific interest. Several key areas of active research involve these microbial communities, some of which have been the subject of several recent publications:

- How do the microbial methanotrophic mats form and what organisms are involved in their viability (Treude et al., 2005a; Treude et al., 2007)?
- Where are the hotspots of activity within these microbial communities (Treude et al., 2007) ?
- How does the process of AOM work within in these microbial communities (Krüger et al., 2003; Meyerdierks et al., 2005)?
- What are the functions of the uncultured members of the microbial communities? (Knittel et al., 2003; Knittel et al., 2005)

Part 4: Sulfide-oxidizing mats

Sulfide is a very remarkable compound; it is toxic to most living organisms, yet it is a very important substrate and product of microbial metabolism. It can be generated via microbial respiration or abiotically during seawater/rock interactions at hydrothermal vents. Sulfide-oxidizing mats typically occupy niches characterized by a relatively high flux of sulfide. They are found in a variety of locations, such as hydrothermal vents (Jannasch et al., 1989), hot springs (Ng et al., 2005), cold seeps (Treude et al., 2003), and reduced sediments (Fossing et al., 1995). As such, they can be indicators of intense subsurface microbial activity, as is the case at cold seeps (Treude et al., 2003) as well as in eutrophic sediments of

upwelling areas (Brüchert et al., 2003). Among the best known examples of deep-sea sulfide oxidizing mats of cold seep ecosystems are the vast mats found at the Haakon Mosby mud volcano in the Barents Sea (Niemann et al., 2006). These mats are composed of *Beggiatoa filaments*, which thrive on the sulfide produced as a result of the anaerobic oxidation of methane (Figure 4) (Niemann et al., 2006).

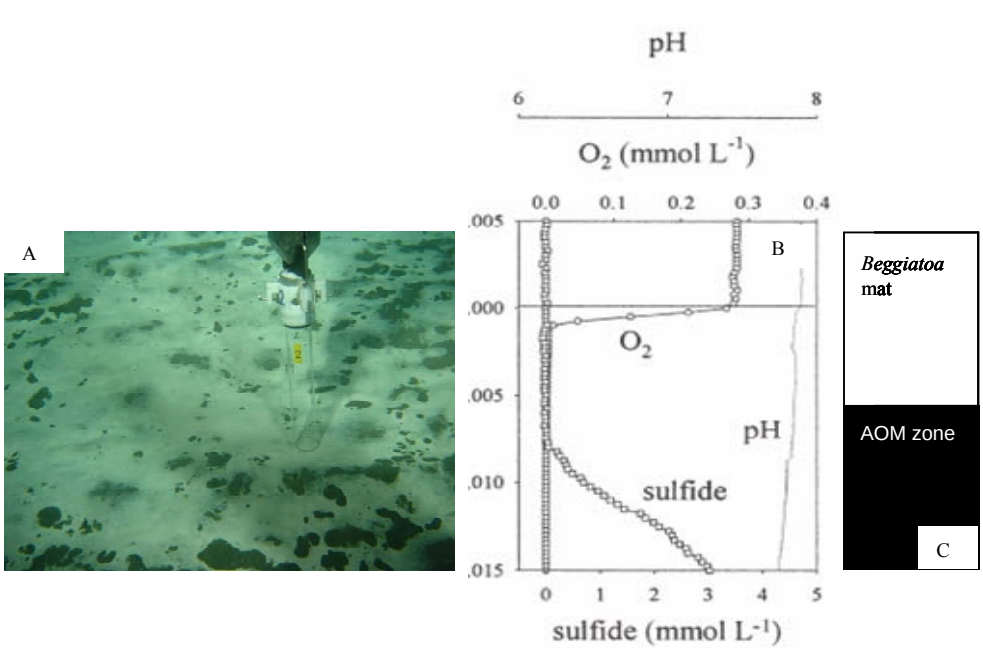

Figure 4: (A) Seafloor image of *Beggiatoa* mats from the Haakon Mosby mud volcano in the North Sea (Image courtesy of IFREMER.). (B) Profiles of O_2, H_2S, and pH from a *Beggiatoa* mat (modified from De Beer *et al.* 2006). Y axis is depth in meters. Sulfide is produced as a result of the anaerobic oxidation of methane. (C) Schematic of mat pictured to the left.

Sulfide oxidation in mats

Sulfide oxidation can be an aerobic (eqn. 5) or anaerobic process, occurring with nitrate (eqn.6), or nitrite depending on the microorganisms involved, as well as the environmental conditions.

$$H_2S + 2O_2 \rightarrow SO_4^{2-} + 2H^+ \quad (5)$$

$$H_2S + NO_3^- + H_2O \rightarrow SO_4^{2-} + NH_4^+ \quad (6)$$

Most known sulfide-oxidizing bacteria are obligate or facultative aerobes. In the complete oxidation from sulfide, electrons are transferred to oxygen, ultimately producing sulfate. It can take place via various intermediates, such as through the formation of elemental S, sulfite (SO_3^{2-}), or thiosulfate ($S_2O_3^{2-}$). The central intermediate for the oxidation of sulfide, S and thiosulfate is sulfite. From this step sulfite is directly oxidized to sulfate via the enzyme sulfite oxidase. The electrons from this process are transferred to cytochrome c, via sulfide

oxidase and then flow through the electron transport chain to oxygen. This electron flow generates a protomotive force that results in the generation of ATP. Alternatively, AMP can be added to sulfite with APS reductase, then sulfate liberated either with adenylylsulfate:phosphate adeylytransferase (APAT) or ATP sulfurase. The activity of these enzymes results in the generation of ADP or ATP (substrate level phosphorylation).

Major organisms involved in sulfide-oxidizing mats

Most known sulfide-oxidizing mats are dominated by one, or only few types of sulfide-oxidizing bacteria. However, associated with mats and the surface sediments underlying them is a relatively high diversity of other organisms, including a variety of grazers such as nematodes or other worms (Van Gaever et al., 2006; Lösekann et al., 2007). Sulfide-oxidizing bacteria encompass many different lineages of prokaryotes. The most well-known sulfide oxidizing bacteria are within the γ-Proteobacteria. They are the giant vacuolated sulfide oxidizing bacteria, *Beggiatoa* (Jannasch et al., 1989), *Thioploca* (Fossing et al., 1995), and *Thiomargarita* (Schulz et al., 1999b) (Figure 5). These organisms are known for the conspicuous white mats that they form at hydrothermal vents, cold seeps and\or above organic rich sediments. The white color is result of elemental S that is stored in internal vacuoles within the cells (Nelson et al., 1989; Schulz et al., 1999a). Other well-known mat forming sulfide-oxidizing bacteria are within the ε-Proteobacteria. They are "*Candidatus* Arcobacter sulfidicus" (Taylor and Wirsen, 1997; Wirsen et al., 2002), and *"Candidatus* Thioturbo danicus" (Thar and Kuhl, 2002; Muyzer et al., 2005), which lack internal vacuoles for the storage of sulfur. Sulfide-oxidizing archaea are represented by thermophiles such *Sulfolobus,* which are present in hot spring mats (Ng et al., 2005).

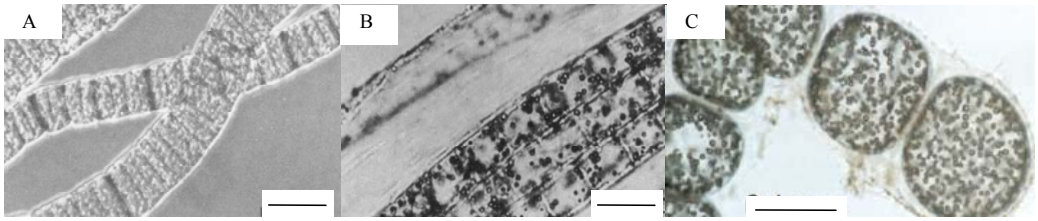

Figure 5: (A) *Beggiatoa* sp. filaments from a hydrothermal vent sediment (modified from Nelson *et al.* 1987). (B) *Thioploca* sp. filaments from the Peruvian shelf sediment (modified from Fossing *et al.*, 1995) (C) Chain of *Thiomargarita namibiensis* from Namibian shelf sediment (modified from Schulz *et al.* 1999). Scale bars indicates 50 µm (A-B) and 100 µm (C).

Major areas of research on sulfide oxidizing mats

Sulfide oxidizing mats are very widespread in the marine environment; however several research questions still surround these types of microbial communities:

- Which environmental factors select for different types of mat forming sulfide oxidizers and their distribution (de Beer et al., 2006)?
- What is the biodiversity of mat-forming sulfide oxidizers in the ocean (Schulz and Jorgensen, 2001)?
- What is the microdiversity and distribution patterns of different sulfide-oxidizer populations (Mussmann et al., 2003)?
- How much carbon is fixed by sulfide oxidizing mats and how is the energy transferred to higher food levels (Levin and Michener, 2002)?

Part 5: Iron-cycling microbial mats

Iron is one of the most abundant elements and constitutes over 4 % of the Earth's crust (Wedepohl, 1995). It is redox active and can be oxidized to gain energy as well as used as an electron acceptor for cellular metabolism by many different prokaryotes. It is also a vital component of many different enzymes. Iron is central to biogeochemical cycling not only because its role in biology, but its role in mineral formation and dissolution, as it can readily react with S, Mn and P containing minerals (Canfield et al., 2005). Iron-cycling mats are microbial mats that are formed by iron-oxidizing bacteria. Their distribution is global and they exist everywhere there is a Fe^{2+} source.

Iron-oxidation in mats

Iron-oxidation can be either aerobic (eqns. 7 and 8) or anaerobic with nitrate (eqn. 9) as an alternative electron acceptor (Edwards et al., 2004). The bacteria in these mats oxidize Fe^{2+} to Fe^{3+}, the Fe^{3+} reacts with water to form Fe(III)-hydroxide, which is responsible for the red color of iron-oxidizing mats (Canfield et al., 2005).

$$4Fe^{2+} + O_2 + 4H^+ \rightarrow 4Fe^{3+} + 2H_2O \quad (7)$$

$$4Fe_2^{+} + O_2 + 10H_2O \rightarrow 4Fe(OH)_3 + 8H^+ \quad (8)$$

$$2Fe^{2+} + NO_3^- + 5H_2O \rightarrow 2Fe(OH)_3 \quad (9)$$

There are in principal two types of iron-oxidizing mats, those that are active at acidic pH and those that are active at circumneutral pH. At acidic pH Fe^{3+} cation is stable (eqn. 7), but

can react with water to form Fe(III)-hydroxide as is the case under neutrophilic conditions (eqns. 8 and 9). Acidophilic iron-oxidizing mats are infamous at acid mine drainage environments. These habitats form where pyrite is exposed to oxygen and water as a result of mining activities. The S in pyrite is oxidized to sulfate, releasing Fe^{2+} and H^{+}. Under these conditions Fe^{2+} is very stable and can be oxidized by bacteria to Fe^{3+}. The Fe^{3+} can then react with pyrite, releasing sulfate, Fe^{2+} and H^{+}.

$$FeS_2 + 14Fe^{3+} + 8H_2O \rightarrow 15Fe^{2+} + 2SO_4^{2-} + 16H^{+} \quad (10)$$

This cycle is continuously repeated, resulting in very acidic conditions and the fowling of the water. Examples of this are Fe-oxidizing mats that form in mine drainages at Iron Mountain, USA (Druschel et al., 2004) and in the Rio Tinto river, Spain (Davis et al., 2000).

Figure 6. Image from the Rio Tinto in Spain. (modified from Davis *et al.*, 1998). Red color is a result of Fe-oxide precipitation.

Neutrophilic iron oxidation typically occurs when Fe^{2+} rich waters reach the oxic zone. Fe^{2+} is supplied by the activities of iron-reducing bacteria, which release Fe^{2+} or through hydrothermal vent fluids. Under these conditions, Fe^{2+} can be oxidized to form iron-oxides ,which precipitate. This situation occurs in groundwater seeps (Emerson and Revsbech, 1994), plant root nodules (Emerson et al., 1999) and at hydrothermal vents (Emerson and Moyer, 2002).

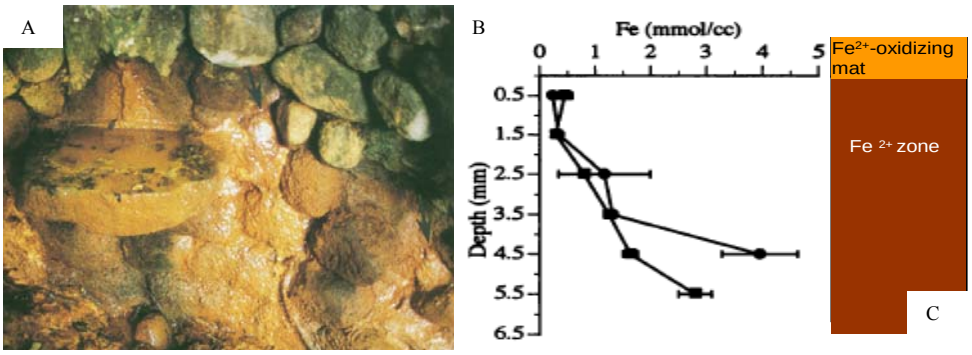

Figure 7. (A) Image from a groundwater seep near Aarhus Denmark (modified from Emerson *et al.*, 1994). (B) Fe^{2+} profile underneath a Fe^{2+}-oxidizing mat (modified from Emerson *et al.*, 1994). (C) Schematic of the Fe^{2+} oxidizing mat picture on the right.

The mechanisms of iron oxidation and reduction by prokaryotes are currently poorly understood. The best known mechanism of iron oxidation is that of the acidophile *Thiobacillus ferrooxidans* (Canfield et al., 2005). It is not known how the electrons are absconded from Fe^{2+}. These electrons, however, are eventually passed to the periplasm protein (rusticyanin), then to a cytochrome and then to O_2 where H_2O is created from H^+ that are pumped into the cell via ATPases. Additionally, NADH necessary for CO_2 fixation can be generated by electrons taken from Fe^{2+}.

Microorganisms involved in iron oxidizing mats

Iron oxidation is very wide spread among prokaryotes. Well known acidophilic strains are in the δ-proteobacterium, such as *Acidithiobacillus ferrooxidans*, and *Leptospirillum ferrooxidans*, both of which are very active in acid mine drainage environments (Rawlings et al., 1999). The most well-known iron-oxidizing archaeon is *Ferroplasma acidarmanus* which is known from low pH biofilms (Edwards et al., 2000). Neutrophilic iron oxidizers are the well-known sheet forming β-Proteobacteria, *Leptothrix* and *Sphaerotilus,* as well as the stalk forming *Gallionella* (Canfield et al., 2005).

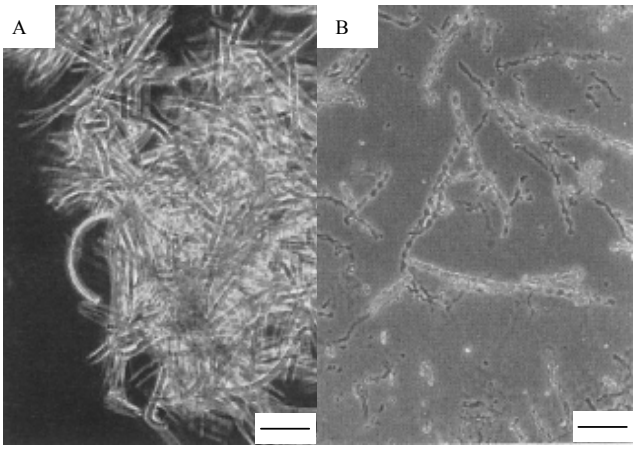

Figure 8. (A) *Leptothrix* sheaths and *Gallionella* stalks from the Fe seep in Figure 7A (modified from Emerson *et al*., 1994). Scale bars indicates 10 μm.

Iron reduction

Iron reduction is somewhat enigmatic, especially in systems where sulfide is present. That is because sulfide can rapidly react with Fe-oxides abiotically to produce Fe^{2+} and FeS (Canfield et al., 2005), or Fe-oxides can be reduced directly by microorganisms. Iron reduction is typically a heterotrophic process where an organic electron donor is used:

$$CH_3COO^- + 8FeOOH \rightarrow 3HCO_3^- + 8Fe^{2+} + 15OH^- \quad (11)$$

The mechanisms for the direct microbial reduction of Fe-oxides is at this point unknown. Fe-oxides present a problem to microbes as they are not soluble. Previous work has suggested, however, that this process can occur via the use of electron shuttles (Straub and Schink, 2003), to which electrons are donated and the electrons delivered to Fe-oxides. Additional work has shown that conductive pili (nanowires) from cells may act as a conduit for the transfer of electrons to Fe-oxides (Reguera et al., 2005). Bacteria of the family Geobacteraceae can couple the oxidation of organic compounds to the reduction of insoluble Fe(III) oxides, and even grow by oxidizing organics with a graphite electrodeas the sole electron acceptor (Bond et al., 2002).

Iron reducing bacteria in mats

Iron reduction is carried out by a wide variety of bacteria and archaea. Most of the known Fe-reducing bacteria are Proteobacteria. Within the δ-Proteobacteria, are *Geobacter*, *Pelobacter*, *Desulfuromonas*, in the ε-Proteobacteria *Sulfurospirillum* and the γ-proteobacteria *Shewanella* (Canfield et al., 2005). These organisms can use multiple electron donors such as H_2 and acetate, lactate and ethanol. In the ε-Proteobacteria there is *Sulfurospirillum deleyianum*, which is interesting as it is able to couple iron reduction to the cycling of S compounds (Straub and Schink, 2004). Iron-reducing archaea are the hypothermophiles *Archaeglobus fulgidus* and *Ferroglobus placidus*.

Major areas of research on iron-cycling mats

Iron-oxidizing mats are a very exciting area of research, because so little information is available on how they actually function. Several research areas are being pursued:

- What organisms are responsible for the formation and functioning of iron-oxidizing mats (Edwards et al., 2004)?
- What is the contribution of abiotic vs. microbially mediated processes (Neubauer et al., 2002; James and Ferris, 2004) ?
- How do iron-utilizing bacteria shuttle electrons to and from iron in Fe reduction and oxidation (Straub and Schink, 2003; Reguera et al., 2005)?

References

Boetius, A., Ravenschlag, K., Schubert, C.J., Rickert, D., Widdel, F., Giesecke, A., Amann, R., Jørgensen, B.B., Witte, U. and Pfannkuche, O., 2000. A marine microbial consortium apparently mediating anaerobic oxidation of methane. Nature, 407: 623-626.

Bond, D.R., Holmes, D.E., Tender, L.M. and Lovley, D.R., 2002. Electrode-reducing microorganisms that harvest energy from marine sediments. Science, 295(5554): 483-485.

Bonin, P.C. and Michotey, V.D., 2006. Nitrogen budget in a microbial mat in the Camargue (southern France). Marine Ecology-Progress Series, 322: 75-84.

Brüchert, V., Jorgensen, B.B., Neumann, K., Riechmann, D., Schlosser, M. and Schulz, H., 2003. Regulation of bacterial sulfate reduction and hydrogen sulfide fluxes in the central Namibian coastal upwelling zone. Geochimica Et Cosmochimica Acta, 67(23): 4505-4518.

Buick, R., Dunlop, J.S.R. and Groves, D.I., 1981. Stromatolite Recognition in Ancient Rocks - an Appraisal of Irregularly Laminated Structures in an Early Archean Chert-Barite Unit from North-Pole, Western-Australia. Alcheringa, 5(3-4): 161-181.

Canfield, D., E., Kristensen, E. and Thamdrup, B., 2005. Microbial Ecosystems, Aquatic Geomicrobiology. Elsevier, San Diego.

Canfield, D.E. and Des Marais, D.J., 1993. Biogeochemical cycles of carbon, sulfur, and free oxygen in a microbial mat. Geochimica et Cosmochimica Acta, 57(16): 3971-3984.

Davey, M.E. and O'Toole, G.A., 2000. Microbial Biofilms: from Ecology to Molecular Genetics. Microbiology and Molecular Biology Reviews, 64(4): 847-867.

Davis, R.A., Welty, A.T., Borrego, J., Morales, J.A., Pendon, J.G. and Ryan, J.G., 2000. Rio Tinto estuary (Spain): 5000 years of pollution. Environmental Geology, 39(10): 1107-1116.

de Beer, D., Sauter, E., Niemann, H., Kaul, N., Foucher, J.P., Witte, U., Schluter, M. and Boetius, A., 2006. In situ fluxes and zonation of microbial activity in surface sediments of the Hakon Mosby Mud Volcano. Limnology and Oceanography, 51(3): 1315-1331.

Druschel, G.K., Baker, B.J., Gihring, T.M. and Banfield, J.F., 2004. Acid mine drainage biogeochemistry at Iron Mountain, California. Geochemical Transactions, 5(2): 13-32.

Edwards, K.J., Bach, W., McCollom, T.M. and Rogers, D.R., 2004. Neutrophilic iron-oxidizing bacteria in the ocean: Their habitats, diversity, and roles in mineral deposition, rock alteration, and biomass production in the deep-sea. Geomicrobiology Journal, 21(6): 393-404.

Edwards, K.J., Bond, P.L., Gihring, T.M. and Banfield, J.F., 2000. An archaeal iron-oxidizing extreme acidophile important in acid mine drainage. Science, 287(5459): 1796-1799.

Emerson, D. and Moyer, C.L., 2002. Neutrophilic Fe-Oxidizing Bacteria Are Abundant at the Loihi Seamount Hydrothermal Vents and Play a Major Role in Fe Oxide Deposition. Applied and Environmental Microbiology, 68(6): 3085-3093.

Emerson, D. and Revsbech, N.P., 1994. Investigation of an Iron-Oxidizing Microbial Mat Community Located near Aarhus, Denmark - Laboratory Studies. Applied and Environmental Microbiology, 60(11): 4032-4038.

Emerson, D., Weiss, J.V. and Megonigal, J.P., 1999. Iron-Oxidizing Bacteria Are Associated with Ferric Hydroxide Precipitates (Fe-Plaque) on the Roots of Wetland Plants. Applied and Environmental Microbiology, 65(6): 2758-2761.

Entcheva-Dimitrov, P. and Spormann, A.M., 2004. Dynamics and control of biofilms of the oligotrophic bacterium Caulobacter crescentus. Journal of Bacteriology, 186(24): 8254-8266.

Fossing, H., Gallardo, V.A., Jørgensen, B.B., Hüttel, M., Nielsen, L.P., Schulz, H., Canfield, D.E., Forster, S., Glud, R.N., Gundersen, J.K., Küver, J., Ramsing, N.B., Teske, A., Thamdrup, B. and Ulloa, O., 1995. Concentration and transport of nitrate by the mat-forming sulphur bacterium *Thioploca*. Nature, 374: 713-715.

Goregues, C.M., Michotey, V.D. and Bonin, P.C., 2005. Molecular, biochemical, and physiological approaches for understanding the ecology of denitrification. Microbial Ecology, 49(2): 198-208.

Hallam, S.J., Putnam, N., Preston, C.M., Detter, J.C., Rokhsar, D., Richardson, P.M. and DeLong, E.F., 2004. Reverse Methanogenesis: Testing the Hypothesis with Environmental Genomics. Science, 305(5689): 1457-1462.

Hanada, S. and Pierson, B.K., 2006. The prokaryotes. Springer-Verlag.

Hinrichs, K.-U. and Boetius, A., 2002. The anaerobic oxidation of methane: new insights in microbial ecology and biogeochemistry. In: G. Wefer et al. (Editors), Ocean Margin Systems. Springer-Verlag, Berlin, pp. 457-477.

Hinrichs, K.-U., Hayes, J.M., Sylva, S.P., Brewer, P.G. and De Long, E.F., 1999. Methane-consuming archaebacteria in marine sediments. Nature, 398: 802-805.

Hoehler, T.M. and Alperin, M.J., 1996. Anaerobic methane oxidation by a methanogen-sulphate reducer consortium: geochemical evidence and biochemical considerations. In: M.E. Lidstrom and F.R. Tabita (Editors), Microbial Growth on C_1 Compounds. Kluwer Academic Publishers, Intercept, Andover, UK, pp. 326-333.

Hoehler, T.M., Bebout, B.M. and Des Marais, D.J., 2001. The role of microbial mats in the production of reduced gases on the early Earth. Nature, 412(6844): 324-327.

James, R.E. and Ferris, F.G., 2004. Evidence for microbial-mediated iron oxidation at a neutrophilic groundwater spring. Chemical Geology, 212(3-4): 301.

Jannasch, H.W., Nelson, D.C. and Wirsen, C.O., 1989. Massive Natural Occurrence of Unusually Large Bacteria (Beggiatoa Sp) at a Hydrothermal Deep-Sea Vent Site. Nature, 342(6251): 834-836.

Jonkers, H.M., Ludwig, R., De Wit, R., Pringault, O., Muyzer, G., Niemann, H., Finke, N. and De Beer, D., 2003. Structural and functional analysis of a microbial mat ecosystem from a unique permanent hypersaline inland lake: `La Salada de Chiprana' (NE Spain). FEMS Microbiology Ecology, 44(2): 175-189.

Joye, S.B., Boetius, A., Orcutt, B.N., Montoya, J.P., Schulz, H.N., Erickson, M.J. and Logo, S.K., 2004. The anaerobic oxidation of methane and sulfate reduction in sediments from Gulf of Mexico cold seeps. Chemical Geology, 205: 219-238.

Jungblut, A.D., Hawes, I., Mountfort, D., Hitzfeld, B., Dietrich, D.R., Burns, B.P. and Neilan, B.A., 2005. Diversity within cyanobacterial mat communities in variable salinity meltwater ponds of McMurdo Ice Shelf, Antarctica. Environmental Microbiology, 7(4): 519-529.

Kasten, S. and Jørgensen, B., B., 2000. Sulfate reduction in marine sediments. In: H. Schulze, D., and M. Zabel (Editors), Marine Geochemistry. Springer, Berlin, pp. 263-281.

Kelley, D.S., Karson, J.A., Blackman, D.K., Fruh-Green, G.L., Butterfield, D.A., Lilley, M.D., Olson, E.J., Schrenk, M.O., Roe, K.K., Lebon, G.T., Rivizzigno, P., Party, A.-S. and, 2001. An off-axis hydrothermal vent field near the Mid-Atlantic Ridge at 30 degrees N. Nature, 412(6843): 145-149.

Knittel, K., Boetius, A., Lemke, A., Eilers, H., Lochte, K., Pfannkuche, O., Linke, P. and Amann, R., 2003. Activity, distribution, and diversity of sulfate reducers and other

bacteria in sediments above gas hydrate (Cascadia margin, Oregon). Geomicrobiology Journal, 20(4): 269-294.
Knittel, K., Losekann, T., Boetius, A., Kort, R. and Amann, R., 2005. Diversity and distribution of methanotrophic archaea at cold seeps. Applied and Environmental Microbiology, 71(1): 467-479.
Krüger, M., Meyerdierks, A., Glockner, F.O., Amann, R., Widdel, F., Kube, M., Reinhardt, R., Kahnt, R., Bocher, R., Thauer, R.K. and Shima, S., 2003. A conspicuous nickel protein in microbial mats that oxidize methane anaerobically. Nature, 426(6968): 878-881.
Levin, L.A. and Michener, R.H., 2002. Isotopic evidence for chemosynthesis-based nutrition of macrobenthos: the lightness if being at Pacific methane seeps. Limnol. Oceanogr., 47(5): 1336-1345.
Ley, R.E., Harris, J.K., Wilcox, J., Spear, J.R., Miller, S.R., Bebout, B.M., Maresca, J.A., Bryant, D.A., Sogin, M.L. and Pace, N.R., 2006. Unexpected Diversity and Complexity of the Guerrero Negro Hypersaline Microbial Mat. Applied and Environmental Microbiology, 72(5): 3685-3695.
Lösekann, T., Knittel, K., Nadalig, T., Fuchs, B., Niemann, H., Boetius, A. and Amann, R., 2007. Diversity and Abundance of Aerobic and Anaerobic Methane Oxidizers at the Haakon Mosby Mud Volcano, Barents Sea. Applied and Environmental Microbiology. Applied and Environmental Microbiology, 73: 3348-3362.
Madigan, M., T., Martinko, J., M., and Parker, J., 2003. Metabolic diversity. In: G. Carlson (Editor), Brock Biology of Microorganims.
Manne, A.S. and Richels, R.G., 2001. An alternative approach to establishing trade-offs among greenhouse gases. Nature, 410(6829): 675-677.
Meyerdierks, A., Kube, M., Lombardot, T., Knittel, K., Bauer, M., Glockner, F.O., Reinhardt, R. and Amann, R., 2005. Insights into the genomes of archaea mediating the anaerobic oxidation of methane. Environmental Microbiology, 7(12): 1937-1951.
Michaelis, W., Seifert, R., Nauhaus, K., Treude, T., Thiel, V., Blumenberg, M., Knittel, K., Gieseke, A., Peterknecht, K., Pape, T., Boetius, A., Aman, A., Jørgensen, B.B., Widdel, F., Peckmann, J., Pimenov, N.V. and Gulin, M., 2002. Microbial reefs in the Black Sea fueled by anaerobic oxidation of methane. Science, 297: 1013-1015.
Michotey, V. and Bonin, P., 1997. Evidence for anaerobic bacterial processes in the water column: denitrification and dissimilatory nitrate ammonification in the northwestern Mediterranean Sea. Marine Ecology Progress Series, 160: 47-56.
Minz, D., Fishbain, S., Green, S.J., Muyzer, G., Cohen, Y., Rittmann, B.E. and Stahl, D.A., 1999a. Unexpected population distribution in a microbial mat community: sulfate-reducing bacteria localized to the highly oxic chemocline in contrast to a eukaryotic preference for anoxia. Applied and Environmental Microbiology, 65(10): 4659-65.
Minz, D., Flax, J.L., Green, S.J., Muyzer, G., Cohen, Y., Wagner, M., Rittmann, B.E. and Stahl, D.A., 1999b. Diversity of sulfate-reducing bacteria in oxic and anoxic regions of a microbial mat characterized by comparative analysis of dissimilatory sulfite reductase genes. Applied and Environmental Microbiology, 65(10): 4666-71.
Mussmann, M., Schulz, H.N., Strotmann, B., Kjaer, T., Nielsen, L.P., Rossello-Mora, R.A., Amann, R.I. and Jorgensen, B.B., 2003. Phylogeny and distribution of nitrate-storing Beggiatoa spp. in coastal marine sediments. Environmental Microbiology, 5(6): 523-533.
Muyzer, G., Yildirim, E., van Dongen, U., Kuhl, M. and Thar, R., 2005. Identification of "Candidatus Thioturbo danicus," a Microaerophilic Bacterium That Builds Conspicuous Veils on Sulfidic Sediments. Applied and Environmental Microbiology, 71(12): 8929-8933.

Nauhaus, K., Boetius, A., Krüger, M. and Widdel, F., 2002. In vitro demonstration of anaerobic oxidation of methane coupled to sulphate reduction in sediment from marine gas hydrate area. Environmental Microbiology, 4(5): 298-305.
Nelson, D.C., Wirsen, C.O. and Jannasch, H.W., 1989. Characterization of Large, Autotrophic Beggiatoa Spp Abundant at Hydrothermal Vents of the Guaymas Basin. Applied and Environmental Microbiology, 55(11): 2909-2917.
Neubauer, S.C., Emerson, D. and Megonigal, J.P., 2002. Life at the Energetic Edge: Kinetics of Circumneutral Iron Oxidation by Lithotrophic Iron-Oxidizing Bacteria Isolated from the Wetland-Plant Rhizosphere. Applied and Environmental Microbiology, 68(8): 3988-3995.
Ng, C.C., Chang, C.C. and Shyu, Y.T., 2005. Archaeal community revealed by 16s rRNA and fluorescence in situ hybridization in a sulphuric hydrothermal hot spring, northern Taiwan. World Journal of Microbiology & Biotechnology, 21(6-7): 933-939.
Niemann, H., Losekann, T., de Beer, D., Elvert, M., Nadalig, T., Knittel, K., Amann, R., Sauter, E.J., Schluter, M., Klages, M., Foucher, J.P. and Boetius, A., 2006. Novel microbial communities of the Haakon Mosby mud volcano and their role as a methane sink. Nature, 443(7113): 854.
Nisbet, E.G. and Fowler, C.M.R., 1999. Archaean metabolic evolution of microbial mate. Proceedings of the Royal Society of London Series B-Biological Sciences, 266(1436): 2375-2382.
Nisbet, E.G. and Sleep, N.H., 2001. The habitat and nature of early life. Nature, 409: 1083-1091.
Omoregie, E.O., Crumbliss, L.L., Bebout, B.M. and Zehr, J.P., 2004a. Comparison of diazotroph community structure in Lyngbya sp and Microcoleus chthonoplastes dominated microbial mats from Guerrero Negro, Baja, Mexico. Fems Microbiology Ecology, 47(3): 305-318.
Omoregie, E.O., Crumbliss, L.L., Bebout, B.M. and Zehr, J.P., 2004b. Determination of nitrogen-fixing phylotypes in Lyngbya sp and Microcoleus chthonoplastes cyanobacterial mats from Guerrero Negro, Baja California, Mexico. Applied and Environmental Microbiology, 70(4): 2119-2128.
Orphan, V.J., House, C.H., Hinrichs, K.-U., McKeegan, K.D. and De Long, E.F., 2001. Methane-consuming Archaea revealed by directly coupled isotopic and phylogenetic analysis. Science, 293: 484-487.
Orphan, V.J., House, C.H., Hinrichs, K.U., McKeegan, K.D. and DeLong, E.F., 2002. Multiple archaeal groups mediate methane oxidation in anoxic cold seep sediments. Proceedings of the National Academy of Sciences of the United States of America, 99(11): 7663-7668.
Paerl, H.W., Steppe, T.F. and Reid, R.P., 2001. Bacterially mediated precipitation in marine stromatolites. Envrionmental Microbiology, 3(2): 123-30.
Papineau, D., Walker, J.J., Mojzsis, S.J. and Pace, N.R., 2005. Composition and Structure of Microbial Communities from Stromatolites of Hamelin Pool in Shark Bay, Western Australia. Applied and Environmental Microbiology, 71(8): 4822-4832.
Raad, I., 1998. Intravascular-catheter-related infections. The Lancet, 351(9106): 898.
Raghoebarsing, A.A., Pol, A., van de Pas-Schoonen, K.T., Smolders, A.J.P., Ettwig, K.F., Rijpstra, W.I.C., Schouten, S., Damste, J.S.S., Op den Camp, H.J.M., Jetten, M.S.M. and Strous, M., 2006. A microbial consortium couples anaerobic methane oxidation to denitrification. Nature, 44: 917-921.
Rawlings, D.E., Tributsch, H. and Hansford, G.S., 1999. Reasons why 'Leptospirillum'-like species rather than Thiobacillus ferrooxidans are the dominant iron-oxidizing bacteria

in many commercial processes for the biooxidation of pyrite and related ores. Microbiology, 145: 5-13.
Reeburgh, W.S., 2007. Oceanic methane biogeochemistry. Chemical Reviews, 107(2): 486-513.
Reguera, G., McCarthy, K.D., Mehta, T., Nicoll, J.S., Tuominen, M.T. and Lovley, D.R., 2005. Extracellular electron transfer via microbial nanowires. Nature, 435(7045): 1098-1101.
Reid, R.P., Visscher, P.T., Decho, A.W., Stolz, J.F., Bebout, B.M., Dupraz, C., Macintyre, I.G., Paerl, H.W., Pinckney, J.L., Prufert-Bebout, L., Steppe, T.F. and DesMarais, D.J., 2000. The role of microbes in accretion, lamination and early lithification of modern marine stromatolites. Nature, 406(6799): 989-92.
Schulz, H.N., Brinkhoff, T., Ferdelman, T.G., Hernández Mariné, M., Teske, A. and Jørgensen, B.B., 1999a. Dense populations of a giant sulfur bacterium in Namibian shelf sediments. Science, 284: 493-495.
Schulz, H.N., Brinkhoff, T., Ferdelman, T.G., Marine, M.H., Teske, A. and Jorgensen, B.B., 1999b. Dense populations of a giant sulfur bacterium in Namibian shelf sediments. Science, 284(5413): 493-495.
Schulz, H.N. and Jorgensen, B.B., 2001. Big bacteria. Annual Review of Microbiology, 55: 105-137.
Stadnitskaia, A., Muyzer, G., Abbas, B., Coolen, M.J.L., Hopmans, E.C., Baas, M., van Weering, T.C.E., Ivanov, M.K., Poludetkina, E. and Sinninghe Damste, J.S., 2005. Biomarker and 16S rDNA evidence for anaerobic oxidation of methane and related carbonate precipitation in deep-sea mud volcanoes of the Sorokin Trough, Black Sea. Marine Geology, 217(1-2): 67-96.
Stal, L. and Caumette, P. (Editors), 1994. Microbial mats: Structure, development and environmental significance. Berlin, Springer-Verlag.
Stal, L., J., Paerl, H., W., Bebout, B., M. and Villbrandt, M., 1994. Heterocystous versus non-heterocystous cyanobacteria in microbial mat. In: L. Stal, J., and P. Caumette (Editors), Microbial mats. Springer-Verlag, Berlin.
Stolz, J.F., 1985. The microbial community at Laguna Figueroa, Baja California Mexico: from miles to microns. Origins of Life and Evolution of Biospheres, 15: 347-52.
Straub, K.L. and Schink, B., 2003. Evaluation of electron-shuttling compounds in microbial ferric iron reduction. Fems Microbiology Letters, 220(2): 229-233.
Straub, K.L. and Schink, B., 2004. Ferrihydrite-dependent growth of *Sulfurospirillum deleyianum* through electron transfer via sulfur cycling. Applied and Environmental Microbiology, 70(10): 5744-5749.
Taylor, C.D. and Wirsen, C.O., 1997. Microbiology and ecology of filamentous sulfur formation. Science, 277(5331): 1483-1485.
Teske, A., Ramsing, N.B., Habicht, K., Fukui, M., Kuver, J., Jorgensen, B.B. and Cohen, Y., 1998. Sulfate-reducing bacteria and their activities in cyanobacterial mats of solar lake (Sinai, Egypt). Applied and Environmental Microbiology, 64(8): 2943-51.
Thar, R. and Kuhl, M., 2002. Conspicuous Veils Formed by Vibrioid Bacteria on Sulfidic Marine Sediment. Applied and Environmental Microbiology, 68(12): 6310-6320.
Tice, M.M. and Lowe, D.R., 2004. Photosynthetic microbial mats in the 3,416-Myr-old ocean. Nature, 431: 549-552.
Treude, T., Boetius, A., Knittel, K., Wallmann, K. and Jørgensen, B.B., 2003. Anaerobic oxidation of methane above gas hydrates at Hydrate Ridge, NE Pacific Ocean. Marine Ecology Progress Series, 264: 1-14.

Treude, T., Knittel, K., Blumenberg, M., Seifert, R. and Boetius, A., 2005a. Subsurface Microbial Methanotrophic Mats in the Black Sea. Applied and Environmental Microbiology, 71(10): 6375-6378.

Treude, T., Niggemann, J., Kallmeyer, J., Wintersteller, P., Schubert, C.J., Boetius, A. and Jorgensen, B.B., 2005b. Anaerobic oxidation of methane and sulfate reduction along the Chilean continental margin. Geochimica et Cosmochimica Acta, 69(11): 2767-2779.

Treude, T., Orphan, V., Knittel, K., Gieseke, A., House, C.H. and Boetius, A., 2007. Consumption of Methane and CO2 by Methanotrophic Microbial Mats from Gas Seeps of the Anoxic Black Sea. Applied and Environmental Microbiology, 73(7): 2271-2283.

Valentine, D.L. and Reeburgh, W.S., 2000. New perspectives on anaerobic methane oxidation. Environ. Microbiol., 2(5): 477-484.

van der Meer, M.T.J., Schouten, S., Bateson, M.M., Nubel, U., Wieland, A., Kuhl, M., de Leeuw, J.W., Damste, J.S.S. and Ward, D.M., 2005. Diel variations in carbon metabolism by green nonsulfur-like bacteria in alkaline siliceous hot spring microbial mats from Yellowstone National Park. Applied and Environmental Microbiology, 71(7): 3978-3986.

Van Gaever, S., Moodley, L., de Beer, D. and Vanreusel, A., 2006. Meiobenthos at the Arctic Hakon Mosby Mud Volcano, with a parental-caring nematode thriving in sulphide-rich sediments. Marine Ecology-Progress Series, 321: 143-155.

Ward, D.M., Bateson, M.M., Ferris, M.J., Kuhl, M., Wieland, A., Koeppel, A. and Cohan, F.M., 2006. Cyanobacterial ecotypes in the microbial mat community of Mushroom Spring (Yellowstone National Park, Wyoming) as species-like units linking microbial community composition, structure and function. Philosophical Transactions of the Royal Society B-Biological Sciences, 361(1475): 1997-2008.

Webb, K.L., Dupaul, W.D., Wiebe, W., Sottile, W. and Johannes, R.E., 1975. Enewetak (Eniwetok) Atoll - Aspects of Nitrogen Cycle on a Coral-Reef. Limnology and Oceanography, 20(2): 198-210.

Wedepohl, K.H., 1995. The Composition of the Continental-Crust. Geochimica et Cosmochimica Acta, 59(7): 1217-1232.

Wiebe, W.J., Johannes, R.E. and Webb, K.L., 1975. Nitrogen-Fixation in a Coral-Reef Community. Science, 188(4185): 257-259.

Wieland, A. and Kuhl, M., 2006. Regulation of photosynthesis and oxygen consumption in a hypersaline cyanobacterial mat (Camargue, France) by irradiance, temperature and salinity. Fems Microbiology Ecology, 55(2): 195-210.

Wieland, A., Zopfi, J., Benthien, A. and Kuhl, M., 2005. Biogeochemistry of an iron-rich hypersaline microbial mat (Camargue, France). Microbial Ecology, 49(1): 34-49.

Wirsen, C.O., Sievert, S.M., Cavanaugh, C.M., Molyneaux, S.J., Ahmad, A., Taylor, L.T., DeLong, E.F. and Taylor, C.D., 2002. Characterization of an autotrophic sulfide-oxidizing marine Arcobacter sp. that produces filamentous sulfur. Applied and Environmental Microbiology, 68(1): 316-25.

Part 6: General questions addressed in chapters II-V and author contributions

There are four publications included in this cumulative dissertation. Chapter II and V deal with microbial communities and their activities within conspicuous photosynthetic and sulfide- and iron-oxidizing mats, respectively. Chapter III and IV deal with AOM communities and their activities. In these two chapters, sediment communities are investigated which form distinct hotspot zones in the ocean seafloor. The major questions that were addressed in each of these publications:

(a) Which microbial populations are responsible for the dominant biogeochemical processes in the investigated habitat?

(b) How abundant are these key microbes within the microbial community and which other microorganisms are associated with them?

(c) How active are the microbes within these communities, and what are their main environmental signatures?

In the following, the individual contributions by the authors are explained:

Publication I (Chapter II): Diversity and function of Chloroflexus-like bacteria in a hypersaline microbial mat: phylogenetic characterization and impact on aerobic respiration

Authors: Ami Bachar, Enoma O. Omoregie, Rutger de Wit, Henk M. Jonkers

This paper has been published by Applied and Environmental Microbiology 73 (2007): 3975-3983. Ami Bachar collected the samples, conducted the microsensor measurements, constructed the 16S rRNA gene library, analyzed pigments recovered in this study, and wrote this manuscript. Enoma Omoregie conducted the 16S rRNA gene phylogenetic analysis, assisted in the construction of the 16S rRNA gene library. Rutger de Wit carried out the pigment analysis. Henk M. Jonkers, assisted in the collection of these samples. All coauthors were involved in the writing of this manuscript.

Publication II (Chapter III): Microbial methane turnover at mud volcanoes of the Gulf of Cadiz

Authors: Helge Niemann, Joana Duarte, Christian Hensen, Enoma Omoregie, Vito H. Magalhães, Marcus Elvert, Luis M. Pinheiro, Achim Kopf, Antje Boetius

This paper was published in Geochimica et Cosmochimica Acta 70:5536-5555, in 2006. Helge Niemann collected the samples used in this study. Laboratory rate measurements and biomarker analysis were conducted by Helge Niemann and Joana Duarte. Sulfate and sulfide concentration measurements and diffusive flux calculations were carried out by Christian Hensen. 16S rRNA gene library was constructed and analyzed by Enoma Omoregie. Vito H. Magalhães and Luis Pinheiro provided seismic sections and areal maps. Achim Kopf was the chief scientist of the cruise and provided insight to the geology of the Cadiz. Antje Boetius assisted in editing of this manuscript. The manuscript was written by Helge Niemann and profited from comments of all coauthors.

Publication III (Chapter IV): Anaerobic oxidation of methane and sulfate reduction at cold seeps in the Eastern Mediterranean sea

Authors: Enoma O. Omoregie, Helge Niemann, Vincent Mastalerz, Gert de Lange, Alina Stadnitskaia, Jean Mascle, Jean-Paul Foucher, Antje Boetius

This manuscript is in preparation for submission to Marine Geology. Enoma Omoregie conducted the biogeochemical measurements, microscopical analyses, constructed and analyzed the 16S rRNA gene libraries and wrote the manuscript. Helge Niemann collected the samples, and conducted part of the initial sample processing. Vincent Mastalerz and Gert de Lange provided sulfate and methane measurements. Alina Stadnitskaia provided the core descriptions. Jean Mascle provided the bathymetric maps. Jean-Paul Foucher was chief scientist of the Nautinil cruise, coordinator of the MEDIFLUX project and provided geological insight to the Nile Deep Sea Fan. Antje Boetius collected part of the samples, assisted in the initial sample processing and in writing of the manuscript.

Publication IV (Chapter V): Biogeochemistry and community composition of iron- and sulfide-oxidizing microbial mats at the Chefren mud volcano (Nile Deep Sea Fan, Eastern Mediterranean)

Authors: Enoma O. Omoregie, Vincent Mastalerz, Gert de Lange, Kristina L. Straub, Andreas Kappler, Hans Røy, Alina Stadnitskaia, Jean-Paul Foucher, Antje Boetius

This manuscript in is preparation for submission to Applied and Environmental Microbiology. Enoma Omoregie conducted the biogeochemical measurements, the microscopy, constructed and analyzed the 16S rRNA gene libraries, and wrote the manuscript. Vincent Mastalerz and Gert de Lange provided sulfate, methane and iron measurements. Kristina Straub and Andreas Kappler conducted the SEM and EDX work as well enrichments for Fe(III)-reducing bacteria. Hans Røy developed the fluid flow model. Alina Stadnitskaia provided the core descriptions. Jean-Paul Foucher was chief scientist of the Nautinil cruise, coordinator of the MEDIFLUX project and provided geological insight to the Nile Deep Sea Fan. Antje Boetius collected part of the samples, assisted in the sample processing and in writing of the manuscript.

Chapter II: Diversity and function of Chloroflexus-like bacteria in a hypersaline microbial mat: phylogenetic characterization and impact on aerobic respiration

Diversity and function of *Chloroflexus*-like bacteria in a hypersaline microbial mat: phylogenetic characterization and impact on aerobic respiration

Running title: Phylogeny and respiration of *Chloroflexus*

Ami Bachar[1], Enoma Omoregie[1], Rutger de Wit[2] and Henk M. Jonkers[1, 3]*

[1]Max-Planck-Institute for Marine Microbiology, Celsiusstrasse 1, D-28359 Bremen, Germany

[2]CNRS and Université Montpellier II UMR 5119, Case 093, Place Eugène Bataillon F-34095 Montpellier Cedex 05, France

[3]Delft University of Technology, Postbox 5048, NL-2600 GA Delft, The Netherlands

* Corresponding author. Mailing address: Delft University of Technology, Postbox 5048, NL-2600 GA Delft, The Netherlands. Phone: +31 152788743. Fax: +31 152786383. E-mail: h.m.jonkers@tudelft.nl

This manuscript has been published in Applied and Environmental Microbiology 73 (2007): 3975-3983

Abstract

We studied the diversity of *Chloroflexus*-like bacteria (CLB) in a hypersaline phototrophic microbial mat and assayed their near-infrared (NIR) light dependent oxygen respiration rates. PCR with primers that were reported to specifically target the 16S rRNA gene from members of the phylum Chloroflexi resulted in the recovery of 49 sequences and 16 phylotypes (sequences of the same phylotype share more than 96% similarity) of which ten sequences (four phylotypes) appeared related to filamentous anoxygenic phototrophic members of the Family Chloroflexaceae. Photopigment analysis revealed the presence of BChl*c*, BChl*d* and γ-carotene, pigments known to be produced by phototrophic CLB. Oxygen microsensor measurements on intact mats revealed a NIR (710-770 nm) light-dependent decrease in aerobic respiration, a phenomenon that we also observed in an axenic culture of *Chloroflexus aurantica*us. The metabolic characteristic of phototrophic CLB to switch from anoxygenic photosynthesis under NIR illumination to aerobic respiration under non-NIR illumination was further used to estimate their contribution to mat community respiration. Steady-state oxygen profiles under dark conditions and visible (VIS; 400 - 700 nm), NIR (710-770 nm) and VIS + NIR were compared. NIR light illumination led to a substantial increase in oxygen concentration in the mat. The observed impact on oxygen dynamics shows that CLB play a significant role in the cycling of carbon in this hypersaline microbial mat ecosystem. This study further demonstrates that the applied method, the combination of microsensor techniques and VIS/NIR illumination, allows a rapid establishment of the presence and significance of CLB in environmental samples.

Introduction

Chloroflexus-like bacteria (CLB) have been reported to be conspicuously present in some microbial mats [4, 14, 16, 19, 23, 24, 29, 32, 34], while in others they seem to be virtually absent. CLB are multicellular filamentous anoxygenic phototrophs (therefore alternatively called FAP's [13]), which can move by gliding and are further characterized by the production of BChl*a* and with in some species the supplemental production of BChl*c* or *d*. All characterized CLB are members of the genera *Chloroflexus*, *Chloronema*, *Oscillochloris*, *Roseiflexus* or *Heliothrix* within the Family Chloroflexaceae within the phylum Chloroflexi (previously called the green nonsulfur bacteria). The phylum Chloroflexi accommodates additional genera including filamentous but non-phototrophic species (*Herpetosiphon*) and even non-filamentous non-phototrophic species (*Thermoleophilum* and *Thermomicrobium*) [13]. Fluorescence microscopy with infrared detection has been used to visualize bacteriochlorophyll-containing CLB in hot spring microbial mats [27]. We have used fluorescence microscopy with blue excitation to discriminate potential CLB from cyanobacteria, because the latter fluoresce in the red visible light range as opposed to the former that do not fluoresce in the red. *Chloroflexus aurantiacus*, which was initially isolated and described by Pierson and Castenholz [28], is the most studied species of the Chloroflexaceae and is characterized by a versatile metabolism as it can grow photohetero- and photoautotrophically as well as chemotrophically by oxygen respiration. It produces BChlc_s characterized by an *In vivo* absorption maximum at 740 nm instead of 745-755 nm of BChl*c* that is produced by the phylogenetically distantly related green sulfur bacteria [22]. Despite the fact that CLB

bacteriochlorophyll synthesis is repressed by oxygen [25, 28] they are often found to be abundant in the fully oxic photic zone of microbial mats [6, 14, 15, 19, 24] where they can utilize organic photosynthetic exudates from oxygenic phototrophs, probably their most preferred substrates [2, 13]. Studies on BChl*a* production in the purple sulfur bacterium *Thiocapsa roseopersicina* have shown that an anoxic period of merely a few hours (the dark period in microbial mats) during a 24-hour period suffices to produce enough photopigment to enable phototrophic growth in the light but oxic period in mats [31, 35]. The same may hold for CLB and explain their observed abundance in the oxic zone of microbial mats, however, *In situ* studies on their function and metabolism are still limited [24, 29, 33, 34]. The aim of the present study was to characterize the impact of CLB on the community carbon and oxygen metabolism of a hypersaline microbial mat, making use of the observed phenomenon that intact mats as well as a pure culture of *C.aurantiacus* showed a significant decrease in aerobic respiration upon near infrared (NIR) light illumination. Therefore, we measured the contribution of CLB to microbial mat community oxygen respiration under different illumination regimes (visible (VIS; 400-700 nm); VIS + NIR (400-700 + 710-770 nm) and dark conditions). In this combined physiological and molecular study we provide quantitative CLB pigment analysis data as well as 16S rRNA gene-based evidence to demonstrate the presence of CLB in the mat and characterize their phylogenetic diversity.

Materials and methods

Sample collection

Microbial mat samples were collected in October 2004 from near shore mats of the hypersaline lake 'La Salada de Chiprana' located in Northeastern Spain (41°14'20N 0°10'55W). Intact mat samples where taken for further studies to Bremen, Germany, where they were incubated in original lake water at 21 ^{0}C under light (300 µmol photons m^{-2} s^{-1}) - dark illumination cycles of 16h/8h in glass aquarium.

Characterization of CLB in Lake Chiprana microbial mats:

Oxygen and hydrogen sulfide dynamics in intact mats

In order to characterize the intact microbial mat, profiles of oxygen and hydrogen sulfide concentrations were measured at 100 µm intervals in the laboratory in a flow-through chamber under artificial illumination (83 and 300 µmol photons m^{-2} s^{-1}) using a fiber-optic lamp (Schott, KL 1500) which has a halogen lamp as the light source. Oxygen profiles were additionally measured under dark conditions and at 33 and 166 µmol photons m^{-2} s^{-1}. Clark-type amperometric oxygen (10 µm tip diameter) and hydrogen sulfide (15 µm tip diameter) microsensors were applied. See references [17, 35] for details on application of oxygen and hydrogen sulfide sensors and calibration procedures. Microsensors were mounted on a motorized micromanipulator connected to a heavy stand. Positioning and data acquisition was performed automatically with a laptop. Before profiling, the

microsensor tip was positioned on the sediment surface of the microbial mat with the aid of binoculars.

Microscopic observations

The topmost 2-mm green stratum, i.e. the photic zone of the mat, was suspended in filtered lake water and aliquots were taken for fluorescence microscopy. Microscopic samples were excited with blue light and in combination with a long-pass filter (> 520 nm) filamentous bacteria that were fluorescent (cyanobacteria) or non-fluorescent in the visible part of the light spectrum could thus be distinguished. Non fluorescent thin filaments without visible sulfur inclusions were considered CLB. Diversity of CLB morphotypes was determined according to filament width and length. Ratio of non-fluorescent to fluorescent filaments was assessed visually from multiple sample preparations.

Photopigment analysis

The photic zone (0-2 mm surface layer) from frozen microbial mat samples was cut off and freeze dried. Pigments were extracted after sonication in HPLC-grade acetone. Two subsequent extractions were combined and the carboxylic groups of extracted pigments were methylated with 2-3 drops of diazomethane dissolved in acetone using a modification of the method recommended by Sigma-Aldrich (cat. Z411736, Aldrich, Milwaukee, WI, USA) using 1-methyl-3-nitro-1-nitrosoguanidine (MNNG) as the precursor. The solvent was evaporated using a speed-vacuum machine for a few hours until complete dryness, leaving pigments in the tube. Pigments were re-dissolved in a 2-ml HPLC elution solution: 45% acetonitrile, 50% methanol and 5% water-based 50 mM ammonium-acetate buffer (pH

7.2). The liquid was filtered through a sterile 0.2 µm pore size filter and a 100 µl aliquot was injected into the HPLC for pigment identification and quantification using a binary protocol as described before [5].

CLB phylotype diversity: DNA extraction, PCR amplification and cloning

In order to estimate the diversity of CLB phylotypes in the studied mat, a clone library was constructed. Genomic DNA was extracted from 0.2 g mat samples as described before [1] and purified with Wizard® DNA clean up system (Promega©). An approximately 400 bp fragment of the 16S rRNA gene was amplified from genomic DNA using primers specific for bacteria of the phylum Chloroflexi (green nonsulfur bacteria) [11], GNSB-941F 5'AGCGGAGCGTGTGGTTT'3; GNSB-1340R 5'CGCGGTTACTAGCAAC'3. Two µl of template were added to a 50 µl reaction mixture with 0.5 U Eppendorf TAQ, 1X Buffer, 4 mM of $MgCl_2$, 4 mM of each dNTP, and 1 µM of each primer. The reaction was run in a Mastercycler thermocycler (Eppendorf, Hamburg, Germany), with the following cycling conditions: 95°C for two minutes, then 30 cycles of 95°C for 30 seconds, 55°C for 30 seconds and 72°C for 1 minute, followed by a final incubation step at 72°C for 10 minutes. The PCR product was visualized on an agarose gel, and the 16S rRNA band excised. The excised PCR product was then purified using the QIAquick Gel Extraction Kit (Qiagen, Hilden, Germany). Two µl of purified product were then ligated into the pGEM T-Easy vector (Promega, Madison, WI) and then transformed into *E. coli* TOP10 cells (Invitrogen, Carlsbad, CA) according to the manufacturer's recommendations. Overnight cultures were prepared from positive transformants in a 2-ml 96 well culturing plate. Plasmid DNA was

extracted and purified using the Montage Plasmid Miniprep 96 kit (Millipore, Billerica, USA).

DNA Sequencing and analysis

Purified plasmids were sequenced in one direction with the M13F primer, using the BigDye Terminator v3.0 Cycle Sequencing kit (Applied Biosystems, Foster City, USA). Samples were run on an Applied Biosystems 3100 Genetic Analyzer (Foster City, USA). A phylogenetic tree was constructed with the ARB software package (http://www.arb-home.de) [21]. First, the partial sequences retrieved and amplified from the mat were grouped into phylotypes based on the criterion that sequences of the same phylotype share more than 96% similarity. Phylogenetic trees were constructed with Maximum-Likelihood and Neighbor-joining, using publicly available sequences that were at least 1100 base pairs. Representative sequences from each phylotype were then added to the phylogenic trees by parsimony.

Functional analysis of CLB in mats and culture:

Aerobic respiration of *Chloroflexus aurantiacus*

In order to determine the influence of different light quality (VIS and/or NIR illumination) on the metabolism of CLB (phototrophy versus aerobic respiration), an axenic culture of the hyperthermophilic strain *Chloroflexus aurantiacus* (DSM 635) was taken as model organism for CLB in the natural environment (even though C. *aurantiacus* might be quite different from CLB present in hypersaline environments, pure cultures of hypersaline CLB

species are not available). *C. aurantiacus* was cultured according to DSMZ recommendations in yeast extract medium amended with 1 mM sulfide. Cultures were incubated anaerobically at 55ºC under a light/dark regime of 16h illumination with incandescent light (approximately 25 µmol photons m^{-2} s^{-1}) and 8h darkness. Oxygen consumption under different light conditions was determined in sulfide depleted cultures. Just before oxygen consumption measurements culture aliquots were aerated and subsequently incubated in 25-ml glass tubes in a water bath at 55^0 C. An oxygen microsensor, fitted in a butyl-rubber stopper, was inserted into the culture (protein content was 0.58 ± 0.03 mg ml^{-1}), without introduction of air bubbles and sealed to avoid contact with ambient air during the measurement. Change in oxygen concentration in time was recorded. Formaldehyde-killed cultures (2% final concentration) were used to correct for abiotic oxygen consumption. Two sets of light/dark shift experiments were performed, the first with a combined visible (VIS) and near infrared (NIR) light source, and the second with a VIS light source only. In the first set of experiments light was provided by a 25-Watt incandescent (visible plus near infrared) light bulb in combination with two 40 mA near infrared light emitting diodes (LED) with peak wavelength at 740 nm and spectral FWHM bandwidth of 30 nm angle (LED-740-524: Roithner LaserTechnik, Austria). Light intensity as determined with a scalar irradiance light sensor (LI-250A, LI-COR Biosciences) was 15 µmol photons m^{-2} s^{-1} near the surface of the culture tube, however, the specific intensity of the NIR light remained unknown as the used light meter is not sensitive in the NIR (> 700 nm) light spectrum. As a light source in the second set of experiments two warm-white high-power LEDs (LXHL-MWGC, Lumileds, USA) were applied. The light range of these LEDs is restricted to only the visible part of the spectrum (400-700 nm). With this light

source a light intensity of 60 µmol photons m^{-2} s^{-1} was measured at the surface of the inundated culture tube.

Aerobic respiration of intact mats under different illumination conditions

In order to elucidate the effect of NIR light illumination on oxygen dynamics, intact mat pieces were incubated in a flow-through chamber at room temperature and illuminated with LEDs of visible radiance (VIS 400-700nm: LXHL-MWGC, Lumileds, USA) and/or with two 40 mA NIR LEDs (LED-740-524: Roithner LaserTechnik, Austria). The advantage of using separate LEDs instead of applying VIS/NIR filters in combination with a full spectrum light source is that the light intensity of the light source with one type of spectrum is not changed when the light source of the other spectral type is switched on or off. VIS LEDs were used to illuminate mats at 60 µmol photons m^{-2} s^{-1} with or without additional NIR light illumination and oxygen profiles were recorded after steady state conditions were reached. The microbial mat areal net oxygen production rates were calculated from the change in oxygen fluxes in the diffusion boundary layer using an oxygen diffusion coefficient of $2.1*10^{-5}$ (25^{o} C, 75 ppt) (see [35] for details on the procedure used). In order to determine whether oxygen evolution occurred under NIR-light illumination, oxygen profiles in only NIR light illuminated mats were measured before and after the addition of 3-(3, 4– Dichlophenyl)-1-1-dimethylurea (DCMU), a specific inhibitor of the oxygen-evolving photosystem II. DCMU was added from a stock solution (1 mM dissolved in 70% ethanol) to a final concentration of 5 µM.

Nucleotide sequence accession numbers

The partial 16S rRNA gene sequences determined in this study have been submitted to the GenBank database and assigned accession numbers DQ973818 to DQ 973833.

Results

Characterization of CLB in Lake Chiprana microbial mats:

Microsensor characterization of the intact microbial mat

The oxygen concentration profiles of illuminated mats show that oxygen is mainly produced in the first millimeter and reaches more then 6 times air-saturation under 300 μmol photons m^{-2} s^{-1} (Fig 1a), while in the dark oxygen penetrated to a maximum depth of only 0.4 mm. Oxygen and hydrogen sulfide co-occurred just above the oxic/anoxic interface in the 1-1.5 mm depth layer (Fig 1b). The mat was entirely anoxic from 1.5 mm downwards while hydrogen sulfide concentration increased below this depth. These measurements thus show that CLB present in the photic zone of the mat (0-2 mm surface layer) encounter high oxygen concentrations during illumination in the topmost part, but also sulfide in the lower part of the photic zone. Both components are relevant for CLB metabolism, as oxygen can be used as electron acceptor in aerobic respiration, while sulfide can be used as electron donor during photoautotrophic growth, or alternatively as electron donor for energy generation in aerobic respiration.

Microscopic observations

The microbial mat comprised an association of filamentous cyanobacteria, mainly *Oscillatoria*-like (2.5 μm diameter), *Microcoleus*-like (up to 8 μm diameter) and *Pseudanabaena*-like (about 3 μm diameter) cyanobacteria, and high densities of filaments that are not fluorescent in the red with two different filament diameter: wider (> 2 μm) and narrower ones (< 1 μm) with various lengths. The non-red-fluorescent filamentous bacteria were likely CLB, as they did not contain intracellular sulfur inclusions, typical of filamentous *Beggiatoa* strains. As CLB specific NIR autofluorescence was not determined in this study, we can not exclude that some of these filaments actually represented other bacteria such as filamentous sulfate-reducing bacteria of the genus *Desulfonema* that were previously found to occur in hypersaline mats [10]. The percentage of non-red-fluorescent filaments amounted to 20-30% of total filamentous bacteria in the photic zone

Microbial mat photopigment analysis

HPLC pigment analysis of the studied microbial mat revealed the presence of BChl*a*, *c* and *d* as well as γ-carotene, pigments that are known to be produced by photosynthetic members of the Family Chloroflexaceae [12]. Figure 2 depicts the chromatograms at 440, 660 and 760 nm of a sample of the top layer of the mat and peak identification is presented in Table 1. The pigment composition reflects a phototrophic community comprising cyanobacteria i.e., chlorophyll *a* (Chl*a*), zeaxanthin and β-carotene; and CLB i.e., BChl*c*/*d*, γ-carotene, and minor amounts of BChl*a*. In addition, degradation products of these

compounds were observed. The BChl*c*/*d* allomers eluted between 13 and 27 minutes (peaks 5-10 and 12, 13, Fig. 2). These retention times were longer than observed for the farnesol-esterified BChl*c* homologs (BChlc_F) found in a culture of *Chlorobium tepidum*. This indicates that the BChl*c*/*d* homologs were more hydrophobic than the BChlc_F homologs and were thus esterified with another alcohol. C. *aurantiacus* contains different allomers of BChl*c* esterified with stearyl, phytyl and geranylgeranyl alcohols. Further identification of the BChl*c*/*d* homologs requires HPLC-MS. In addition, BChl*a* (peak 11) was found in the mats and we also observed two late-eluting BChl*d*-like compounds. Different BChl degradation products were identified as Bacteriopheophorbide *c*, Bacteriopheophytin *a*, *c* and *d*. A number of peaks were quantified (see Table 2). The ratio of BChl*c*: BChl*d*: BChl*a* was 72: 26: 1 on average

CLB phylotype diversity

A total of 49 sequences were recovered by 16S rRNA PCR using Chloroflexi specific primers designed by Gich et al [11]. This primer set targeted the 16S rRNA gene from various members of the phylum Chloroflexi, which includes isolated and characterized members of the anoxygenic phototrophic filamentous genera *Chloroflexus, Chloronema, Oscillochloris*, *Heliothrix* and *Roseiflexus*. A total of 8 major clusters (Fig. 3) of sequences that were well supported in several Maximum likelihood and Neighbor-joining trees were identified. There was significant diversity among the sequences that were recovered. Thus, we distinguished 16 different phylotypes each comprising sequences that shared above 96 % sequence similarity. A representative sequence was selected from each phylotype that

was considered in the phylogenetic analysis. Accordingly, most sequences were most closely related to those from uncultured bacteria retrieved from various microbial mats, soils, sediments and sludges. In general, the sequences recovered in this study were about 75-86% identical to sequences recovered in other studies. Ten of 49 sequences from this study clustered with sequences derived from members of the Family Chloroflexaceae (clusters I-II), the remaining 39 sequences clustered with sequences from various other uncultured groups of bacteria distantly related to the Family Chloroflexaceae (clusters III-VIII) but still within the phylum Chloroflexi. Some of these appear distantly related to *Dehalococcoides* (phylum Chloroflexi, class Dehalococcoides). Seven sequences (cluster I) represented by LCC01 (2 sequences), LCC77 (4 sequences) and LCC57 were 90-99% identical to sequences recovered from a hypersaline microbial mat, Guerrero Negro, Mexico [23]. Three sequences represented by LCC39 (cluster II) shared an identity of 88% with *C. aurantiacus*. They were the most closely related sequences to any 16S rRNA gene from a cultured organism.

Functional analysis of CLB impact on microbial mat oxygen respiration:

Aerobic respiration of *Chloroflexus aurantiacus*

C.aurantiacus pre-grown under anoxic/light conditions was subjected to aerobic conditions by aeration of culture aliquots just before measuring aerobic respiration rates. Examples of oxygen consumption measurements during Incandescent light bulb + NIR LED / dark- or VIS LED / dark shifts are presented in Figure 4. Calculated oxygen consumption rates at different illumination conditions are presented in Table 3. Oxygen consumption rate at

NIR-light illumination was significantly lower (ca 50%) compared to dark or only VIS-light illumination. No significant difference in oxygen consumption rate between dark and only VIS-light illumination was observed. The dark respiration calculated from the first experimental series was somewhat lower than that of the second series (Table 3). This may have been due to the lower initial oxygen concentration in the first series. The glutaraldehyde-killed culture showed no measurable oxygen uptake in time. The NIR light applied to the *C. aurantiacus* culture was the maximum intensity that could be reached with the NIR LED configuration applied in this study. It may well be that this applied intensity was not sufficiently high to saturate anoxygenic photosynthesis of the *C. aurantiacus* culture.

Effect of NIR light illumination on microbial mat community respiration

The effect of NIR illumination on microbial mat community oxygen consumption was inferred from the steady-state oxygen profiles acquired under the different light conditions. Upon illumination with only NIR light, oxygen penetration significantly increased compared to dark condition from 0.40 to 0.55 mm (Fig 5). A comparable phenomenon was found when VIS and NIR light were combined, i.e., the oxygen penetration depths were 0.7 and 0.9 mm, when VIS was applied alone and when VIS and NIR light were combined, respectively. Under VIS alone illumination (60 μmol photons m^{-2} s^{-1}) oxygen reached a maximum concentration of 190 μM at a depth of 0.1 mm. When NIR light was subsequently added to the white light, the oxygen maximum increased to 230 μM and moved deeper to a depth of 0.175 mm. Calculated microbial mat areal net oxygen

production or consumption values from the oxygen profiles measured under the different light conditions are presented in Table 4. Controls done with NIR-only illuminated mats in which oxygen profiles were measured before and after DCMU addition, showed no difference in oxygen concentration and penetration depth. These observations indicate that NIR illumination did not result in oxygenic photosynthesis in this specific hypersaline microbial mat. If so, in DCMU inhibited mats oxygen concentration would have been decreased due to continued respiration but ceased oxygenic photosynthesis. The unchanged oxygen concentration profile after DCMU addition also shows that the addition of ethanol (part of the DCMU stock solution) to this mat does not result in increased aerobic respiration rates on the short term. The latter also supports the finding by Ludwig et al [20] that aerobic respiration in Lake Chiprana microbial mats is not limited by organic carbon compounds.

Discussion

The investigated microbial mat from the hypersaline Lake Chiprana, Spain, appeared to be rich in CLB in the photic zone as was demonstrated by microscopy, pigment analysis and diversity of CLB-related partial 16S rRNA gene sequences. The fact that CLB not only occur in hot spring microbial mats but also in hypersaline mats was also found in previously published studies [14, 23, 19, 32], however, their *In situ* metabolic function in carbon cycling remains largely to be clarified. In this study we developed a method that allows us to evaluate the proportion of the oxygen and carbon metabolism that is directly attributed to the metabolic activity of CLB in the mat. For that we made use of the

characteristic that CLB can switch their metabolism from anoxygenic photosynthesis under NIR illumination to aerobic respiration in its absence. We corroborated this characteristic for a pure culture of *C.aurantiacus*. As the electromagnetic spectrum of sunlight comprises both VIS and NIR light we decided to use artificial illumination with specific LEDs and not filters as originally have been used [9]. The latter may decrease the light intensity or otherwise affect the non-target light field and may thus influence e.g. the VIS light intensity and simultaneously also oxygenic photosynthesis rates, what would have influenced the mats oxygen concentration and thus hampered the quantification of CLB respiration rates. In this study NIR light illumination with a spectrum of 740 ± 30 nm in addition to dark or only VIS light illumination (with a spectrum of 400-700 nm) led to a substantial increase in net areal mat oxygen production rate. As 740 nm is the specific absorption wavelength of BChl*c*$_s$, which is known to be produced by *C.aurantiacus*, and to a lesser extend of BChl*c* and *d* which are also produced by CLB species, we conclude that the observed effect in mat community oxygen dynamics was due to the metabolic activity of CLB species. Similarly as CLB, in the presence of oxygen, purple sulfur bacteria (PSB) [7] and purple non-sulfur bacteria may switch immediately their metabolism from anoxygenic photosynthesis to aerobic respiration when the NIR illumination is suddenly stopped. However, these bacteria have a very low absorption cross section at 740 nm and, therefore, virtually do not use the light of the LED used in this study. Moreover, microscopic observations showed only very small quantities of typical PSB morphotypes and, in general, specific respiration rates of Chromatiaceae (PSB) [7, 46] are 1-2 orders of magnitude lower than we found for *Chloroflexus aurantiacus*. Green sulfur bacteria that also contain BChl*a*, BChl*c* and BChl*d*, have been found in some microbial mats. However, these bacteria are strict anaerobes that

are confined to the permanent anoxic layers of the mat and cannot contribute to oxygen respiration. Recently, a cyanobacterium that produces Chl*d* and absorbs light in the NIR light spectrum was isolated [18]. Whether such presumably oxygen-producing organisms comprise a substantial part of the microbial community in this mat remains to be investigated, although no Chl*d* has been detected in this study. However, we conclude that if present, such organisms could not be responsible for the observed increase in oxygen concentration upon additional NIR light illumination as control experiments with DCMU, a specific inhibitor of photosystem II and thus oxygen production, did not result in a decrease in oxygen concentration when applied to only NIR light illuminated mats.

The role CLB play in the local carbon cycle can be inferred from their respiration rate under non-NIR light conditions. Axenic culture experiments with *C.aurantiacus* showed that its oxygen respiration decreased by about 50% upon NIR light illumination. CLB can switch from anoxygenic phototrophy, which provides energy due to cyclic electron transport in photosystem I, to aerobic respiration to sustain energy generation under dark conditions [13]. It can thus be assumed that the amount of oxygen respired under non-NIR light condition at least equals the equivalent of energy that was produced by anoxygenic photosynthesis by active CLB under NIR light illumination. One way therefore to estimate the role of CLB in the local carbon cycle is to compare its non-NIR light respiration to total community respiration. In the dark, total community respiration, as inferred from microbial mat areal oxygen uptake, decreased from 0.13 to 0.10 nmol O_2 cm^{-2} sec^{-1}, a decrease of 25% upon NIR illumination. When NIR light was additionally supplied to VIS light the net community areal oxygen production increased from 0.03 to 0.07 nmol O_2 cm^{-2} sec^{-1}, i.e. more than doubling the apparent net primary production, likely the result

of a decrease in CLB respiration due to a switch to anoxygenic phototrophy for energy generation.

The measurable change in oxygen dynamics upon NIR illumination (740 nm) of intact mats can thus be attributed to CLB activity. However, as this metabolic shift is directly linked to the mode of energy generation, no conclusions can be drawn as to whether a shift in electron donor for autotrophic growth (e.g. reduced sulfur compounds) or carbon source (organic or inorganic) for hetero- or autotrophic growth also occurs. CLB are known to be able to use various inorganic compounds as electron donor during autotrophic growth as well as inorganic and various organic compounds as carbon source during phototrophic or heterotrophic growth [13, 34]. The reason why CLB can be found in high densities in microbial mats is likely due to this versatile metabolism. In mats light intensity, oxygen-, reduced sulfur compound- as well as dissolved inorganic- and organic carbon concentrations change rapidly during a full 24-hour diel cycle, conditions to which CLB are thus maximally adapted. In such systems they would have a competitive advantage over more specialized but metabolically more restricted organisms.

The capacity to switch from anoxygenic photosynthesis to respiration has thus been clearly demonstrated for *C.aurantiacus* in culture experiments and has been inferred for the CLB in this microbial mat from oxygen profiles. This ability, which is apparently widespread among CLB has important consequences for the quantification of gross photosynthesis in mats using the traditional light/dark shift method, which was introduced by Revsbech et al in 1981 [30] and applied in numerous studies since. This method is based among others on the assumption, that in a microbial mat under steady state (stable oxygen profile) conditions, community oxygen consumption rate remains initially unchanged (at

least for a few seconds) when switched from light to darkness. The rate of oxygen disappearance at the start of the dark period would then equal the rate of oxygen production in the light [30]. This assumption, however, does not hold when *C.aurantiacus* or other CLB make up a significant part of the microbial community, as they may switch within seconds from anoxygenic photosynthesis in the light to aerobic respiration in the dark. That this effect can be substantial is shown in this study where apparent net photosynthesis more then doubled when NIR light was additionally supplied to VIS light illumination. Hence, using the traditional light/dark shift method, gross photosynthesis rates will be substantially overestimated in CLB rich microbial mats. However, this effect can be compensated for, if as a light source only VIS illumination (400-700 nm) is used (CLB will behave as aerobic bacteria, i.e. continuously respire) or, alternatively, an additional NIR light source remains continuously on (CLB will continue anoxygenic phototrophy, and not switch to aerobic respiration when VIS light is switched off) during measurements.

The high diversity in 16S rRNA gene phylotypes affiliated to the phylum Chloroflexi indicates, that besides a number of sequences that group within the Family Chloroflexaceae, non-filamentous and even non-phototrophic Chloroflexi may be present in this mat. It is difficult to infer the type of chlorophyll that a bacterium will poses based on our 16S rRNA data given the paucity of 16S rRNA gene sequences available from cultured members of the Chloroflexaceae. However, the three sequences represented by LCC39 (cluster II) group with sequences from two characterized *Chloroflexus* species, and are therefore likely to represent BChl*c*-producing CLB active in this system. The 6 sequences from cluster I that were recovered from this study are most closely related to the 16S rRNA gene from *Heliothrix oregonensis*, a CLB that does not, like *Chloroflexus* species, produce

BChl*c* or *d* in addition to BChl*a*. The organisms responsible for these sequences may thus not have contributed to the observed changes in community oxygen respiration upon 740 nm NIR light manipulations. The three sequences represented by LCC39 from this mat are the ones that are most closely related to the 16S rRNA gene from *C.aurantiacus* which originated from a hot spring microbial mat, and which is so far the most intensely studied and characterized species from the Family Chloroflexaceae. However, they only share a sequence identity of 88%. Highest sequence identity obtained from this hypersaline mat (cluster I) was found with those that originated from Guerrero Negro, Mexico (AJ309642 and AJ309636) [23], also a hypersaline microbial mat but from a different continent. Sequence similarity between these sequences was up to 99% what indicates that at least some hypersaline Chloroflexaceae may have a cosmopolitan distribution.

This study focused on CLB, i.e. filamentous phototrophic bacteria that are members of the Family Chloroflexaceae. Although the clone library from this study retrieved 10 out of 49 sequences that grouped within the Family Chloroflexaceae it is not known whether these all indeed represent filamentous phototrophic bacteria, as only few sequences from this group represent well characterized strains. The clone library shows furthermore that sequences retrieved in this study that fall outside the Family Chloroflexaceae, but still cluster within the Chloroflexi phylum, are all most closely related to sequences from uncultured organisms. The apparently high but uncharacterized diversity of Chloroflexi related sequences retrieved from this specific hypersaline mat seems typical as other studies from various hot spring [24, 29] and hypersaline mats [19, 23] as well as other ecosystems [3, 11] reported the same. Intriguing question remains as what kind of

species these sequences belong to and which ecological role they play in these ecosystems. Future cultivation and eco-physiological characterization studies must resolve this question.

Acknowledgements

We thank Alfredo Legaz (guard of COMENA, Caspe) and the local authorities in Chiprana for granting permission to Lake Chiprana and take microbial mat samples. We are grateful to Dirk de Beer and Lubos Polerecky for discussion and technical help. A. Bachar was supported by a grant (DFG JO-412) from the German Research Foundation. R. de Wit acknowledges support from the Deutscher Akademischer Austausch Dienst (DAAD) and the Agence National de la Recherche (program CYANOCARBO).

References

1. **Abed, R. M. M., and F. Garcia-Pichel.** 2001. Long-term compositional changes after transplant in a microbial mat cyanobacterial community revealed using a polyphasic approach. Environ. Microbiol. **3:**53-62.

2. **Bateson, M. M., and D. M. Ward.** 1988. Photoexcretion and fate of glycolate in a hot-spring cyanobacterial mat. Appl. Environ. Microbiol. **54:**1738-1743.

3. **Bjornsson, L., P. Hugenholtz, G. W. Tyson, and L. L. Blackall.** 2002. Filamentous Chloroflexi (green non-sulfur bacteria) are abundant in wastewater treatment processes with biological nutrient removal. Microbiology-Sgm **149:**2309-2318.

4. **Boomer, S. M., D. P. Lodge, B. E. Dutton, and B. Pierson.** 2002. Molecular characterization of novel red green nonsulfur bacteria from five distinct hot spring communities in Yellowstone National Park. Appl. Environ. Microbiol. **68:**346-355.

5. **Buffan-Dubau, E., O. Pringault, and R. DeWit.** 2001. Artificial cold-adapted microbial mats cultured from Antarctic lake samples. 1. Formation and structure. Aquat. Microbiol. Ecol. **26:**115-125.

6. **D'Amelio, E. D., Y. Cohen, and D. J. DesMarais.** 1987. Association of a new type of gliding, filamentous, purple phototrophic bacterium inside bundles of *Microcoleus chthonoplastes* in hypersaline microbial mats. Arch. Microbiol. **147:**213-220.

7. **DeWit, R., and H. VanGemerden.** 1987. Chemolithotrophic growth of the phototrophic sulfur bacterium *Thiocapsa roseopersicina*, FEMS Microbiol. Ecol. **45:**117-126.

8. **DeWit, R., and H. VanGemerden.** 1990. Growth and metabolism of the purple sulfur bacterium *Thiocapsa roseopersicina* under combined light dark and oxic anoxic regimens. Arch. Microbiol. **154:**459-464.

9. **DeWit, R., L. Falcón, and C. Charpy-Roubaud.** 2005. Heterotrophic dinitrogen fixation (acetylene reduction) in phosphate-fertilised *Microcoleus chthonoplastes* microbial mat from the hypersaline inland lake "la Salada de Chiprana" (NE Spain). Hydrobiol. **534:**245 - 253.

10. **Fukui, M., A. Teske, B. Assmus, G. Muyzer, and F. Widdel.** 1999. Physiology, phylogenetic relationships, and ecology of filamentous sulfate-reducing bacteria (genus *Desulfonema*). Arch. Microbiol. **172:**193-203.

11. **Gich, F., J. Garcia-Gil, and J. Overmann.** 2001. Previously unknown and phylogenetically diverse members of the green nonsulfur bacteria are indigenous to freshwater lakes. Arch. Microbiol. **177:**1-10.

12. **Gich, F., R. L. Airs, M. Danielsen, B. J. Keely, C. A. Abella, J. Garcia-Gil, M. Miller, and C. M. Borrego.** 2003. Characterization of the chlorosome antenna of the filamentous anoxygenic phototrophic bacterium *Chloronema* sp. strain UdG9001. Arch. Microbiol. **180:**417-426.

13. **Hanada, S., and B. K. Pierson.** November 2002. The Family Chloroflexaceae. *In* M. Dworkin et al. (ed.), The Prokaryotes: an evolving electronic resource for the microbiological community, 3rd edition, release 3.11. [Online.] http://link.springer-ny.com/link/service/books/10125. Springer-Verlag, New York. Accessed 28 August 2006.

14. **Jonkers, H. M., R. Ludwig, R. DeWit, O. Pringault, G. Muyzer, H. Niemann, N. Finke, and D. DeBeer.** 2003. Structural and functional analysis of a microbial mat ecosystem from a unique permanent hypersaline inland lake: 'La Salada de Chiprana' (NE Spain). FEMS Microbiol. Ecol. **44:**175-189.

15. **Jørgensen, B. B., and D. C. Nelson.** 1988. Bacterial zonation, photosynthesis, and spectral light-distribution in hot-spring microbial mats of Iceland. Microbiol. Ecol. **16:**133-147.

16. **Klappenbach, J. A., and B. K. Pierson.** 2004. Phylogenetic and physiological characterization of a filamentous anoxygenic photoautotrophic bacterium ‘Candidatus Chlorothrix halophila’ gen. nov., sp. nov. recovered from hypersaline microbial mats. Arch. Microbiol. **181:**17-25.

17. **Kühl, M., C. Steuckart, G. Eickert, and P. Jeroschewski.** 1998. A H_2S microsensor for profiling biofilms and sediments: application in an acidic lake sediment. Aquat Microb. Ecol. **15:**201-209.

18. **Kühl, M., M. Chen, P. J. Ralph, U. Schreiber, and A. W. D. Larkum.** 2005. A niche for cyanobacteria containing chlorophyll d. Nature **433:**820-820.

19. **Ley, R. E., J. K. Harris, J. Wilcox, J. R. Spear, S. R. Miller, B. M. Bebout, J. A. Maresca, D. A. Bryant, M. L. Sogin, and N. R. Pace.** 2006. Unexpected diversity and complexity of the Guerrero Negro hypersaline microbial mat. Appl. Environ. Microbiol. **72:**3685-3695.

20. **Ludwig, R., O. Pringault, R. DeWit, D. DeBeer, and H. M. Jonkers.** 2006. Limitation of oxygenic photosynthesis and oxygen consumption by phosphate and organic nitrogen in a hypersaline microbial mat: a microsensor study. FEMS Microbiol. Ecol. **57:**9-17

21. **Ludwig, W., O. Strunk, R. Westram, L. Richter, H. Meier, Yadhukumar, A. Buchner, T. Lai, S. Steppi, G. Jobb, W. Forster, I. Brettske, S. Gerber, A. W. Ginhart, O. Gross, S. Grumann, S. Hermann, R. Jost, A. Konig, T. Liss, R. Lussmann, M. May, B. Nonhoff, B. Reichel, R. Strehlow, A. Stamatakis, N. Stuckmann, A. Vilbig, M. Lenke, T. Ludwig, A. Bode, and K. H. Schleifer.** 2004. ARB: a software environment for sequence data. Nucleic Acids Res. **32:**1363-1371.

22. **Madigan, M. T., J. M. Martinko, and J. Parker.** 2000. Brock - Biology of microorganisms (9^{th} edition). Prentice-Hall, Inc. New Jersey.

23. **Nübel, U., M. M. Bateson, M. T. Madigan, M. Kühl, and D. M. Ward.** 2001. Diversity and distribution in hypersaline microbial mats of bacteria related to *Chloroflexus* spp. Appl. Environ. Microbiol. **67:**4365-4371.

24. **Nübel, U., M. M. Bateson, V. VanDieken, A. Wieland, M. Kühl, and D. M. Ward.** 2002. Microscopic examination of distribution and phenotypic properties of phylogenetically diverse Chloroflexaceae-related bacteria in hot spring microbial mats. Appl. Environ. Microbiol. **68:**4593-4603.

25. **Oelze, J.** 1992. Light and oxygen regulation of the synthesis of bacteriochlorophylls a and c in *Chloroflexus aurantiacus*. J. Bacteriol. **174:**5021-5026.

26. **Overmann, J., and N. Pfennig.** 1992. Continuous growth and respiration of Chromatiaceae species at low oxygen concentrations. Arch. Microbiol. **158:**59-67.

27. **Pierson, B. K., and H. M. Howard.** 1972. Detection of bacteriochlorophyll containing microorganisms by infrared fluorescence photomicrography. J. Gen. Microbiol. **73:**359-363.

28. **Pierson, B. K., and R. W. Castenholz.** 1974. Studies of pigments and growth in *Chloroflexus aurantiacus*, a phototrophic filamentous bacterium. Arch. Microbiol. **100:**283-305.

29. **Pierson, B. K., D. Valdez, M. Larsen, E. Morgan, and E. E. Mack.** 1994. *Chloroflexus*-like organisms from marine and hypersaline environments - distribution and diversity. Photosynt. Res. **41:**35-52.

30. **Revsbech, N. P., B. B. Jørgensen, and O. Brix.** 1981. Primary production of microalgae in sediments measured by oxygen microprofile, H-CO-14(3)-fixation, and oxygen-exchange methods. Limnol. Oceanogr. **26:**717-730.

31. **Schaub, B. E. M., and H. VanGemerden.** 1994. Simultaneous phototrophic and chemotropic growth in the purple sulfur bacterium *Thiocapsa roseopersicina* M1. FEMS Microbiol. Ecol. **13:**185-195.

32. **Sorensen, K. B., D. E. Canfield, A. P. Teske, and A. Oren.** 2005 Community composition of a hypersaline endoevaporitic microbial mat. Appl. Environ. Microbiol. **71:**7352-7365.

33. **VanDerMeer, M. T. J., S. Schouten, J. S. S. Damste, J. W. DeLeeuw, and D. M. Ward.** 2003. Compound-specific isotopic fractionation patterns suggest different carbon metabolisms among *Chloroflexus*-like bacteria in hot-spring microbial mats. Appl. Environ. Microbiol. **69:**6000-6006.

34. **VanDerMeer, M. T. J., S. Schouten, M. M. Bateson, U. Nübel, A. Wieland, M. Kühl, J. W. De Leeuw, J. S. S. Damste, and D. M. Ward.** 2005. Diel variations in carbon metabolism by green nonsulfur-like bacteria in alkaline siliceous hot spring microbial mats from Yellowstone National Park. Appl. Environ. Microbiol. **71:**3978-3986.

35. **Wieland, A., and M. Kühl.** 2000. Short-term temperature effects on oxygen and sulphide cycling in a hypersaline cyanobacterial mat (Solar Lake, Egypt). Mar. Ecol. Prog. Ser. **196:**87-102.

Tables

Table 1: Pigment identification, retention times and λ-max of the different peaks shown in the chromatograms of Fig. 4

Peak N°	Rt (min)	Compound	λ max
1	6.13	unknown carotenoid	448
2	7.50	Bacteriopheaophorbide c - methyl ester	438, 505, 662
3	9.66	phaeophorbide a - methyl ester	411, 661
4	12.29	zeaxanthin	451, 475
5	13.90	Bacteriochlorophyll c	434, 663.
6	19.04	Bacteriochlorophyll c	430, 662
7	20.06	Bacteriochlorophyll d	427, 652
8	21.49	Bacteriochlorophyll c	431, 668
9	22.40	Bacteriochlorophyll d	428, 653
10	24.30	Bacteriochlorophyll d	428, 653
11	25.00	Bacteriochlorophyll a	373, 761
12	25.50	Bacteriochlorophyll c	434, 663
13	26.10	Bacteriochlorophyll c	435, 660
14	28.50	Bacteriopheaophytine c	412, 661
15	29.13	Bacteriopheaophytine d	409, 654
16	29.90	Bacteriopheaophytine c	411, 661
17	30.50	Chlorophyll a	431, 660
18	31.70	allomer Chlorophyll a	431, 659
19	33.20	Bacteriopheaophytine a	358, 525, 740
20	33.98	Bacteriochlorophyll d-like	435, 652
21	34.75	Bacteriochlorophyll d-like	433, 652
22	35.80	Bacteriopheaophytine a	359, 531, 666, 740
23	36.68	Phaeophytin a	409, 661
24	37.10	γ-carotene	434, 460
25	38.70	β-carotene	454, 480
26	39.10	Pyrophaeophytin a	409, 661

Table 2: Pigment quantification of Lake Chiprana microbial mat September 2004; Concentrations are presented as μg cm^{-2}. Ratio of BChl*a*, *c* and *d* indicate that CLB are abundant in this mat

Pigment	Mean	SD
Total BChl*c*	10.7	2.6
Total BChl*d*	3.9	1.8
Chl*a*	11.2	2.8
Total Phaeophytin *a* + Pyrophaeophytin *a*	9.5	0.8
Bchl*a*	0.15	0.06
Zeaxanthin	0.72	0.20
γ-carotene	0.25	0.14
β-carotene	1.14	0.26

Table 3: *Chloroflexus aurantiacus* aerobic respiration rates in aerated axenic culture aliquots (n=4) at different illumination conditions. Respiration rates under dark and visible (VIS) light illumination are not significantly different. However, respiration rate under near-infrared (NIR) light (25 Watts incandescent light bulb + two 40 mA NIR LEDs) illumination and dark condition are significantly different

Experiment	Light condition (Intensity 400-700nm: μmol photons m^{-2} s^{-1})	Respiration rate (μmol O_2 g^{-1} protein min^{-1})
Series 1	Bulb + NIR LEDs (15 μE)	2.48 (± 0.17)
	Dark	4.47 (± 0.59)
Series 2	VIS LEDs (60 μE)	5.44 (± 0.29)
	Dark	5.75 (± 0.50)

Table 4: Calculated net areal oxygen production rates (negative values denote net consumption) from oxygen concentration profiles (see Fig. 4) in Lake Chiprana microbial mats at different illumination conditions. Dark; visible (VIS) light only; near-infrared (NIR) light only; VIS + NIR light illumination

Light condition	Net areal O_2 production (nmol O_2 cm^{-2} s^{-1})
Dark	-0.13
NIR	-0.10
VIS	0.03
VIS + NIR	0.07

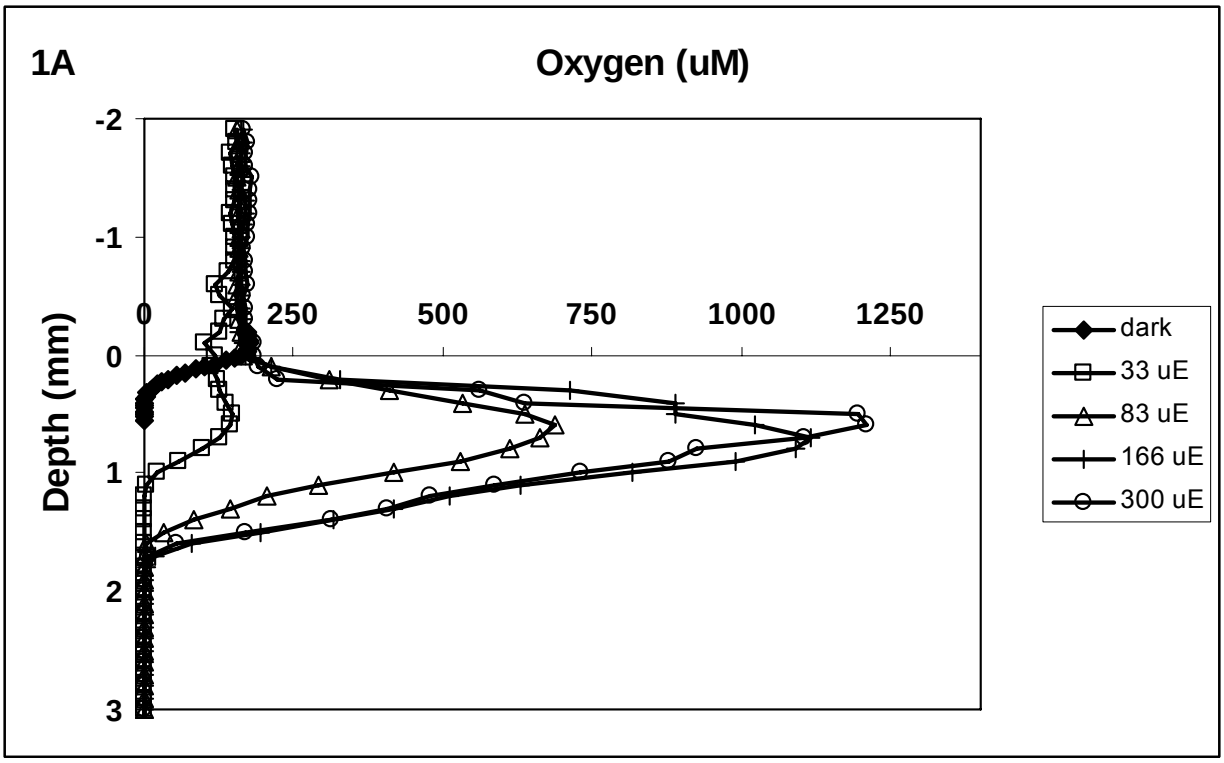

Figure 1A. Oxygen concentration profiles in Lake Chiprana microbial mat at different light intensities (µE denotes µmol photons m^{-2} s^{-1}). Oxygen reaches up to 6-times air saturation at higher light intensities, indicating that CLB in the photic zone have to cope with high and fluctuating oxygen concentrations.

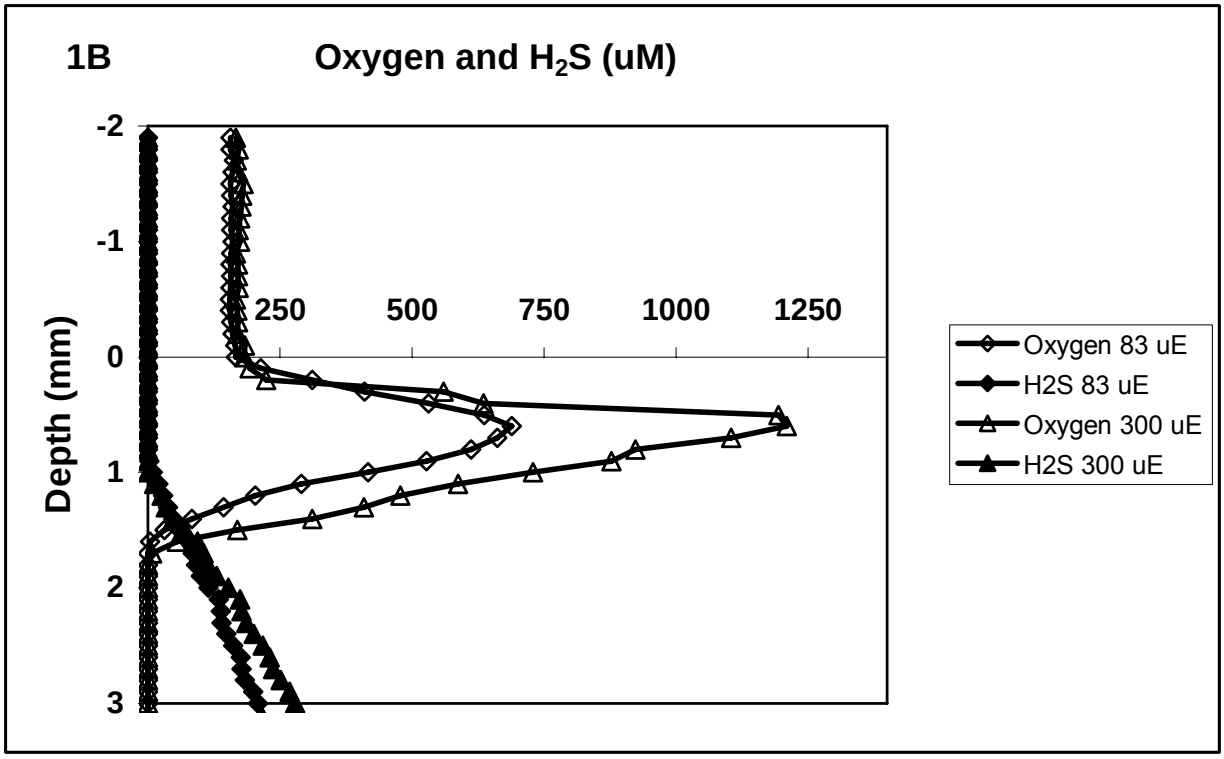

Figure 1B. Oxygen and sulfide (H_2S) concentration profiles measured at light intensities of 83 and 300 μmol photons m^{-2} s^{-1} (μE). Oxygen and sulfide co-occur in the depth zone between 1 and 1.5 mm, a zone were CLB would be able to oxidize sulfide both phototrophically and chemotrophically, in the latter case using oxygen as electron acceptor

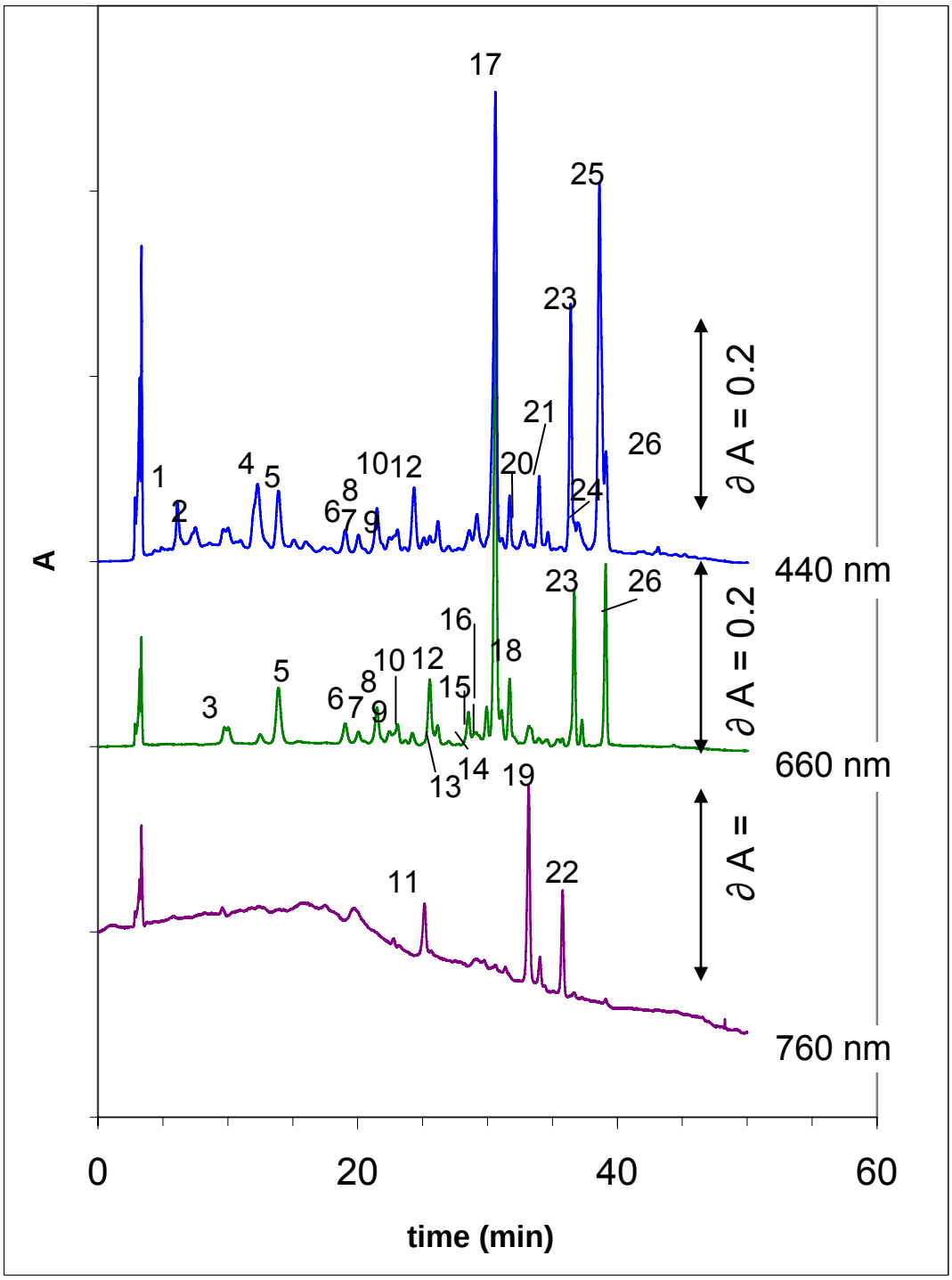

Figure 2. HPLC chromatograms of 440, 660 and 760 nm of a sample from the top 5-mm of the Lake Chiprana microbial mat. Identified pigment molecules represented in numbers, are presented in table 2. Main pigments are chlorophyll a (peak 17) and BChl*c* allomers (peaks 5-6, 8, 12-14 and 16)

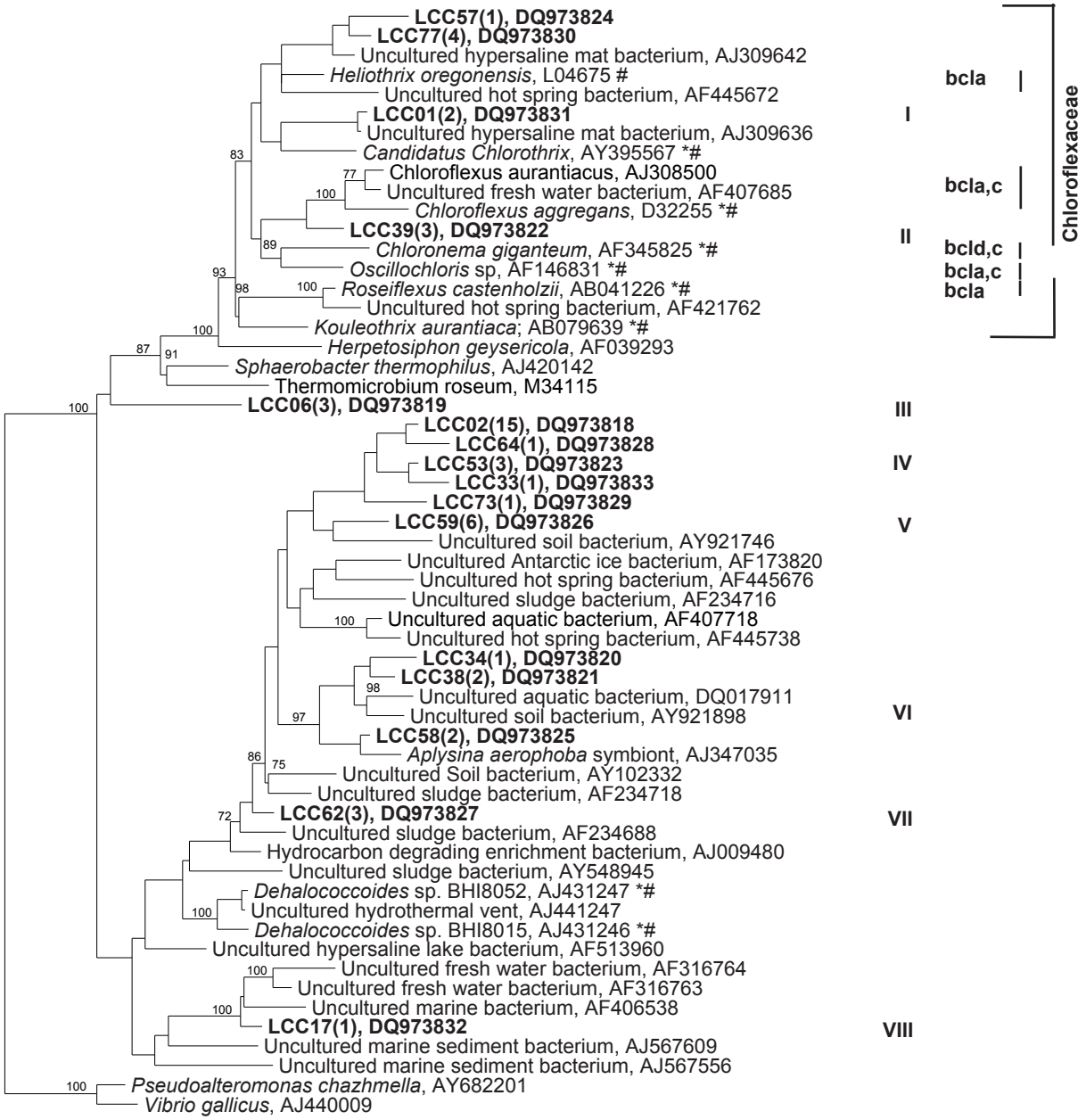
LCC57(1), DQ973824
LCC77(4), DQ973830
Uncultured hypersaline mat bacterium, AJ309642
Heliothrix oregonensis, L04675 #
Uncultured hot spring bacterium, AF445672
LCC01(2), DQ973831
Uncultured hypersaline mat bacterium, AJ309636
Candidatus Chlorothrix, AY395567 *#
Chloroflexus aurantiacus, AJ308500
Uncultured fresh water bacterium, AF407685
Chloroflexus aggregans, D32255 *#
LCC39(3), DQ973822
Chloronema giganteum, AF345825 *#
Oscillochloris sp, AF146831 *#
Roseiflexus castenholzii, AB041226 *#
Uncultured hot spring bacterium, AF421762
Kouleothrix aurantiaca; AB079639 *#
Herpetosiphon geysericola, AF039293
Sphaerobacter thermophilus, AJ420142
Thermomicrobium roseum, M34115
LCC06(3), DQ973819
LCC02(15), DQ973818
LCC64(1), DQ973828
LCC53(3), DQ973823
LCC33(1), DQ973833
LCC73(1), DQ973829
LCC59(6), DQ973826
Uncultured soil bacterium, AY921746
Uncultured Antarctic ice bacterium, AF173820
Uncultured hot spring bacterium, AF445676
Uncultured sludge bacterium, AF234716
Uncultured aquatic bacterium, AF407718
Uncultured hot spring bacterium, AF445738
LCC34(1), DQ973820
LCC38(2), DQ973821
Uncultured aquatic bacterium, DQ017911
Uncultured soil bacterium, AY921898
LCC58(2), DQ973825
Aplysina aerophoba symbiont, AJ347035
Uncultured Soil bacterium, AY102332
Uncultured sludge bacterium, AF234718
LCC62(3), DQ973827
Uncultured sludge bacterium, AF234688
Hydrocarbon degrading enrichment bacterium, AJ009480
Uncultured sludge bacterium, AY548945
Dehalococcoides sp. BHI8052, AJ431247 *#
Uncultured hydrothermal vent, AJ441247
Dehalococcoides sp. BHI8015, AJ431246 *#
Uncultured hypersaline lake bacterium, AF513960
Uncultured fresh water bacterium, AF316764
Uncultured fresh water bacterium, AF316763
Uncultured marine bacterium, AF406538
LCC17(1), DQ973832
Uncultured marine sediment bacterium, AJ567609
Uncultured marine sediment bacterium, AJ567556
Pseudoalteromonas chazhmella, AY682201
Vibrio gallicus, AJ440009
I
II
III
IV
V
VI
VII
VIII
bcla
bcla,c
bcld,c
bcla,c
bcla
Chloroflexaceae
0.10 substitutions per site

Figure 3. 16S Maximum likelihood tree of representative sequences recovered in this study (bold), and those retreived from the databse. Sequences from this study represent groups of sequences that shared greater than 96% identity; numbers in brackets represent the number of sequences in such as group. Symbols represent known phototrophic species (*) as well as previously isolated and described species (#). Group I represents *Heliothrix* (chlorosome-less BChl*a* but not BChl*c* or *d*-producing species) related sequences; Group II represents *Chloroflexus* / *Chloronema* / *Oscillochloris* (chlorosome and BChla + c or d-producing species) as well as *Roseiflexus* (chlorosome-less BChl*a* but not BChl*c* or *d*-producing species) related sequences; Groups III-VIII represent subclusters which all accommodate sequences found in Chiprana microbial mats, but all these are distantly related to the Family Chloroflexaceae, but still within the phylum Chloroflexi

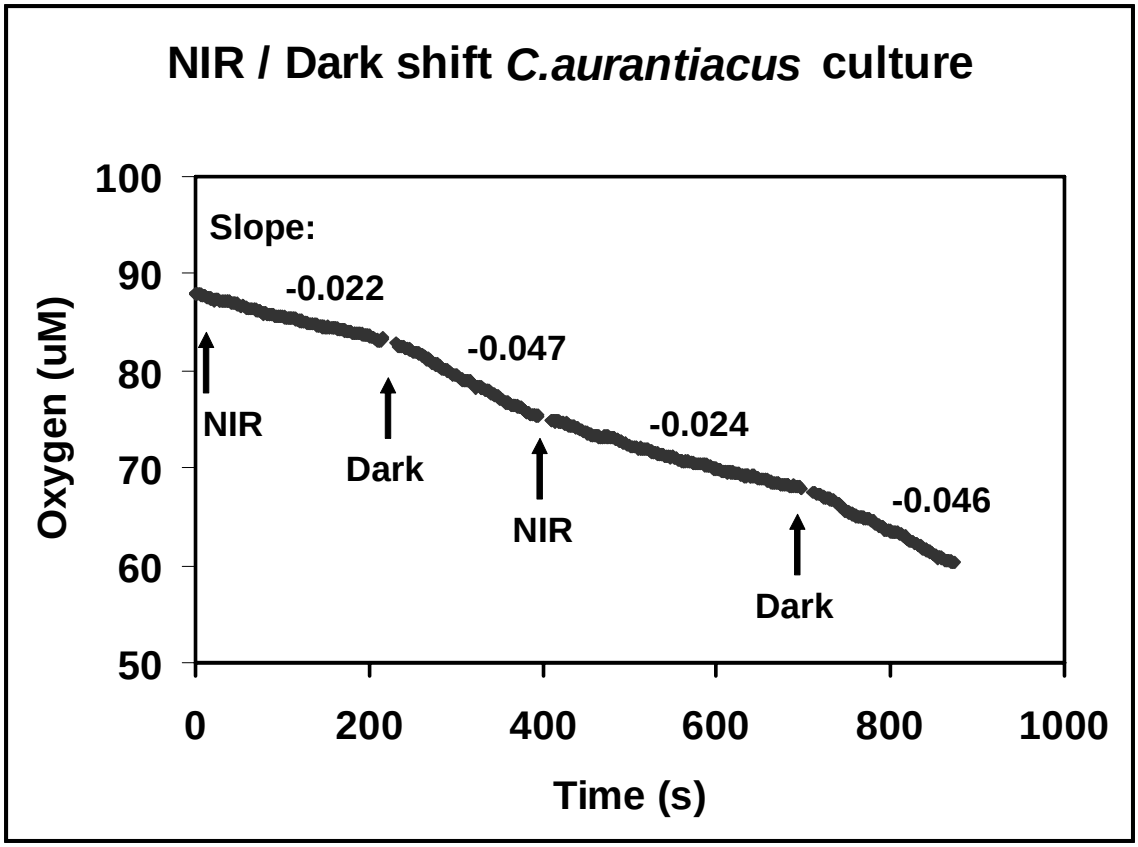
NIR / Dark shift C.aurantiacus culture
Oxygen (uM)
100
90
80
70
60
50
Slope:
-0.022
-0.047
-0.024
-0.046
NIR
Dark
NIR
Dark
0
200
400
600
800
1000
Time (s)

Figure 4a

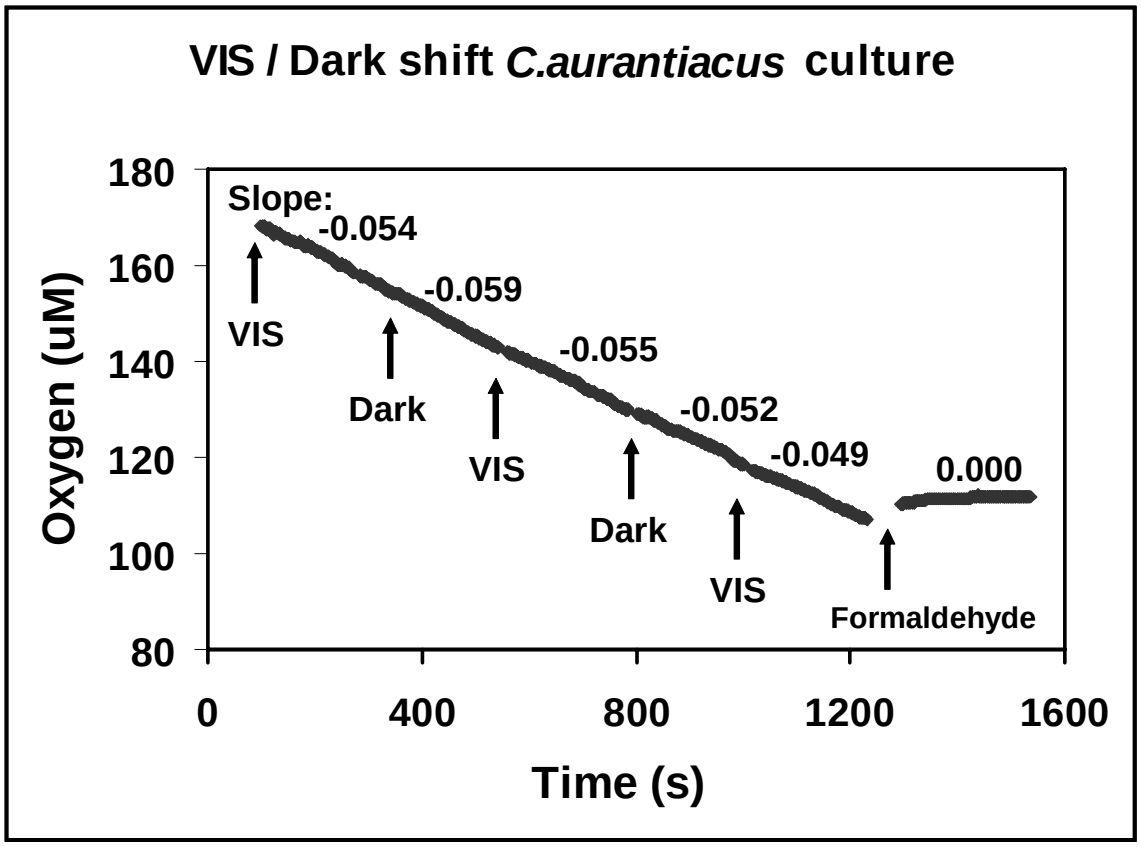

Figure 4b

Figure 4. Oxygen consumption in aerated axenic cultures of *C.aurantiacus* under different illumination conditions. Fig 4a: Alternating NIR (25 Watts incandescent lightbulb + two 40 mA NIR (710-770 nm) LEDs) illumination and darkness; Fig 4b: Alternating VIS (two VIS (400-700 nm) LEDs) illumination and darkness as well as formaldehyde killed control. See Table 3 for calculated specific respiration rates

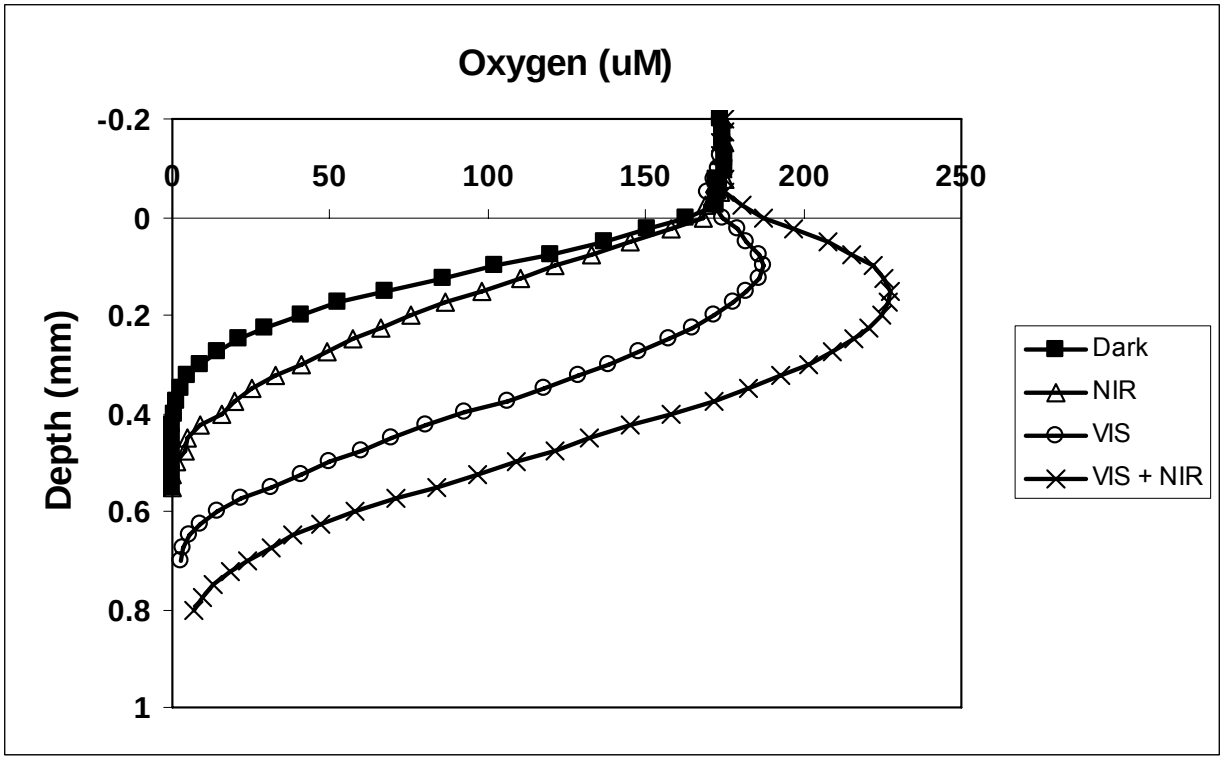

Figure 5. Steady state oxygen concentration profiles in Lake Chiprana microbial mat at four different light conditions; 1: dark, 2: NIR (two 40 mA, 710-770 nm NIR LEDs), 3: VIS (two 400-700 nm VIS LEDs; 60 µmol photons m^{-2} s^{-1}) and 4: two NIR plus two VIS LEDs

Chapter III: Microbial methane turnover at mud volcanoes of the Gulf of Cadiz

Microbial methane turnover at mud volcanoes of the Gulf of Cadiz

Niemann, H.[1,2]; Duarte, J.[3]; Hensen, C.[4]; Omoregie, E.[1,7]; Magalhães, V.H.[3,5]; Elvert, M.[6]; Pinheiro, L, M.[3]; Kopf, A. [6]; Boetius, A.[1,7]

[1] Max Planck Institute for Marine Microbiology Bremen, Celsiusstr.1, 28359 Bremen, Germany
[2] Alfred Wegener Institute for Polar and Marine Research, 27515 Bremerhaven, Germany
[3] Geosciences Department and CESAM, University of Aveiro, Campus de Santiago, 3810-193 Aveiro, Portugal
[4] Leibniz Institute of Marine Sciences, IfM-GEOMAR, 24148 Kiel, Germany
[5] Department National Institute of Engineering, Technology and Innovation, Alfragide, 2720-866 Amadora, Portugal
[6] Research Center Ocean Margins, University of Bremen, 28359 Bremen, Germany
[7] International University Bremen, 28759 Bremen, Germany

Author to whom correspondence should be addressed:

Helge Niemann
email: hniemann@mpi-bremen.de, phone +49-421-2028653

Running head: Mud volcanoes of the Gulf of Cadiz

Index terms: mud volcano, Gulf of Cadiz, cold seep, methane, AOM, anaerobic oxidation of methane, sulphate reduction, chemosynthesis, carbonate, ANME, biomarker

This manuscript has been published in Geochimica et Cosmoschimica Acta 70 (2006): 5336-5355

ABSTRACT

The Gulf of Cadiz is a tectonically active area of the European continental margin and characterised by a high abundance of mud volcanoes, diapirs, pockmarks and carbonate chimneys. During the R/V SONNE expedition "GAP- Gibraltar Arc Processes (SO-175)" in December 2003, several mud volcanoes were surveyed for gas seepage and associated microbial methane turnover. Pore water analyses and methane oxidation measurements on sediment cores recovered from the centres of the mud volcanoes Captain Arutyunov, Bonjardim, Ginsburg, Gemini and a newly discovered, mud volcano-like structure called "No Name" show that thermogenic methane and associated higher hydrocarbons rising from deeper sediment strata are completely consumed within the seabed. The presence of a distinct sulphate-methane transition zone (SMT) overlapping with high sulphide concentrations suggests that methane oxidation is mediated under anaerobic conditions with sulphate as the electron acceptor. Anaerobic oxidation of methane (AOM) and sulphate reduction (SR) rates show maxima at the SMT, which was found between 20 to 200 cm below sea floor at the different mud volcanoes. In comparison to other methane seeps, AOM activity (<383 mmol m^{-2} yr^{-1}) and diffusive methane fluxes (<321 mmol m^{-2} yr^{-1}) in mud volcano sediments of the Gulf of Cadiz are low to mid range. Corresponding lipid biomarker and 16S rDNA clone library analysis give evidence that AOM is mediated by a mixed community of anaerobic methanotrophic archaea and associated sulphate reducing bacteria (SRB) in the studied mud volcanoes. Little is known about the variability of methane fluxes in this environment. Carbonate crusts littering the sea floor of mud volcanoes in the northern part of the Gulf of Cadiz had strongly ^{13}C-depleted lipid signatures indicative of higher seepage activities in the past. However, actual sea floor video observations showed only scarce traces of methane seepage and associated biological processes at the seafloor. No active fluid or free gas escape to

the hydrosphere was observed visually at any of the surveyed mud volcanoes, and biogeochemical measurements indicate a complete methane consumption in the seafloor. Our observations suggest that the emission of methane to the hydrosphere from the mud volcano structures studied here may be insignificant at present.

1. INTRODUCTION

Constraining global sources and sinks of the greenhouse gas methane, and understanding the climate change coupled to variations in atmospheric methane, are important rationales of current biogeochemical research. Anthropogenic sources as well as natural emission from wetlands contribute significantly to the global emission of methane to the atmosphere, but the role of the ocean in global methane fluxes is not well understood (Reeburgh, 1996; Judd et al., 2002). Recently, marine mud volcanism has been identified as an important escape pathway for methane and higher hydrocarbons (Dimitrov, 2002; Judd et al., 2002; Dimitrov, 2003). Mud volcanism is caused by various geological processes at continental margins such as tectonic accretion and faulting, rapid burial of sediments and emission of gases and fluids. Such processes may lead to high pore fluid pressures and sediment instabilities, and consequently cause mud extrusions. Since subsurface muds and shales of productive continental margins often contain methane and other hydrocarbons of thermogenic and/or microbial origin, mud flows can be accompanied by gas expulsion (Milkov, 2000; Kopf, 2002; Charlou et al., 2003; Somoza et al., 2003). Mud volcanoes (MVs) are structurally diverse, ranging in shape from amorphous mud pies to conical structures, and in size from a few meters to kilometres in diameter, attaining heights of up to a few hundred meters (Dimitrov, 2002; Kopf, 2002). While there are only 650 to 900 known terrestrial mud volcanoes (Kopf, 2003), global estimates for marine mud volcanoes range between 800 and 100000 (Milkov, 2000; Dimitrov, 2002; Dimitrov, 2003; Kopf, 2003; Milkov et al., 2003). It is unknown how many of these submarine mud volcanoes are actively emitting methane to the hydrosphere. As a result, global estimates of methane emissions from these structures vary considerably. Recent estimates suggest that terrestrial and shallow water mud volcanoes contribute between 2.2 and 6 Tg yr^{-1} of methane to the atmosphere (Dimitrov, 2003;

Milkov et al., 2003) and that 27 Tg yr^{-1} of methane may escape from deep water mud volcanoes (Milkov et al., 2003). Revised estimates of the total methane emission from MVs ranges between 35-45 Tg yr^{-1} (Etiope and Milkov, 2004), 30-70 Tg yr^{-1} (Etiope and Klusman, 2002), and – when using only known MVs and correcting for size of the edifice – between 0.3 Tg yr^{-1} (Kopf, 2003) and 1.4 Tg yr^{-1} (Kopf, 2002). Clearly, a better understanding of mud volcano activity and methane turnover at these structures is needed, to evaluate the contribution of mud volcanism to the total annual methane emission to the atmosphere (535 Tg yr^{-1}, Judd et al., 2002).

The main sink for methane in the ocean is the anaerobic oxidation of methane (AOM) with sulphate as the terminal electron acceptor (Barnes and Goldberg, 1976; Reeburgh, 1976; Iversen and Jørgensen, 1985; Hinrichs and Boetius, 2002; Nauhaus et al., 2002; Treude et al., 2003). This process is mediated by archaea, operating most likely in cooperation with sulphate reducing bacteria (SRB) (Hinrichs et al., 1999; Boetius et al., 2000; Orphan et al., 2001). So far, two groups of anaerobic methanotrophic archaea (ANME-1, ANME-2) have been identified (Hinrichs et al., 1999; Boetius et al., 2000; Orphan et al., 2001; Michaelis et al., 2002; Knittel et al., 2005). They usually occur together with SRB from a distinct, yet uncultivated cluster within the *Desulfosarcina*/*Desulfococcus* group (Seep-SRB1; Knittel et al. 2003). Generally, microbial methane oxidation is characterized by a strong discrimination against the heavy, stable carbon isotope ^{13}C, leading to a significant depletion in the ^{13}C-content of metabolites and biomass (Reeburgh and Heggie, 1977; Whiticar et al., 1986; Summons et al., 1994; Elvert et al., 1999; Thiel et al., 1999; Whiticar, 1999; Orphan et al., 2001). Such conspicuous isotope signatures of lipid biomarkers for the archaeal and bacterial partners in AOM mediating communities have been a main tool in studying the diversity and functioning of cold seep ecosystems (Hinrichs et al., 1999; Pancost et al., 2000; Elvert et al., 2001; Orphan et al., 2001; Michaelis et al., 2002; Elvert et al., 2003; Blumenberg et al., 2004; Elvert et al., 2005; Niemann et al., 2005). Active

mud volcanoes in the Mediterranean Sea, eg. Napoli, Amsterdam and Kazan (Pancost et al., 2000; Aloisi et al., 2002; Haese et al., 2003; Werne et al., 2004); the Black Sea, e.g. Dvurechenskii and Odessa (Bohrmann et al., 2003; Stadnitskaia et al., 2005); and the Barents Sea, e.g. Håkon Mosby (Vogt et al., 1997a; Vogt et al., 1997b; Damm and Budéus, 2003; De Beer et al., 2006) are characterised by steep gradients of pore water solutes due to upward fluid and gas flow and high rates of AOM and sulphate reduction (SR). Several of these geo-bio-systems were also found to support enormous biomasses of chemosynthetic symbiotic tubeworms and bivalves, which are fuelled by methane and/or sulphide, and mats of giant sulphide oxidising bacteria, (Southward et al., 1981; Fisher, 1990; Olu et al., 1997a; Gebruk et al., 2003).

During the UNESCO program "Training through Research (TTR)" with R/V Prof. Logachev, numerous mud volcanoes hosting methane-hydrate were discovered in the Gulf of Cadiz (Kenyon et al., 2000; Gardner, 2001; Kenyon et al., 2001; Mazurenko et al., 2002; Somoza et al., 2002; Pinheiro et al., 2003). However, the geochemical and microbiological activity of these potential seep structures and the occurrence of methane emission to the hydrosphere remained unknown. As part of the Gibraltar Arch Project (GAP), we studied several mud volcanoes with the aid of sea-floor video imaging as well as video-guided sampling of sediments and carbonate crusts during a cruise with R/V Sonne in 2003 (SO-175). The main goals of this investigation were to survey the occurrence of methane seepage at mud volcanoes in the Gulf of Cadiz, to compare the distribution and magnitude of AOM by rate measurements and diffusive flux calculations, as well as to identify the key methanotrophs using lipid biomarker and 16S rDNA methods.

2. MATERIALS AND METHODS

2.1. Geological Setting and Videographic Observations

The Gulf of Cadiz is located west of the Gibraltar Arc, between Iberia and the African plate (Fig. 1). This area has experienced a complex tectonic history with several episodes of extension, strike-slip and compression related to the closure of the Tethys Ocean, the opening of the N-Atlantic, and the African-Eurasian convergence since the Cenozoic (Maldonado et al., 1999). During the Tortonian, a large olistrostome body made of eroded material from the Betic Cordillera (Spain) and Rif Massif (Morocco) was emplaced west of the Straits of Gibraltar (Maldonado and Comas, 1992; Somoza et al., 2003). Due to the ongoing compression, these rapidly deposited sediments dewater intensely and form MVs and fluid escape structures (Diaz-Del-Rio et al., 2003). The Gulf of Cadiz has been intensely surveyed with geophysical tools, leading to the discovery of the first MVs, mud diapirs and pockmarks in 1999 (Kenyon et al., 2000; Gardner, 2001; Pinheiro et al., 2003). In addition, an extensive field of mud volcanoes and diapiric structures covered with carbonate chimneys and crusts was discovered along or in close proximity of the main channels of the Mediterranean outflow water (Kenyon et al., 2000; Kenyon et al., 2001; Diaz-Del-Rio et al., 2003; Somoza et al., 2003; Kopf et al., 2004).

In the present study, Captain Arutyunov (Capt. Arutyunov), Bonjardim, Ginsburg, Gemini, Hesperides and Faro MV and a newly discovered structure termed “No Name”, were investigated (Fig. 1, Tab. 1). Prior to biogeochemical sampling, a few transects across the selected MVs were surveyed with the video-sled Ocean Floor Observation System (OFOS), or with a video-guided multiple-corer (MUC, Tab. 1). Both systems are equipped with powerful lamps and a video

camera. Video observations were made from a vertical perspective at ca. 1-2 m above the sea bottom to monitor an area of approximately 1 m^2. The systems were passively towed at minimum speed (<1.84 km h^{-1}) along 2-3 transects of 1 to 3 km crossing the rim and apex of the edifices with a total bottom observation time of approximately 8 h per mud volcano (Tab. 1, Kopf et al., 2004). The video-guided MUC was also used to select representative sampling positions and to retrieve undisturbed surface sediments (next section).

2.2. Sample collection and storage

Sediments from several mud volcanoes were sampled by gravity coring in the central crater region (Tab. 1, Fig. 2), retrieving up to 5 m of sediment. Additionally, surface sediments of Capt. Arutyunov and Bonjardim MV were obtained with a video-guided MUC because the top decimetres of sediment cover are often lost during gravity core retrieval. Video-guided MUC sampling enabled the retrieval of undisturbed surface sediments of up to 50 cm sediment depth. With this method, the seafloor can be observed when the MUC is towed at minimum speed at about 1-2 m above bottom. The MUC is launched immediately when targeted seafloor structures are observed. Compared to the gravity core, MUC cores contained a broader horizon of hemipelagic surface sediments providing further evidence for a loss of surface sediments during gravity coring. To account for this loss, we aligned the depth of gravity cores obtained from Capt. Arutyunov and Bonjardim MV according to the vertical sulphate profiles of MUC-cores recovered from one site, assuming that sulphate concentrations are mainly a function of depth in proximate cores. According to this procedure, the top of the gravity cores recovered from Capt. Arutyunov and Bonjardim MV were from 40 and 12.5 cm sediment depth, respectively. Aligning proximate core sections is an approach to account for a loss of an unknown quantity of surface

sediments during gravity coring. However, this can be problematic if the spatial variability of geochemical gradients is high.

Upon recovery, gravity cores were sectioned into 1 m pieces, which were cut longitudinally into halves, just before sub sampling. All cores were immediately transferred into a cold room and subsampled for concentration measurements of pore water constituents (methane, sulphate, sulphide), AOM and SR rate measurements as well as for lipid biomarker and 16S rDNA analyses (Tab. 1). Sediments for measurements of methane and sulphate concentrations and turnover rate measurements were subsampled vertically with push cores (acrylic core liners, 26 mm diameter, n = 3) from MUC-cores (Jørgensen, 1978; Treude et al., 2003). Gravity cores were subsampled by plugging glass tubes (60 mm length, 10 mm diameter, n = 5) into selected ca. 10 cm wide sediment horizons (every 20 to 30 cm). The tubes were then sealed with butyl rubber stoppers to prevent gas loss during the anaerobic incubation. Sediment samples for pore water extraction, biomarker and 16S rDNA analyses were collected from 2 cm sections of MUC cores and from ca. 10 cm wide sediment horizons (every 20 to 30 cm) of gravity core sections. Directly after subsampling, pore water from these sediment horizons was extracted by pressure filtration (5 bars) through Teflon squeezers provided with 0.2 µm cellulose acetate filters according to previous works (Reeburgh, 1967; Niewöhner et al., 1998; Hensen et al., 2003). Subsequently, the pore water was immediately fixed (next section). Lipid and DNA samples were stored in cleaned glass vials at –20°C until extraction in the home laboratory. Carbonate crusts from Hesperides and Faro MV were collected with a video guided grab-sampler (Tab.1). Because Hesperides MV consist of 6 individual cones, the grab sample was taken from the apex of the highest (north-eastern) summit. The grab sampler allows to retrieve samples down to a depth of ca. 0.5 m below sea floor (bsf). The videographic observation and sampling procedure is similar to the technique

used for video-guided coring as explained above. Upon recovery, carbonate crusts for lipid biomarker analyses were transferred into plastic bags and stored at –20°C until extraction.

2.3. Methane Concentrations

Methane concentrations in sediments were determined according to the "head space" method from 5 ml sediment fixed with 10 ml NaOH (2.5%, w/v) in glass vials (20 ml) as described previously by Treude and co-workers (2003). A vertical resolution of 2 cm was chosen for surface samples from MUC cores, and of 20-30 cm for subsurface samples from gravity cores. The concentrations presented here are *ex situ* methane concentrations. As a result of depressurisation and warming of the core during sediment retrieval, concentrations above 1.4 mM (saturation at 1 bar and 4°C) would have led to degassing during retrieval and sediment subsampling. Also, dissociation of gas hydrates upon recovery may lead to biased methane concentrations in the cores. We tried to minimize the problem by (a) subsampling immediately after opening the core and (b) subsampling of deeper sediments below the longitudinal opening plane of the gravity core with glass syringes. Methane concentrations were determined shortly after the cruise (<2 month) from 200 µl aliquots of the head space using a gas chromatograph (5890A, Hewlett Packard) equipped with a packed stainless steal Porapak-Q column (6 ft, 0.125 in, 80/100 mesh, Agilent Technologies) and a flame ionisation detector (Treude et al., 2003). The carrier gas was helium at a flow rate of 30 ml min^{-1}. The column temperature was 40°C. The chromatography system was calibrated for a concentration range of 0.001 to 5 mM methane (final concentration in the sediment). Sediment samples from Capt. Arutyunov and Bonjardim MV were additionally analysed for the concentrations of the higher hydrocarbons (C_{2+}) ethane, propane, isobutene and butane (Σbutane) using the above-described chromatography setting with

a temperature gradient. Subsequent to injection at 40°C, the temperature was increased at a rate of 2°C min^{-1} to 200°C and held for 20 min. Identity and concentrations of methane and C_{2+}-compounds were determined with standards of known hydrocarbon compositions.

2.4. Sulphate and Sulphide Concentrations

Sulphate and sulphide concentrations were analysed according to modified methods from Cline (1969) and Small et al. (1975), respectively, as described elsewhere (Grasshoff et al., 1983). Briefly, sulphide concentrations were determined immediately after pore water squeezing by adding 1 ml of pore water to 50 µl of a zinc acetate gelatine solution. Zinc acetate gelatine solution consists of 50 mg gelatine and 261 mg ZnAc dissolved in 25 ml O_2-free water. Sulphide was quantitatively removed as ZnS and kept in colloidal solution. After adding 10µl of 4% N,N-Dimethyl-1,4-phenylenediamine-dihydrochloridethe dissolved in 6 N HCl (w/v), the concentration was determined photometrically by measuring the absorbance after 1 hour at 670 nm. Sulphate concentrations were determined on 2 ml sub-samples of filtered pore water using a Sykam-S ion chromatography system equipped with an anion exchange column (LCA A14). 7.5 mM Na_2CO_3-solution was used as an eluent at a flow rate of 1.75 ml min^{-1}. Samples were diluted by 1:54 with the eluent prior to injection. Sulphate concentrations were determined with a Sykam S3110 conductivity detector.

2.5. Diffusive Flux Calculations

Diffusive fluxes were calculated to compare areal rates of AOM and SR, to estimate the activity of Ginsburg and Gemini mud volcano as well as the No Name structure and to compare the

surveyed systems to other seeps in the world oceans. This approach bears several problems, namely potential artefacts in the ex situ concentrations of porewater species due to degassing, the assumption of steady state in the porewater system, and the alignment of sediment cores. At Bonjardim mud volcano, the alignment of pore water profiles was discontinuous, while the resolution of pore water gradients was not well resolved at Ginsburg and Gemini mud volcano. Where possible, we determined two concentration gradients: one from the aligned profile and the other from the profile of the gravity core in order to provide a possible range of the sulphate and sulphide fluxes.

Local fluxes (J) were calculated from the vertical profiles of pore water constituents (methane, sulphate, sulphide) according to Fick's first law of diffusion assuming steady state conditions (e.g. Niewöhner et al., 1998; Berner 1980 and references therein):

$$J = -\phi D_s \frac{\delta C}{\delta x} \quad (1)$$

where D_s is the diffusion coefficient in the sediments (in $cm^2\ yr^{-1}$) , ϕ the porosity (in %) and $\frac{\delta C}{\delta x}$ the local concentration gradient (in cm^{-4}). $\frac{\delta C}{\delta x}$ was determined from the depth intervals where the concentration change was maximal. D_s was determined from the molecular diffusion coefficient after Boudreau (1997):

$$D_s = \frac{D_0}{1 - \ln(\phi)^2} \quad (2)$$

For each mud volcano, D_0 values were corrected for temperature (3 to 12°C, depending on the actual bottom water temperature), resulting in values ranging between 291 to 392, 178 to 244 and 356 to 434 for methane, sulphate and sulphide, respectively (Boudreau, 1997). ϕ was determined

from the weight loss per volume of wet sediment after drying to stable weight at 60°C. In general, ϕ decreased with depth showing values of 57 - 76% in the top sections and 51 - 60% in the bottom sections of the retrieved MUC and GC cores (data shown for the SMT, Tab. 2).

2.6. Ex-situ AOM and SR Rate Measurements

Sediment for turnover rate measurements recovered from Capt. Arutyunov and Bonjardim MV were incubated on board according to previously described methods (Jørgensen, 1978; Treude et al., 2003; Treude et al., 2005). Briefly, 25µl $^{14}CH_4$ (dissolved in water, 2.5 kBq) or 5 µl $^{35}SO_4^{2-}$ tracer (dissolved in water, 50 kBq) were injected into butyl rubber sealed glass tubes from gravity core sub-sampling, and in 1 cm intervals into small push cores (whole core injection) used for MUC core sub-sampling. Incubations were carried out for 24 h at *in situ* temperature in the dark. Subsequently, incubated AOM and SR rate samples were fixed in 25 ml NaOH (2.5%, w/v) and 25 ml zinc acetate solution (20%, w/v), respectively. Further processing of AOM and SR rate samples was performed according to Treude et al (2003) and references therein. Turnover rates were calculated according to the following formulas:

$$\mathrm{AOM} = \frac{^{14}\mathrm{CO_2}}{^{14}\mathrm{CH_4} + ^{14}\mathrm{CO_2}} \times \frac{\mathrm{conc.CH_4}}{\mathrm{incubat.Time}} \quad (3)$$

$$\mathrm{SRR} = \frac{\mathrm{TRI}^{35}\mathrm{S}}{^{35}\mathrm{SO_4}^{2-} + \mathrm{TRI}^{35}\mathrm{S}} \times \frac{\mathrm{conc.SO_4}^{2-}}{\mathrm{incubat.Time}} \quad (4)$$

Here, $^{14}CO_2$, $^{35}SO_4^{2-}$ and $TRI^{35}S$ are the activities (Bq) of carbon dioxide, sulphate and total reduced sulphur species, respectively, whereas $conc.CH_4$ and $conc.SO_4^{2-}$ are the concentrations of methane and sulphate (per volume of fresh sediment) at the beginning of the incubation. To compare *ex situ* microbial rates with the diffusive fluxes of methane and sulphate, AOM and SR

rates were integrated over depth (0 to 80 cm below sea floor) from the alignments of cores 9036-2 and 9041-4 as well as 9051-1 and 9051-2, respectively. *Ex situ* rate measurements may differ from *in situ* rates due to the effect of depressurisation on concentrations of gaseous and dissolved components.

2.7. Extraction of Sediment and Carbonate Samples and Preparation of Derivates

Sediments from Capt. Arutyunov and Bonjardim MV as well as carbonate crusts from Hesperides and Faro MV were analysed for lipid biomarker signatures. The extraction procedure and preparation of fatty acid methyl esters (FAMES) was carried out according to previously described methods (Gillian et al., 1981; Elvert et al., 2003; Niemann et al., 2005). Briefly, total lipid extracts (TLE) were obtained from ca. 20 g of wet sediment and from authigenic carbonates disintegrated with HCL (2M) prior to extraction. The TLE was extracted by subsequent ultrasonication using organic solvents of decreasing polarity (dichloromethane/methanol (1:2, v/v), dichloromethane/methanol (2:1 (v/v), dichloromethane). Internal standards of known concentration and carbon isotopic compositions were added prior to extraction. Fatty acid moieties present in glyco and phospholipids were cleaved by saponification with methanolic KOH-solution. After extraction of the neutral lipid fraction from this mixture, fatty acids (FAs) were methylated with BF_3 in methanol yielding FAMES. Double bond positions of monoenoic FAs were determined by analysis of dimethyl disulphide adducts according to methods described elsewhere (Nichols et al., 1986; Moss and Lambertfair, 1989).

Neutral lipids were further separated into hydrocarbons, ketones and alcohols on a SPE silica glass cartridge (0.5 g packing) with solvents of increasing polarity (*n*-hexane/dichloromethane (95:5, v/v), *n*-hexane/dichloromethane (2:1, v/v), dichloromethane/acetone (9:1, v/v)) (Niemann

et al., 2005). Alcohols were derivatised with bis(trimethylsilyl)triflouracetamid (BSTFA) forming trimethylsilyl (TMS) ethers prior to analyses.

2.8. Gas Chromatography

Concentrations of single lipid compounds were determined by gas chromatography analysis using a Varian 30 m apolar CP-Sil 8 CB fused silica capillary (0.25 mm internal diameter [ID], film thickness 0.25 μm) in a Hewlett Packard 6890 Series gas chromatograph equipped with an on column injector and a flame ionisation detector. Initial oven temperature was 80°C. Subsequently to injection, the initial temperature was increased to 130°C at a rate of 20°C min^{-1}, then raised to 320°C at a rate of 4°C min and held at 320°C for 30 min. The carrier was helium at a constant flow of 2 ml min^{-1} and the detector temperature was set to 310°C. Concentrations were calculated relative to internal standards present within the respective lipid fraction.

2.9. Gas Chromatography-Mass Spectrometry (GC-MS), Gas Chromatography-Isotope Ratio Mass Spectrometry (GC-IRMS)

Identity and stable carbon isotope ratios of individual compounds were determined by GC-MS and GC-IRMS analysis, respectively. Instrument specifications and operation modes of the GC-MS and GC-IRMS units were set according to Elvert et al. (2003). Identities of acquired mass spectra were compared to known standards and published data. Stable isotope ratios are given in the δ-notation against Pee Dee Belemnite. $\delta^{13}C$-values of FAs and alcohols were corrected for the introduction of additional carbon atoms during derivatisation. Internal standards were used to

monitor precision and reproducibility during measurements. Reported $\delta^{13}C$-values have an analytical error of ±1‰.

2.10. DNA extraction and clone library construction

Total community DNA was extracted from sediments (ca. 1 g) collected from the SMT of Capt. Arutyunov MV (30-40 cm) using the FastDNA spin kit for soil (Q-Biogene, Irvine, California, USA). Samples were bead-beat in a Fastprep machine (Q-Biogene, Irvine, California, USA) at speed 4.5 for 30 seconds. All other steps in the DNA extraction procedure were preformed according to the manufacturer's recommendations. Almost full-length archaeal and bacterial 16S rRNA genes were amplified from sediments samples using the primers 20f (Massana et al., 1997) and Uni1392R (Lane et al., 1985) for *Archaea* and GM3F (Muyzer et al., 1995) and GM4R (Kane et al., 1993) for *Bacteria*. Polymerase chain reactions (PCRs) were performed with TaKaRa Ex Taq (TaKaRa, Otsu Japan), using 2.5 U of enzyme, 1X Buffer, 4 mM of $MgCl_2$, 4 mM of each dNTP, 1 µM of each primer and 2 µl of template in a 50 µl reaction. PCR reactions were preformed in a Mastercycler machine (Eppendorf, Hamburg, Germany), with the following cycling conditions: 95°C for two minutes, then 30 cycles of 95°C for 30 seconds, 60°C (*Archaea*) or 50°C (*Bacteria*) for 30 seconds and 72°C for 3 minutes, followed by a final incubation step at 72°C for 10 minutes. PCR products were visualized on an agarose gel, and the 16S band excised. PCR products were purified using the QIAquick Gel Extraction Kit (Qiagen, Hilden, Germany). Two microliters of purified DNA were ligated in the pGEM T-Easy vector (Promega, Madison, WI) and transformed into competent E. coli TOP10 cells (Invitrogen, Carlsbad, CA) according to the manufacturer's recommendations. Transformation reactions were plated on LB-agarose plates. Overnight cultures were prepared from individual colonies picked from these plates using

the Montage Plasmid Miniprep 96 kit (Millipore, Billerica, USA). Purified plasmids were sequenced in one direction, with either the 958R (*Archaea*) or GM1F (*Bacteria*) primers using the BigDye Terminator v3.0 Cycle Sequencing kit (Applied Biosystems, Foster City, USA). Samples were sequenced on an Applied Biosystems 3100 Genetic Analyser (Foster City, USA). A total of 39 archaeal and 47 bacterial clones were partially sequenced (~ 0.5 kb). Using the ARB software package, the sequences were calculated into existing phylogentic trees by parsimony without allowing a change in the tree topology. Representative sequences of each cluster were then fully sequenced (~1.3 kb) and matched against the NCBI database (http://www.ncbi.nlm.nih.gov/BLAST). Sequences were submitted to the Genbank database (http://www.ncbi.nlm.nih.gov/) and are accessible under the following accession numbers: DQ004661 to DQ004676 and DQ004678 to DQ004680.

3. RESULTS

3.1. Field Observations

A detailed description of sea floor video observations, sedimentology and sampling locations is provided in the cruise report of R/V SONNE expedition SO-175 (Kopf et al., 2004). The mud volcanoes Capt. Arutyunov, Bonjardim, Ginsburg, Gemini, and Faro studied here are cone shaped structures with a relief of up to 200 m and a maximum diameter of 4.9 km kilometres (Fig. 2a, b; Tab.1). Hesperides MV has comparable dimensions but is composed of 6 individual cones. A new structure was discovered east of the TTR MV and termed "No Name" (Fig. 1). Video observations of the mud volcanoes Capt. Arutyunov, Bonjardim, Ginsburg, Hesperides, and Faro did not reveal indications for recent gas, fluid or mud expulsion during the transects across the central craters of each structure . The centres of Capt. Arutyunov, Bonjardim and Ginsburg MV were covered with light beige sediments (shown for Capt. Arutyunov MV, Fig. 3a). At Capt. Arutyunov MV, some sediment stretches were scattered with accretions, interpreted as mud clasts, which may indicate past mud eruptions (Fig. 3b). At Ginsburg MV, a few small carbonate crusts (<0.5 m) were observed on the seafloor. Beside these observations, no other distinctive geological or biological features indicating gas or fluid seepage were visible on video images at Ginsburg MV. Surface sediments recovered from Capt. Arutyunov MV contained very thin tubeworms (diameter <1 mm), which extended down to 20 cm into the sediment. These were not visible on video images due to their low abundance and small diameter. Tubeworms are regarded as indicator species for reduced environments because the known species harbour methane or sulphide oxidising symbionts, indicating sulphide and/or methane availability in the sediments (Southward et al., 1981; Southward et al., 1986; Schmaljohann and Flugel, 1987; Sibuet and Olu,

1998; Kimura et al., 2003; Southward et al., 2005). The central areas of Hesperides and Faro MV were littered with fragments of carbonate chimneys and carbonate crusts (shown for Hesperides MV, Fig. 3c). Both, chimneys and crusts were ranging in size from several centimetres to meters in length and diameter, respectively. At Faro MV, a few, small patches covered with microbial mats possibly consisting of filamentous sulphide oxidising bacteria were observed (Fig. 3d). Moreover, TV-guided grab samples recovered from this MV also contained a few specimens of the deep-dwelling chemosynthetic clam *Acharax sp.* usually harbouring sulphide oxidising bacteria in their gills (Felbeck, 1983; Krueger and Cavanaugh, 1997; Peek et al., 1998; Sibuet and Olu, 1998). Video observations were not carried out at Gemini MV and the "No Name" structure. The MUC-cores retrieved from Capt. Arutyunov and Bonjardim MV contained yellowish, muddy sediments in the top sections from 0-20 and 0-40 cm bsf, respectively. The bottom sections of the MUC-cores contained mud breccia, a mud matrix with clasts extruded from greater depth below these edifices (Cita et al., 1981; Akhmanov and Woodside, 1998). The gravity cores retrieved from these MVs as well as those retrieved from Ginsburg and Gemini also contained mud breccia. The gravity core recovered from the "No Name" structure contained a matrix of cold water coral fragments and greyish mud but no mud breccia. Hence, the relation of the "No Name" geo-structure to mud-volcanism remains unknown. Grab samples from Hesperides and Faro MV contained carbonate fragments and mud breccia. After recovery, the temperature in the top sediment section (~1 m) at Bonjardim MV was ca. 3°C. In contrast, the temperature was considerably higher at Capt. Arutyunov (12°C), Ginsburg MV, Gemini MV and the "No Name" structure (10°C, respectively) most probably as a result of the warm Mediterranean outflow water, which contributes to the bottom water at these MVs.

3.2. Captain Arutyunov Mud Volcano

3.2.1. Methane, C_{2+}, Sulphate and Sulphide

Methane concentrations in surface sediments (0-20 cm, Fig. 4a) were <0.001 mM indicating a complete consumption of methane rising from deeper sediment strata. A distinct SMT was observed in the lower half of the MUC-core section (25 - 40 cm bsf.) with *ex situ* methane concentrations above saturation at atmospheric pressure, and sulphate concentrations dropping below 0.5 mM. The steepest gradients of methane and sulphate found in this zone amounted to 0.4 and –1.12 µmol cm^{-4}, respectively (Fig. 4a, Tab. 2). Small gas hydrate chips were found throughout the whole gravity core section from 44 to 235 cm bsf (1941-1). Similar to methane, concentrations of C_{2+}-compounds decreased across the SMT (Fig. 4b). Hydrocarbons in the sediment comprised methane (>99%), ethane (<0.4%), propane (<0.07%) with trace amounts of butane and isobutene present indicating a thermogenic origin of these gases (Nuzzo et al. 2006; Stadnitskaia et al., 2006 and references therein). Sulphide concentrations peaked in the SMT with 4.8 mM at 39 cm bsf (Fig. 4d). The steepest sulphide gradient was 0.63 µmol cm^{-4} (Fig. 4d, Tab. 2). A downward sulphide gradient could not be determined because highest sulphide concentrations were observed in the lowest sediment horizon of the MUC-core at Capt. Arutyunov MV. Unfortunately, the sulphide profile could not be aligned with the gravity core section.

3.2.2. AOM, SR Rates and Diffusive Fluxes

AOM and SR rates at Capt. Arutyunov MV were highest in the SMT at 39 cm bsf with maximum values of 11 and 25 nmol cm^{-3} d^{-1}, respectively (Fig. 4c). AOM and SR rates sharply decreased above and below this horizon. Replicate AOM and SR rate measurements showed a standard error of 33 and 37% of the average value, respectively. The areal integration resulted in 1.8 higher SR rates compared to AOM (Tab. 2). The areal AOM and SR rate were in good agreement with diffusive flux calculations showing a 1.7-fold higher sulphate flux compared to the methane flux. The sulphide flux to the surface (upward flux) was comparable to the total downward flux of sulphate (Tab. 2).

3.2.3. Lipid Biomarker

Diagnostic archaeal and bacterial lipid concentrations were strongly increased in sediments at the SMT (Fig. 4e,g). Here, stable carbon isotope analysis revealed highest depletion in ^{13}C with minimum values of –92‰ (*sn2*-hydroxyarchaeol) in archaeal specific diether lipids and –82‰ ($cyC_{17:0\omega5,6}$) in bacterial specific FAs (Tab. 3, Fig. 4f, g) indicating the incorporation of methane derived carbon in archaeal and bacterial biomass (sample from 31 cm bsf). The concentration of both archaeal and bacterial lipids decreased just above and below this sediment horizon. At the SMT, the ratio of *sn2*-hydroxyarchaeol relative to archaeol was 1.6:1 (Tab. 3). Other diagnostic archaeal isoprenoidal hydrocarbons such as 2,6,11,15-tetramethylhexadecane (crocetane) could not be quantified due to an unresolved complex mixture of hydrocarbons (UCM) in all of the hydrocarbon fractions. Similarly, specific archaeal diethers and bacterial FAs could not be resolved from this background below 40 cm sediment depth. The concentrations of diagnostic

archaeal lipids were roughly one order of magnitude lower in comparison to specific bacterial FAs.

The FA fraction in sediments at the SMT was dominated by the FAs $C_{16:1\omega5}$ and $cyC_{17:0\omega5,6}$ which are putatively specific for SRB involved in AOM (Elvert et al., 2003) and contained comparably high amounts of FA $C_{17:1\omega6}$ (Tab. 3). Both, $C_{16:1\omega5}$ and $cyC_{17:0\omega5,6}$ were the most ^{13}C-depleted FAs. However, all other FAs in the C_{14} to C_{17} range carried significantly ^{13}C-depleted isotope signatures as well with values ranging between -65‰ ($C_{16:1\omega9}$) to –75‰ ($C_{14:0}$). C_{18}-FAs were comparably enriched in ^{13}C with $\delta^{13}C$-values ranging between -25‰ ($C_{18:0}$) to -31‰ ($C_{18:1\omega7}$) most likely indicating a planktonic origin of these compounds. Concentrations of mono- and dialkyl glycerol ethers (MAGEs and DAGEs, respectively), presumably of bacterial origin (Pancost et al., 2001), were low in all samples recovered during cruise SO-175. Thus, a detailed analysis of these compounds was not carried out. However, sediments at the SMT of Capt. Arutyunov MV comprised comparably high contents of MAGEs relative to DAGES with $\delta^{13}C$ values ranging from –65‰ to -85‰ (data not shown). The MAGEs comprised a suite of alkyl moieties, which is comparable to those of the fatty acids found at Capt. Arutyunov MV. The suite of fatty acids extracted from the tubeworms comprised dominant amounts of the FAs $C_{16:1\omega7}$ and $C_{18:1\omega7}$ and to a lesser degree $C_{16:0}$ and $C_{18:0}$ with uniform $\delta^{13}C$-values of about -40‰, indicating chemoautotrophic carbon fixation (data not shown). The alcohol and hydrocarbon fractions were not analysed.

3.2.4. Phylogenetic diversity

An archaeal and a bacterial clone library was constructed to study the 16S rDNA-based microbial diversity in sediments at the SMT of Capt. Arutyunov MV (30-40 cm bsf). The 16S rDNA

archaeal clone library consisted of 9 phylogenetic groups (Tab. 4). Closest relatives of these groups were found among seep-endemic, uncultured microorganisms. The majority of sequences obtained were related to the ANME-2 group (59% ANME-2a, 3% ANME-2c of all archaeal sequences) which is known to mediate AOM (Boetius et al., 2000; Orphan et al., 2002; Knittel et al., 2005). The second most abundant group (18% of all archaeal sequences) was found to belong to the ANME-1 cluster which is also known to mediate AOM (Hinrichs et al., 1999; Michaelis et al., 2002; Orphan et al., 2002). The bacterial clone library consisted of 10 uncultivated bacterial lineages. Similar to the archaeal sequences, the next relatives of all bacterial 16S rDNA sequences belonged to uncultivated organisms that are commonly found at methane seeps (Knittel et al., 2003, Tab. 4). The closest relatives of the most abundant cluster of sequences (81%) belonged to the Seep-SRB1 group which comprises the bacterial partners of ANME-1 and ANME-2 (Knittel et al., 2003). Other phylogenetic groups of *Bacteria* were represented by single sequences (<2%).

3.3. Bonjardim MV

3.3.1. Methane, C_{2+}, Sulphate and Sulphide

A distinct SMT was observed in the top meter of the gravity core section with *ex situ* methane concentrations above saturation at atmospheric pressure and sulphate concentrations dropping below 0.2 mM. After aligning the sulphate profile of the gravity core with the MUC core section, the actual depth of the SMT was determined between 45 and 70 cm bsf (Fig. 5a). Methane concentrations in surface sediments (0 – 52 cm sediment depth) were <0.001 mM indicating a complete consumption of methane in the SMT. As the two core sections overlapped,

concentration gradients were determined from the gravity core section and also from aligned profiles in the overlapping zone (Fig. 5a,d). The steepest methane and sulphate gradients in the gravity core section were determined with 0.09 and –0.76 µmol cm^{-4}, respectively (Fig. 5a, Tab. 2). Aligning the gravity core and MUC-core sections, the steepest sulphate gradient was –1.67 µmol cm^{-4}. Methane concentrations declined below the depth at which the two core sections overlap (Fig. 5a). Hence, no further concentration gradient was determined. In comparison to Capt. Arutyunov MV, C_{2+}-concentrations were high with values of >0.25 mM at a sediment depth below 1 m (Fig. 5b). Similar to methane, concentrations of C_{2+}-compounds decreased across the SMT indicating a consumption of these compounds. Gaseous hydrocarbons comprised methane (>81%), ethane (<14%), propane (<4.5%) and Σbutane (<0.4%) indicating a thermogenic origin of these gases (Stadnitskaia et al., 2006). Sulphide concentrations peaked in the SMT with 5.3 mM at 52.5 cm bsf (Fig. 5d). In the gravity core section, the steepest sulphide gradients were determined as 0.23 (upward) and –0.07 (downward) µmol cm^{-4}, respectively (Tab. 2). Aligning the two core sections, the steepest (upward) sulphide gradient was determined with 0.73 µmol cm^{-4}.

3.3.2. AOM, SR Rates and Diffusive Fluxes

AOM and SR rates were highest in the SMT at 58 cm bsf with maximum values of 2.6 and 15.4 nmol cm^{-3} d^{-1}, respectively (Fig. 5c). Comparably low values of AOM and SR rates were measured in over- and underlying sediment horizons. Replicate AOM and SR rate measurements showed a high standard error of 92 and 85% of the average value, respectively, possibly indicating a high small scale variability on a metre scale. The 19-fold higher areal SR compared to AOM suggests a decoupling of these two processes (Tab. 2). Accordingly, the concentration

gradients (determined from unaligned and aligned profiles) translate to a 5.1- to 11-fold higher diffusive downward flux of sulphate compared to the upward flux of methane. The cumulative sulphide flux (upward and downward) accounted for 77% to 92% of the sulphate flux.

3.3.3. Lipid Biomarker

A moderate increase of diagnostic archaeal and bacterial lipid concentrations was observed at the SMT in sediments of Bonjardim MV (Fig. 5e,g). At this horizon (-57 cm bsf), stable carbon isotope analysis revealed highest depletions in ^{13}C with minimum values of –83‰ (*sn2*-hydroxyarchaeol) in archaeal diether lipids and –49‰ ($C_{16:1\omega5}$) in bacterial FAs (Tab. 3, Fig. 5f, g). At the SMT, the ratio of *sn2*-hydroxyarchaeol relative to archaeol was 0.7:1 and therefore lower in comparison to Capt. Arutyunov MV (Tab. 3). Similar to Capt. Arutyunov MV, other diagnostic archaeal isoprenoidal hydrocarbons could not be measured due to a high UCM background. Equally high amounts of the FAs $C_{16:1\omega5}$ and ai-$C_{15:0}$, both of which were the most ^{13}C-depleted FAs (Tab. 3), were detected in sediments at the SMT. The FA cy$C_{17:0\omega5,6,}$ which was abundant at Capt. Arutyunov MV could not be detected in sediments of Bonjardim MV. Furthermore, dominant FAs such as $C_{16:1\omega7}$, $C_{16:0}$, $C_{18:1\omega9}$ and $C_{18:1\omega7}$ carried $\delta^{13}C$-signatures ≥-34‰, indicating that AOM was not the main energy and carbon delivering process to the microbial community. In contrast to Capt. Arutyunov MV, the concentrations of diagnostic archaeal lipids were roughly 4-fold higher compared to specific bacterial FAs (Tab. 3). A further analysis of the diversity of microbial organism using 16S rDNA methods was not carried out at Bonjardim MV.

3.4. Ginsburg MV, Gemini MV and "No Name"

3.4.1. Methane, Sulphate and Sulphide

The SMT was located in the upper metre of the sediment cores retrieved from Ginsburg and Gemini MV and at 2-3 m bsf at the "No Name" structure, respectively (Fig. 6a, c, e). Methane concentrations in sediments overlying the SMT at these structures were <0.001 mM, and reached *ex situ* concentrations above (Gemini MV and "No Name") and just below saturation (1.3 mM, Ginsburg MV) below the SMT. Sediments retrieved from Ginsburg MV had a distinct smell of petroleum below 40 cm bsf. No depth corrections were made as only gravity cores were taken from these MVs. The actual depth of the SMTs was therefore most likely 10 to 40 cm below the sediment depth indicated in Figure 6. In contrast to the observed depletion of sulphate to concentrations <0.4 mM below the SMT at Gemini MV and the "No Name" structure, sulphate concentrations showed a minimum between 30 to 70 cm and an increase to values ≥17 mM with depth below 90 cm at Ginsburg MV. The total diffusive sulphate flux was therefore calculated from both, the upward and the downward gradients at Ginsburg MV. At Ginsburg MV, Gemini MV and the "No Name" structure, methane and downward sulphate gradients ranged from 0.02 to 0.05 and –0.11 to -0.92 μmol cm^{-4}, respectively (Tab. 2). The upward sulphate gradient at Ginsburg MV was 0.35 μmol cm^{-4}. Sulphide concentrations peaked in the SMTs with values between 4.7 to 7.6 mM (Fig. 6 b, d, f) and steepest gradients were determined with values between 0.04 to 0.32 (upward) and –0.06 to –0.15 (downward) μmol cm^{-4}, respectively (Tab. 2).

3.4.2. Diffusive Fluxes

The diffusive flux calculations from pore water profiles of Ginsburg MV, Gemini MV and the "No Name" structure indicate that the diffusive sulphate fluxes exceeded the methane fluxes (by 15.5-, 18.5- and 2.5-fold, respectively according to the calculation). This suggests a decoupling of AOM and SR at these structures similar to the observations made at Bonjardim MV (Tab. 2). The calculated cumulative (upward + downward) sulphide flux accounted for 66, 70 and 146% of the sulphate fluxes at Ginsburg MV, Gemini MV and the "No Name" structure, respectively. The composition of the microbial community was not investigated here.

3.5. Lipid biomarkers of carbonate crusts

Exposed carbonate crusts were observed at the mud volcanoes Ginsburg, Hesperides and Faro. Additionally, high amounts of broken carbonate chimneys were found at Hesperides and Faro MV. Both crusts and chimney pieces were absent at Capt. Arutyunov MV, Bonjardim MV and the "No Name" structure according to our visual inspections. We could retrieve crust samples from the summits of Hesperides and Faro MV for further analyses of the lipid signatures of the crusts.

3.5.1. Hesperides MV

Carbonate crusts of Hesperides MV contained archaeal and bacterial lipids diagnostic for methanotrophic communities and processes. Archaeal lipids were strongly depleted in $\delta^{13}C$ with minimum values of –97‰ (archaeol) whereas bacterial FAs were only moderately depleted with

minimum values of –43‰ (ai-$C_{15:0}$, Tab. 3). Only trace amounts of *sn2*-hydroxyarchaeol were detected among the archaeal diethers. Isoprenoidal hydrocarbons were dominated by 2,6,10,15,19-pentamethylicosane (PMI:0) and contained comparably low amounts of a crocetane / 2,6,10,14-tetramethylhexadecane (phytane) mixture and ΣPMI:1 (comprising 2 isomers). The FA fraction in the carbonate was dominated by $C_{16:0}$ followed by $C_{18:0}$ with $\delta^{13}C$-values >-28‰ (Tab. 3). FAs putatively specific for SRB involved in AOM such as $C_{16:1\omega5}$, i-$C_{15:0}$ and ai-$C_{15:0}$ (Elvert et al., 2003; Blumenberg et al., 2004), were approximately 3 to 4.8 times lower in concentration compared to $C_{16:0}$. However, in contrast to abundant FAs, stable carbon isotope compositions of i-$C_{15:0}$, ai-$C_{15:0}$ and $C_{16:1\omega5}$ showed a moderate depletion in ^{13}C (Tab. 3). Moreover, in comparison to specific archaeal lipids, diagnostic bacterial FAs were roughly an order of magnitude lower in concentration.

3.5.2. Faro MV

All archaeal and bacterial lipids found in the carbonate crust of Faro MV were strongly depleted in ^{13}C (Tab. 3) with minimum $\delta^{13}C$ values of –114‰ (archaeol) in diagnostic archaeal diether lipids and –99‰ (i-$C_{15:0}$) in specific bacterial FAs (Tab. 3). Archaeal diether lipids were dominated by archaeol and contained comparably low amounts of *sn2*-hydroxyarchaeol. Isoprenoidal hydrocarbons were dominated by PMI:2 (9 isomers) followed by PMI:1 (2 isomers) and relatively high amounts of crocetane/phytane. Specific FAs showed comparably small differences in abundance and $\delta^{13}C$-values (Tab. 3). However, ai-$C_{15:0}$ was the most dominant FA with a roughly 2-fold higher concentration compared to i-$C_{15:0}$ and $C_{16:1\omega5}$. The FA cy$C_{17:0\omega5,6}$ was not detected. Concentrations of specific FAs were comparable to specific archaeal lipids.

4. DISCUSSION

4.1. Evidence of Methane-Driven Geochemical and Biological Activity at Mud Volcanoes of the Gulf of Cadiz

Active marine mud volcanoes have been identified as important escape pathways of hydrocarbon gases and may even contribute to atmospheric green house gases (Dimitrov, 2002; Judd et al., 2002; Kopf, 2002; Damm and Budéus, 2003; Dimitrov, 2003; Sauter et al., 2006). However, high methane fluxes reaching surface sediments may support high biomasses of methane-oxidizing microorganisms, and via their sulphide production also thiotrophic, giant bacteria and other chemosynthetic fauna which form a filter against gas emission to the hydrosphere (Olu et al., 1997b; Sahling et al., 2002; Werne et al., 2002; Boetius and Suess, 2004; Milkov et al., 2004; Cordes et al., 2005). Furthermore, methane venting is often associated with the precipitation of authigenic carbonates which sequester methane derived CO_2 at the seafloor (Aloisi et al., 2000; Kopf, 2002; Boetius and Suess, 2004; Hensen et al., 2004). These carbonates may also serve as paleo-indicators of previously active phases of quiescent or fossil seeps (Ritger et al., 1987; Peckmann et al., 1999; Thiel et al., 1999).

The Gulf of Cadiz is characterised by numerous mud volcanoes (Fig. 1) which have been intensely surveyed since their discovery in 1999 (Kenyon et al., 2000; Kenyon et al., 2001; Somoza et al., 2002; Pinheiro et al., 2003). Among the findings indicative of high past and present methane seepage are the occurrence of hydrate-bearing sediments, authigenic carbonates and seep related biota at several mud volcanoes (Gardner, 2001; Diaz-Del-Rio et al., 2003; Pinheiro et al., 2003; Somoza et al., 2003). Yet, the present activity of these structures in relation to methane emission to the hydrosphere remains unknown. The observations during cruise SO-

175 revealed only few traces of methane reaching surface sediment horizons (here referring to the upper decimetres bsf reachable by biota) at the centres of the mud volcanoes Capt. Arutyunov, Bonjardim, Ginsburg and Hesperides, and the "No Name" structure. No visible fluid or gas escape to the hydrosphere was detected with video observations, indicating that the mud volcanoes may be relatively inactive and that the methane flux may be consumed within subsurface sediment horizons. In contrast, highly active seep systems such as Hydrate Ridge, the Gulf of Mexico or Håkon Mosby Mud Volcano show maximal methane consumption and sulphide production at the sediment surface, and emit methane into the hydrosphere through focused gas and fluid escape pathways, despite the high methane and sulphate turnover rates consuming substantial fractions of the methane flux (Boetius et al., 2000; Damm and Budéus, 2003; Treude et al., 2003; Joye et al., 2004; De Beer et al., 2006; Sauter et al., 2006).

The high sulphide fluxes from anaerobic methane consumption at active seeps are utilised by thiotrophic communities, e.g. mats of giant bacteria like *Beggiatoa sp.*, various chemosynthetic bivalves like *Calyptogena sp.*, *Acharax sp.*, *Bathymodiolus sp.* and by several siboglinid tubeworm species (Sibuet and Olu, 1998). Such communities often colonise large areas at highly active seeps. Furthermore, these organisms are adapted to different geochemical settings and can be used as indicators for high methane fluxes and turnover in surface sediments. Three types of indicator communities were so far observed at low abundances at the investigated mud volcanoes. Some small (ca. 20 cm diameter) blackish sediment patches covered with white bacterial mats were observed by towed camera systems at Faro MV indicating locally elevated fluxes of sulphide (likely AOM-derived) reaching the surface of the seafloor (Fig. 6d). Few specimen of the deep dwelling thiotrophic bivalve *Acharax sp.* were recovered from Faro MV and previously from Ginsburg MV (Gardner, 2001). Members of the family *Solemyidae* to which *Acharax sp.* belongs are mostly deep burrowing and occur in seep habitats with low or moderate methane and

sulphide fluxes where they can take up sulphide through their foot from subsurface accumulations (Sibuet and Olu, 1998; Sahling et al., 2002; Treude et al., 2003). At Hydrate Ridge for instance, *Acharax sp.* mines subsurface sediments for sulphide pockets below 15 cm sediment depth (Sahling et al., 2002). As a third indicator species, tubeworms were recovered from Capt. Arutyunov and previously observed at Bonjardim MV (Pinheiro et al., 2003). As adult animals, these worms are lacking a mouth, gut and anus and are hence depending on energy and carbon sources provided by symbiotic, thiotrophic or methanotrophic bacteria (Southward et al., 1981; Dando et al., 1994; Gebruk et al., 2003; Southward et al., 2005). At Capt. Arutyunov MV, the moderate ^{13}C-depletion of worm-derived membrane lipids (ca. -40‰) indicates a thiotrophic or mixed methanotrophic/thiotrophic feeding mode of the tubeworm symbionts. This is concluded on the basis of the δ^{13}C-value of -48‰ of the source methane (Nuzzo et al., 2005). Aerobic methanotrophic bacteria are characterised by a considerable depletion in the ^{13}C-content of membrane lipids in comparison to source methane (Hanson and Hanson, 1996), which was not reflected in the tubeworm isotope signature.

4.2. Hotspots of hydrocarbon turnover at the mud volcanoes of the Gulf of Cadiz

The observed patterns of seep related biota is in good agreement with the observed geochemical gradients. All mud volcanoes investigated here showed a complete depletion of methane and sulphate within the subsurface SMT. At Capt. Arutyunov and Bonjardim MV, the SMT was positioned at 25 to 40 cm and 45 to 70 cm bsf, respectively (Fig. 4a, 5a), and reflected in elevated AOM and SR rates within this zone. Generally, integrated rate measurements were comparable to the diffusive fluxes at Capt. Arutyunov and Bonjardim MV (Tab. 3). Also, concentration measurements of methane and sulphate and the resulting estimates of diffusive methane and

sulphate fluxes at Ginsburg MV, Gemini MV and the "No Name" structure indicate that sulphate-dependent AOM is a widespread microbial process in the centres of the mud volcanoes of the Gulf of Cadiz. However, as we cannot exclude a potential advective transport component in sediments of the surveyed mud volcanoes and due to shortcomings in the vertical resolution of pore water profiles, the estimates of fluxes presented here should be considered with caution.

With respect to methane fluxes and microbial turnover rates at the time of our investigation, Capt. Arutyunov MV was the most active of the investigated structures followed by Bonjardim, Ginsburg and Gemini MV, while "No Name" was the least active structure (Tab. 2). Furthermore, highest turnover rates and fluxes coincided with the shallowest SMT comparing all investigated MVs. Hence, compared to other marine gas seeps and methane-rich environments, the Gulf of Cadiz MVs investigated here showed a low or medium range in methane turnover rates, reflecting the relatively low methane fluxes. At the Namibian continental slope, the north western Black Sea and Chilean shelf and the western Argentinean basin for instance, the SMT is located several meters bsf and methane fluxes are low with values usually <55 mmol m^{-2} yr^{-1} (Niewöhner et al., 1998; Jørgensen et al., 2001; Hensen et al., 2003; Treude et al., 2005). These values are comparable to Ginsburg and Gemini MV as well as to the "No Name" structure. The AOM activity and diffusive methane fluxes at Capt. Arutyunov and Bonjardim MV were substantially higher than those at Ginsburg MV, Gemini MV and the "No Name" structure. However, areal rates and diffusive fluxes at Capt. Arutyunov and Bonjardim MV are still two orders of magnitude lower in comparison to other cold seeps, which bear gas hydrates at their stability limit such as Håkon Mosby Mud Volcano, Hydrate Ridge and the Gulf of Mexico. In such environments with active fluid flow (>100 cm yr^{-1}) and gas emission via ebullition, methane fluxes were estimated with values >8.5 mol m^{-2} yr^{-1} (Torres et al., 2002; Luff and Wallmann,

2003; De Beer et al., 2006) and AOM reached values >4 mol m^{-2} yr^{-1}, i.e. >0.5 µmol cm^{-3} d^{-1} (Treude et al., 2003; Joye et al., 2004).

In vitro experiments with sediment slurries and *ex situ* tracer injection assays have previously shown that AOM and SR are in a 1:1 molar stoichiometry if methane is the sole carbon source (Nauhaus et al., 2002; Treude et al., 2003). In spite of the putative loss of methane during subsampling, the deviation from the 1:1 stoichiometry between AOM and SR as well as between the sulphate and methane fluxes (Tab. 2) indicates the presence of electron donors other than methane for SR at the investigated MVs. SRR were always highest at the depth of the SMT but just above detection limit in the overlying sediments of Capt. Arutyunov and Bonjardim MV (Figs. 4c, 5c). Hence, a substantial contribution to SR by pelagic organic matter input can be ruled out. However, our data provide evidence for the presence of other hydrocarbons beside methane in the subsurface sediments of several mud volcanoes. Sulphate reducing bacteria can use a variety of short and long chain alkanes and complex aliphatic and aromatic compounds (Rueter et al., 1994; Widdel and Rabus, 2001). At Capt. Arutyunov and Bonjardim MV the presence of complex hydrocarbons is indicated by the strong unresolved complex mixture (UCM) of hydrocarbons in sediment samples from the SMT and deeper sediment horizons. Furthermore, C_2-C_4 compounds declined at the depth of the SMT (Figs. 4b, 5b), indicating their consumption in this zone. At Bonjardim MV, the deviation between AOM and SR was higher compared to Capt. Arutyunov MV coinciding with higher concentrations of C_{2+} compounds. Furthermore, Mazurenko et al. (2003) observed a composition of hydrocarbon gases at Ginsburg MV similar to those detected at Bonjardim MV. Nuzzo et al. (2005) and Stadnitskaia et al. (2006) showed that methane is commonly of a thermogenic origin at mud volcanoes in the Gulf of Cadiz. Hence, SR fuelled by higher hydrocarbons could be an important microbial process in the MV sediments of the Gulf of Cadiz in addition to methane oxidation. Similar results were obtained in a study of

cold seeps of the Gulf of Mexico where SR rates exceed AOM rates up to 10-fold, fuelled by a variety of hydrocarbons and petroleum in the sediments (Joye et al., 2004).

In conclusion, our biogeochemical measurements as well as biological and geological observations indicate that elevated methane fluxes are associated with the centres of the MVs studied during cruise SO-175. However, at the investigated sites, all methane was consumed anaerobically in subsurface sediments and we could not observe any emission of methane to the hydrosphere. However, there is evidence for extensive fluid and/or gas escape in the past as indicated by the widespread occurrence of massive carbonate chimneys and crusts (Diaz-Del-Rio et al., 2003; Somoza et al., 2003), of which at least the latter bear AOM signals. Another geological evidence for temporally varying activities of mud volcanism in the Gulf of Cadiz are the typical "Christmas tree" structures observed on high-resolution seismic profiles (Somoza et al., 2002; Somoza et al., 2003). Such patterns are probably caused by eruptive events followed by phases of dormancy. This so-called multiphase activity is a common behaviour in many terrestrial mud volcanoes (e.g. Lokbatan MV; Aliyev et al., 2002; Dimitrov, 2003; Kholodov, 2002). It is therefore possible that mud volcanism in the Gulf of Cadiz is in a transient state of low activity at present.

4.4. Identity of Methane Oxidising Communities in Sediments and Carbonate Crusts

Fingerprinting of diagnostic lipids is a common tool for the chemotaxonomic identification of microorganisms (Madigan et al., 2000; Boschker and Middelburg, 2002). This approach has been used extensively to examine anaerobic methanotrophic organisms, because the carbon isotope fractionation associated with AOM leads to specific, very depleted $\delta^{13}C$-signatures of lipid biomarkers (Hinrichs et al., 1999; Elvert et al., 2001; Blumenberg et al., 2004). The dominance of

bacterial and archaeal lipids with low $\delta^{13}C$-values in sediments and carbonates indicate that AOM is a major biomass-generating process at the investigated MVs. Differences in the abundances of specific archaeal isoprenoidal diethers, hydrocarbons and bacterial FAs, as well as varying $\Delta\delta^{13}C$ values of these lipids (compared to source methane) indicate that several phylogenetic groups of methanotrophic communities mediate AOM in the Gulf of Cadiz. Elevated concentrations and associated low $\delta^{13}C$-signatures of specific archaeal and bacterial membrane lipids corresponded with elevated AOM and SR rates in sediments of the SMT at Capt. Arutyunov and Bonjardim MV (Fig. 4e-g, 5e-g, Tab. 3). In combination with 16S rDNA analysis, the biomarker patterns give evidence that AOM is mediated by a microbial community consisting of methanotrophic archaea and SRB phylogenetically related to those which were previously found at other methane seeps (Boetius et al., 2000; Michaelis et al., 2002; Orphan et al., 2002; Teske et al., 2002; Niemann et al., 2005). Furthermore, the presence of a similar suite of ^{13}C-depleted lipids in abundant authigenic carbonates recovered from Hesperides and Faro MV (Tab.3) indicates higher activities and a more widespread microbial methane turnover in the past.

4.4.1. Methanotrophic Archaea

Previous publications revealed dominant amounts of *sn2*-hydroxarchaeol relative to archaeol in ANME-2 dominated habitats, whereas the reverse was observed in ANME-1 dominated systems (Blumenberg et al., 2004; Elvert et al., 2005; Niemann et al., 2005). Moreover, ANME-2 communities were found to comprise high contents of crocetane, whereas it seems to be present at low concentrations in ANME-1 (Elvert et al., 1999; Boetius et al., 2000; Blumenberg et al., 2004). Stable carbon isotope fractionations were found to be higher in ANME-2 compared to ANME-1 dominated habitats (Orphan et al., 2002) with $\Delta\delta^{13}C$-values (archaeol relative to the

source methane) ranging between 34 to 53‰ and 11 to 37‰, respectively (Hinrichs et al., 1999; Boetius et al., 2000; Elvert et al., 2001; Orphan et al., 2002; Teske et al., 2002; Blumenberg et al., 2004; Niemann et al., 2005).

In the Gulf of Cadiz, a high *sn2-hydroxy*archaeol to archaeol ratio of 1.7:1 was detected at Capt. Arutyunov MV indicating that this system is dominated by ANME-2 archaea (Blumenberg et al., 2004; Elvert et al., 2005). Accordingly, a high $\Delta\delta^{13}$C-value of 42‰ of archaeol compared to the source methane (-48‰, Nuzzo et al., 2005) was observed. Furthermore, the dominance of ANME-2 compared to ANME-1 sequences in the clone library from Capt. Arutyunov MV suggests a dominance of ANME-2 in this SMT. However, the SMT of Capt. Arutyunov MV also contained other typical seep associated 16S rDNA sequences, including crenarcheota of the Marine Benthic Group B, which are often found at methane seeps, but whose function remains unknown (Knittel et al. 2005). At Bonjardim MV, a lower *sn2*-hydroxyarchaeol to archaeol ratio of 0.7:1 combined with lower $\Delta\delta^{13}$C-values between the biomarkers (e.g. archaeol, 31.5‰) relative to the source methane (-49.5 to -51 ‰, Nuzzo et al., 2005; Stadnitskaia et al., 2006) lie between published values from systems dominated by either ANME-1 or ANME-2 (Blumenberg et al., 2004; Elvert et al., 2005; Niemann et al., 2005). This suggests a mixed ANME community in these sediments. Similar characteristics have been observed in carbonate crusts at Faro MV. At this mud volcano, substantial amounts of ^{13}C-depleted crocetane were detected giving additional indications for an involvement of ANME-2 in AOM at the time of carbonate precipitation. At Hesperides MV, only trace amounts of *sn2*-hydroxyarchaeol were detected, and thus indicate the dominance of ANME-1 communities. No distinct environmental preferences have been found for either group, most likely because the taxonomic level investigated comprises a relatively large diversity of microorganisms.

4.4.2. Sulphate Reducing Bacteria

At many different cold seep settings, ANME-1 and ANME-2 archaea have been found in consortium with SRB of the Seep-SRB1 cluster belonging to the *Desulfosarcina/Desulfococcus* group (Knittel et al., 2003). However, this cluster apparently comprises physiologically different ecotypes that are distinguished by very specific FA patterns according to their association to either ANME-1 or to ANME-2 (Elvert et al., 2003; Blumenberg et al., 2004). FA signatures in environmental systems dominated by ANME-1 / Seep-SRB1 communities comprise high contents of ai-$C_{15:0}$ relative to i-$C_{15:0}$ (Blumenberg et al., 2004; Elvert et al., 2005), whereas systems dominated by ANME-2 / Seep-SRB1 communities comprise the unusual FA cy$C_{17:1\omega5,6}$ and dominant contents of $C_{16:1\omega5}$ but almost balanced ratios of ai-$C_{15:0}$ relative to i-$C_{15:0}$ (Elvert et al., 2003; Blumenberg et al., 2004).

The dominance of the unusual FAs $C_{16:1\omega5}$ and cy$C_{17:1\omega5,6}$ and an almost equal ratio of the iso- and anteiso- branched $C_{15:0}$ FAs in sediments of the SMT at Capt. Arutyunov MV are in very good agreement with the archaeal lipid data and published lipid signatures of the Seep-SRB1 ecotype associated with ANME-2. This finding is also in accordance with the predominance of Seep-SRB1 sequences in the bacterial clone library. As expected from the detection of potentially diverse ANME communities at Bonjardim MV, the FA signature shows characteristics of both SRB ecotypes previously identified as bacterial partners in AOM. The high ratio of ai-$C_{15:0}$ compared to i-$C_{15:0}$ (8.4:1) is indicative for the Seep-SRB1 ecotype associated with ANME-1 while the high abundance of $C_{16:1\omega5}$ indicates the ecotype associated with ANME-2. This finding is similar to results obtained from a carbonate crust at Faro MV where a comparable fatty acid pattern has been detected. At Bonjardim MV, however, several FAs carry δ^{13}C-signatures that are comparable to the source methane and do not show any fractionation. This suggests a

contribution to carbon biomass from processes other than methane consumption. A similar mixture of carbon sources to biomass could also explain the unspecific signature of FAs in the carbonate of Hesperides MV.

Another striking difference is the comparably high lipid concentration in the carbonate recovered from Faro compared to that recovered from Hesperides MV. A rather recent formation of the sampled carbonate from Faro MV appears likely, as these were stained black from sulphide and recovered together with some living specimens of the chemosynthetic bivalve *Acharax sp.* A possible explanation for the difference in AOM-derived lipid contents could be that the sampled carbonate crust from Hesperides is older than that recovered from Faro MV and has been exposed to oxic sea water and lipid diagenesis for a longer time which is indicated by the dominant abundance of saturated FAs relative to unsaturated FAs. This may also explain the dominance of PMI's with higher degrees of saturation at Hesperides compared to Faro MV assuming that the diagenetic alteration of unsaturated isoprenoid hydrocarbons is similar to that of FAs.

5. CONCLUSIONS

At the centres of the mud volcanoes Captain Arutyunov, Bonjardim, Ginsburg, Gemini and Faro as well as at the "No Name" structure, several indications for a slow upward fluid and gas flux were found. Our data suggest a complete consumption of methane and higher hydrocarbons in the sediments of the studied mud volcanoes at depths of 20-300 cm below seafloor. We found no indication of hydrocarbons reaching near surface sediments or the hydrosphere except from the visual observation of small patches of reduced sediments covered by giant sulphide-oxidizing bacteria indicating localised near-surface AOM activities. However, with respect to the limited extend of video surveys and sediment sampling in this study, a potential seepage of hydrocarbons into the water column can not be ruled out. The overlap of methane and sulphate depletion with sulphide production shows that methane oxidation processes are mediated microbially under anaerobic conditions. Correspondingly, anaerobic oxidation of methane and sulphate reduction rates show a peak in a distinct, narrow methane-sulphate transition zone in the subsurface sediments of the mud volcano centres. Highest turnover rates and fluxes coincided with the shallowest SMT depths with Capt. Arutyunov MV as the most active system in the study area, followed by the mud volcanoes Bonjardim, Ginsburg, and Gemini and finally the "No Name" structure. In comparison to other gas seeps, methane fluxes and turnover rates are low to mid range in the Gulf of Cadiz. In addition to AOM, the anaerobic oxidation of higher hydrocarbons could be an important process fuelling SR. Lipid biomarker patterns and 16S rDNA clone sequences from the sediments and carbonates of the AOM hotspots provide evidence that both of the previously described ANME-1 / Seep-SRB1 and ANME-2 / Seep-SRB1 communities mediate AOM at mud volcanoes in the Gulf of Cadiz. The finding of their lipid signatures in carbonate crusts at the centres of the investigated mud volcanoes indicates that at least some of

the vast amounts of carbonates littering mud volcanoes and diapiric ridges in the northern part of the Gulf of Cadiz are linked to methane seepage.

Acknowledgements - The authors thank the captain and crew as well as the shipboard scientific community of the R/V SONNE for their help at sea. We also thank Tomas Wilkop, Imke Müller and Viola Beier for technical assistance with laboratory analyses. Scientific exchange and collaboration were supported by the CRUP-ICCTI/DAAD Portuguese/German Joint Action *Geophere/Biosphere Coupling Processes in the Gulf of Cadiz* (A-15/04; Boetius, Pinheiro). This work was also supported by the ESF Eurocores/Euromargins MVSEIS project (01-LEC_EMA24F; PDCTM72003/DIV/40018-MVSEIS), as well as by the IRCCM (International Research Consortium on Continental Margins at International University Bremen, Germany), the Max Planck Society and the project MUMM (Mikrobielle Umsatzraten von Methan in gashydrathaltigen Sedimenten, FN 03G0608A) supported by the German Ministry of Education and Research (BMBF). This is publication GEOTECH-234 of the program GEOTECHNOLOGIEN of the BMBF and German Research Foundation (DFG).

REFERENCES

Akhmanov, G. and Woodside, J., 1998. Mud volcanic samples in the context of the mediterranean ridge mud diapiric belt. In: Robertson, A. H. F., Emeis, K.-C., Richter, C., and Camerlenghi, A. Eds.), *Proceedings of the Ocean Drilling Program, Scienctific Results*. Ocean Drilling Program, College Station, TX.

Aloisi, G., Bouloubassi, I., Heijs, S. K., Pancost, R. D., Pierre, C., Damste, J. S. S., Gottschal, J. C., Forney, L. J., and Rouchy, J. M., 2002. CH4-consuming microorganisms and the formation of carbonate crusts at cold seeps. *Earth and Planetary Science Letters* **203**, 195-203.

Aloisi, G., Pierre, C., Rouchy, J.-M., Foucher, J.-P., Woodside, J., and Party, T. M. S., 2000. Methane-related authigenic carbonates of eastern Mediterranean Sea mud volcanoes and their possible relation to gas hydrate destabilisation. *Earth and Planetary Science Letters* **184**, 321-338.

Barnes, R. O. and Goldberg, E. D., 1976. Methane Production and Consumption in Anoxic Marine-Sediments. *Geology* **4**, 297-300.

Berner, R. A., 1980. *Early Diagenesis - A Theoretical Approach*. Princeton University Press, Princeton, New Jersey.

Blumenberg, M., Seifert, R., Reitner, J., Pape, T., and Michaelis, W., 2004. Membrane lipid patterns typify distinct anaerobic methanotrophic consortia. *Proc Natl Acad Sci U S A* **101**.

Boetius, A., Ravenschlag, K., Schubert, C., Rickert, D., Widdel, F., Gieseke, A., Amann, R., Jørgensen, B. B., Witte, U., and Pfannkuche, O., 2000. A marine microbial consortium apparently mediating anaerobic oxidation of methane. *Nature* **407**, 623-626.

Boetius, A. and Suess, E., 2004. Hydrate Ridge: a natural laboratory for the study of microbial life fueled by methane from near-surface gas hydrates. *Chemical Geology* **205**, 291-310.

Bohrmann, G., Ivanov, M., Foucher, J. P., Spiess, V., Bialas, J., Greinert, J., Weinrebe, W., Abegg, F., Aloisi, G., Artemov, Y., Blinova, V., Drews, M., Heidersdorf, F., Krabbenhoft, A., Klaucke, I., Krastel, S., Leder, T., Polikarpov, I., Saburova, M., Schmale, O., Seifert, R., Volkonskaya, A., and Zillmer, M., 2003. Mud volcanoes and gas hydrates in the Black Sea: new data from Dvurechenskii and Odessa mud volcanoes. *Geo-Marine Letters* **23**, 239-249.

Boschker, H. T. S. and Middelburg, J. J., 2002. Stable isotopes and biomarkers in microbial ecology. *FEMS Microbiol Ecol* **40**, 85-95.

Boudreau, B. P., 1997. *Diagenetic models and their implementation: modelling transport and reactions in aquatic sediments*. Springer, Berlin.

Charlou, J. L., Donval, J. P., Zitter, T., Roy, N., Jean-Baptiste, P., Foucher, J. P., and Woodside, J., 2003. Evidence of methane venting and geochemistry of brines on mud volcanoes of the eastern Mediterranean Sea. *Deep-Sea Research Part I-Oceanographic Research Papers* **50**, 941-958.

Cita, M. B., Ryan, W. B. F., and Paggi, L., 1981. Prometheus Mud Breccia: an example of shale diapirism in the western Mediterranean Ridge, *Annales Ge´ologiques Des Pays Helle´niques*.

Cline, J. D., 1969. Spectrophotometric Determination of Hydrogen Sulfide in Natural Waters. *Limnol Oceanogr* **14**, 454-458.

Cordes, E. E., Arthur, M. A., Shea, K., Arvidson, R. S., and Fisher, C. R., 2005. Modeling the mutualistic interactions between tubeworms and microbial consortia. *Plos Biology* **3**, 497-506.

Damm, E. and Budéus, G., 2003. Fate of vent-derived methane in seawater above the Hakon Mosby mud volcano (Norwegian Sea). *Mar Chem* **82**, 1-11.

Dando, P. R., Bussmann, I., Niven, S. J., O'hara, S. C. M., Schmaljohann, R., and Taylor, L. J., 1994. A methane seep area in the Skagerrak, the habitat of the pogonophore *Siboglinum poseidoni* and the bivalve mollusc *Thyasira sarsi*. *Mar Ecol Prog Ser* **107**, 157-167.

De Beer, D., Sauter, E., Niemann, H., Kaul, N., Foucher, J. P., Witte, U., Schluter, M., and Boetius, A., 2006. In situ fluxes and zonation of microbial activity in surface sediments of the Hakon Mosby Mud Volcano. *Limnol Oceanogr* **51**, 1315-1331.

Diaz-Del-Rio, V., Somoza, L., Martinez-Frias, J., Mata, M. P., Delgado, A., Hernandez-Molina, F. J., Lunar, R., Martin-Rubi, J. A., Maestro, A., Fernandez-Puga, M. C., Leon, R., Llave, E., Medialdea, T., and Vazquez, J. T., 2003. Vast fields of hydrocarbon-derived carbonate chimneys related to the accretionary wedge/olistostrome of the Gulf of Cadiz. *Marine Geology* **195**, 177-200.

Dimitrov, L. I., 2002. Mud volcanoes - the most important pathway for degassing deeply buried sediments. *Earth-Science Reviews* **59**, 49-76.

Dimitrov, L. I., 2003. Mud volcanoes - a significant source of atmospheric methane. *Geo-Marine Letters* **23**, 155-161.

Elvert, M., Boetius, A., Knittel, K., and Jorgensen, B. B., 2003. Characterization of specific membrane fatty acids as chemotaxonomic markers for sulfate-reducing bacteria involved in anaerobic oxidation of methane. *Geomicrobiol J* **20**, 403-419.

Elvert, M., Greinert, J., Suess, E., and Whiticar, M. J., 2001. Carbon isotopes of biomarkers derived from methane-oxidizing microbes at Hydrate Ridge, Cascadia convergent margin. In: Paull, C. K. and Dillon, W. P. Eds.), *Natural gas hydrates: Occurrence, distribution, and dynamics*. American Geophysical Union, Washington DC.

Elvert, M., Hopmans, E. C., Treude, T., Boetius, A., and Hinrichs, K.-U., 2005. Spatial variatons of archaeal-bacterial assambladges in gas hydrate bearing sediments at a cold seep: Implications from a high resolution molecular and isotopic approach. *Geobiology* **3**, 195-209.

Elvert, M., Suess, E., and Whiticar, M. J., 1999. Anaerobic methane oxidation associated with marine gas hydrates: superlight C-isotopes from saturated and unsaturated C_{20} and C_{25} irregular isoprenoids. *Naturwissenschaften* **86**, 295-300.

Etiope, G. and Klusman, R. W., 2002. Geologic emissions of methane to the atmosphere. *Chemosphere* **49**, 777-789.

Etiope, G. and Milkov, A. V., 2004. A new estimate of global methane flux from onshore and shallow submarine mud volcanoes to the atmosphere. *Environmental Geology* **46**, 997-1002.

Felbeck, H., 1983. Sulfide Oxidation and Carbon Fixation by the Gutless Clam Solemya-Reidi - an Animal-Bacteria Symbiosis. *J Comp Physiol* **152**, 3-11.

Fisher, C. R., 1990. Chemoautotrophic and Methanotrophic Symbioses in Marine-Invertebrates. *Reviews in Aquatic Sciences* **2**, 399-436.

Gardner, J. M., 2001. Mud volcanoes revealed and sampled on the Western Moroccan continental margin. *Geophysical Research Letters* **28**, 339-342.

Gebruk, A. V., Krylova, E. M., Lein, A. Y., Vinogradov, G. M., Anderson, E., Pimenov, N. V., Cherkashev, G. A., and Crane, K., 2003. Methane seep community of the Hakon Mosby mud volcano (the Norwegian Sea): composition and trophic aspects. *Sarsia* **88**, 394-403.

Gillian, F. T., Johns, R. B., Verheyen, T. V., Nichols, P. D., Esdaile, R. J., and Bavor, H. J., 1981. Monounsaturated fatty acids as specific bacterial markers in marine sediments, *Advances in Organic Geochemistry*.

Grasshoff, K., Ehrhardt, M., and Kremling, K., 1983. *Methods of seawater analysis*. Verlag Chemie, Weinheim.

Haese, R. R., Meile, C., Van Cappellen, P., and De Lange, G. J., 2003. Carbon geochemistry of cold seeps: Methane fluxes and transformation in sediments from Kazan mud volcano, eastern Mediterranean Sea. *Earth and Planetary Science Letters* **212**, 361-375.

Hanselmann, K. W., 1991. Microbial Energetics Applied to Waste Repositories. *Experientia* **47**, 645-687.

Hanson, R. S. and Hanson, T. E., 1996. Methanotrophic bacteria. *Microbiological Reviews* **60**, 439-&.

Hensen, C., Wallmann, K., Schmidt, M., Ranero, C. R., and Suess, E., 2004. Fluid expulsion related to mud extrusion off Costa Rica - A window to the subducting slab. *Geology* **32**, 201-204.

Hensen, C., Zabel, M., Pfeifer, K., Schwenk, T., Kasten, S., Riedinger, N., Schulz, H. D., and Boettius, A., 2003. Control of sulfate pore-water profiles by sedimentary events and the significance of anaerobic oxidation of methane for the burial of sulfur in marine sediments. *Geochimica Et Cosmochimica Acta* **67**, 2631-2647.

Hinrichs, K.-U. and Boetius, A., 2002. The anaerobic oxidation of methane: New insights in microbial ecology and biogeochemistry. In: Wefer, G., Billett, D., and Hebbeln, D. Eds.), *Ocean Margin Systems*. Springer-Verlag, Berlin, Berlin.

Hinrichs, K.-U., Hayes, J. M., Sylva, S. P., Brewer, P. G., and Delong, E. F., 1999. Methane-consuming archaebacteria in marine sediments. *Nature* **398**, 802-805.

Iversen, N. and Jørgensen, B. B., 1985. Anaerobic methane oxidation rates at the sulfate-methane transition in marine sediments from Kattegat and Skagerrak (Denmark). *Limnol Oceanogr* **30**, 944-955.

Jørgensen, B. B., 1978. A comparison of methods for the quantification of bacterial sulphate reduction in coastal marine sediments. I. Measurements with radiotracer techniques. *Geomicrobiol J* **1**, 11-27.

Jørgensen, B. B., Weber, A., and Zopfi, J., 2001. Sulfate reduction and anaerobic methane oxidation in Black Sea sediments. *Deep-Sea Research Part I-Oceanographic Research Papers* **48**, 2097-2120.

Joye, S. B., Boetius, A., Orcutt, B. N., Montoya, J. P., Schulz, H. N., Erickson, M. J., and Lugo, S. K., 2004. The anaerobic oxidation of methane and sulfate reduction in sediments from Gulf of Mexico cold seeps. *Chemical Geology* **205**, 219-238.

Judd, A. G., Hovland, M., Dimitrov, L. I., Gil, S. G., and Jukes, V., 2002. The geological methane budget at Continental Margins and its influence on climate change. *Geofluids* **2**, 109-126.

Kane, M. D., Poulsen, L. K., and Stahl, D. A., 1993. Monitoring the Enrichment and Isolation of Sulfate-Reducing Bacteria by Using Oligonucleotide Hybridization Probes Designed from Environmentally Derived 16s Ribosomal-Rna Sequences. *Appl Environ Microbiol* **59**, 682-686.

Kenyon, N. H., Ivanov, M. K., Akhmetzhanov, A. M., and Akhmanov, G., 2001. Interdisciplinary Approaches to Geoscience on the North East Atlantic Margin and Mid-Atlantic Ridge. IOC Technical Series no. 60.

Kenyon, N. H., Ivanov, M. K., Akhmetzhanov, A. M., and Akhmanov, G. G., 2000. Multidisciplinary Study of Geological Processes on the North East Atlantic and Western Mediterranean Margins. IOC Technical Series no. 56.

Kholodov, V. N., 2002. Mud Volcanoes: Distribution Regularities and Genesis (Communication 2. Geological–Geochemical Peculiarities and Formation Model). *Lithology and Mineral Resources* **37**, 293-310.

Kimura, H., Sato, M., Sasayama, Y., and Naganuma, T., 2003. Molecular characterization and in situ localization of endosymbiotic 16S ribosomal RNA and RuBisCO genes in the pogonophoran tissue. *Mar Biotechnol* **5**, 261-269.

Knittel, K., Boetius, A., Lemke, A., Eilers, H., Lochte, K., Pfannkuche, O., Linke, P., and Amann, R., 2003. Activity, distribution, and diversity of sulfate reducers and other bacteria in sediments above gas hydrate (Cascadia margin, Oregon). *Geomicrobiol J* **20**, 269-294.

Knittel, K., Lösekann, T., Boetius, A., Kort, R., and Amann, R., 2005. Diversity and distribution of methanotrophic archaea at cold seeps. *Appl Environ Microbiol* **71**, 467-479.

Kopf, A., Bannert, B., Brückmann, W., Dorschel, B., Foubert, A. T. G., Grevemeyer, I., Gutscher, M. A., Hebbeln, D., Heesemann, B., Hensen, C., Kaul, N. E., Lutz, M., Magalhaes, V. H., Marquardt, M. J., Marti, A. V., Nass, K. S., Neubert, N., Niemann, H., Nuzzo, M., Poort, J. P. D., Rosiak, U. D., Sahling, H., Schneider Von Deimling, J., Somoza, L., Thiebot, E., and Wilkop, T. P., 2004. Report and preliminary results of Sonne Cruise SO175, Miami - Bremerhaven, 12.11 - 30.12.2003. Fachbereich Geowissenschaften der Universität Bremen.

Kopf, A. J., 2002. Significance of mud volcanism. *Reviews of Geophysics* **40**, B-1 - B49.

Kopf, A. J., 2003. Global methane emission through mud volcanoes and its past and present impact on the Earth's climate. *International Journal of Earth Sciences* **92**, 806-816.

Krueger, D. M. and Cavanaugh, C. M., 1997. Phylogenetic diversity of bacterial symbionts of Solemya hosts based on comparative sequence analysis of 16S rRNA genes. *Appl Environ Microbiol* **63**, 91-98.

Lane, D. J., Pace, B., Olsen, G. J., Stahl, D. A., Sogin, M. L., and Pace, N. R., 1985. Rapid-Determination of 16s Ribosomal-Rna Sequences for Phylogenetic Analyses. *Proc Natl Acad Sci U S A* **82**, 6955-6959.

Luff, R. and Wallmann, K., 2003. Fluid flow, methane fluxes, carbonate precipitation and biogeochemical turnover in gas hydrate-bearing sediments at Hydrate Ridge, Cascadia Margin: Numerical modeling and mass balances. *Geochimica Et Cosmochimica Acta* **67**, 3403-3421.

Madigan, M. T., Martinko, J. M., and Parker, J., 2000. *Brock Biology of Microorganisms*. Prentice-Hall, Inc.

Maldonado, A. and Comas, M. C., 1992. Geology and Geophysics of the Alboran Sea - an Introduction. *Geo-Marine Letters* **12**, 61-65.

Maldonado, A., Somoza, L., and Pallares, L., 1999. The Betic orogen and the Iberian-African boundary in the Gulf of Cadiz: geological evolution (central North Atlantic). *Marine Geology* **155**, 9-43.

Massana, R., Murray, A. E., Preston, C. M., and Delong, E. F., 1997. Vertical distribution and phylogenetic characterization of marine planktonic Archaea in the Santa Barbara Channel. *Appl Environ Microbiol* **63**, 50-56.

Mazurenko, L. L., Soloviev, V. A., Belenkaya, I., Ivanov, M. K., and Pinheiro, L. M., 2002. Mud volcano gas hydrates in the Gulf of Cadiz. *Terra Nova* **14**, 321-329.

Michaelis, W., Seifert, R., Nauhaus, K., Treude, T., Thiel, V., Blumenberg, M., Knittel, K., Gieseke, A., Peterknecht, K., Pape, T., Boetius, A., Amann, R., Jorgensen, B. B., Widdel, F., Peckmann, J. R., Pimenov, N. V., and Gulin, M. B., 2002. Microbial reefs in the Black Sea fueled by anaerobic oxidation of methane. *Science* **297**, 1013-1015.

Milkov, A. V., 2000. Worldwide distribution of submarine mud volcanoes and associated gas hydrates. *Marine Geology* **167**, 29-42.

Milkov, A. V., Sassen, R., Apanasovich, T. V., and Dadashev, F. G., 2003. Global gas flux from mud volcanoes: A significant source of fossil methane in the atmosphere and the ocean. *Geophysical Research Letters* **30**.

Milkov, A. V., Vogt, P. R., Crane, K., Lein, A. Y., Sassen, R., and Cherkashev, G. A., 2004. Geological, geochemical, and microbial processes at the hydrate-bearing Hakon Mosby mud volcano: a review. *Chemical Geology* **205**, 347-366.

Moss, C. W. and Lambertfair, M. A., 1989. Location of Double-Bonds in Monounsaturated Fatty-Acids of Campylobacter-Cryaerophila with Dimethyl Disulfide Derivatives and Combined Gas Chromatography-Mass Spectrometry. *Journal of Clinical Microbiology* **27**, 1467-1470.

Muyzer, G., Teske, A., Wirsen, C. O., and Jannasch, H. W., 1995. Phylogenetic relationships of Thiomicrospira species and their identification in deep-sea hydrothermal vent samples by denaturing gradient gel electrophoresis of 16S rDNA fragments. *Arch Microbiol* **164**, 165-172.

Nauhaus, K., Boetius, A., Kruger, M., and Widdel, F., 2002. In vitro demonstration of anaerobic oxidation of methane coupled to sulphate reduction in sediment from a marine gas hydrate area. *Environmental Microbiology* **4**, 296-305.

Nichols, P. D., Guckert, J. B., and White, D. C., 1986. Determination of monounsaturated fatty acid double-bond position and geometry for microbial monocultures and complex consortia by capillary GC-MS of their dimethyl disulphide adducts. *J Microbiol Methods* **5**, 49-55.

Niemann, H., Elvert, M., Hovland, M., Orcutt, B., Judd, A. G., Suck, I., Gutt, J., Joye, S. B., Damm, E., Finster, K., and Boetius, A., 2005. Methane emission and consumption at a North Sea gas seep (Tommeliten area). *Biogeosciences* **2**, 335-351.

Niewöhner, C., Hensen, C., Kasten, S., Zabel, M., and Schulz, H. D., 1998. Deep sulfate reduction completely mediated by anaerobic methane oxidation in sediments of the upwelling area off Namibia. *Geochimica et Cosmochimica Acta* **62**, 455-464.

Nuzzo, M., Hensen, C., Hornibrook, E., Brueckmann, W., Magalhaes, V. H., Parkes, R. J., and Pinheiro, L. M., 2005. Origin of Mud Volcano Fluids in the Gulf of Cadiz (E-Atlantic)*EGU General Assembly*, Vienna.

Olu, K., Lance, S., Sibuet, M., Henry, P., Fialamedioni, A., and Dinet, A., 1997a. Cold seep communities as indicators of fluid expulsion patterns through mud volcanoes seaward of the Barbados accretionary prism. *Deep-Sea Research Part I-Oceanographic Research Papers* **44**, 811-&.

Olu, K., Lance, S., Sibuet, M., Henry, P., Fiala-Médioni, A., and Dinet, A., 1997b. Cold seep communities as indicators of fluid expulsion patterns through mud volcanoes seaward of the Barbados accretionary prism. *Deep-Sea Research I* **44**, 811-841.

Orphan, V. J., House, C. H., Hinrichs, K. U., Mckeegan, K. D., and Delong, E. F., 2001. Methane-consuming archaea revealed by directly coupled isotopic and phylogenetic analysis. *Science* **293**, 484-487.

Orphan, V. J., House, C. H., Hinrichs, K. U., Mckeegan, K. D., and Delong, E. F., 2002. Multiple archaeal groups mediate methane oxidation in anoxic cold seep sediments. *Proc Natl Acad Sci U S A* **99**, 7663-7668.

Pancost, R. D., Bouloubassi, I., Aloisi, G., and Damste, J. S. S., 2001. Three series of non-isoprenoidal dialkyl glycerol diethers in cold-seep carbonate crusts. *Organic Geochemistry* **32**, 695-707.

Pancost, R. D., Sinninghe Damsté, J. S., De Lint, S., Van Der Maarel, M. J. E. C., Gottschal, J. C., and Party, T. M. S. S., 2000. Biomarker evidence for widespread anaerobic methane oxidation in Mediterranean sediments by a consortium of methanogenic archaea and bacteria. *Appl Environ Microbiol* **66**, 1126-1132.

Peckmann, J., Thiel, V., Michaelis, W., Clari, P., Gaillard, C., Martire, L., and Reitner, J., 1999. Cold seep deposits of Beauvoisin (Oxfordian; southeastern France) and Marmorito (Miocene; northern Italy): microbially induced authigenic carbonates. *International Journal of Earth Sciences* **88**, 60-75.

Peek, A. S., Feldman, R. A., Lutz, R. A., and Vrijenhoek, R. C., 1998. Cospeciation of chemoautotrophic bacteria and deep sea clams. *Proc Natl Acad Sci U S A* **95**, 9962-9966.

Pinheiro, L. M., Ivanov, M. K., Sautkin, A., Akhmanov, G., Magalhaes, V. H., Volkonskaya, A., Monteiro, J. H., Somoza, L., Gardner, J., Hamouni, N., and Cunha, M. R., 2003. Mud volcanism in the Gulf of Cadiz: results from the TTR-10 cruise. *Marine Geology* **195**, 131-151.

Reeburgh, W. S., 1967. An Improved Interstitial Water Sampler. *Limnol Oceanogr* **12**, 163-&.

Reeburgh, W. S., 1976. Methane consumption in Cariaco Trench waters and sediments. *Earth and Planetary Science Letters* **28**, 337-344.

Reeburgh, W. S., 1996. "Soft spots" in the global methane budget. In: Lidstrom, M. E. and Tabita, F. R. Eds.), *Microbial Growth on C_1 Compounds*. Kluwer Academic Publishers, Dordrecht.

Reeburgh, W. S. and Heggie, D. T., 1977. Microbial methane consumption reactions and their effect on methane distributions in freshwater and marine environments. *Limnol Oceanogr* **22**, 1-9.

Ritger, S., Carson, B., and Suess, E., 1987. Methane-derived authigenic carbonates formed by subduction-induced pore-water expulsion along the Oregon/Washington margin. *Geological Society of American Bulletin* **98**, 147-156.

Rueter, P., Rabus, R., Wilkes, H., Aeckersberg, F., Rainey, F. A., Jannasch, H. W., and Widdel, F., 1994. Anaerobic Oxidation of Hydrocarbons in Crude-Oil by New Types of Sulfate-Reducing Bacteria. *Nature* **372**, 455-458.

Sahling, H., Rickert, D., Lee, R. W., Linke, P., and Suess, E., 2002. Macrofaunal community structure and sulfide flux at gas hydrate deposits from the Cascadia convergent margin, NE Pacific. *Marine Ecology-Progress Series* **231**, 121-138.

Sauter, E. J., Muyakshin, S. I., Charlou, J.-L., Schluter, M., Boetius, A., Jerosch, K., Damm, E., Foucher, J.-P., and Klages, M., 2006. Methane discharge from a deep-sea submarine mud volcano into the upper water column by gas hydrate-coated methane bubbles. *Earth and Planetary Science Letters* **243**, 354-365.

Schmaljohann, R. and Flugel, H. J., 1987. Methane-Oxidizing Bacteria in Pogonophora. *Sarsia* **72**, 91-99.

Sibuet, M. and Olu, K., 1998. Biogeography, biodiversity and fluid dependence of deep-sea cold-seep communities at active and passive margins. *Deep-Sea Research Part II-Topical Studies in Oceanography* **45**, 517-567.

Small, H., Stevens, T. S., and Bauman, W. C., 1975. Novel Ion-Exchange Chromatographic Method Using Conductimetric Detection. *Anal Chem* **47**, 1801-1809.

Somoza, L., Diaz-Del-Rio, V., Leon, R., Ivanov, M., Fernandez-Puga, M. C., Gardner, J. M., Hernandez-Molina, F. J., Pinheiro, L. M., Rodero, J., Lobato, A., Maestro, A., Vazquez, J. T., Medialdea, T., and Fernandez-Salas, L. M., 2003. Seabed morphology and hydrocarbon seepage in the Gulf of Cadiz mud volcano area: Acoustic imagery, multibeam and ultra-high resolution seismic data. *Marine Geology* **195**, 153-176.

Somoza, L., Diaz-Del-Rio, V., Vaszquez, J. T., Pinheiro, L. M., and Hernandez-Molina, F. J., 2002. Numerous methane gas-related sea floor structures identified in Gulf of Cadiz. *EOS* **83**, 541-547.

Southward, A. J., Southward, E. C., Dando, P. R., Barrett, R. L., and Ling, R., 1986. Chemoautotrophic Function of Bacterial Symbionts in Small Pogonophora. *J Mar Biol Assoc U K* **66**, 415-437.

Southward, A. J., Southward, E. C., Dando, P. R., Rau, G. H., Felbeck, H., and Fluegel, H., 1981. Bacterial symbionts and low $^{13}C/^{12}C$ ratios in tissues of Pogonophora indicate unusual nutrition and metabolism. *Nature* **293**, 616-620.

Southward, E. C., Schulze, A., and Gardiner, S. L., 2005. Pogonophora (Annelida): form and function. *Hydrobiologia* **535-536**, 227-251.

Stadnitskaia, A., Ivanov, M. K., Blinova, V., Kreulen, R., and Van Weering, T. C. E., 2006. Molecular and carbon isotopic variability of hydrocarbon gases from mud volcanoes in the Gulf of Cadiz, NE Atlantic. *Marine and Petroleum Geology* **23**, 281-296.

Stadnitskaia, A., Muyzer, G., Abbas, B., Coolen, M. J. L., Hopmans, E. C., Baas, M., Van Weering, T. C. E., Ivanov, M. K., Poludetkina, E., and Damste, J. S. S., 2005. Biomarker and 16S rDNA evidence for anaerobic oxidation of methane and related carbonate precipitation in deep-sea mud volcanoes of the Sorokin Trough, Black Sea. *Marine Geology* **217**, 67-96.

Summons, R. E., Jahnke, L. L., and Roksandic, Z., 1994. Carbon isotopic fractionation in lipids from methanotrophic bacteria: Relevance for interpretation of the geochemical record of biomarkers. *Geochimica Et Cosmochimica Acta* **58**, 2853-2863.

Teske, A., Hinrichs, K. U., Edgcomb, V., Gomez, A. D., Kysela, D., Sylva, S. P., Sogin, M. L., and Jannasch, H. W., 2002. Microbial diversity of hydrothermal sediments in the Guaymas Basin: Evidence for anaerobic methanotrophic communities. *Appl Environ Microbiol* **68**, 1994-2007.

Thiel, V., Peckmann, J., Seifert, R., Wehrung, P., Reitner, J., and Michaelis, W., 1999. Highly isotopically depleted isoprenoids: molecular markers for ancient methane venting. *Geochimica et Cosmochimica Acta* **63**, 3959-3966.

Torres, M. E., Mcmanus, J., Hammond, D. E., De Angelis, M. A., Heeschen, K. U., Colbert, S. L., Tryon, M. D., Brown, K. M., and Suess, E., 2002. Fluid and chemical fluxes in and out of sediments hosting methane hydrate deposits on Hydrate Ridge, OR, I: Hydrological provinces. *Earth and Planetary Science Letters* **201**, 525-540.

Treude, T., Boetius, A., Knittel, K., Wallmann, K., and Jorgensen, B. B., 2003. Anaerobic oxidation of methane above gas hydrates at Hydrate Ridge, NE Pacific Ocean. *Marine Ecology-Progress Series* **264**, 1-14.

Treude, T., Niggemann, J., Kallmeyer, J., Wintersteller, P., Schubert, C. J., Boetius, A., and Jorgensen, B. B., 2005. Anaerobic oxidation of methane and sulfate reduction along the Chilean continental margin. *Geochimica et Cosmochimica Acta* **69**, 2767-2779.

Vogt, P. R., Cherkashev, A., Ginsburg, G. D., Ivanov, G. I., Crane, K., Lein, A. Y., Sundvor, E., Pimenov, N. V., and Egorov, A., 1997a. Haakon Mosby mud volcano: A warm methane

seep with seafloor hydrates and chemosynthesis-based Ecosystem in late Quantemary Slide Valley, Bear Island Fan, Barents Sea passive margin. *EOS Transactions of the American Geophysical Union Supplement* **78**, 187-189.

Vogt, P. R., Cherkashev, G., Ginsburg, G., Ivanov, G. I., Milkov, A., Crane, K., Lein, A., Sundvor, E., Pimenov, N. V., and Egorov, A., 1997b. Haakon Mosby Mud Volcano Provides Unusual Example of Venting. *EOS Transactions of the American Geophysical Union Supplement* **78**, 549, 556-557.

Werne, J. P., Baas, M., and Damste, J. S. S., 2002. Molecular isotopic tracing of carbon flow and trophic relationships in a methane-supported benthic microbial community. *Limnol Oceanogr* **47**, 1694-1701.

Werne, J. P., Haese, R. R., Zitter, T., Aloisi, G., Bouloubassi, L., Heijs, S., Fiala-Medioni, A., Pancost, R. D., Damste, J. S. S., De Lange, G., Forney, L. J., Gottschal, J. C., Foucher, J. P., Mascle, J., and Woodside, J., 2004. Life at cold seeps: a synthesis of biogeochemical and ecological data from Kazan mud volcano, eastern Mediterranean Sea. *Chemical Geology* **205**, 367-390.

Whiticar, M. J., 1999. Carbon and hydrogen isotope systematics of bacterial formation and oxidation of methane. *Chemical Geology* **161**, 291-314.

Whiticar, M. J., Faber, E., and Schoell, M., 1986. Biogenic methane formation in marine and freshwater environments: CO_2 reduction *vs*. acetate fermentation - Isotope evidence. *Geochimica et Cosmochimica Acta* **50**, 693-709.

Widdel, F. and Rabus, R., 2001. Anaerobic biodegradation of saturated and aromatic hydrocarbons. *Curr Opin Biotechnol* **12**, 259-276.

Figure Captions

Figure 1. Bathymetric chart of the Gulf of Cadiz showing the locations of known mud volcanoes, diapirs and areas where carbonate chimneys and crusts were discovered. The structures studied during the SO-175 expedition are in bold face letters.

Figure 2. Seismic images and 3D images of multibeam bathymetry of Captain Arutyunov (a) and Bonjardim mud volcano (b). Seismic images show the central conduit below the mud volcanoes and sampling position of the cores recovered during the SO-175 expedition. Captain Arutyunov and Bonjardim MV are conical shaped structures with a relief of 80 and 100 m and a diameter of ca. 2 and 1 km, respectively. Colours denote the bathymetry (m below sea surface). Seismic images were modified after Kenyon et al. (2001) (a) and Pinheiro et al. (2003) (b).

Figure 3. Seafloor images (ca. 1 m^2) of Capt. Arutyunov (a,b), Hesperides (c) and Faro MV (d). The surface of Capt. Arutyunov, Bonjardim, Ginsburg MV were found to be covered by pelagic sediments as shown in panel a. The holes are burrows of crabs. Some sediment stretches at Capt. Arutyunov MV contained accretions that are interpreted as clasts (b) indicating past mud flows. Hesperides and Faro mud volcano were littered with carbonate chimneys and crusts as shown for Hesperides MV in panel (c). At Faro mud volcano, also a few dark sediment patches probably covered with whitish, giant sulphide oxidizing bacteria were observed (d).

Figure 4. Captain Arutyunov mud volcano. A distinct SMT, highlighted in grey, was found between 25 and 40 cm bsf (a). At this horizon, concentrations of higher hydrocarbons also decline (b). Note that AOM and SR rates (c), sulphide concentrations (d), concentrations (e) and stable carbon isotope values of diagnostic, bacterial fatty acids (f) and concentrations of isoprenoidal

diethers (g) all peak at the SMT. Panels (a) and (d) illustrate steepest gradients determined for methane, sulphate and sulphide (bold lines). Circles represent multiple corer and triangles gravity corer samples. Errors are given as standard errors.

Figure 5. Bonjardim mud volcano. A distinct SMT, highlighted in grey, was found between 50 and 70 cm bsf (a). At this horizon, concentrations of higher hydrocarbons also decline (b). Note that concentrations of C_{2+}-compounds are ~35-fold higher compared to Captain Arutyunov MV. AOM and SR rates (c), sulphide concentrations (d), concentrations (e) and stable carbon isotope values of diagnostic, bacterial fatty acids (f) and concentrations of isoprenoidal diethers (g) peak at the SMT. Panels (a) and (d) illustrate steepest gradients determined for methane, sulphate and sulphide (bold lines). Concentration gradients for sulphate and sulphide were determined from concentration profiles of the gravity core samples as well as from aligned gravity core and multiple-corer concentration profiles. Circles represent multiple corer and triangles gravity corer samples. Errors are given as standard errors.

Figure 6. The SMT, highlighted in grey, was found in the top most m at Ginsburg (a) and Gemini (c) and between 2 and 3 m at No Name MV (e; note the different scale chosen for depth). In these horizons, also sulphide concentrations peak (b, d, f). Bold lines illustrate steepest gradients determined for methane, sulphate and sulphide.

Table 1. Mud volcanoes investigated during the cruise SO-175. The water depth refers to the highest elevation of the mud volcanoes. V = video observations, CH_4 = methane concentration measurements, SO_4^{2-} = sulphate concentration measurements, C_{2+} = concentration measurements

of higher hydrocarbons, F = diffusive methane and sulphate flux calculation, R = AOM and SR rate measurements, L = Lipid analyses, D = DNA analysis.

Table 2. Concentrations gradients, diffusive fluxes and *ex situ* AOM and SR rates integrated over depth. A negative concentration gradient indicates downward directed flux; a positive value indicates upward flux. Flux values are given without algebraic signs. * and ‡ denote gradients and total sulphate fluxes determined from aligning multiple- and gravity cores. Gradients in brackets indicate upward diffusing sulphate and downward diffusing sulphide, respectively.

Table 3. Bacterial fatty acids, archaeal diether and isoprenoidal hydrocarbons analysed in sediments at the SMT of Captain Arutyunov and Bonjardim MV as well as in carbonate crusts from Hesperides and Faro MV. Abundances of fatty acids were normalised to i-$C_{15:0}$, archaeal diethers to archaeol and archaeal isoprenoidal hydrocarbons to PMI:0. Specific lipid components are highlighted in grey.

Table 4. Archaeal and bacterial 16S rDNA clone libraries obtained from sediments of the SMT of Captain Arutyunov MV. The Archaeal clone library is dominated by sequences belonging to the ANME-2 cluster and the bacterial library by sequences belonging to the Seep-SRB1 cluster.

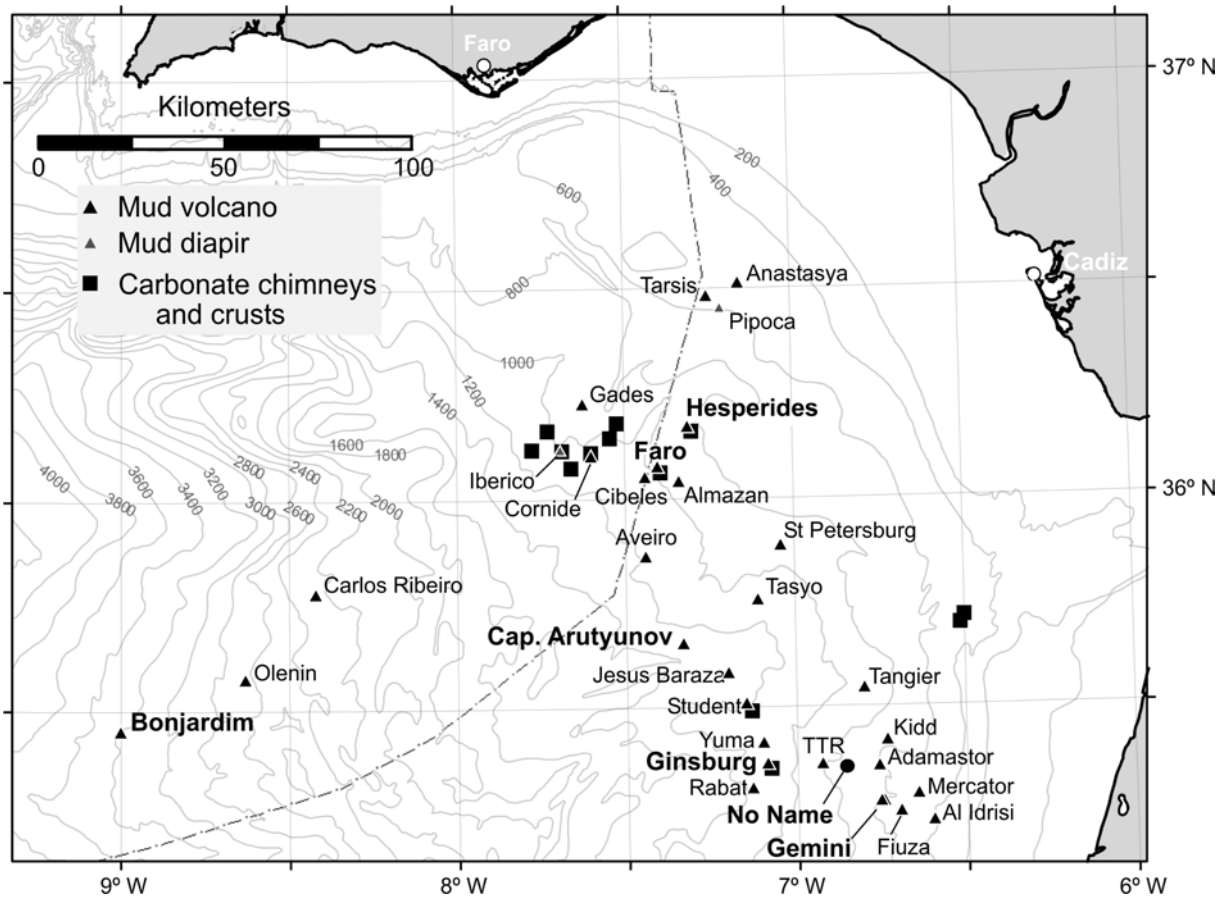

Figure 1. Bathymetric chart of the Gulf of Cadiz showing the locations of known mud volcanoes, diapirs and areas where carbonate chimneys and crusts were discovered. The structures studied during the SO-175 expedition are in bold face letters.

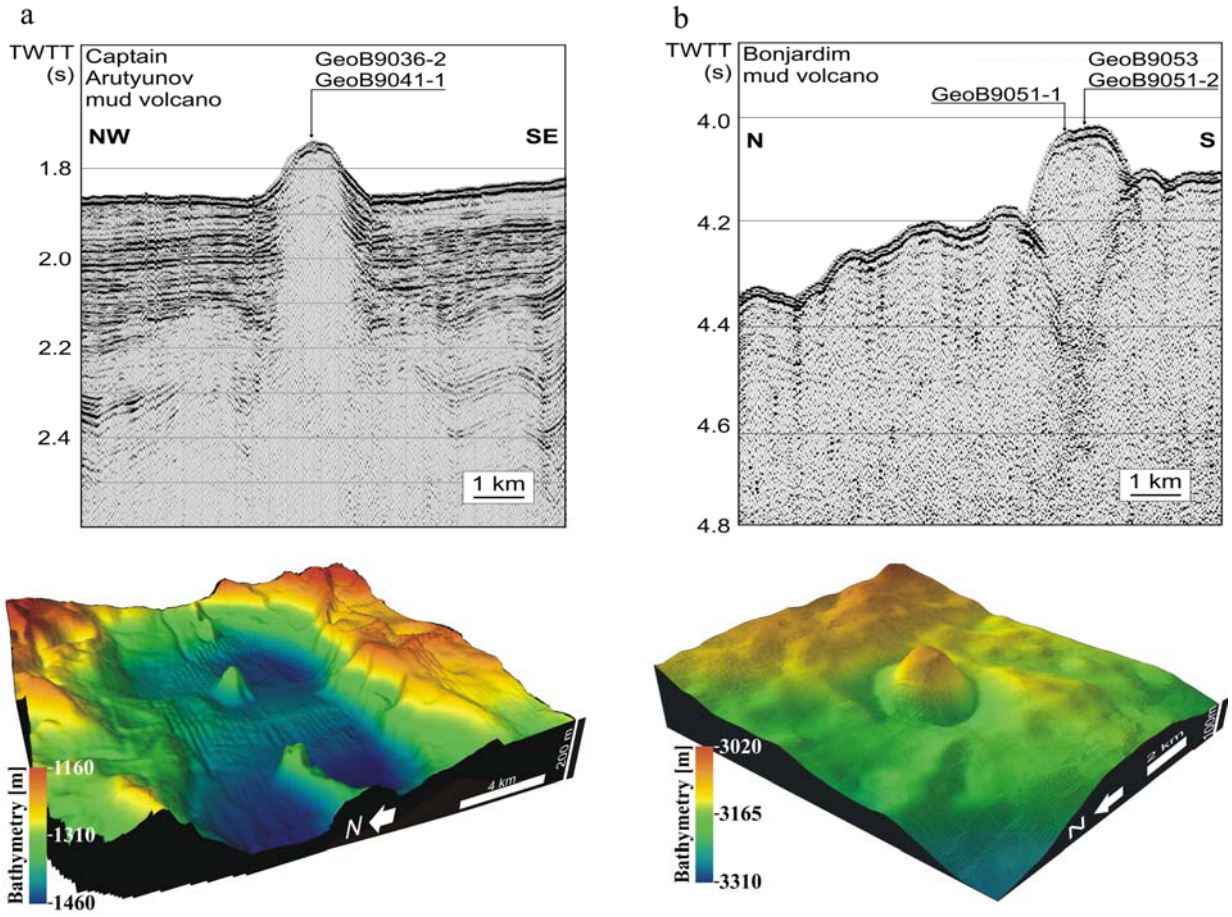

Figure 2. Seismic images and 3D images of multibeam bathymetry of Captain Arutyunov (a) and Bonjardim mud volcano (b). Seismic images show the central conduit below the mud volcanoes and sampling position of the cores recovered during the SO-175 expedition. Captain Arutyunov and Bonjardim MV are conical shaped structures with a relief of 80 and 100 m and a diameter of ca. 2 and 1 km, respectively. Colours denote the bathymetry (m below sea surface). Seismic images were modified after Kenyon et al. (2001) (a) and Pinheiro et al. (2003) (b).

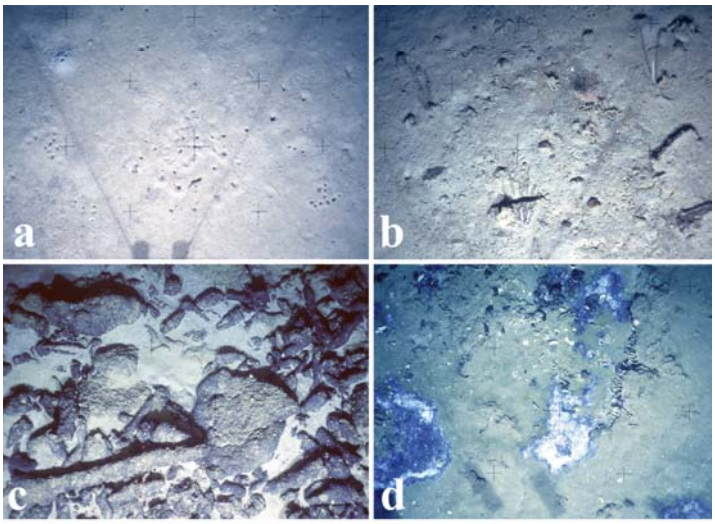

Figure 3. Seafloor images (ca. 1 m^2) of Capt. Arutyunov (a,b), Hesperides (c) and Faro MV (d). The surface of Capt. Arutyunov, Bonjardim, Ginsburg MV were found to be covered by pelagic sediments as shown in panel a. The holes are burrows of crabs. Some sediment stretches at Capt. Arutyunov MV contained accretions that are interpreted as clasts (b) indicating past mud flows. Hesperides and Faro mud volcano were littered with carbonate chimneys and crusts as shown for Hesperides MV in panel (c). At Faro mud volcano, also a few dark sediment patches probably covered with whitish, giant sulphide oxidizing bacteria were observed (d).

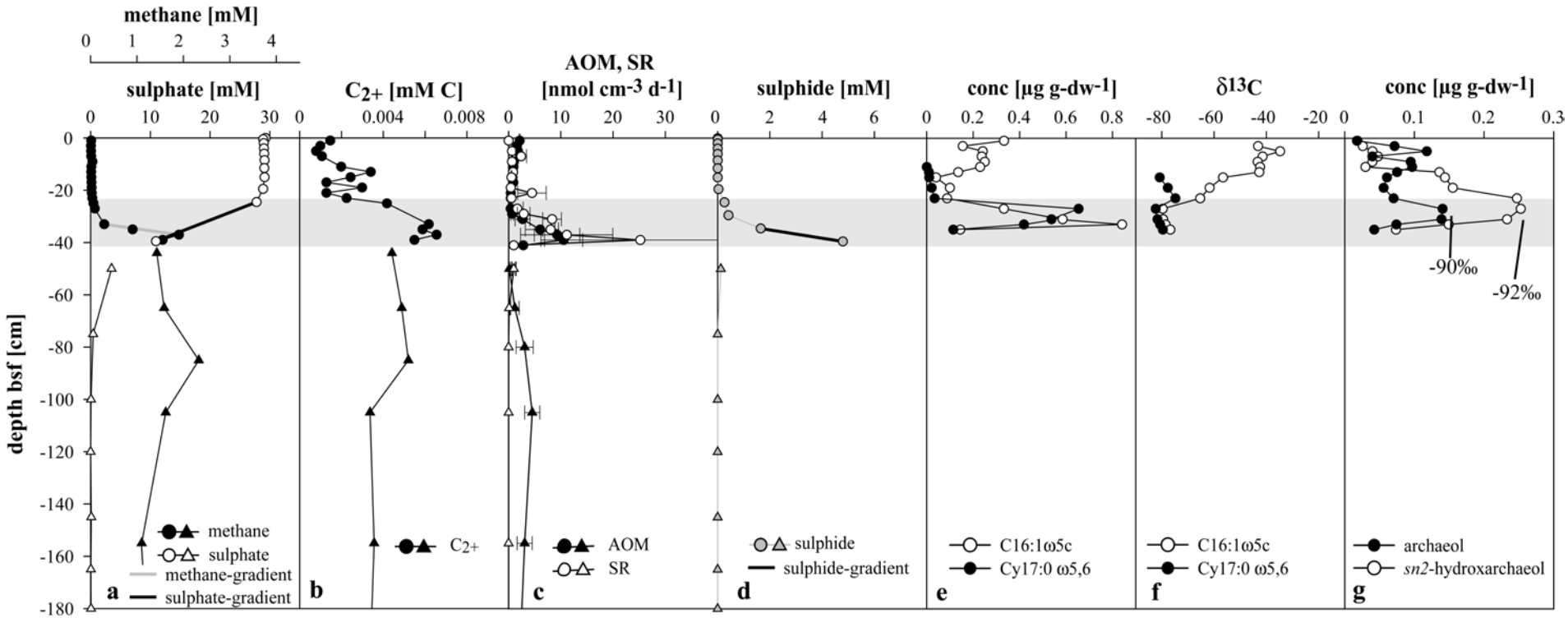

Figure 4. Captain Arutyunov mud volcano. A distinct SMT, highlighted in grey, was found between 25 and 40 cm bsf (a). At this horizon, concentrations of higher hydrocarbons also decline (b). Note that AOM and SR rates (c), sulphide concentrations (d), concentrations (e) and stable carbon isotope values of diagnostic, bacterial fatty acids (f) and concentrations of isoprenoidal diethers (g) all peak at the SMT. Panels (a) and (d) illustrate steepest gradients determined for methane, sulphate and sulphide (bold lines). Circles represent multiple corer and triangles gravity corer samples. Errors are given as standard errors.

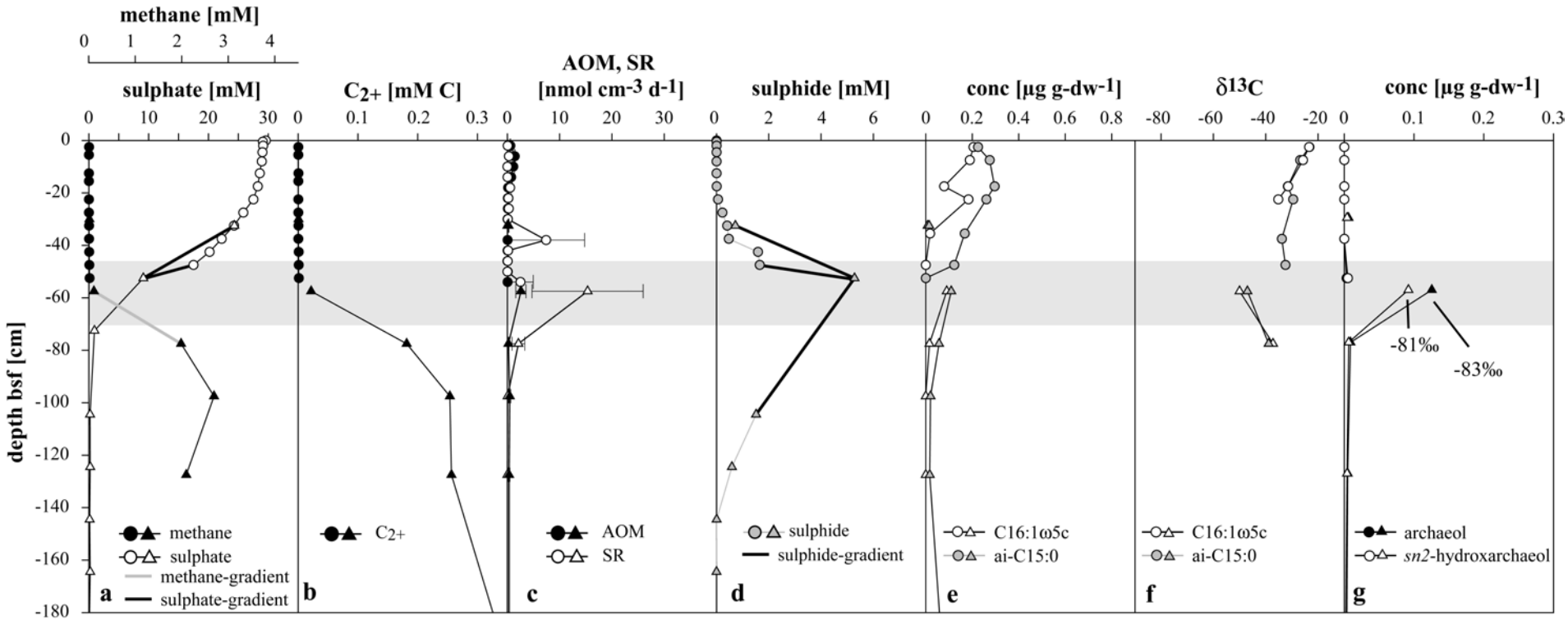

Figure 5. Bonjardim mud volcano. A distinct SMT, highlighted in grey, was found between 50 and 70 cm bsf (a). At this horizon, concentrations of higher hydrocarbons also decline (b). Note that concentrations of C_{2+}-compounds are ~35-fold higher compared to Captain Arutyunov MV. AOM and SR rates (c), sulphide concentrations (d), concentrations (e) and stable carbon isotope values of diagnostic, bacterial fatty acids (f) and concentrations of isoprenoidal diethers (g) peak at the SMT. Panels (a) and (d) illustrate steepest gradients determined for methane, sulphate and sulphide (bold lines). Concentration gradients for sulphate and sulphide were determined from concentration profiles of the gravity core samples as well as from aligned gravity core and multiple-corer concentration profiles. Circles represent multiple corer and triangles gravity corer samples. Errors are given as standard errors.

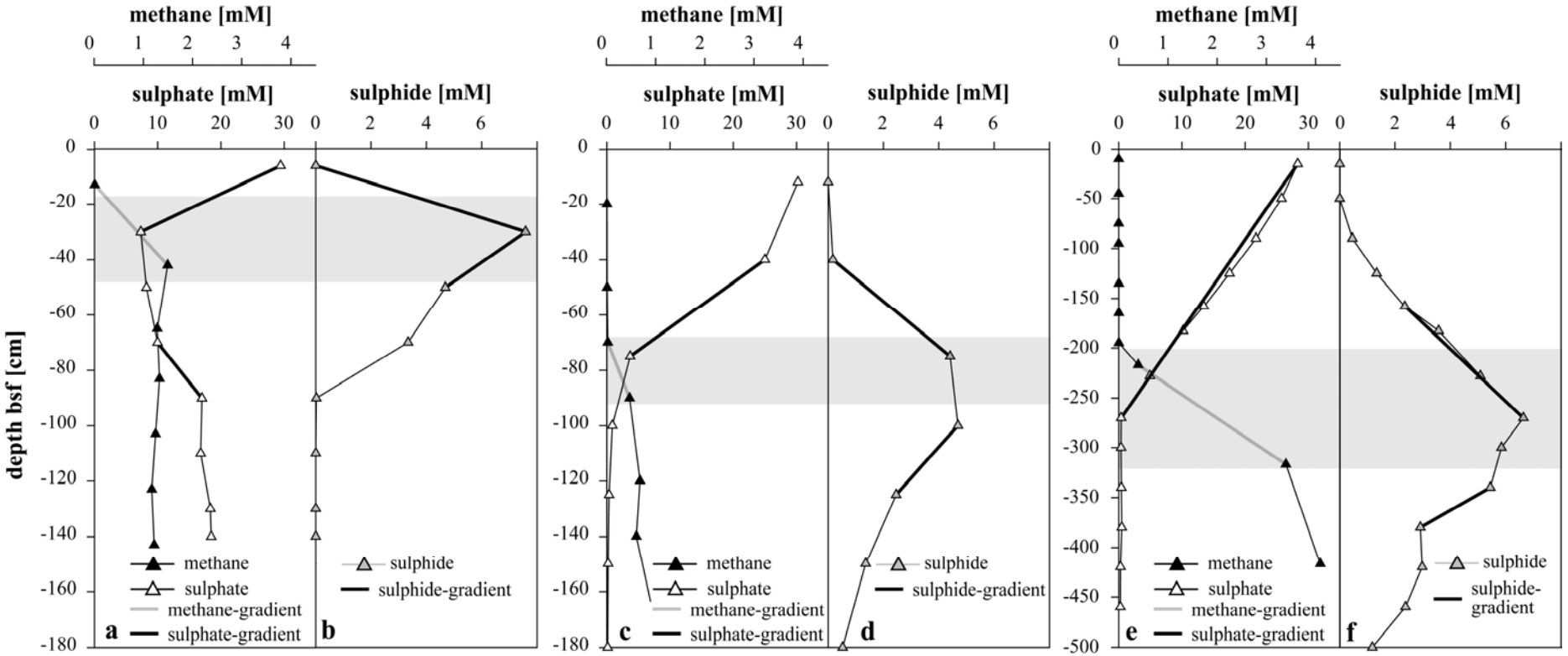

Figure 6. The SMT, highlighted in grey, was found in the top most m at Ginsburg (a) and Gemini (c) and between 2 and 3 m at No Name MV (e; note the different scale chosen for depth). In these horizons, also sulphide concentrations peak (b, d, f). Bold lines illustrate steepest gradients determined for methane, sulphate and sulphide.

Table 1. Mud volcanoes investigated during the cruise SO-175. The water depth refers to the highest elevation of the mud volcanoes. V = video observations, CH_4 = methane concentration measurements, SO_4^{2-} = sulphate concentration measurements, C_{2+} = concentration measurements of higher hydrocarbons, F = diffusive methane and sulphate flux calculation, R = AOM and SR rate measurements, L = Lipid analyses, D = DNA analysis.

Structure	Relief [m]	Diam. [km]	Water depth [m]	Device	Core/Grab	Lat. N	Long. W	Applied Methods
CAMV	80	2.0	1315	MUC	GeoB 9036-2	35° 39.72'	07° 19.98'	V, CH_4, SO_4^{2-}, C_{2+}, H_2S, F, R, L, D
				GC	GeoB 9041-1	35° 39.70'	07° 19.97'	CH_4, SO_4^{2-}, C_{2+}, H_2S
Bonjardim	100	1.0	3090	MUC	GeoB 9051-1	35° 27.72'	08° 59.98'	V, CH_4, SO_4^{2-}, C_{2+}, H_2S, R, L
				GC	GeoB 9051-2	35° 27.61'	09° 00.03'	CH_4, SO_4^{2-}, C_{2+}, H_2S, F, R, L
Ginsburg	150	4.0	910	GC	GeoB 9061-1	35° 22.42'	07° 05.29'	V, CH_4, SO_4^{2-}, H_2S, F
Gemini	200	4.9	435	GC	GeoB 9067-1	35° 16.92'	06° 45.47'	CH_4, SO_4^{2-}, H_2S, F
No Name	150	3.7	460	GC	GeoB 9063-1	35° 21.99'	06° 51.92'	CH_4, SO_4^{2-}, H_2S, F
Hesperides	160	3.0	690	Grab	GeoB 9023-1	36° 10.73'	07° 18.39'	V, L
Faro	190	2.6	810	Grab	GeoB 9029-3	36° 05.68'	07° 24.12'	V, L

Table 2. Concentrations gradients, diffusive fluxes and *ex situ* AOM and SR rates integrated over depth. A negative concentration gradient indicates downward directed flux; a positive value indicates upward flux. Flux values are given without algebraic signs. * and ‡ denote gradients and total sulphate fluxes determined from aligning multiple- and gravity cores. Gradients in brackets indicate upward diffusing sulphate and downward diffusing sulphide, respectively.

			Conc. gradient [µmol cm^{-4}]			Diffusive fluxes [mmol m^{-2} yr^{-1}]			Microbial turnover [mmol m^{-2} yr^{-1}]	
Structure	**Core GeoB**	**Porosity [%]**	**CH_4**	**SO_4^{2-}**	**Sulphide**	**CH_4**	**ΣSO_4^{2-}**	**ΣSulphide**	**AOM**	**SR**
Capt. Arutyunov	9036-2	56	0.40	-1.12	0.63	407	708	702	383	577
Bonjardim	9051-2	58	0.09	-0.76,-1.67*	0.23,0.73* (-0.07)	76	388,867‡	299,795‡	36	690
Ginsburg	9061-1	60	0.05	-0.92 (0.35)	0.32 (-0.15)	55	852	565		
Gemini	9067-1	56	0.02	-0.61	0.12 (-0.09)	21	388	272		
No Name	9063-1	57	0.03	-0.11	0.04 (-0.06)	29	74	108		

Table 3. Bacterial fatty acids, archaeal diether and isoprenoidal hydrocarbons analysed in sediments at the SMT of Captain Arutyunov and Bonjardim MV as well as in carbonate crusts from Hesperides and Faro MV. Abundances of fatty acids were normalised to i-$C_{15:0}$, archaeal diethers to archaeol and archaeal isoprenoidal hydrocarbons to PMI:0. Specific lipid components are highlighted in grey.

			Sediment		Carbonate	
			Captain Arutyunov	Bonjardim	Hesperides	Faro
Normalised abundance (δ^{13}C-values)	Bacterial fatty acids	$C_{14:0}$	1.3 (-75)	2.0 (-37)	1.1 (-31)	2.3 (-93)
		i-$C_{15:0}$	1.0 (-71)	1.0 (-42)	1.0 (-39)	1.0 (-99)
		ai-$C_{15:0}$	1.3 (-73)	8.4 (-47)	1.5 (-43)	1.9 (-95)
		$C_{15:0}$	0.6 (-73)	1.4 (nd)	0.3 (-45)	0.4 (-96)
		i-$C_{16:0}$	0.2 (-73)	nd	0.2 (nd)	0.2 (-87)
		$C_{16:1\omega9}$	0.7 (-65)	nd	nd	0.1 (-92)
		$C_{16:1\omega7}$	0.8 (-67)	14.6 (-34)	0.6 (-27)	1.8 (-93)
		$C_{16:1\omega5}$	7.7 (-80)	8.4 (-49)	0.1 (-41)	0.7 (-96)
		$C_{16:0}$	2.4 (-67)	7.8 (-21)	4.8 (-27)	1.6 (-77)
		10 Me$C_{16:0}$	0.3 (-67)	nd	nd	1.0 (-94)
		i-$C_{17:0}$	0.3 (-69)	nd	0.3 (-32)	0.3 (-96)
		ai-$C_{17:0}$	0.1 (nd)	1.1	0.5 (-38)	0.3 (-99)
		$C_{17:1\omega7}$	0.9 (-68)	1.9	0.5 (-31)	0.4 (-93)
		$C_{17:1\omega6}$	1.9 (-74)	nd	nd	0.1 (nd)
		cy$C_{17:0\omega5,6}$	7.1 (-82)	nd	nd	nd
		$C_{17:0}$	nd	nd	0.2 (nd)	0.1 (nd)
		$C_{18:1\omega9}$	1.0 (-27)	6.4 (-27)	0.2 (nd)	0.3 (-77)
		$C_{18:1\omega7}$	0.9 (-31)	13.7 (-31)	0.4 (-37)	1.5 (-84)
		$C_{18:0}$	0.2 (-25)	3.5 (-25)	1.8 (-28)	0.4 (-67)
	Archaeal lipids	Archaeol	1.0 (-90)	1.0 (-81)	1.0 (-97)	1.0 (-114)
		sn2-hydroxyarchaeol	1.7 (-92)	0.7 (-83)	tr	0.2 (-111)
		Crocetane / Phytane			0.5 (-47)	3.3 (-110)
		PMI:0			1.0 (-87)	1.0 (-111)
		ΣPMI:1			0.3 (nd)	4.6 (-113)
		ΣPMI:2			nd	8.3 (-113)
		ΣPMI:3			nd	0.3 (-101)
Concentration [µg g-dw^{-1}]	Bacterial fatty acids	i-$C_{15:0}$	0.08	0.01	0.1	8.7
		ai-$C_{15:0}$	0.1	0.09	0.15	16.77
		$C_{16:1\omega5}$	0.6	0.09	0.01	6.05
		$C_{17:1\omega6}$	0.14	nd	n d	0.5
		cy$C_{17:0\omega5,6}$	0.56	nd	n d	nd
	Archaeal lipids	Archaeol	0.14	0.4	2.39	41.58
		sn2-hydroxyarchaeol	0.23	0.3	0.02	8.31
		Crocetane / Phytane			0.23	4.59
		PMI:0			0.44	1.4
Putative origin			ANME2 Seep-SRB1	ANME1 Seep-SRB1 & ANME2 Seep-SRB1	ANME1 Seep-SRB1 (?)	ANME1 Seep-SRB1 & ANME2 Seep-SRB1

Table 4. Archaeal and bacterial 16S rDNA clone libraries obtained from sediments of the SMT of Captain Arutyunov MV. The Archaeal clone library is dominated by sequences belonging to the ANME-2 cluster and the bacterial library by sequences belonging to the Seep-SRB1 cluster.

Phylogenetic group		Clones	Representative clone	Next relative	Sequence similarity
Archaea		39			
Euryarchaeota	ANME 2a	23	CAMV300A948 (DQ004662)	Uncultured cold seep archaeal clone BS-K-H6 (AJ578128)	99%
	ANME 2c	1	CAMV301A975 (DQ004668)	Uncultured hydrocarbon seep archaeal clone C1_R019 (AF419638)	99%
	ANME 1	7	CAMV300A952 (DQ004664)	Uncultured hydrocarbon seep archaeal clone HydCal61 (AJ578089)	99%
	Marine Benthic Group D	1	CAMV300A963 (DQ004667)	Uncultured hydrothermal vent archaeal clone pMC2A203 (AB019737)	98%
	Marine Benthic Group D	1	CAMV300A951 (DQ004663)	Uncultured contaminated aquifer archaeal clone WCHD3-02 (AF050616)	90%
	Marine Benthic Group D	1	CAMV301A980 (DQ004669)	Uncultured hydrothermal vent archaeal clone VC2.1 Arc6 (AF068817)	87%
	Unclassified Archaea	1	CAMV300A960 (DQ004666)	Uncultured cold seep archaeal clone BS-SR-H5 (AJ578148)	98%
	Uncalssified Archaea	3	CAMV301A993 (DQ004661)	Uncultured hydrothermal vent archaeal clone NT07-CAT-A24 (AB111475)	80%
Crenarchaeota	Marine Benthic Group B	1	CAMV300A958 (DQ004665)	Uncultured archaeal clone BS-K-D4 (AJ578124)	99%
Bacteria		47			
δ Proteobacteria	Seep SRB 1	38	CAMV300B922 (DQ004675)	Uncultured hydrocarbon seep bacterial clone Hyd89-04 (AJ535240)	99%
	Desulfobulbacteraceae	1	CAMV301B937 (DQ004679)	Uncultured Echinocardium cordatum hindgut bacterial clone Del 7 (AY845643)	96%
	Desulfobulbaceae	1	CAMV300B921 (DQ004674)	Uncultured hydrocarbon seep bacterial clone Hyd89-51 (AJ535252)	99%
γ Proteobacteria	Stenotrophomonas	1	CAMV301B944 (DQ004671)	Stenotrophomonas maltophilia (AB008509)	99%
Clostridia	Clostridiales	1	CAMV300B902 (DQ004670)	Uncultured bacterial clone DR9IPCB16SCT8 (AY604055)	98%
Spirochaetes	Spirochaeta	1	CAMV301B941 (DQ004680)	Uncultured Spirochaeta sp. (AF424377)	96%
	Spirochaeta	1	CAMV300B915 (DQ004672)	Uncultured spirochete clone IE052 (AY605138)	96%
	Unclassified bacteria	1	CAMV300B916 (DQ004673)	Uncultured hydrocarbon seep bacterial clone Hyd24-12 (AJ535232)	97%
	Unclassified bacteria	1	CAMV301B934 (DQ004678)	Uncultured hydrocarbon seep bacterial clone 1B-41 (AY592596)	93%
	Unclassified bacteria	1	CAMV300B923 (DQ004676)	Uncultured hydrocarbon seep bacterial clone GCA025 (AF154106)	98%

Chapter IV: Anaerobic oxidation of methane and sulfate reduction at cold seeps in the Eastern Mediterranean

Anaerobic oxidation of methane and sulfate reduction at cold seeps in the Eastern Mediterranean Sea

Running title: Cold seeps of the Eastern Mediterranean Sea

*[1,2]Enoma O. Omoregie, [1]Helge Niemann, [3]Vincent Mastalerz, [3]Gert de Lange, [4]Alina Stadnitskaia, [5]Jean Mascle, [6]Jean-Paul Foucher, *[1,2,7]Antje Boetius

*[1]Max Planck Institute for Marine Microbiology, Bremen, Germany

[2]Jacobs University Bremen, Bremen, Germany

[3]Department of Earth Sciences, Utrecht University, Utrecht, The Netherlands

[4]Royal Netherlands Institute for Sea Research (NIOZ), Texel, The Netherlands

[5]Geosciences-Azur, Villefranche sur mer, France

[6]Department of Marine Geosciences, IFREMER Centre de Brest, Plouzane Cedex, France

[7]Alfred Wegener Institute for Polar and Marine Research, Bremerhaven, Germany

This manuscript will be submitted to Marine Geology

Keywords: methane oxidation, sulfate reduction, archaea, cold seeps, mud volcano, pockmarks, Nile Deep Sea Fan

* Corresponding authors: eomoregi@mpi-bremen.de; aboetius@mpi-bremen.de

Max Planck Institute for Marine Microbiology, Celsiusstr. 1, Bremen, Germany

Phone: (+49) 421-2028-869; (+49) 421-2028-869

Fax: (+49) 421-2028-870

Abstract

The Eastern Mediterranean hosts a variety of active cold seep systems such as mud volcanoes, and pockmarks, in water depths of 500 to 3200 m. In the framework of ESF EUROCORES project MEDIFLUX, the NAUTINIL expedition with RV L'Atalante and the submersible Nautile in 2003 was the first to sample the active seep systems of the Nile Deep Sea Fan. Here we compare rates of the anaerobic oxidation of methane (AOM) and sulfate reduction (SR), as well as the microbial community structure of a variety of cold seep systems sampled during the NAUTINIL expedition. Our results revealed strong differences in microbial activity and diversity among the different seep systems of the Eastern, Central and Western provinces of the Nile Deep Sea Fan (NDSF), as well as the Olimpi field (Central Mediterranean Ridge). Integrated over the top 10 cm below seafloor, SR rates ranged from 0.1 - 66 mmoles*m^{-2}*d^{-1} and AOM rates from 0.1 - 3.6 mmoles*m^{-2}*d^{-1}. The lowest rates were associated with pockmarks and carbonate pavements, and highest rates with the mud volcano centers. Sulfate reduction was often considerably higher than methane oxidation, indicating that other electron donors were utilized besides methane. 16S rRNA gene analysis together with fluorescence in situ hybridization (FISH), revealed the presence of all known groups of marine methane oxidizing archaea (i.e. ANME-1, -2, -3) and also of methane oxidizing bacteria (i.e. *Methylobacter* sp. and relatives) in the seep sediments. The microbial community structure differed between the different types of seeps. Generally, microbial activity related to methane turnover was lower at the seeps of the Eastern Mediterranean than at other seeps despite the high availability of methane and sulfate.

Introduction

Cold seeps are geologically and geochemically active systems, which can host very active biological ecosystems, which are fueled by fluids and gases emitted to the sea floor (Treude et al., 2003; Niemann et al., 2006a; Niemann et al., 2006b; Omoregie et al., 2007). A variety of such cold seep systems have recently been detected on active and passive continental margins of the Eastern Mediterranean, including mud volcanoes, pockmarks and brine lakes. Accumulations of such structures are found at the Eastern Mediterranean ridge accretionary prism (Camerlenghi et al., 1992; Fusi and Kenyon, 1996; Woodside et al., 1998; Huguen et al., 2004; Zitter et al., 2005), on the Nile Deep-Sea Fan off the coast of Egypt (Mascle et al., 2001; Loncke et al., 2004; Loncke et al., 2006) and Israel (Coleman and Ballard, 2001). Due to the important role of methane as a greenhouse gas, increasing attention has been given to the structure, function and distribution of cold seep communities, which may act as biological barrier against methane emission ((Hinrichs and Boetius, 2002; Sibuet and Olu-Le Roy, 2002; Reeburgh, 2007) and references therein).

One of the main biogeochemical processes underlying energy flow in most cold seep ecosystems is the anaerobic oxidation of methane (AOM) via sulfate reduction (SR). This process significantly affects seep habitats by inducing the precipitation of carbonate (Ritger et al., 1987), as well as by producing sulfide, both of which provide additional niches to a variety of microbial communities and benthic fauna, including chemosynthetic microbe-animal symbioses such as siboglinid tubeworms, mytilid and vesicomyid bivalves (Ritger et al., 1987; Sibuet and Olu-Le Roy, 2002). AOM is mediated by a syntrophic association between archaea (ANME groups 1-3), related to

Methanosarcinales, Methanomicrobiales and *Methanococcoides*, and sulfate-reducing bacteria (SRB) of the *Desulfosarcina*/*Desulfococcus* or the *Desulfobulbus* clusters (Boetius et al., 2000a; Orphan et al., 2001; Knittel et al., 2005; Lösekann et al., 2007). A distinct variety of other bacteria and archaea with yet unknown function have been repeatedly detected in cold seep systems, which form characteristic microbial communities (Teske et al., 2002; Knittel et al., 2003; Knittel et al., 2005).

Active cold seep systems in the Eastern Mediterranean have been the subject of several studies that have included MVs on the Eastern Mediterranean Ridge, such as the Napoli and Milano MVs in the Olimipi area, and Amsterdam and Kazan in the Anaximander mountains (Camerlenghi et al., 1992; Cita et al., 1996; Limonov et al., 1996; Silva et al., 1996; Volgin and Woodside, 1996; Woodside et al., 1998; Aloisi et al., 2000; Pancost et al., 2000; Aloisi et al., 2002; Charlou et al., 2003; Haese et al., 2003; Heijs, 2005). Highly ^{13}C-depleted archaeal biomarkers (i.e. archeaol, PMI and others) indicative of AOM have been recovered from carbonates and sediments at these seeps (Aloisi et al., 2000; Pancost et al., 2000; Aloisi et al., 2002; Heijs, 2005; Bouloubassi et al., 2006; Heijs et al., 2006). Evidence for SR coupled to AOM at these sites has been made primarily on the basis of ^{13}C-depleted bacterial lipids believed to originate from methane dependent sulfate reducing bacteria (Aloisi et al., 2000; Pancost et al., 2000; Aloisi et al., 2002; Heijs, 2005; Bouloubassi et al., 2006; Heijs et al., 2006). Furthermore, 16S rRNA gene surveys of sediments from these mud volcanoes have revealed the presence of anaerobic methane oxidizing archaea, i.e. ANME-1 and 2, as well as their sulfate reducing partners related to the *Desulfosarcina* and *Desulfococcus* (Heijs, 2005; Heijs et al., 2005).

Here we present the first AOM and SR activity measurements, in relation to microbial community structure of cold seep systems in the Nile Deep Sea Fan (NDSF). We focused on cold seeps of the Eastern (Amon, Isis mud volcanoes), Central (North Alex, pockmark area) and Western (Chefren mud volcano) NDSF. For comparison, the Napoli mud volcano of the Olimpi field on the Central Mediterranean Ridge was also studied. We used whole core tracer injection methods to quantify rates of methane oxidation and sulfate reduction as well as 16S rDNA-based molecular tools to investigate the microbial community structure. The main questions addressed in this study are: (1) How high is microbial methane and sulfate consumption at the various seeps of the NSDF, and in comparison to other known seep systems? (2) Which microorganisms are responsible for this activity at the mud volcanoes in the Eastern Mediterranean?

Material and Methods

Sampling sites of the NAUTINIL expedition. Napoli MV is located within the Olimpi area on the Central part of the Eastern Mediterranean Ridge (Fig. 1). The mud volcanoes Amon and Isis of the Eastern NDSF, North Alex of the Central NDSF and Chefren and Mykerinos of the Western NDSF, were sampled for the first time with the submersible Nautile (IFREMER) during the NAUTINIL expedition in 2003 (Fig. 1). These mud volcanoes are circular features (1-3 km in diameter) in water depths of 500 - 3000 m with elevations of up to 100 m above the seabed. They are located above well-developed feeder channels, clearly seen on the seismic data (Loncke et al., 2004; Dupré et al., 2007; Huguen et al., 2007). In the deeper central province of the NDSF we sampled

a field characterized by abundant pockmarks of 3-15 m diameter between extensive flat carbonate pavements covering the seafloor.

At all these sites, **s**ediment samples were collected by push and blade corers *Nautile***.** Immediately upon returning to the RV Atalante the cores were taken to the cold room, sub-sampled and processed for the multidisciplinary measurements outlined below.

Methane concentration. Sediment were sectioned horizontally (2 cm intervals, corresponding to 2 ml of sediment) and sections were placed in 18 ml glass vials containing 10 ml of 2.5% NaOH. The vials were immediately sealed with a rubber stopper. Alternatively, sections were equilibrated with a saturated NaCl solution (ca. 300 g/l) in rubber sealed glass vials for at least 12 hours. The sediment slurries were shaken, and 100 µl of headspace removed by a glass syringe. Methane concentrations were measured by injecting 100 µl of head space in a Hewlett Packard 5890A or a Shimadzu GC-14B gas chromatograph.

Methane oxidation. Methane oxidation rates were measured using $^{14}CH_4$ gas, based on previously described methods (Iversen and Blackburn, 1981; Treude et al., 2003). Pre-drilled cores were used to sub-sample the push cores. The holes were spaced 1 cm apart and sealed with silicone prior to sub-sampling. After quickly sub-sampling the push cores, the subcores were sealed with a rubber stopper, and placed in the dark at in the in situ temperature of 14°C for 1 - 2 hours. Ten microliters of $^{14}CH_4$ (~0.25 kBq) were then injected through the silicon plugs into the sediment, and the sub-cores incubated in the dark at *in situ* temperature for 24 hr. The cores were then quickly sectioned into 2 cm layers, and the sections fixed in 2.5% NaOH as for methane concentration determinations. Further processing was done according to Treude et al.

(Treude et al., 2003). Rates were calculated according to the equation below, where $^{14}CO_2$ = activity of CO_2 produced, $^{14}CH_4$= activity of residual tracer, CH_4 = residual CH_4, *V*= sediment volume and *t*= time.

$$\text{AOM rate} = (^{14}CO_2/(^{14}CO_2 + {}^{14}CH_4)) * [CH_4] * 1/V / t$$

Sulfate concentration. Sediment subcores were sectioned horizontally (2 cm intervals, corresponding to 2 ml of sediment) and sections placed in 15 ml polypropylene vials with 20 % zinc acetate and shaken thoroughly. The sediment slurry was then centrifuged at 5000 rpm for five minutes and the supernatants removed to clean polypropylene vials. The supernatants were analyzed using non-suppressed ion chromatography with an anion exchange column (LCA A14, Sykam) and a conductivity detector (S3110, Sykam). Alternatively sulfate samples were measured as S using ICP-AES.

Sulfate reduction. Sulfate reduction rates were measured by $^{35}SO_4^{-2}$ whole core injection incubations. Parallel to the methane oxidation samples, sediment subcores were pre-incubated, injected with 5 µl of $^{35}SO_4^{-2}$ (10 kBq) and incubated for 24 hours at *in situ* temperature before fixation in 20% zinc acetate. The samples were then processed according the method described by Kallmeyer et al. (Kallmeyer et al., 2004). Rates were calculated according to the equation below, where $TRIS^{35}S$ = activity of total reduced inorganic sulfur, $^{35}SO4$ = activity of residual tracer, SO_4^{-2} = residual SO_4^{-2} within the sample, *V* = sediment volume, and *t* = time.

$$\text{SR rate} = (TRI^{35}S/(TRI^{35}S + {}^{35}SO_4^{-2})) * [SO_4^{-2}] * 1/V / t$$

Acridine Orange Direct Counts (AODC) and Fluorescence In Situ Hybridization (FISH). Two milliliters of sediment were placed in a 20 ml plastic tube with 9 ml of a 2 % formalin and artificial seawater solution for 4 hr at room temperature. At the end of the incubation period, half of the mixture was processed for FISH, the other half was stored at 4°C for AODC. AODC (Boetius and Lochte, 1996), FISH (Snaidr et al., 1997) and CARD-FISH (Ishii et al., 2004) were all performed according to previously described methods. All FISH and CARD-FISH slides were counter-stained with DAPI (4´,6´- diamidino-2-phenylindole). At least 30 - 50 grids were counted randomly from each slide for AODC, FISH and CARD-FISH. Probe hybridization details are given in Table 2. No signal was observed using ANME-2, and Mγ705 CARD-FISH probes, therefore ANME-2 and Mγ705 targeted cells were enumerated using monolabeled FISH probes. Cell numbers within conspicuous ANME-SRB aggregates were estimated using a semi-direct method. All aggregates and cells were assumed to be spherical. The average cell volume was estimated to be 0.26 μm^3. The volume of an average aggregate (82 μm^3) was divided by the cell volume, and a ratio of 2:1 archaeal to bacterial cells was used to calculate bacterial and archaeal cells within the consortium (Boetius et al., 2000b).

16S rDNA library construction and analysis. Sediments were sectioned into 2 cm intervals and frozen at -20°C until further processing. 16S rDNA libraries for archaeal and bacterial communities were created after Niemann et al. (Niemann et al., 2006a). Briefly, total DNA was extracted from the first 4 cm of sediment (~ 0.3 g) using the FastDNA spin kit for soil (Q-Biogene, Irvine, California, USA). Partial archaeal and bacterial 16S genes were amplified using the primers ARCH20F (Massana et al., 1997)

and Uni1392R (Lane et al., 1985) for Archaea and GM3F (Muyzer et al., 1995) and GM4R (Kane et al., 1993) for Bacteria. Amplification products were then cloned and sequenced in one direction on an ABI 3100 genetic analyzer. Single directional reads were then analyzed using the ARB software package (Ludwig et al., 2004). P-tests were conducted for comparisons between sequences in this study using the program S-LIBSHUFF version 1.22 (Schloss et al., 2004). Distance matrices were created in ARB (Ludwig et al., 2004) using the Neighbor-joining tool. Sequences were submitted to the GenBank database (http://www.ncbi.nlm.nih.gov/) and are accessible under the following accession numbers: XXXX-XXXX.

Results and Discussion

The Eastern Mediterranean basin is known as one of the most oligotrophic areas of the world's oceans, it is characterized by low particle flux rates, deep oxygen and sulfate penetration into the seafloor due to low rates of organic matter diagenesis, and low microbial cell numbers already at the seafloor (Boetius et al., 1996). Hence, any type of sulfidic environment at the seafloor of the Eastern Mediterranean deep sea must be associated with local advection of electron donors from the deep subsurface, such as fluid flow and gas seepage. Offshore Egypt, the Nile continental margin is characterized by a large deep-water turbiditic system known as the Nile Deep Sea Fan. Here, detailed geological and geophysical study of the Nile Deep Sea Fan by the expeditions 'Prismed II', 'Fanil', and 'Medisis' in 1998, 2000 and 2002 revealed an abundance of seafloor structures associated with gas chimneys and active salt tectonics in water depths of 500 - 3000 m (Mascle et al., 2006). A variety of these targets, including mud volcano and

pockmark structures were visited in 2003 by the expedition NAUTINIL. Most strikingly, almost all structures showed signs of active gas seepage, fluid flow, mud volcanism and authigenic carbonate formation (Dupré et al., 2007). Hence, the abundance of cold seeps, chemosynthetic communities and anoxic microbial ecosystems in the highly oligotrophic Eastern Mediterranean is much greater than previously considered.

Eastern province of the NDSF

Visible observations

Five dives were dedicated to investigating the methane turnover and microbiology of active sites of the Amon and Isis MVs (Figs. 1a,b and Table 1). For detailed geological and morphological descriptions of Amon and Isis see Dupre et al. (Dupré et al., 2007). Visual observations of both mud volcanoes provided evidence for active seepage and methane consumption in the center of both MVs. We found areas of highly disturbed seafloor, with fresh cracks, troughs and grayish mud breccia. Also, blackish, reduced patches of sediment of 0.5 - 4 m in diameter were observed around the freshly disturbed areas and were frequently covered with mats of sulfide-oxidizing bacteria (Fig. 2a,b). Our sampling effort concentrated on those sites as the presence of sulfide-oxidizing bacterial mats point to active subsurface processes producing and transporting sulfide to the seafloor (Treude et al., 2003; Niemann et al., 2006b).

The sedimentology of all push cores from the active centers of both MVs showed evidence of mud volcanism (Fig. 3a,b). Two sediment push cores were recovered from the center of Amon (Table 1, Fig. 2a: NL11PC1, NL12PC2) and three from the center of Isis (Table 1, Fig. 2b: NL8PC1(4), NL18PC3(1) and NL13PC4(7)). The surfaces of both

cores from Amon were covered with sulfide-oxidizing bacterial mats above reduced sediments followed by lighter grayish mud breccia below (Fig. 3a). Sporadic gas ebullition from the seafloor was observed at Amon and Isis upon sampling and submersible touch-down in the center. All three cores (Fig. 3b) recovered from Isis contained dark grey mud breccia, two cores had small whitish aggregates at the surface indicating the presence of sulfide oxidizing bacteria (NL8PC1(4), NL8PC3(1)).

Sulfate reduction and anaerobic oxidation of methane

Large methane plumes with high concentrations of methane have been detected above the centers of Amon and Isis (0.5 and 0.7 μM, respectively) (Dupré et al., 2007) Mastalerz et al., unpublished data). When retrieved to deck, all cores from the center of Isis and Amon MV had cracks within the sediment indicating gas escape during recovery. Accordingly, methane concentrations measured in all recovered sediment cores from both MV centers exceeded 1 mM (Fig. 3a,b), and some cores still contained gas bubbles during sub-sampling. Despite high methane concentrations, sulfate concentrations exceeded 5 mM throughout the cores, with moderate anaerobic oxidation of methane (AOM) rates (0.1 - 3.7 mmoles m^{-2} d^{-1}). Sulfate reduction (SR) rates (0.7 - 24 mmoles m^{-2} d^{-1}) were much higher (Table 3). The peaks in SR coincided with reduced sediment layers stained black by FeS precipitation in the cores from Amon (Fig. 3a) and NL8PC1(4). In two cores from Isis (NL8PC3(1) and NL13PC4(7)), SR activity was distributed evenly throughout the cores but blackish sediment layers were not observed. Other hydrocarbons transported together with methane may have been responsible for the observed high SR activity exceeding that of AOM by several-fold. C_2 and higher

hydrocarbons have been detected in sediments and bottom waters of Amon and Isis (Mastalerz et al., unpublished data). A decoupling of AOM and SR in the presence of higher hydrocarbons has already been observed in seep sediments of the Gulf of Mexico (Joye et al., 2004), as well as the in Gulf of Cadiz (Niemann et al., 2006a).

Microbial community structure

Total cell numbers were ca 10^9 cells*ml^{-1} in surface sediments of both MVs (Table 4), which were on the lower end of numbers observed at other active seep settings (>10^{10} cells*ml^{-1}) (Michaelis et al., 2002; Knittel et al., 2003; Tina Lösekann et al., 2007). Fluorescence in situ hybridization (FISH) (Tables 4) as well as 16S rRNA gene analysis (Table 5) were carried out on representative cores from Amon (NL12PC1) and Isis (NL13PC4(7)). The dominance (36 - 58 %) of δ-proteobacterial sequences in the bacterial library from surface sediments below bacterial mats of both MVs were in accordance with the relatively high SR rates. A large portion of the 16S rDNA sequences were related to SRB of the genres *Desulfosarcina*, *Desulfococcus*, *Desulfocapsa* and *Desulfobulbus*, which are ubiquitous at seeps and have been previously implicated as partners of methanotrophic archaea (ANME) (Knittel et al., 2003). Using the probe DSS658, which targets the *Desulfosarcina/Desulfococcus* cluster, showed that most of these cells were aggregated with ANME-2 cells at Amon, whereas at Isis most of the DSS658 targeted cells were single cells. Interestingly, the core NL12PC1 from Amon also showed considerably closer coupling of AOM to SR. The dominance of the archaeal libraries by sequences most closely related to ANME-2, and their relatively high cell numbers was matched by relatively high AOM rates. ANME-1 and 3 cells were also

detected, but their numbers were below 1% of the total cells. Several sequences belonging to methanogens of the genus *Methanococcoides* were detected in sediments of both MVs. Incubations with these sediments under methanogenic conditions with methanol produced substantial enrichments of *Methanococcoides* (T. Holler, unpublished data), indicating that these organisms are viable within these sediments. These archaea are capable of growing on C-1 compounds and could contribute to local methane concentrations, however, their source of energy in the investigated sediments remains unknown. Also several other typical groups of cold-seep associated archaea and bacteria were detected (e.g. γ-proteobacteria, crenarcheota of the MBGD group); but the metabolic function and environmental role of these organisms was not further investigated here. Interestingly, at both MVs a significant portion of the bacteria (EUB) cells in consortium with ANME cells were not targeted by DSS658 or DBB660, indicating that other bacterial partners may be present. Despite differences in rates, and abundances of microbial groups, P-tests (> 5 %) between the 16S rDNA archaeal and bacterial libraries indicated that microbial communities at both MVs were not significantly different.

Central province of the NDSF

Visual observations

Three dives were dedicated to investigating different seafloor structures in the central province (Fig.1a,c): The active center of the North Alex mud volcano, and a region characterized by pockmarks and vast areas of carbonate crusts. For detailed morphological and geological descriptions of North Alex and the pockmarks see Dupre et

al. (Dupré et al., 2007) and Bayon *et al*. (Bayon et al., 2007). The central NDSF is comprised of three domains: an upper, middle and lower slope. The upper slope hosts large gas chimneys associated with mud volcanoes such as North Alex. The seafloor of the center of North Alex MV was much less disturbed than that of Amon and Isis, and was essentially flat (Fig. 2d). However, the center sediments were over pressurized with gas, as evidenced from spontaneous gas ebullition observed during the dive. The single blade core recovered from center was gas saturated and contained mud breccia interspersed with small chunks of carbonate (Figure 3c). Bacterial mats were not observed in the center of North Alex.

The middle slope area was characterized by a flat seafloor covered by vast areas of carbonate pavement (> 1 km), interspersed by reduced, grayish sediments, as well as many pockmarks (Fig. 2e). The pockmarks were circular depressions of about ca. 3 - 15 m in diameter and up to 3 m depth below the surrounding seafloor. Carbonate crusts and litter (Fig. 2e) were observed in the central depression of the pockmarks, indicating a connection between gas flow, microbial methane oxidation and carbonate precipitation (Bayon et al., 2007). One core was taken within a small pockmark (NL6PC1), and another one (NL7PC1) from relatively pelagic sediments of light brown color just outside a carbonate-covered area.

The area on the lower slope showed extensive (~ 500 m) flat and partially broken carbonate crusts, which hosted seep-associated fauna and lots of shell debris. Outside of the flat area many small carbonate mounds and small (3 m) pockmarks were observed. One core was taken within a pockmark, one close to a small carbonate mound in light brown sediments (NL14PC2; Fig. 2f). The larger carbonate pavements on the middle and

lower slope were interspersed by reduced blackish sediments (Fig. 2g), littered by shell debris. They hosted a variety of small chemosynthetic bivalves as well as small patches of living siboglinid tube worms (Fig. 2h). These organisms likely dependeds on the sulfide flux derived from hydrocarbon-fueled sulfate reduction in sediments below the crust. In contrast to Amon, Isis and North Alex, the pockmarks appeared to be an area of ancient, continuous and diffuse seepage activity as discussed by Bayon et al. (Bayon et al., 2007).

Sulfate reduction and anaerobic oxidation of methane

Methane concentrations of up to 0.2 μM in the bottom water above the centre of North Alex indicated that this mud volcano actively emitted methane, similar to Amon and Isis MVs (Mastalerz et al. unpublished data; (Dupré et al., 2007). According to the visual observations, the sediments were gas-saturated at the seafloor. Methane concentrations in retrieved cores from North Alex were up to 1.8 mM. In contrast, the bottom water from the middle and lower slope areas next to the pockmarks and carbonate pavements showed no or very low methane anomalies (Bayon et al., 2007). Correspondingly, sediment cores from these areas contained less than 10 μM methane.

SR and AOM rates measured (Fig. 3c and Table 3) at North Alex were 4 and 3.4 mmol cm^{-2} d^{-1} within the top 10 cm, showing a tight coupling (~ 1:1) between SR and AOM. Again, neither methane nor sulfate concentrations were depleted in this zone. In contrast, the cores taken outside the carbonate and pockmark area and within a pockmark, SR and AOM rates were generally < 0.1 mmol m^{-2} d^{-1}. Only the core from dive NL14 to the lower slope taken close to the carbonate mound showed higher rates (2.8 mmol m^{-2} d^{-}

^{1}) below 10 cm sediment depth. This is consistent with observations from Bayon et al.(Bayon et al., 2007), which suggest that the sediments beneath the crusts are active in methane turnover.

Microbial community structure

We chose the most active samples for analysis of the distribution of different microbial groups, the core from the center of North Alex (NL15BC1) and the core next to a small carbonate mound on the lower slope (NL14PC2). Cell numbers at North Alex were $>10^{9}$*cells*ml^{-1} in the surface sediments, however, only few consortia were detected (Table 4). They were not targeted by DSS658, indicating that an unknown bacterial partner(s) was involved in the AOM consortia. The vast majority of cells were unknown single cell bacteria; only 10 % of these were targeted by DSS658. ANME-1 and -2 cells were only a small part of the archaeal cells that were detected in both sediments. The cell numbers from the pockmarks region were considerably lower (0.4 - 0.9 10^{9}*cells*ml^{-1}) and methane-oxidizing archaea were virtually absent from these sediments. However, microbial biomarker analysis of carbonates from this site indicated that ANME-2 were the dominant group within the carbonates (Gontharet, unpublished data, Stadnitskaia unpublished data). Unfortunately, the active sediments below these carbonates could not be sampled.

Brine-influenced gas seeps: Western Province of the NDSF and the Olimpi mud volcano field

Visual observations

Three dives were dedicated to investigating sites of hydrocarbon and brine seepage in the Western Province of the NSDF and the Olimpi field of the Central Mediterranean Ridge (Table 1). The Chefren MV is located within the Menes caldera in the Western Province ((Huguen et al., 2007); Fig. 1a,d). The center of this MV hosted a large submarine lake filled with fluid mud and brines, which were partially covered by mats of sulfide oxidizers and their precipitates (Fig. 4a). The edges of the central lake were covered by clear brines (Fig. 4b). In contrast, the center of the Napoli MV, had many smaller sized brine pools some of which were empty (Fig. 4d). This area was previously investigated and further details of its geological, geochemical and biological characteristics have been published elsewhere (Charlou et al., 2003; Olu-Le Roy et al., 2004; Haese et al., 2006). We recovered 5 samples from the slope (NL4PC1, NL18PC2(7) and PC4(6)) and center of Chefren (NL19PC1(5) and PC3(8)), as well as 4 cores from the center of Napoli (NL1PC2, NL21PC5(1) and PC6(2), NL22PC7(3)) (Table 1). All cores recovered from seafloor areas were covered by visible bacterial mats and their mineral precipitates, which varied considerably in color and composition.

On the slope of Chefren, colorful white and orange microbial mats were detected associated with brine seepage (Fig. 4c). These mats and their associated microbial community were described in detail elsewhere (Omoregie et al., 2007). Briefly, the orange mats were composed of sheaths of iron-oxidizing bacteria as well as iron oxide precipitates. The white mats consisted mostly of sulfur filaments produced by

"*Candidatus* Arcobacter sulfidicus". Two cores (NL4PC1 and NL18PC4) were retrieved from the sulfide-oxidizing mats, as well as one core from iron-oxidizing mats (NL18PC2) at the bottom of the north-western slope of Chefren MV (Tab. 1). The mats at this site were associated with brine seepaged. Brine was observed flowing over the sulfide-oxidizing mats (Omoregie et al., 2007). The cores from the sulfide-oxidizing mats showed a highly reduced, blackish sediment horizon directly below the surface followed by dark grey mud breccia (Fig. 5a). In contrast, the core from the iron-oxidizing mat (Fig. 5b) had a reduced layer in the middle of the core, which was surrounded by brownish sediment. The two cores from the center of the Chefren MV were taken directly from the edge of a large brine lake in an area covered by clear brine (NL19PC1(5), PC3(8)). A thin line of bacterial mats formed directly between the interface of the brine and the seafloor (Fig. 4b). Both cores had reduced layers at the surface followed by dark brown sediment.

In the center of Napoli abundant patches of white mats presumably formed by sulfide oxidizing bacteria (Fig. 4e) as well as extensive carbonate crusts were visible at the seafloor (Fig. 4f). These carbonate crusts were also frequently perforated with tube worms similar to the pockmark area of the Central NDSF. Two cores from thin sulfide oxidizing mats (NL1PC2M and NL22PC3) and two cores from exposed blackish sediment between crusts (NL21PC1 and 2) were recovered from Napoli. All cores showed reduced sediment layers at the surface, and dark grey sediment interspersed with carbonate.

Sulfate reduction and anaerobic oxidation of methane

Methane concentrations in the bottom waters above the center of Chefren were relatively high (40 μM) in contrast to Napoli MV (20 nM) Mastalerz et al. unpublished data). The brines from both Chefren and Napoli (salinity of up to 153 and 268) contained high amounts of methane (up to 0.7 and 2.5 mM) and sulfide (up to 7.1 and 2.1) (Caprais et al., unpublished data). The sediments sampled from Chefren contained similar amounts of methane as at the other seeps of the NDSF (0.2 - 2 mM). At Napoli methane concentrations in the sediments were low (0.04 - 0.08 mM). The samples recovered from Chefren and Napoli MV showed a wide range of SR and AOM rates (0.2 - 66.5 and 0.1 - 2.3 mmol cm^{-2} d^{-1}, 0 -10 cm). Generally, SR exceeded AOM considerably, pointing to the presence of other hydrocarbon sources besides methane (Fig. 5a-c and Table 3). The highest rates were generally located close to the surface similar to the other cores investigated in this study. SR and AOM rates were similar to those investigated at other seeps in this study, suggesting that the presence of brines did not necessarily have a negative effect on the rates. Sulfate concentrations remained very high throughout the cores, even close to the peaks of SR (Fig. 5).

Microbial community structure

Similar to the 16S rRNA gene libraries of the Amon and Isis MV samples, those from the slope of Chefren were dominated by sequences from δ-proteobacteria and ANME-2 (Table 5). Sequences of aerobic methanotrophs were also abundant. Total cell numbers in samples from the slope of Chefren MV were slightly lower than those of the Amon and Isis MVs (Table 4). ANME-2 and -3 cells only made up a small proportion of

total archaeal cells, indicating that other archaeal groups, such as benthic crenarcheota may represent a significant biomass in these sediment zones. In contrast, a relatively high proportion of the bacterial cells were identified as sulfate reducers targeted by the DSS658 probe.

The cell numbers at the surface of Napoli were very high, but decreased to numbers similar to the other MVs in this study within a few cm below the surface. The archaeal composition at Napoli was different from other cold seeps in the NDSF. ANME-1 cells appeared to be the dominant ANME in the core from Napoli and ANME-2 were absent. Very few consortia were detected in the Napoli sediments. Bacteria of the *Desulfosarcina*/*Desulfococcus* cluster were abundant as free-living cells. This matched previous work conducted on sediments and carbonates recovered from Napoli (Pancost et al., 2000; Aloisi et al., 2002; Heijs, 2005). These studies detected highly ^{13}C-depleted biomarkers of archaea and SRB, as well as 16S rRNA gene sequences from Napoli sediments, which were representative of ANME-1 and DSS groups.

Comparisons between the bacterial libraries of sediments underlying the sulfide- and iron-oxidizing mats at Chefren indicated that they were significantly different (P value < 1 %). Details of this comparison are given elsewhere (Omoregie et al., 2007). Despite the proximity of the cores (<2 m distance), the difference in microbial community structure was not surprising giving the markedly different geochemistry between these two mats, especially with regard to dissolved iron and sulfide in the porewaters (Omoregie et al., 2007). This was also true for comparisons with the bacterial clone libraries from Amon and Isis MVs (P value < 5%). The archaeal libraries did not show significant differences between the sediments (P value > 5%), except for the

sulfide-oxidizing mat from Chefren (P value < 1%). The 16S rRNA gene data suggest that the presence of brine may affect bacterial diversity.

Summary

Here, we have provided the first AOM and SR measurements from cold seeps in the Eastern Mediterranean, which are considerably influenced by these processes in their geology, chemistry as well as biology (Pancost et al., 2000; Aloisi et al., 2002; Olu-Le Roy et al., 2004). AOM and SR also were the dominant biogeochemical processes at cold seeps of the NDSF. Our results show that the rates across the various cold seeps in the eastern Mediterranean were variable, both within different sites at the seeps, as well as between these seeps. Only some of the sediments investigated in this study showed a relatively tight coupling between AOM and sulfate reduction (e.g. North Alex, Amon). At most sites compounds other than methane were fueling sulfate reduction. In general, SR and especially AOM rates were lower than at other known seep systems, such as Hydrate Ridge and the Bush Hill site of the Gulf of Mexico, where AOM and SR rates of 50 - 100 mmol m^{-2} d^{-1} were reached (Treude et al., 2003; Joye et al., 2004). Rates of 1-10 mmol m^{-2} d^{-1} as measured at the active centres of the Amon, Isis, North Alex, Chefren and Napoli MVs were found at seeps either limited by electron donor flux such as at the Gulf of Cadiz MVs (Niemann et al., 2006a) or by electron acceptor availability as at Haakon Mosby MV on the Norwegian margin (Niemann et al., 2006b). In contrast to any other type of seep system previously investigated, the sediments were saturated with methane, but sulfate concentrations were always above 5 mM within the top 20 cm of sediment, and we did not reach the sulfate-methane transition zone in most of the cores.

The reason for this anomaly with regard to sulfate remains unknown. The relatively lower SR and AOM rates at the investigated sites match the relatively low biomass of methanotrophic archaea, and the low numbers of AOM consortia. A factor other than energy supply must control the standing stock of these key microorganisms at the cold seeps of the Eastern Mediterranean. Consequently, methane accumulates in the sediments of the MV centers and can pass the microbial filter. Accordingly, strong methane anomalies were observed in the water columns of all mud volcanoes investigated in this study. This indicates that the microbial filter is not efficient in eliminating the methane flux to the ocean at these sites, for reasons that require future investigation.

Acknowledgements

We would like to thank the crew and captain of RV L'Atalante, the NAUTILE team as well as the NAUTINIL team for their excellent support with work at sea. Also we thank Viola Beier, Imke Müller, Tomas Wilkop, Afua Asante-Poku and Abena Asante-Poku for help with analyses, and Katrin Knittel and Alban Ramette for scientific advice. The work of E.O., H.N., and A.B. in the ESF EUROCORES EUROMARGIN project MEDIFLUX was financially supported by ESF, DFG and the Max Planck Society.

References

Aloisi, G., Bouloubassi, I., Heijs, S.K., Pancost, R.D., Pierre, C., Damste, J.S.S., Gottschal, J.C., Forney, L.J. and Rouchy, J.M., 2002. CH4-consuming microorganisms and the formation of carbonate crusts at cold seeps. Earth and Planetary Science Letters, 203(1): 195-203.

Aloisi, G., Pierre, C., Rouchy, J.M., Foucher, J.P., Woodside, J. and Party, M.S., 2000. Methane-related authigenic carbonates of eastern Mediterranean Sea mud volcanoes and their possible relation to gas hydrate destabilisation. Earth and Planetary Science Letters, 184(1): 321-338.

Amann, R.I., Binder, B.J., Olson, R.J., Chisholm, S.W., Devereux, R. and Stahl, D.A., 1990. Combination of 16S rRNA-targeted oligonucleotide probes with flow cytometry for analyzing mixed microbial populations. Appl. Environ. Microbiol., 56: 1919-1925.

Bayon, G., Loncke, L., Dupré, S., Caprais, J.-C., Ducassou, E., Duperron, S., Foucher, J.-P., Fouquet, Y., Gontharet, S., Henderson, G.M., Etoubleau, J., Klaucke, I., Mascle, J., Migeon, S., Ondréas, H., Pierre, C., Huguen, C., Stadnitskaia, A., Woodside, J. and Sibuet, M., 2007. In situ investigation of the Centre Nile margin: Linking fluid seepage and continental-slope instabilities. Deep-Sea Research Part I Oceanographic Research Papers, Submitted.

Boetius, A., Ferdelman, T. and Lochte, K., 2000a. Bacterial activity in sediments of the deep Arabian Sea in relation to vertical flux. Deep-Sea Research Part I Oceanographic Research Papers, 47: 2835-2875.

Boetius, A. and Lochte, K., 1996. Effect of organic enrichments on hydrolytic potentials and growth of bacteria in deep-sea sediments. Mar. Ecol. Prog. Ser., 140: 239-250.

Boetius, A., Ravenschlag, K., Schubert, C.J., Rickert, D., Widdel, F., Giesecke, A., Amann, R., Jørgensen, B.B., Witte, U. and Pfannkuche, O., 2000b. A marine microbial consortium apparently mediating anaerobic oxidation of methane. Nature, 407: 623-626.

Boetius, A., Scheibe, S., Tselepides, A. and Thiel, H., 1996. Microbial biomass and activities in deep-sea sediments of the Eastern Mediterranean: trenches are benthic hotspots. Deep-Sea Research Part I Oceanographic Research Papers, 43: 1439-1460.

Bouloubassi, I., Aloisi, G., Pancost, R.D., Hopmans, E., Pierre, C. and Damste, J.S.S., 2006. Archaeal and bacterial lipids in authigenic carbonate crusts from eastern Mediterranean mud volcanoes. Organic Geochemistry, 37(4): 484-500.

Camerlenghi, A., Cita, M.B., Hieke, W. and Ricchiuto, T., 1992. Geological Evidence for Mud Diapirism on the Mediterranean Ridge Accretionary Complex. Earth and Planetary Science Letters, 109(3-4): 493-504.

Charlou, J.L., Donval, J.P., Zitter, T., Roy, N., Jean-Baptiste, P., Foucher, J.P., Woodside, J., Party, M.S. and, 2003. Evidence of methane venting and geochemistry of brines on mud volcanoes of the eastern Mediterranean Sea. Deep-Sea Research Part I Oceanographic Research Papers, 50(8): 941-958.

Cita, M.B., Ivanov, M.K. and Woodside, J.M., 1996. The Mediterranean Ridge Diapiric Belt - Introduction. Marine Geology, 132(1-4): 1-6.

Coleman, D.F. and Ballard, R.D., 2001. A highly concentrated region of cold hydrocarbon seeps in the southeastern Mediterranean Sea. Geo-Marine Letters, 21(3): 162-167.

Daims, H., Brühl, A., Amann, R. and Schleifer, K.H., 1999. The domain-specific probe EUB338 is insufficient for the detection of all Bacteria: Development and evaluation of a more comprehensive probe set. Systematic and Applied Microbiology, 22: 434-444.

Devereux, R., Kane, M.D., Winfrey, J. and Stahl, D.A., 1992. Genus- and group specific hybridization probes for determinative and environmental studies of sulfate-reducing bacteria. Systematic and Applied Microbiology, 15: 601-609.

Dupré, S., Woodside, J.M., Foucher, J.-P., de Lange, G., Mascle, J., Boetius, A., Mastalerz, V., Stadnitskaia, A., Ondreas, H., Huguen, C., Harmégnies, F., Gontharet, S., Loncke, L., Deville, E., Niemann, H., Omoregie, E., Olu-Le Roy, K., Fiala-Médioni, A., Dählmann, A., Caprais, J.-C., Prinzhofer, A., Sibuet, M., Pierre, C., Sinninghe Damsté, J. and Party, N.S., 2007. Seafloor geological studies above active gas chimneys off Egypt (Central Nile Deep Sea Fan). Deep-Sea Research Part I Oceanographic Research Papers, In Press.

Eller, G., Stubner, S. and Frenzel, P., 2001. Group-specific 16S rRNA targeted probes for the detection of type I and type II methanotrophs by fluorescence in situ hybridisation. Fems Microbiology Letters, 198(2): 91-97.

Fusi, N. and Kenyon, N.H., 1996. Distribution of mud diapirism and other geological structures from long-range sidescan sonar (GLORIA) data, in the Eastern Mediterranean Sea. Marine Geology, 132(1-4): 21-38.

Haese, R.R., Hensen, C. and de Lange, G.J., 2006. Pore water geochemistry of eastern Mediterranean mud volcanoes: Implications for fluid transport and fluid origin. Marine Geology, 225(1-4): 191-208.

Haese, R.R., Meile, C., Van Cappellen, P. and De Lange, G.J., 2003. Carbon geochemistry of cold seeps: Methane fluxes and transformation in sediments from Kazan mud volcano, eastern Mediterranean Sea. Earth and Planetary Science Letters, 212(3-4): 361-375.

Heijs, S., 2005. Microbial communiteis at deep-sea mud volcanoes in the Eastern Mediterranean Sea. PhD dissertation.

Heijs, S.K., Aloisi, G., Bouloubassi, I., Pancost, R.D., Pierre, C., Damste, J.S.S., Gottschal, J.C., van Elsas, J.D. and Forney, L.J., 2006. Microbial community structure in three deep-sea carbonate crusts. Microbial Ecology, 52(3): 451-462.

Heijs, S.K., Damste, J.S.S. and Forney, L.J., 2005. Characterization of a deep-sea microbial mat from an active cold seep at the Milano mud volcano in the Eastern Mediterranean Sea. Fems Microbiology Ecology, 54(1): 47-56.

Hinrichs, K.-U. and Boetius, A., 2002. The anaerobic oxidation of methane: new insights in microbial ecology and biogeochemistry. In: G. Wefer et al. (Editors), Ocean Margin Systems. Springer-Verlag, Berlin, pp. 457-477.

Huguen, C., Foucher, J.P., Mascle, J., Ondreas, H., Thouement, M., Gonthat, S., Stadnitskaia, A., Pierre, C., Bayon, G., Loncke, L., Boetius, A., Bouloubassi, I., Lange, G.d., Y. Fouquet, Woodside, J. and Party, N.S., 2007. The Western Nile Margin Fluid seepages features: “in situ” observations of the Menes caldera (NAUTINIL Expedition, 2003). In preparation.

Huguen, C., Mascle, J., Chaumillon, E., Kopf, A., Woodside, J. and Zitter, T., 2004. Structural setting and tectonic control of mud volcanoes from the Central Mediterranean Ridge (Eastern Mediterranean). Marine Geology, 209(1-4): 245-263.

Ishii, K., Mussmann, M., MacGregor, B.J. and Amann, R., 2004. An improved fluorescence in situ hybridization protocol for the identification of bacteria and archaea in marine sediments. FEMS Microbiology Ecology, 50(3): 203-213.

Iversen, N. and Blackburn, T.H., 1981. Seasonal rates of methane oxidation in anoxic marine sediments. Applied and Environmental Microbiology, 41(6): 1295-1300.

Joye, S.B., Boetius, A., Orcutt, B.N., Montoya, J.P., Schulz, H.N., Erickson, M.J. and Logo, S.K., 2004. The anaerobic oxidation of methane and sulfate reduction in sediments from Gulf of Mexico cold seeps. Chemical Geology, 205: 219-238.

Kallmeyer, J., Ferdelman, T.G., Weber, A., Fossing, H. and Jørgensen, B.B., 2004. Evaluation of a cold chromium distillation procedure for recovering very small amounts of radiolabeled sulfide related to sulfate reduction measurements. Limnology and Oceanography Methods, 2: 171-180.

Kane, M.D., Poulsen, L.K. and Stahl, D.A., 1993. Monitoring the Enrichment and Isolation of Sulfate-Reducing Bacteria by Using Oligonucleotide Hybridization Probes Designed from Environmentally Derived 16s Ribosomal-Rna Sequences. Applied and Environmental Microbiology, 59(3): 682-686.

Knittel, K., Boetius, A., Lemke, A., Eilers, H., Lochte, K., Pfannkuche, O., Linke, P. and Amann, R., 2003. Activity, distribution, and diversity of sulfate reducers and other bacteria in sediments above gas hydrate (Cascadia margin, Oregon). Geomicrobiology Journal, 20(4): 269-294.

Knittel, K., Losekann, T., Boetius, A., Kort, R. and Amann, R., 2005. Diversity and distribution of methanotrophic archaea at cold seeps. Applied and Environmental Microbiology, 71(1): 467-479.

Lane, D.J., Pace, B., Olsen, G.J., Stahl, D.A., Sogin, M.L. and Pace, N.R., 1985. Rapid-Determination of 16s Ribosomal-Rna Sequences for Phylogenetic Analyses. Proceedings of the National Academy of Sciences of the United States of America, 82(20): 6955-6959.

Limonov, A.F., Woodside, J.M., Cita, M.B. and Ivanov, M.K., 1996. The Mediterranean Ridge and related mud diapirism: A background. Marine Geology, 132(1-4): 7-19.

Loncke, L., Gaullier, V., Mascle, J., Vendeville, B. and Camera, L., 2006. The Nile deep-sea fan: An example of interacting sedimentation, salt tectonics, and inherited subsalt paleotopographic features. Marine and Petroleum Geology, 23(3): 297-315.

Loncke, L., Mascle, J., Parties, F.S. and, 2004. Mud volcanoes, gas chimneys, pockmarks and mounds in the Nile deep-sea fan (Eastern Mediterranean): geophysical evidences. Marine and Petroleum Geology, 21(6): 669-689.

Lösekann, T., Knittel, K., Nadalig, T., Fuchs, B., Niemann, H., Boetius, A. and Amann, R., 2007. Diversity and Abundance of Aerobic and Anaerobic Methane Oxidizers at the Haakon Mosby Mud Volcano, Barents Sea. Applied and Environmental Microbiology. Applied and Environmental Microbiology, 73: 3348-3362.

Ludwig, W., Strunk, O., Westram, R., Richter, L., Meier, H., Yadhukumar, Buchner, A., Lai, T., Steppi, S., Jobb, G., Forster, W., Brettske, I., Gerber, S., Ginhart, A.W.,

Gross, O., Grumann, S., Hermann, S., Jost, R., Konig, A., Liss, T., Lussmann, R., May, M., Nonhoff, B., Reichel, B., Strehlow, R., Stamatakis, A., Stuckmann, N., Vilbig, A., Lenke, M., Ludwig, T., Bode, A. and Schleifer, K.-H., 2004. ARB: a software environment for sequence data. Nucleic Acids Research, 32(4): 1363-1371.

Manz, W., Eisenbrecher, M., Neu, T.R. and Szewzyk, U., 1998. Abundance and spatial organization of Gram-negative sulfate-reducing bacteria in activated sludge investigated by in situ probing with specific 16S rRNA targeted oligonucleotides. FEMS Microbiology Ecology, 25: 43-61.

Mascle, J., Sardou, O., Loncke, L., Migeon, S., Camera, L. and Gaullier, V., 2006. Morphostructure of the Egyptian continental margin: Insights from swath bathymetry surveys. Marine Geophysical Researches, 27(1): 49-59.

Mascle, J., Zitter, T., Bellaiche, G., Droz, L., Gaullier, V., Loncke, L., Party, P.S. and, 2001. The Nile deep sea fan: preliminary results from a swath bathymetry survey. Marine and Petroleum Geology, 18(4): 471-477.

Massana, R., Murray, A.E., Preston, C.M. and DeLong, E.F., 1997. Vertical distribution and phylogenetic characterization of marine planktonic Archaea in the Santa Barbara Channel. Applied and Environmental Microbiology, 63(1): 50-56.

Michaelis, W., Seifert, R., Nauhaus, K., Treude, T., Thiel, V., Blumenberg, M., Knittel, K., Gieseke, A., Peterknecht, K., Pape, T., Boetius, A., Aman, A., Jørgensen, B.B., Widdel, F., Peckmann, J., Pimenov, N.V. and Gulin, M., 2002. Microbial reefs in the Black Sea fueled by anaerobic oxidation of methane. Science, 297: 1013-1015.

Muyzer, G., Teske, A., Wirsen, C.O. and Jannasch, H.W., 1995. Phylogenetic-Relationships of Thiomicrospira Species and Their Identification in Deep-Sea Hydrothermal Vent Samples by Denaturing Gradient Gel-Electrophoresis of 16s Rdna Fragments. Archives of Microbiology, 164(3): 165-172.

Niemann, H., Duarte, J., Hensen, C., Omoregie, E., Magalhaes, V.H., Elvert, M., Pinheiro, L.M., Kopf, A. and Boetius, A., 2006a. Microbial methane turnover at mud volcanoes of the Gulf of Cadiz. Geochimica et Cosmochimica Acta, 70(21): 5336.

Niemann, H., Losekann, T., de Beer, D., Elvert, M., Nadalig, T., Knittel, K., Amann, R., Sauter, E.J., Schluter, M., Klages, M., Foucher, J.P. and Boetius, A., 2006b. Novel microbial communities of the Haakon Mosby mud volcano and their role as a methane sink. Nature, 443(7113): 854.

Olu-Le Roy, K., Sibuet, M., Fiala-Medioni, A., Gofas, S., Salas, C., Mariotti, A., Foucher, J.P. and Woodside, J., 2004. Cold seep communities in the deep eastern Mediterranean Sea: composition, symbiosis and spatial distribution on mud volcanoes. Deep-Sea Research Part I Oceanographic Research Papers, 51(12): 1915-1936.

Omoregie, E.O., Mastalerz, V., Lange, G.d., Straub, K.L., Kappler, A., Roey, H., Stadnitskaia, A., Foucher, J.-P. and Boetius, A., 2007. Biogeochemistry and community composition of iron- and sulfide-oxidizing microbial mats at the Chefren mud volcano. In preparation.

Orphan, V.J., House, C.H., Hinrichs, K.-U., McKeegan, K.D. and De Long, E.F., 2001. Methane-consuming Archaea revealed by directly coupled isotopic and phylogenetic analysis. Science, 293: 484-487.

Pancost, R.D., Damste, J.S.S., de Lint, S., van der Maarel, M.J.E.C., Gottschal, J.C. and Party, M.S.S., 2000. Biomarker evidence for widespread anaerobic methane oxidation in Mediterranean sediments by a consortium of methanogenic archaea and bacteria. Applied and Environmental Microbiology, 66(3): 1126-1132.

Reeburgh, W.S., 2007. Oceanic methane biogeochemistry. Chemical Reviews, 107(2): 486-513.

Ritger, S., Carson, B. and Suess, E., 1987. Methane-Derived Authigenic Carbonates Formed by Subduction Induced Pore-Water Expulsion Along the Oregon Washington Margin. Geological Society of America Bulletin, 98(2): 147-156.

Schloss, P.D., Larget, B.R. and Handelsman, J., 2004. Integration of microbial ecology and statistics: a test to compare gene libraries. Applied and Environmental Microbiology, 70(9): 5485-5492.

Sibuet, M. and Olu-Le Roy, K., 2002. Cold Seep Communities on Continental Margins: Structure and Quantitative Distribution Relative to Geological and Fluid Venting Patterns, Ocean Margin System. Springer Verlag, pp. 235-251.

Silva, I.P., Erba, E., Spezzaferri, S. and Cita, M.B., 1996. Age variation in the source of the diapiric mud breccia along and across the axis of the Mediterranean Ridge Accretionary Complex. Marine Geology, 132(1-4): 175-202.

Snaidr, J., Amann, R., Huber, I., Ludwig, W. and Schleifer, K.H., 1997. Phylogenetic analysis and in situ identification of bacteria in activated sludge. Applied and Environmental Microbiology, 63(7): 2884-2896.

Teske, A., Hinrichs, K.U., Edgcomb, V., de Vera Gomez, A., Kysela, D., Sylva, S.P., Sogin, M.L. and Jannasch, H.W., 2002. Microbial diversity of hydrothermal sediments in the Guaymas Basin: evidence for anaerobic methanotrophic communities. Applied and Environmental Microbiology, 68(4): 1994-2007.

Tina Lösekann, Katrin Knittel, Thierry Nadalig, Bernhard Fuchs, Helge Niemann, Antje Boetius and Amann, R., 2007. Diversity and abundance of aerobic and anaerobic methane oxidizers at the Haakon Mosby Mud Volcano, Barents Sea. Applied and Environmental Microbiology, 73: 3348-3362.

Treude, T., Boetius, A., Knittel, K., Wallmann, K. and Jørgensen, B.B., 2003. Anaerobic oxidation of methane above gas hydrates at Hydrate Ridge, NE Pacific Ocean. Marine Ecology Progress Series, 264: 1-14.

Treude, T., Knittel, K., Blumenberg, M., Seifert, R. and Boetius, A., 2005. Subsurface Microbial Methanotrophic Mats in the Black Sea. Applied and Environmental Microbiology, 71(10): 6375-6378.

Volgin, A.V. and Woodside, J.M., 1996. Sidescan sonar images of mud volcanoes from the Mediterranean Ridge: Possible causes of variations in backscatter intensity. Marine Geology, 132(1-4): 39-53.

Wallner, G., Steinmetz, I., Bitter-Suermann, D. and Amann, R., 1996. Flow cytometric analysis of activated sludge with rRNA-targeted probes. Applied and Environmental Microbiology, 19: 569-576.

Woodside, J.M., Ivanov, M.K., Limonov, A.F. and Shipboard Scientist of the, A.E., 1998. Shallow gas and gas hydrates in the Anaximander Mountains region, eastern Mediterranean Sea. Geological Society, London, Special Publications, 137(1): 177-193.

Zitter, T.A.C., Huguen, C. and Woodside, J.M., 2005. Geology of mud volcanoes in the eastern Mediterranean from combined sidescan sonar and submersible surveys. Deep-Sea Research Part I Oceanographic Research Papers, 52(3): 457-475.

Dive	Location[a]	Site	Latitude	Longitude	Depth (m)	Core ID	SO_4^{2-}	CH_4	SR	AOM	16S	FISH	Dive observation
11	E	Amon, SE center	32 22.1444	31 42.6481	1121	NL11PC1	x	x	x	x	-	-	sulfide oxidizing mat
12	E	Amon, SW center	32 22.1418	31 42.5926	1120	NL12PC2	x	x	x	x	x	x	sulfide oxidizing mat
8	E	Isis, center	32 21.6619	31 23.3714	992	NL8PC1(4)	-	x	x	x	-	-	sulfide oxidizing mat
8	E	Isis, center	32 21.6678	31 23.3572	992	NL8PC3(1)	x	x	x	x	-	-	gas saturated grayish sediment
13	E	Isis, NW center	32 21.6779	31 23.3370	991	NL13PC4(7)	x	x	x	x	x	x	sulfide oxidizing mat
6	C	Pockmarks, middle slope	32 38.1418	29 56.1236	2114	NL6PC1	x	x	x	x	-	-	within a pockmark
7	C	Pockmarks, middle slope	32 31.6062	30 20.6553	1691	NL7PC1	-	x	x	x	-	-	away from pockmarks and carbonate
14	C	Pockmarks, lower slope	32 38.4402	29 54.9764	2127	NL14PC2	-	x	x	x	-	x	close to carbonate
15	C	North Alex, E center	31 58.1897	30 08.2229	507	NL15BC1	x	x	x	x	x	-	grey sediment without mats
4	W	Chefren, NW slope	32 06.7373	28 10.3497	3023	NL4PC1	-	x	x	x	-	-	sulfide oxidizing mat
18	W	Chefren, NW slope	32 06.7406	28 10.3487	3024	NL18PC2(7)	x	x	x	x	x	x	iron oxidizing mat
18	W	Chefren, NW slope	32 06.7397	28 10.3510	3022	NL18PC4(6)	x	x	x	x	x	x	sulfide oxidizing mat
19	W	Chefren, S center	32 06.4872	28 10.6767	2968	NL19PC1(5)	x	x	x	x	-	-	the edge of a brine lake
19	W	Chefren, S center	33 06.4872	28 10.6774	2968	NL19PC3(8)	x	-	x	x	-	x	the edge of a brine lake
1	MR	Napoli, center	33 43.4759	24 41.0472	1939	NL1PC2	x	x	x	x	-	x	sulfide oxidizing mat
21	MR	Napoli, NW center	33 43.6553	24 40.8541	1946	NL21PC5(1)			x	x	-	-	sulfide oxidizing mat
21	MR	Napoli, NW center	34 43.6553	24.40.8541	1946	NL21PC6(2)	x	x	x	x	-	-	sulfide oxidizing mat
22	MR	Napoli, S center	33 43.3569	24 41.0522	1940	NL22PC7(3)	x	x	x	x	-	-	sulfide oxidizing mat

Table 1. Sediment cores, and analysis conducted within this study.

a. Location within the Eastern (E), Central (C) and Western (W) Nile Deep-Sea fan, as well as the Mediterranean Ridge (MR).

Probe	Target Group	Taxon	Sequence (5' to 3')	Type	%Formamid	°C Hybrid/Wash	Reference
ARCH915	Most Archaea	Archaea	GTG CTC CCC CGC CAA TTC CT	CARD	35	46/48	Amann et al. 1990
ANME-1-350	ANME-1	Euryarchaeota	GTG CTC CCC CGC CAA TTC CT	CARD	40	46/48	Boetius *et al.* 2000
ANME-2-538	ANME-2	Euryarchaeota	GGC TAC CAC TCG GGC CGC	FISH	50	46/48	Treude *et al.* 2005
ANME-3-1249	ANME-3	Euryarchaeota	TCG GAG TAG GGA CCC ATT	CARD	20	46/48	Lösekann *et al.* 2007
EUB I	Most bacteria	Bacteria	GCT GCC TCC CGT AGG AGT	CARD	35	46/48	Amann et al. 1990
EUB II	Planctomycetales	Bacteria	GCA GCC ACC CGT AGG TGT	CARD	35	46/48	Daims *et al.* 1999
EUB III	Verrucomicrobiales	Bacteria	GCT GCC ACC CGT AGG TGT	CARD	35	46/48	Daims *et al.* 1999
Non338	negative hybridization probe	-	ACTCCTACGGGAGGCAGC	CARD/FISH	variable	46/48	Wallner *et al.* 1993
DSS658	*Desulfosarcina-Desulfococcus*	δ-Proteobacteria	TCCACTTCCCTCTCCCAT	CARD	50	46/48	Manz *et al.* 1998
DBB660	*Desulfobulbus*	δ-Proteobacteria	GAA TTC CAC TTT CCC CTC TG	CARD	60	46/48	Devereux *et al.* 1992
Mγ705	Type I Methanotrophs	γ-Proteobacteria	CTG GTG TTC CTT CAG ATC	FISH	20	46/48	Gulledge *et al.* 1992

Table 2. Oligonucleotide probes and hybridization conditions used in this study. EUB-I, II, III were mixed into a single solution.

Location	Core	SR(0-4)	AOM(0-4)	SR/AOM	SR (4-10)	AOM(4-10)	SR/AOM	SR(0-10)	AOM(0-10)	SR/AOM	SR (10-)	AOM(10-)	SR/AOM	core depth
Amon	NL11PC1	2.0	0.1	**15**	8.5	3.0	**3**	10.5	3.1	**3**	10.7	0.8	**14**	(23cm)
Amon	NL12PC2	9.9	2.2	**5**	6.8	3.7	**2**	16.7	5.8	**3**	2.8	0.8	**3**	(15cm)
Isis	NL8PC1(4)	3.2	0.2	**14**	0.7	0.1	**6**	3.8	0.3	**12**	-	-	**-**	
Isis	NL8PC3(1)	3.3	0.2	**14**	5.3	0.1	**57**	8.6	0.3	**26**	-	-	**-**	
Isis	NL13PC4(7)	24.8	1.5	**17**	19.1	2.1	**9**	44.0	3.6	**12**	-	-	**-**	
Pockmarks	NL6PC1	0.1	<	**-**	<	<	**-**	0.1	<	**-**	-	-	**-**	
Pockmarks	NL7PC1	<	<	**-**	<	<	**-**	<	<	**-**	-	-	**-**	
Pockmarks	NL14PC2	0.1	0.1	**1**	0.1	<	**-**	0.1	0.1	**2**	2.8	<	**-**	(21cm)
North Alex	NL15BC1	1.2	0.9	**1**	2.8	2.5	**1**	4.0	3.5	**1**	-	-	**-**	
Chefren	NL4PC1	42.7	0.6	**72**	23.9	0.3	**79**	**66.5**	**0.9**	**75**	2.1	0.2	**10**	(25cm)
Chefren	NL18PC4(6)	4.1	0.1	**72**	0.3	0.1	**3**	4.4	0.2	**28**	-	-	**-**	
Chefren	NL18PC2(7)	0.8	0.2	**4**	4.6	0.3	**16**	5.3	0.5	**11**	0.6	0.1	**6**	(15cm)
Chefren	NL19PC3(8)	0.2	0.2	**1**	<	0.1	**-**	0.2	0.3	**1**	-	-	**-**	
Chefren	NL19PC1(5)	0.5	1.2	**-**	0.1	1.1	**-**	0.7	2.3	**-**	-	-	**-**	
Napoli	NL1PC2	8.7	<	**-**	0.1	<	**-**	8.8	<	**-**	-	-	**-**	
Napoli	NL21PC6(2)	2.0	<	**-**	0.1	<	**-**	2.1	<	**-**	-	-	**-**	
Napoli	NL21PC5(1)	4.4	0.1	**70**	3.6	<	**-**	8.0	0.1	**87**	27.1	<	**-**	(13cm)
Napoli	NL22PC7(3)	0.6	<	**-**	3.6	<	**-**	4.2	<	**-**	-	-	**-**	

Table 3. Depth integrated sulfate reduction (SR) and anaerobic oxidation of methane (AOM) rates in different sediment horizons (mmoles*m-2*d-1). "<" indicates less than 0.01 mmoles*m-2*d-1.

			ARC915			ANME1			ANME2			EUBI-III			DSS658			Mγ705		
	Depth	Total Cells 1x10^9	Free Cells 1x10^9	Cells in Agg1x10^9	Percent Total	Free Cells 1x10^9	Cells in Agg1x10^9	Percent Total	Free Cells 1x10^9	Cells in Agg1x10^9	Percent Total	Free Cells 1x109	Cells in Agg1x109	Percent Total	Free Cells 1x109	Cells in Agg1x109	Percent Total	Free Cells 1x109	Cells in Agg1x109	Percent Total
Amon	**0-2cm**	2.87	0.05	1.07	39	<	<	<	<	0.57	20	0.99	0.54	53	0.05	0.63	24	<	<	<
NL12PC1	**2-4cm**	2.63	0.06	0.99	40	<	<	<	<	0.24	9	0.95	0.50	55	0.08	0.36	17	<	<	<
	10-12cm	0.30	0.01	0.00	5	<	<	<	<	<	<	0.11	0.00	38	0.01	nd	2	<	<	<
Isis	**0-2cm**	2.83	0.26	0.42	24	<	<	<	<	0.17	6	1.65	0.21	66	0.09	0.01	4	<	<	<
NL13PC4(7)	**2-4cm**	2.84	0.05	0.96	36	<	<	<	<	0.81	29	0.73	0.48	43	0.21	0.00	7	<	<	<
	10-12cm	1.76	0.11	0.46	32	<	<	<	<	-	-	0.86	0.23	62	0.07	0.00	4	<	<	<
PockM	**0-2cm**	0.67	0.11	<	17	<	<	<	<	<	<	0.32	<	47	<	<		<	<	<
NL14PC2	**2-4cm**	0.88	0.02	<	2	<	<	<	<	<	<	0.22	<	24	<	<		0.01	<	2
	10-12cm	0.41	0.01	<	3	<	<	<	<	<	<	0.08	<	19	<	<			<	<
North A.	**0-2cm**	2.77	0.11	0.16	10	0.02	<	1	<	0.15	5	2.08	0.08	78	0.25	0.00	9	<	<	<
NL15BC1	**2-4cm**	2.99	0.04	0.13	6	0.01	<	0	<	<	<	2.44	0.06	84	0.30	0.00	10	<	<	<
	10-12cm	1.85	0.09	0.18	14	0.03	<	2	<	0.06	3	0.16	0.09	14	0.06	0.00	3	<	<	<
Chefren	**0-2cm**	0.90	0.06	<	7	<	<	<	<	<	<	0.47	<	52	0.21	<	23	<	<	<
NL18PC4(6)	**2-4cm**	1.20	0.07	0.19	22	<	<	<	<	0.12	10	0.49	0.09	48	0.16	0.05	18	<	<	<
	10-12cm	0.42	0.07	<	17	<	<	<	<	<	<	0.13	<	30	<	<	<	<	<	<
Chefren	**0-2cm**	1.17	0.02	0.02	4	<	<	<	<	0.03	3	0.77	0.01	67	0.13	0.01	12	0.03	<	2
NL18PC2(7)	**2-4cm**	3.47	0.27	0.27	15	<	<	<	<	0.31	9	1.09	0.13	35	0.09	0.31	11	<	<	<
	10-12cm	1.78	0.34	<	19	<	<	<	<	<	<	0.16	<	9	0.13	<	7	<	<	<
Napoli	**0-2 cm**	15.69	3.27	0.99	27	1.04	<	7	<	<	<	5.96	0.50	41	2.35	<	15	0.06	<	1
NL1PC2	**2-4 cm**	1.80	0.32	<	18	0.16	<	9	<	<	<	0.76	<	42	0.13	<	7	0.00	<	1
	10-12 cm	1.99	0.66	<	33	0.43	<	22	<	<	<	0.54	<	27	<	<	0	<	<	<

Table 4. Cell numbers as well as FISH counts for archaea and bacteria. ANME-3 and DBB660 targeted cells were less than 1 % of total cell numbers. Numbers are ml-1 of sediment

Phylogenetic group	Amon (NL12PC1)	Isis (NL12PC1)	Chefren (NL18PC4(6))	Chefren (NL18PC2(7))
Total number of bacterial clones	**79**	**64**	**87**	**88**
% α-proteobacteria	**1**	**5**	**0**	**1**
% γ-proteobacteria	**25**	**20**	**9**	**34**
Type I methanothrophs	8	5	2	7
% δ-proteobacteria	**58**	**36**	**43**	**31**
Desulfobacteraceae	37	28	32	17
Desulfobulbaceae	18	5	8	10
Desulfuromonadaceae	3	0	0	1
% ε-proteobacteria	**1**	**6**	**0**	**7**
Arcobacter sp.	0	0	0	0
Sulfospirillum sp.	0	0	0	0
Sulfurimonas sp.	0	0	0	0
% Other bacteria	**11**	**28**	**24**	**16**
% Unidentified bacteria	**3**	**5**	**24**	**11**
Total number of archaeal clones	**65**	**71**	**70**	**67**
% Euryarcheaota	**100**	**97**	**96**	**99**
Methanococcoides	3	1	0	0
ANME-undesignated	3	1	0	3
ANME-2A	51	31	19	51
ANME-2C	12	8	1	3
ANME-3	0	0	56	0
MBG-D	15	51	16	53
% Crenarcheaota	**0**	**3**	**4**	**1**
MBG-B	0	1	4	1
MBG-1	0	1	0	0

Table 5. Breakdown of 16S rRNA gene sequences, in percentages obtained from selected cores in this study.

Figure legends

Figure 1A. Bathymetric map of the Eastern Mediterranean. Small and large and rectangles are the Olimpi mud volcano field and the Nile Deep Sea Fan, respectively. Numbers indicate the locations of the Napoli (1), Chefren (2), North Alex (5) Isis (6), and Amon (7) mud volcanoes as well as the pockmark region in the middle (3) and lower slope (4). (B) 3D-Bathymetric maps of Amon and Isis, (C) the pockmark region and the Menes cladera (D). After (Mascle et al., 2006; Dupré et al., 2007).

Figure 2. Seafloor images taken submersible Nautile. (A) Troughs at Amon covered with sulfide oxidizing mats. (B) Troughs at Isis covered with sulfide-oxidizing mats. (C) Flat seabed at Isis with sulfide-oxidizing mats (NL8PC1(4), NL13PC4(7)) and grey patches (NL8PC3(1)). (D) Flat seabed of North Alex (NL15BC). (E) Pockmark from middle slope (Dive NL7). (F) Edge of carbonate pavement of the lower slope (NL14PC2). (G) Carbonate crust from the lower slope. (H) Close up of tube worms and shell debris associated with a carbonate crust.

Figure 3. Sulfate reduction, and anaerobic oxidation of methane, as well as pore water chemistry measurements for selected cores. Core descriptions are located to the right. (A) Sulfide oxidizer mat from Amon (NL12PC1). (B) Sulfide oxidizer mat from Isis (NL13PC4(7)). (C) Next to a carbonate crust (NL14PC1). (D) Gas saturated sediment from North Alex (NL15BC1). Note the different scales on the x-axes. The solid lines represent methane and sulfate concentrations.

Figure 4. Seafloor images taken submersible Nautile. (A) Brine pool at Chefren covered with sulfide-oxidizing mats. (B) Sediment (upper left) and brine transition, bisected by sulfide-oxidizing mats at Chefren (NL19PC1(5) and PC3(8)). (C) Sulfide and iron oxidizing mats at Chefren (NL4PC1, NL18PC2(7), PC4(6)). (D) Brine lake at Napoli. (E) Sulfide-oxidizing mats and reduced sediment at Napoli (NL1PC2, NL21PC5(1), PC6(2) and NL22PC7(3)). (F) Carbonate crusts at Napoli.

Figure 5. Sulfate reduction, and anaerobic oxidation of methane, as well as pore water chemistry measurements for selected cores of brine-impacted sites. Core descriptions are located to the right, for explanations see Fig. 3. (A) Sulfide-oxidizing mat from Chefren (NL18PC4(6)). (B) Iron-oxidizing mat from Chefren (NL18PC2(7)). (C) Sulfide-oxidizing mat from Napoli (NL1PC2). Note the different scales on the x-axis.

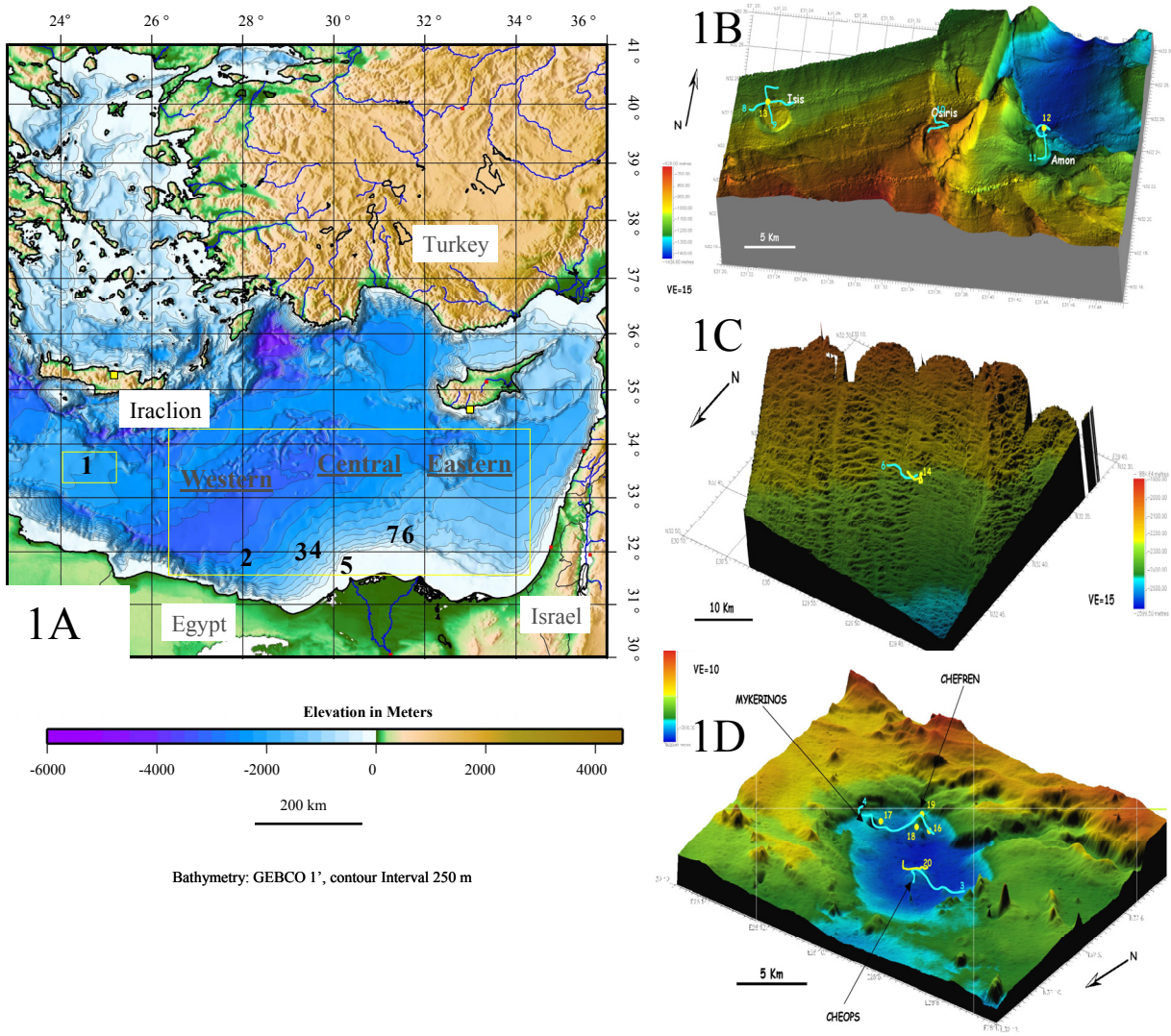

Bathymetry: GEBCO 1', contour Interval 250 m

Figure 1

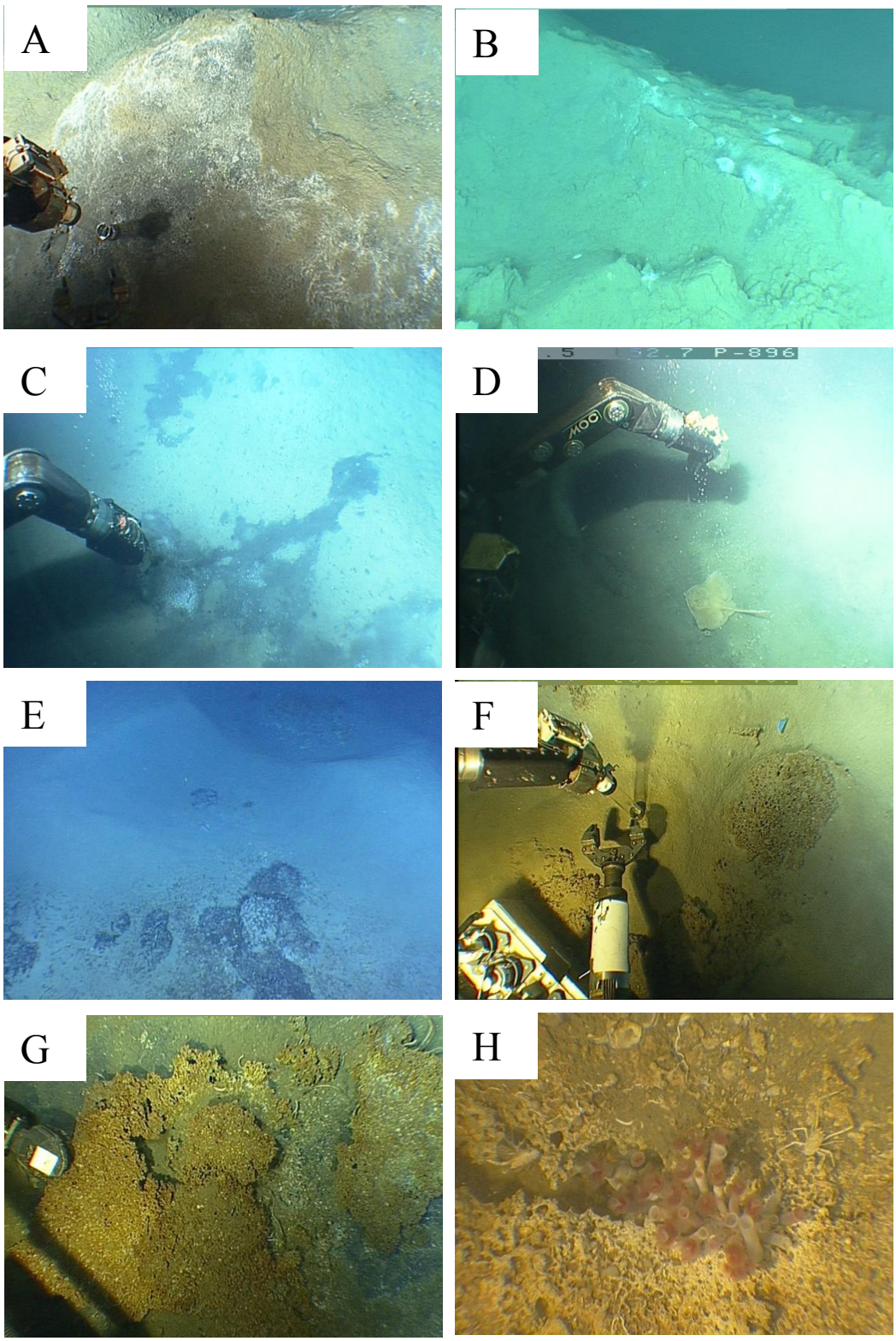

Figure 2

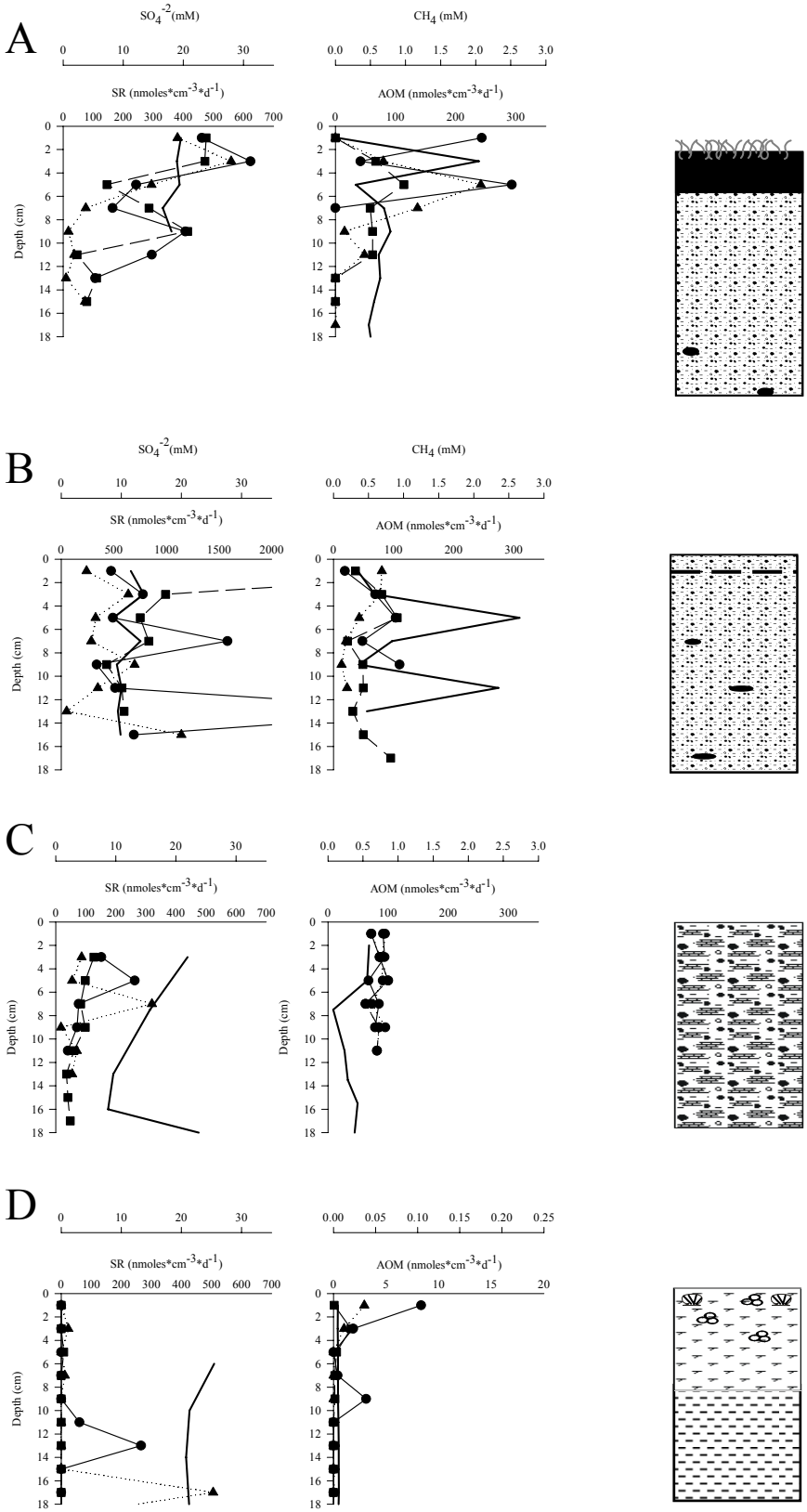
A
B
C
D
SO_4^{-2}(mM)
CH_4 (mM)
SR (nmoles*cm^{-3}*d^{-1})
AOM (nmoles*cm^{-3}*d^{-1})
Depth (cm)
Microbial filaments
Sulfur precipitate
MARL
MUD /CLAY
MUD BRECCIA
Fe oxide precipitate
Shells
Iron sulfide layer

Figure 3

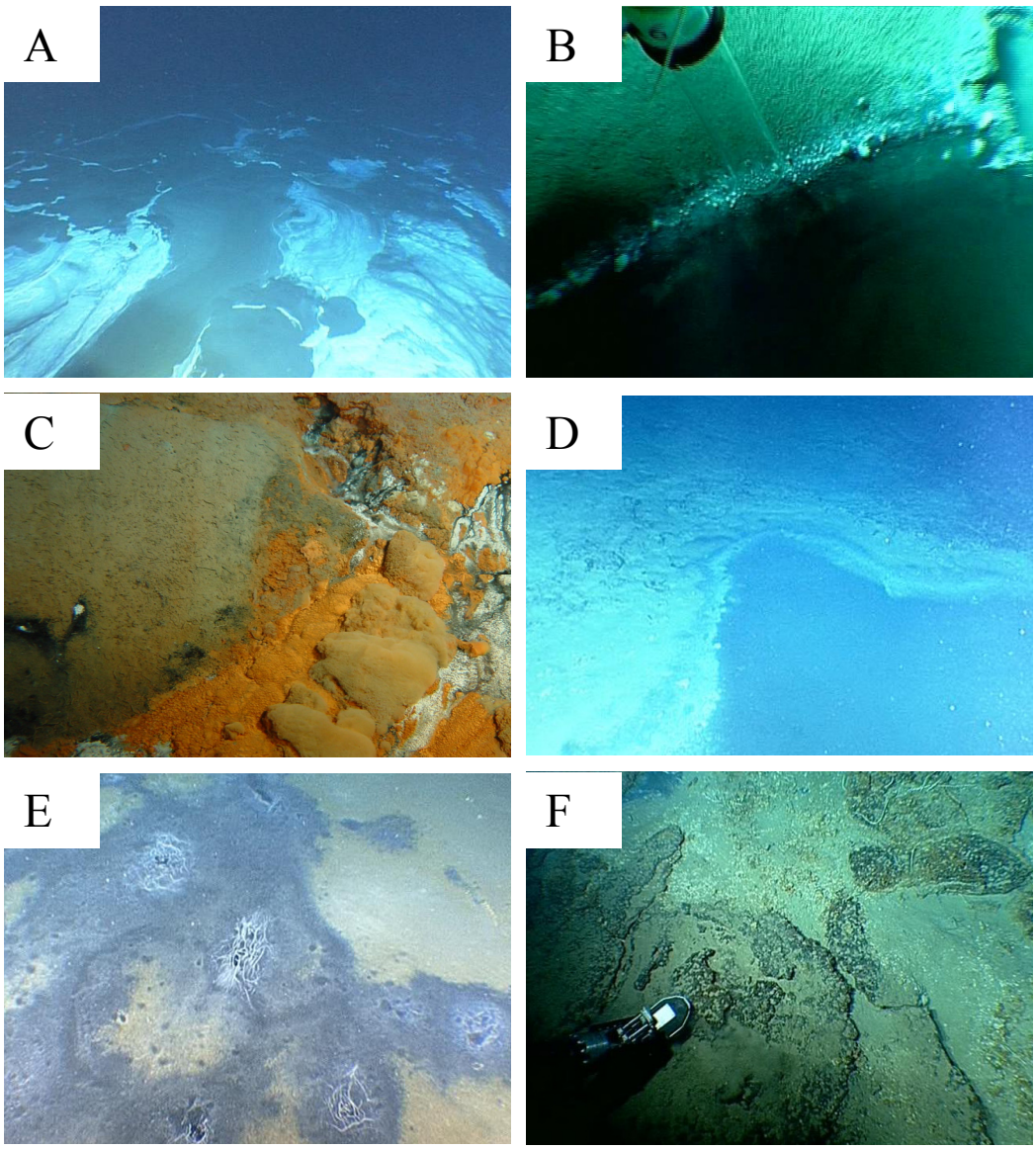

Figure 4

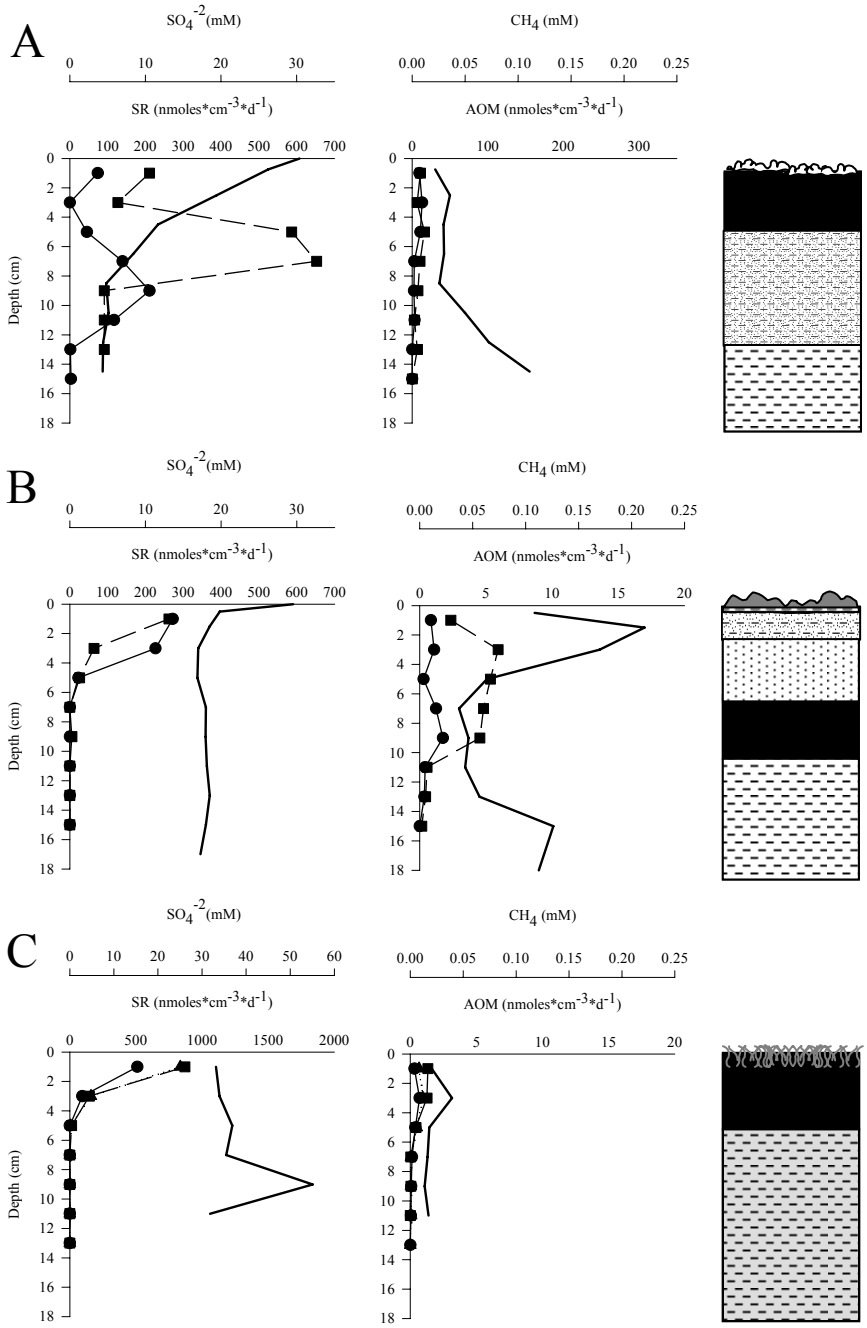
A
SO_4^{-2}(mM)
CH_4 (mM)
SR (nmoles*cm^{-3}*d^{-1})
AOM (nmoles*cm^{-3}*d^{-1})
Depth (cm)
B
SO_4^{-2}(mM)
CH_4 (mM)
SR (nmoles*cm^{-3}*d^{-1})
AOM (nmoles*cm^{-3}*d^{-1})
Depth (cm)
C
SO_4^{-2}(mM)
CH_4 (mM)
SR (nmoles*cm^{-3}*d^{-1})
AOM (nmoles*cm^{-3}*d^{-1})
Depth (cm)

Figure 5

Chapter V: Biogeochemistry and community composition of iron- and sulfide-oxidizing microbial mats at the Chefren mud volcano (Nile Deep Sea Fan, Eastern Mediterranean)

Biogeochemistry and community composition of iron- and sulfide-oxidizing microbial mats at the Chefren mud volcano (Nile Deep Sea Fan, Eastern Mediterranean)

Running title: Iron- and sulfide-oxidizing mats at a mud volcano

[*1,2]Enoma O. Omoregie, [3]Vincent Mastalerz, [3]Gert de Lange, [4#]Kristina L. Straub, [4]Andreas Kappler, [1]Hans Røy, [5]Alina Stadnitskaia, [6]Jean-Paul Foucher, [*1,2,7]Antje Boetius

[*1]Max Planck Institute for Marine Microbiology, Bremen, Germany, [2]Jacobs University, Bremen, Germany, [3]Department of Earth Sciences, Utrecht University, Utrecht, The Netherlands, [4]Center for Applied Geosciences, Eberhard-Karls-University, Tübingen, Germany, [5]Royal Netherlands Institute for Sea Research (NIOZ), Texel, The Netherlands [6]Department of Marine Geosciences, IFREMER Centre de Brest, Plouzane Cedex, France, [7]Alfred Wegener Institute for Polar and Marine Research, Bremerhaven, Germany

Present address: Department of Biogeochemistry, Vienna University, Vienna, Austria

* Corresponding authors: eomoregi@mpi-bremen.de; aboetius@mpi-bremen.de

Max Planck Institute for Marine Microbiology, Celsiusstr. 1, Bremen, Germany

Phone: (+49) 421-2028-869; (+49) 421-2028-869

Fax: (+49) 421-2028-870

Keywords: iron-oxidation, sulfide-oxidation, sulfate reduction, methane oxidation, *Arcobacter*, *Leptothrix*, cold seeps, mud volcanoes, Nile Deep Sea Fan

This Manuscript will be submitted to Applied and Environmental Microbiology

Abstract

At active mud volcanoes, methane and other energy-rich compounds are transported from deep subsurface reservoirs to the seafloor where they support chemosynthetic bacterial and faunal communities. In this study we identified the composition and underlying biogeochemistry of novel, brightly colored white and orange microbial mats at the surface of a brine seep at the outer rim of the Chefren mud volcano (Western Nile Deep Sea Fan). These mats were interspersed with one another but their underlying sediment biogeochemistry differed considerably. Microscopy revealed the white mats to be granules composed of elemental S filaments morphologically similar to those produced by the sulfide-oxidizing ε-proteobacterium "*Candidatus* Arcobacter sulfidicus". Fluorescence in situ hybridization (FISH) indicated that microorganisms targeted by a "C. sulfidicus"-specific oligonucleotide probe (Arc94) constituted up to 25% of the total cells within this mat. Several 16S rRNA genes were identified from organisms closely related to "C. sulfidicus" as well as other sulfide-oxidizing ε-proteobacteria. In contrast, the orange mat consisted mostly of bright orange flakes partially covered by yellow fluffy material. The flakes were composed of Fe(III)-(hydr)oxides coated microbial sheaths similar to those produced by the neutrophilic Fe(II)-oxidizing γ-proteobacterium *Leptothrix ochracea*. However, none of the 16S rRNA gene sequences obtained in this study were closely related to known neutrophilic aerobic Fe(II)-oxidizing bacteria. FISH with the Mγ705 probe revealed sheathed bacteria with similar morphology to the type I methanotrophs *Crenothrix polyspora* and *Clonothrix fusca* within these flakes. 16S rRNA gene sequences related to both these bacteria were recovered from the flakes and the underlying sediment. The sediments

below the white mats showed relatively high sulfate reduction (SR) rates (max. 350 - 400 nmol*cm^{-3}*d^{-1}) fueled only in small part by methane oxidation (max. 10 - 20 nmol*cm^{-3}*d^{-1}). In the SR zone below the white mat, excess pore water sulfide was depleted by microbial sulfide oxidation within the surface layer. In contrast, below the orange mat excess dissolved Fe(II) reached the surface layer, and was depleted in part by microbial Fe(II) oxidation. Both mats as well as the sediments underneath them hosted very diverse microbial communities and mineral precipitates, most likely due to differences in fluid flow patterns.

Introduction

Submarine mud volcanoes are geological structures formed by episodic eruption of gases and muds from deep subsurface reservoirs. Some mud volcanoes continuously expel reduced muds, fluids and gases to the ocean, supplying chemical energy to cold seep organisms, such as dense mats of giant sulfur-oxidizing bacteria, siboglinid tubeworms, and a variety of bivalves (Sibuet and Olu, 1998). Active mud volcanoes, with such cold seep ecosystems are known from the Central Mediterranean Ridge (Dupré, et al., 2007, Olu-Le Roy, et al., 2004, Zitter, et al., 2005), as well as from the Central American continental margin (Mau, et al., 2006), the Gulf of Cadiz (Niemann, et al., 2006) and the Barents Sea (Niemann, et al., 2006). In the Eastern Mediterranean, active mud volcanism and diverse associated ecosystems have recently been detected on the Nile Deep Sea Fan (Dupré, et al., 2007, Loncke, et al., 2006, Mascle, et al., 2005)(Omoregie et al., in preparation).

At mud volcanoes as well as many other cold seeps, methane and sometimes higher hydrocarbons are transported upwards with rising fluids and muds, and can escape to the hydrosphere in the form of gas or oil bubbles (Michaelis, et al., 2002, Niemann, et al., 2006, Sassen, et al., 2001). Anaerobic hydrocarbon degradation forms the basis of a steep sequence of biogeochemical processes connecting the carbon and sulfur cycles (Aharon and Fu, 2000, Sassen, et al., 1993) at these sites. When hydrocarbons reach the sulfate penetrated sediment zones, they are utilized by sulfate reducing bacteria (SRB) as energy and carbon sources. The products of sulfate respiration with methane and higher hydrocarbons are sulfide and bicarbonate (Aharon and Fu, 2000, Boetius, et al., 2000, Joye, et al., 2004). Hence, hydrocarbon seepage is generally associated with high sulfide

fluxes (Niemann, et al., 2006, Treude, et al., 2003). At methane seeps, most of the sulfide is produced via the anaerobic oxidation of methane (AOM) ((Hinrichs and Boetius, 2002), and references therein). However, several cold seep systems (Joye, et al., 2004, Niemann, et al., 2006) including some in the Eastern Mediterranean (Omoregie et al., in preparation) have been discovered where anaerobic degradation of higher hydrocarbons or oil coupled to sulfate reduction was the dominant sulfide source.

Sulfide is central to biogeochemical cycling in marine sediments as an energy-rich microbial substrate and the principle product of one of the most quantitatively important respiratory processes in ocean sediments, namely sulfate reduction (Kasten and Jørgensen, 2000). Sulfide reacts spontaneously with Fe(III) and Fe(II) (Thamdrup, et al., 1994) and Mn(II) and Mn(IV) (Burdige and Nealson, 1986) and is used as an electron donor for a variety of aerobic and anaerobic sulfide-oxidizing microorganisms. Well known marine sulfide-oxidizing organisms include the giant vacuolated γ-proteobacteria, such as *Beggiatoa* and *Thiomargarita* spp., which use oxygen or nitrate for respiration and often form dense mats above hydrocarbon seeps (Boetius, et al., 2000, Kalanetra, et al., 2005, Niemann, et al., 2006, Nikolaus, et al., 2003). Other types of sulfide-oxidizing bacteria mostly known from hydrothermal vent systems, but also sporadically found at cold seep systems belong to the ε-proteobacteria clade (Campbell, et al., 2006). Little is known about the nature and functioning of other types of bacteria and archaea, which appear commonly associated with cold seep ecosystems (Knittel, et al., 2003, Knittel, et al., 2005).

Here we report on our investigation of the biogeochemistry and microbial community structure of two types of closely associated bacterial mats that were

discovered during a dive with the submersible *Nautile* (IFREMER) to a brine seep at the bottom of the Chefren mud volcano located in a large caldera of the western Nile Deep Sea Fan (Menez Caldera). Similar types of mats have been seen at hydrothermal vents (Emerson and Moyer, 2002, Staudigel, et al., 2006, Taylor and Wirsen, 1997), but to date have not been described in association with cold seeps. The object of this study was to combine microscopic, biogeochemical and molecular biological analyses to identify how small-scale variations in geochemical gradients are reflected in diversity, activity and distribution of sediment and mat-forming microorganisms. This work was part of the ESF EUROCORES EUROMARGIN project MEDIFLUX, which is an integrated study of fluid and gas seepage through the seabed of the Nile Deep Sea Fan.

Materials and Methods

Sampling location. The Chefren mud volcano of the MENES Caldera was discovered by bathymetry surveys of the Western Nile Deep Sea Fan during the "FANIL" expedition in 2000 (Mascle et al. 2006) and for the first time visited by submersible during the expedition "NAUTINIL" with the RV *L'Atalante* and *Nautile* (IFREMER) in September 2003. The Menes Caldera (Fig. 1A) is a 8 km diameter circular depression of *ca*. 50-100 m depth, located at about 3,000 m water depth in the western province of the Nile Deep Sea Fan. This caldera hosts three mud volcanoes (MV), Chefren, Cheops and Mykerinos. Chefren MV is about 500 m in diameter and rises to about 60 m above the bottom of the Caldera (3020 m) (Fig. 1B). The center of this MV is filled by a large and deep brine and

mud lake. For a more detailed description of the Menes Caldera and associated structures, see Huguen et al. (Huguen, et al., In preparation).

Sampling. Sediment cores were recovered from the orange and white mats on 26 September 2003 by the submersible *Nautile* (Fig. 2A,B; N 32° 06.74', E 028° 10.35', 3,024 m water depth). Sediment samples were collected using 6 cm diameter push cores. Two push cores were taken from the orange mat (NL18PC1(8); NL18PC2(7); Fig. 2E) and 2 from the white mat above black sediments (NL18PC3(5); NL18PC4(6); Fig. 2F), as well as 2 blade cores (NL18BC1(L3), NLBC2(L7)) from the nearby sediments. Upon returning to the RV *L'Atalante*, cores were immediately taken to the cold room and sub-sampled by 1 cm diameter sub-cores for further analyses as described below. Cores NL18PC3(5) and NL18PC1(8) were used for microbiological analyses as well as rate measurements, whereas cores NL18PC4(6) and NL18PC2(7) were used for geochemical analyses.

Methane concentration. Sub-cores were sectioned and preserved with 2.5% NaOH in rubber sealed glass vials. Alternatively, sections were equilibrated with a saturated NaCl solution (ca. 300 g/l) in rubber sealed glass vials for at least 12 hours. Methane concentrations were measured by injecting 100 µl of head space in a Hewlett Packard 5890A or a Shimadzu GC-14B gas chromatograph.

Methane oxidation rate determinations. Methane oxidation rates were measured using $^{14}CH_4$ gas, based on previously described methods (Iversen and Blackburn, 1981, Treude,

et al., 2003). Subcores were injected with 10 µl of $^{14}CH_4$ (2.5 kBq total, dissolved in ddH_2O) and incubated for 24 hr in the dark at *in situ* temperature of 14°C. Following the incubations the cores were sectioned and fixed with 2.5% NaOH. Further processing was done according to Treude et al. (Treude, et al., 2003). Rates were determined using the equation below, where $^{14}CO_2$ = activity of CO_2 produced, $^{14}CH_4$= activity of residual injected $^{14}CH_4$, $[CH_4]$ = CH_4 concentration, *V*= sediment volume and *t*= time.

$$\text{AOM rate} = (^{14}CO_2/(^{14}CO_2 + {}^{14}CH_4)) * [CH_4] * 1/V / t$$

Sulfate reduction rate determination. Sulfate reduction rate measurements were made using $^{35}SO_4^{-2}$ based on previously described methods (Jørgensen, 1978). Subcores were injected with 5 µl $^{35}SO_4^{-2}$ (100 kBq total, dissolved in ddH_2O) and incubated for 24 hours at *in situ* temperature in the dark. Following the incubations, the sediment was sectioned and placed in a polypropylene tube containing 20% zinc acetate. Further processing was done according to Kallmeyer et al (Kallmeyer, et al., 2004). Rates were calculated according to the equation below, where $TRIS^{35}S$ = activity of total reduced inorganic sulfur, $^{35}SO_4^{2-}$ = activity of residual $^{35}SO_4^{-2}$ tracer, $[SO_4^{-2}]$ = SO_4^{-2} concentration within the sample, *V* = sediment volume, and *t* = time.

$$\text{SR rate} = (TRI^{35}S/(TRI^{35}S + {}^{35}SO_4^{-2})) * [SO_4^{-2}] * 1/V / t$$

Geochemical measurements. For sulfide analysis, 10 µl of 0.1 N NaOH was added to 2 ml pore water sub-samples. Sub-samples were measured on board using a TRAACS800 continuous flow analyzer, applying colorimetric methods after Grasshoff et al. 1983 (Grasshoff, et al., 1983). Pore-water major element analyses was conducted with

inductively coupled plasma atomic emission spectroscopy (ICP-AES), 2 ml sub-samples were acidified by adding 100 µl of suprapur HNO_3 acid (1 M), bubbled to remove sulfide, and stored in the dark at 4°C. Sulfate concentrations were measured as S. The standard deviation for all measurements was 3% or better. The geochemical composition of the solid phase was also determined by ICP-AES after total dissolution of sediments in an acid mixture of $HClO_4$, HNO_3, and HF (Reitz, et al., 2006). Organic carbon content was determined according to the method described by Van Santvoort et al., (vanSantvoort, et al., 1996). International and in-house standards and duplicates were processed to monitor precision and accuracy.

Light and epifluorescence microscopy. Sediment sections were preserved in 2% formalin and artificial seawater for Acridine orange (AO) staining as well as for light microscopy. FISH (Fluorescence In Situ Hybridization) and CARD-FISH (Catalyzed Reporter Deposition) samples were initially fixed in a 2% formalin and seawater solution, washed several times with PBS and finally stored in a PBS/ethanol solution (1:1). AO staining (Boetius and Lochte, 1996), FISH (Snaidr, et al., 1997) and CARD-FISH (Ishii, et al., 2004) were all performed according to previously described methods. All FISH and CARD-FISH slides were counter-stained with DAPI (4´,6´- diamidino-2-phenylindole). At least 30 grids were counted randomly from each slide for AO, FISH and CARD-FISH counts. Probe hybridization details are given in Table 1. Cell numbers within conspicuous ANME-SRB aggregates were estimated using a semi-direct method. All aggregates and cells were assumed to be spherical. The average cell volume was estimated to be 0.26 μm^3. The volume of an average aggregate (82 μm^3) was divided by the cell volume, and a

ratio of 2:1 archaeal to bacterial cells was used to calculate bacterial and archaeal cell numbers within the consortium (Boetius, et al., 2000).

SEM-EDX. Formalin-fixed samples were analyzed with the scanning electron microscope LEO 1550VP equipped with an inlense detector. Element analysis was performed with an INCA Energy 300 System equipped with a Si(Li) detector.

16S rRNA gene construction and phylogenetic analysis. Sectioned sediment samples were frozen at -20°C until processing. 16S rRNA gene, archaeal and bacterial libraries were created after Niemann et al. (Niemann, et al., 2006). Briefly, total community DNA was extracted from sediment sections and orange flakes using the FastDNA spin kit for soil (Q-Biogene, Irvine, California, USA). Total DNA was extracted from formalin preserved white granules using Chelex-100 resin. Granules were boiled at 100°C in presence of Chelex-100, the beads were allowed to settle and the supernatant was used for PCR. The 16S rRNA gene was amplified from archaea using the primers ARCH20F (Massana, et al., 1997) and Uni1392R (Lane, et al., 1985), and from bacteria using GM3F (Muyzer, 1995) and GM4R (Kane, et al., 1993). Amplification products were cloned, and purified plasmid sequenced using an ABI 3100 genetic analyzer. Plasmids were initially sequenced in one direction (*ca*. 0.6 kb). Selected clones were then sequenced fully (ca. 1.5 kb) and used for subsequent phylogenetic analysis within the ARB (Ludwig, et al., 2004) software package. Statistical analysis on 16S rRNA gene libraries was performed using the s-libshuff program by Schloss et al. (Schloss, et al., 2004)

Fluid flow models. Mass transfer models including fluid flow and molecular diffusion were created in the modeling suite Comsol-Multiphysics and calibrated against the measured Cl^- concentration. As Cl^- can be regarded as non reactive, the mass balance is governed by diffusion and advection according to the equation below, where Cl^- = pore water Cl^- concentration, z = vertical distance, φ= porosity, Ds = diffusion coefficient for Cl^- in the pore space and v = the vertical velocity.

$$o = \varphi * Ds * d^2C/dz^2 - v\,\varphi\, dC/dz$$

Diffusion coefficients were corrected for tortuosity via the interpolated porosity in each depth following the procedure from Iversen and Jorgensen (Iversen and Jørgensen, 1993). Concentrations at the surface were set to the Cl^- concentration measured in the bottom water of the push cores and the concentration at the lower boundary of the modeled regime (1 m) was set to the concentration measured below 15 cm (below white mat) or 17 cm (below orange mat) in both cores. This leaves the pore water flow as the only unknown, which can be estimated by numerically finding the best fit to the measured Cl^- profiles. Each steady state calculation was followed by 10 hours of stagnation to include the time the sediment was contained in the core liner before sectioning.

Results

Visual observations. White mats and orange mats were located at a small seep on a steep slope at the bottom of a small mound adjourning the northwestern rim of the Chefren mud volcano (Fig. 1B), at 3,020 m water depth. The mats showed a patchy distribution

and covered about 25 m^2 (Fig. 2A,B). Shimmering brine fluid flowed downwards from black sediments above the white mats (Fig. 2B). Associated with the orange patches at this site, but also at other areas of Chefren MV we observed many crabs feeding on the sediments, which were populated by small worm tubes sticking out 1-2 cm above the sediment (Fig. 2C). The surfaces of the cores recovered from the white mat were composed of thick white granules (Fig. 2D) that resembled cotton balls and were composed of elemental sulfur precipitates. Polychaete larvae (Fig. 2D) were observed crawling through the white mats as well as through the surface of the core. The surfaces of the cores from orange mat were composed of a thick layer of fluffy yellow material, as well as flaky, bright orange particles, resembling Fe(III)-(hydr)oxides (Fig. 2E). Similar to the core from the white mat, polychaete larvae were also associated with the orange mat.

We followed the orange and white mat structure to the SW along the same depth contour for about 50 m. Irregular patches of orange mat occurred within a band of about 2 m in diameter, and also in association with the edge of the brine lake in the center of the MV (Fig. 2F). When using the manipulator arm of *Nautile* to dig in the orange patches we could observe that the subsurface sediments were dark grey to blackish while the surrounding seafloor was of light brown-beige color typical for pelagic sediments in the deep Eastern Mediterranean. No traces of gas ebullition were observed upon disturbance of the seafloor. Wide areas of the brine lake located at the top of Chefren were covered with white mats (Fig. 2G,H) similar to those observed on the sediments at the small brine seep at the NW rise of Chefren MV.

Microscopy. Examination of white granules recovered from the surface of the white mat (Fig. 3A), revealed the presence of tufts of thin filaments (Fig. 3B), morphologically similar to those produced by the ε-proteobacterium "*Candidatus* Arcobacter sulfidicus" (Taylor and Wirsen, 1997, Taylor, et al., 1999). Scanning electron microscopy (SEM) coupled to energy dispersive X-ray analysis (EDX) revealed these filaments to be associated with high amounts of Fe and S (Fig. 3C). Framboidal pyrite grains (not shown) were also detected within these granules. Fluorescence in Situ Hybridization (FISH) with probe Arc94 (Fig. 3D), which targets "C. sulfidicus" and related species indicated that this group of organisms constituted up to 25% of the total cells within the white granules and in the underlying black sediment (Table 2). However, several morphotypes (e.g. filamentous, coccoid) of cells, which hybridized with the probe were observed, some of which were not the typical crescent shaped "C. sulfidicus" cells.

Microscopic examination of flakes recovered from the surface of the orange mat (Fig. 2E and Fig 3E) revealed numerous microbial sheaths of assorted sizes (Fig. 3F, G) similar to those produced by or attributed to the neutrophilic Fe(II)-oxidizing bacterium *Leptothrix ochracea* (Emerson and Moyer, 2002, Emerson and Revsbech, 1994, van Veen, et al., 1978). EDX revealed that many of these sheaths were associated with high amounts of Fe and O, indicating encrustation by Fe(III)-(hydr)oxides. Most sheaths were sheared and empty (Fig. 3G). DAPI and AODC staining both showed that only very few sheaths (< 1%) were populated with cells. FISH with EUB I-III revealed that these contained bacteria some of which that could be targeted by Mγ705 a probe (Fig. 3H) for type I methanotrophs, but not by domain specific probes for α, β or γ-proteobacteria. Two morphotypes of sheathed bacteria were targeted by the Mγ705 probe; one with

rectangular cells similar to *Clonothrix fusca* (Vigliotta, et al., 2007), and the other square cells similar to *Crenothrix polyspora* (Stoecker, et al., 2006). These two morphotypes often appeared bundled together.

Fluid flow model. The orange mats had a shallow Cl^- gradient indicative of relatively low fluid flow. Hence, the 10 hours stagnation of the flow in the core liners had little effect on the shape of the profile and the upward fluid flow velocity could be calculated with good accuracy to 0.6 m a^{-1} (Fig. 4B). The white mats were associated with a much steeper Cl^- gradient indicating higher fluid flow velocities. The relaxation of the gradient during the 10 hour recovery caused the maximum velocity to be uncertain, but the minimum upward fluid flow under the white mat was estimated to be 15 m a^{-1} (Fig. 4A). The central brine lake at Chefren had a salinity of 150‰, sulfate concentrations of around 50 mM, and sulfide and methane concentrations of around 1mM (Caprais, pers. Comm.). Unfortunately, the small brine flow across the white mats could not be quantitatively sampled, but likely had elevated salinity and sulfate concentrations.

Biogeochemistry. Pore water sulfate concentrations under the white mat (Fig. 5A) were close to seawater values at the surface and decreased to about 19 mM immediately below the surface, possibly reflecting sulfate concentrations in the upward seeping fluids. Cl^- and Na^+ concentrations were up to 1.8 times higher than in the bottom water (water overlying the sediment in the core), indicating upward brine flow through the sediments (Table 3). Sulfate reduction (SR) rates (Fig. 5A) were highest in the top 4 cm (300 nmol*cm^{-3}*d^{-1}) and 70-fold higher than anaerobic oxidation of methane (AOM) rates

(Fig 5B). Methane concentrations (Fig. 5B) ranged from 0.1 mM at the top of the core to about 0.05 mM at the bottom. AOM rates were low throughout the top 12 cm of sediment, with a maximum (10 nmol*cm^{-3}*d^{-1}) at 2 - 4 cm sediment depth (Fig. 5B). Sulfide concentrations (Fig. 5C) approached 1 mM within the zone of highest SR activity. Concurrently, Fe(II) (Fig. 5C) was depleted to <0.01 mM above 5 cm, but increased to about 0.2 mM below this zone. These gradients match visual characteristics of the core, namely the precipitation of Fe(II) with excess sulfide in the black, highly reduced sediment horizon of up to 6 cm below the white mat (Fig. 5D). In this layer, the Fe and S content (Table 3) of the solid phase was several times higher than in underlying sediments, indicating a high content of FeS and pyrite.

Below the orange mat, sulfate concentrations decreased from 28 mM at the surface to about 5 mM at 8 cm sediment depth (Fig. 5E). Cl^- and Na^- concentrations indicated that these sediments were also brine impacted, although to a lesser extent than the sediment underlying the white mat (Table 3). Maximum SR rates (400 nmol*cm^{-3}*d^{-1}) (Fig. 5E) were located between 6 - 10 cm. This coincided with blackish, reduced sediment similar to that observed directly beneath the white mat. A second SR maximum (150 nmol*cm^{-3}*d^{-1}) was detected at 0 - 2 cm just below the orange mat. Methane concentrations (Fig. 5F) under the orange mat ranged from less than 0.01 mM at the surface to about 0.1 mM at the bottom of the core (Fig. 5F). AOM rates were highest in the first few centimeters (13 nmol*cm^{-3}*d^{-1}). SR in these sediments also exceeded AOM rates by several-fold. Sulfide concentrations under the orange mat were below 0.01 mM. In contrast, Fe(II) concentrations decreased from 0.7 mM just below the sediment surface to zero below 16 cm sediment depth (Fig. 5G). Fe(II) was completely consumed in the

surface layer below the orange mat. Solid phase Fe and S contents (Table 3) were high throughout the core, but Fe was elevated in the orange mat and in the 5 - 7 cm zone. In view of the Fe and much lower S content, it is likely that both horizons contained substantial amounts of Fe oxides.

Organic carbon content (Table 3) in both cores were low with 0.18 - 0.77% in both cores, which is typical for oligotrophic Eastern Mediterranean deep-sea sediments, indicating that the energy source for microbial reactions was not detritus-based.

CARD-FISH and FISH-counts. Total cell numbers (Table 2) for both cores were around 10^9 cells*cm^{-3} in the upper 10 cm. In the white mat and its underlying sediment, total cell numbers decreased to 10^8 cells*cm^{-3} after 10 cm, whereas below the orange mat total cell numbers were more or less stable over the first 18 cm of sediment. Archaeal cells accounted for less than 3% of the total cells in both mats, but generally accounted for 12 - 35% of the total cells in the underlying sediments. In accordance with the biogeochemistry of the cores, anaerobic methanotrophic archaea (ANME) were detected in the top 6 cm of both cores (Table 2 and Fig. 6A,C). ANME-2 cells formed consortia with SRB belonging to the *Desulfosarcina* and *Desulfococcus* cluster (Fig. 6A). Free-living ANME-2 cells were not detected in the sediments. In contrast, ANME-3 were all single cells, and comprised 6 - 27% of the total cells in the 6 - 10 cm zone under the white mat and 7% in the 8 - 12 cm zone under the orange mat (Table 2 and Fig. 6B).

The mats as well as the top 2 cm of sediment from both cores were dominated by bacteria (52 - 67% of total cells in the sediments, Table 2). DSS658-targeted SRBs made up less than 1% of the white mat community (Table 2 and Fig. 6C), increased to 5 - 23%

of the total cells in the top 6 cm of sediment underneath it, where the SR rate maximum was detected, and dropped again < 1% in deeper sediment. DSS658-targeted SRBs were more abundant in the orange mat and underlying sediment where they comprised 8 - 15% of the total cells.

Arc94-targeted cells made up 8 - 24% of the white mat and top 4 cm of underlying sediment (Table 2 and Fig. 3D). These cells comprised 4% of the total cells within the orange mat and < 1% of the total cells in the underlying sediment. Type I methanotrophs targeted by Mγ705 (Table 2, Fig 3H) comprised < 1% in the white mat and in the sediment, but 2 - 8% in the orange mat and the 2 cm interval beneath it.

16 rRNA gene analyses. 16S rRNA gene libraries for bacteria were constructed for both mats and the top 4 cm of sediment beneath them, whereas archaeal libraries were only constructed for the sediments. Phylotypes identified from bacterial libraries from the mats as well as the underlying sediment were very diverse, and corresponded to microorganisms capable of many types of C, N, O and S transformations. Sequences from the δ-proteobacteria represented the largest group of sequences from any of the libraries except from the orange mat (Table 4 and Fig. 7). Most of these sequences were closely related to those of the SRB clades *Desulfobacteraceae* and *Desulfobulbaceae*. Sequences belonging to relatives of the *Desulfuromonadaceae* were recovered from the sediments underneath the orange mat as well as within the white mat (Table 4 and Fig. 7). Members of this family are capable of Fe(III) and S reduction (Lovley, et al., 1995, Roden and Lovley, 1993).

γ-proteobacteria were the largest group of bacterial sequences (74 - 34%) from the orange mat and a major group of sequences in the sediment underneath it (Table 4 and Fig. 8). Most of these sequences belonged to type I methanotrophs (46 - 12%), with the most closely related cultivated isolates (< 91%) being *Methylobacter marinu*s, *Crenothrix olyspora*, *Clonothrix fusca* and others. Sequences most closely related (> 95%) to "C. sulfidicus" and *Sulfurimonas autotrophica* made up 32% of the sequences recovered from the white mat. Sequences from *Sulfurospirillum arcachonense* (> 95%) were also recovered from both mats.

Sequences from ANME-2a, ANME-2c and ANME-3 made up 63 - 78% of archaeal sequences from the sediment below the white and orange mats (Table 4 and Fig. 9). ANME-3 sequences were only detected under the white mat and not under the orange, although ANME-3 cells were detected by FISH in both sediments. The ubiquitous seep- and subsurface sediment-associated groups of *Crenarcheota*, marine benthic groups B and D (MBGB and MBGD) made up significant portions (25 - 37%) of the sequences recovered from both cores.

Discussion

Primary productivity and organic matter fluxes to the seafloor have varied greatly in the history of the Eastern Mediterranean Sea, but today it is one of the most oligotrophic seas. Its bottom waters are fully oxygenated and burial of organic matter in the sediments is very low (Boetius, et al., 1996, Krom, et al., 1991, Nijenhuis, et al., 1999). Surface-exposed reduced sediments and accumulations of organisms such as

sulfide-oxidizing bacteria, tubeworms and bivalves (Figs 2 and 3) are clear indications of seepage of energy-rich compounds such as methane, higher hydrocarbons, or sulfide. Living cold seep communities and biogeochemically active, fluid-flow impacted sediments have been found along the Eastern Mediterranean Ridge system (Olu-Le Roy, et al., 2004). Many of these seeps show evidence of anaerobic oxidation of methane as a main process providing sulfide for the chemosynthetic communities associated with the seeps (Aloisi, et al., 2002, Heijs, et al., 2006, Pancost, et al., 2000). A variety of mud volcanoes, pockmarks and gas chimneys were sampled only at the passive margin off Egypt (Bayon, et al., 2007, Dupré, et al., 2007, Loncke, et al., 2006, Loncke, et al., 2004). At depths of 500-3,000 m SR and AOM rates ranged between 0.1 - 66 mmol*m^{-2}*d^{-1} and 0.1 - 3.6 mmol*m^{-2}*d^{-1}, respectively (Omoregie et al, in preparation).

Generally at cold seeps, sites of high sulfide fluxes across the seafloor are marked by mat-forming filamentous and unicellular bacteria, which oxidize sulfide to sulfur or sulfate, using oxygen or nitrate as the electron acceptor. These cells are often mobile and can bridge the gap between sulfide and oxygen penetration in the sediments by transporting the electron acceptor to the subsurface sulfide. The giant vacuolated sulfide oxidizers store elemental sulfur internally which lends the mats characteristic white color (Kalanetra, et al., 2005, Nelson, et al., 1989, Nikolaus, et al., 2003). Mats formed by giant vacuolated sulfide oxidizers typically appear smooth (Niemann, et al., 2006), furry (attached vacuolated filamentous cells) (Nikolaus, et al., 2003) or crusty (i.e. *Thiomargarita* spp. cold seep mats (Kalanetra, et al., 2005)). The mats described here have a different appearance both macroscopically (cotton ball structure) as well as microscopically (external sulfur storage).

To our knowledge, the orange mats have not been previously described from marine cold seeps, but similar mats are known from a few hydrothermal vent settings (Emerson and Moyer, 2002, Kennedy, et al., 2003, Staudigel, et al., 2006) and ground water Fe(II) seeps (Emerson and Revsbech, 1994). At these sites, they are thought to be created by Fe(II)-oxidizing β- or γ-proteobacteria belonging to the genera *Gallionella*, *Leptothrix* or *Marinobacter*, as well as the γ-proteobacterium PV-1. Both, the orange and white mats investigated here appear to represent important communities at brine-impacted cold seeps of the Eastern Mediterranean, and were commonly observed floating on the brine (white mats, e.g. Fig 2G, H) or at the edge of brine lakes (Fig. 2F, orange mat).

Composition of the white mats and orange mats. The granules recovered from the white mat were composed of elemental S filaments as shown by light microscopy, SEM and EDX (Fig. 3). These filaments were most likely produced by chemoautotrophic sulfide-oxidizing organisms related to "*Candidatus* Arcobacter sulfidicus" as indicated by 16S rRNA gene analysis and FISH showing that up to 25% of the cells within the mat were made up by close relatives of this strain. "C. sulfidicus" secretes long S filaments as a byproduct of sulfide oxidation (Sievert, et al., 2006). "C. sulfidicus" like bacteria have received recent attention due to their ability to form highly dense accumulations of elemental S at hydrothermal vent settings (Sievert, et al., 2006), and in laboratory bioreactors (Taylor and Wirsen, 1997) but has also been detected at cold seep settings (Robinson, et al., 2004). These environments are typically sulfidic, high fluid-flow environments where sulfide and oxygen gradients overlap due to advective processes.

Sequences closely related to *Desulfocapsa sulfoexigens*, which is capable of S disproportionation into sulfide, sulfate and H^+ (Finster, et al., 1998), were another significant portion of the sequences from the white mat. Their activities within this mat would likely enhance S cycling as it would consume S, as well as provide additional sulfide.

The flakes that made up the orange mat were composed of Fe(III)-(hydr)oxide encrusted sheaths (Fig. 3) similar to those produced by the neutrophilic Fe(II)-oxidizing β-proteobacterium *Leptothrix ochracea* (van Veen, et al., 1978). Similar sheaths identified in several hydrothermal vent settings (Emerson and Moyer, 2002, Kennedy, et al., 2003, Staudigel, et al., 2006) have been shown to be encrusted with Fe(III)-(hydr)oxides (Kennedy, et al., 2003, Staudigel, et al., 2006). The metabolism of *Leptothrix ochracea* is unclear as it has not been obtained in pure culture. Yet, it is generally regarded as a heterotroph and is often found in organic-rich environments. It is unlikely that the low organic carbon content of the Chefren sediments provide energy to heterotrophic mat-forming iron-oxidizers (Table 3). Hence we speculate that the organisms responsible for the mat formation are unknown chemoautotrophs, which gain energy from aerobic Fe(II) oxidation utilizing the high flux of upward flowing, Fe(II) rich porewater.

Fe(II)-oxidizing bacteria are thought to form Fe-oxide encrusted sheaths in order to locate the electron transfer process close to the cell as well as provide a means for the cell to escape encrustation by Fe(III)-(hydr)oxides. The energetic yield of this process is very low; therefore large amounts of Fe(II) need to be turned over in order to provide enough energy for growth, leading to high amounts of Fe-oxides but very few cells

(Emerson and Moyer, 2002). Neutrophilic Fe(II) oxidation, although it occurs in a variety of environments such as hydrothermal vents (Emerson and Moyer, 2002), freshwater springs (James and Ferris, 2004), and plant root nodules (Emerson, et al., 1999), remains somewhat enigmatic, as under these conditions Fe(II) spontaneously oxidizes to Fe(III). However, neutrophilic Fe(II)-oxidizing bacteria have been shown to increase Fe oxidation rates by up to 4 times over abiotic rates (James and Ferris, 2004, Neubauer, et al., 2002). The exact mechanism of this process is currently unknown, but has been suggested to occur through the binding and sequestration of Fe(II) by bacterial exopolymers (Neubauer, et al., 2002).

It is likely that the Mγ705 targeted sheaths corresponded to organisms similar to *Crenothrix polyspora* and *Clonothrix fusca* (Vigliotta, et al., 2007). They often occur bundled together, as observed in this study. It is unclear as to whether these organisms can oxidize Fe(II) in addition to methane, as they have only recently been cultivated. They, however, are often described in environments where there is likely to be Fe(II) and methane present, such as ground water springs. Additionally, there are several reports of *C. polyspora* sheaths incrusted in Fe(III)-(hydr)oxides (Taylor, et al., 1997, Volker, et al., 1977). No 16S rDNA sequences recovered from the orange mat were similar to known Fe(II)-oxidizing species (e.g. sheath forming *Leptothrix* spp., stalk forming *Gallionella* spp., PV-1 and others). 16S rRNA gene sequences were recovered that grouped with *C. polyspora* and *C. fusca,* but it is unclear whether these correspond to microorganisms similar to the cultivated strains.

Many sequences from organisms, which could possibly constitute the reductive part of the Fe cycle were detected within the orange mat. Interestingly, sequences that

grouped with *Sulfurospirillum deleyianum,* which is capable of Fe(III)-reduction via S cycling were detected within this mat (Straub and Schink, 2004). Activities of these organisms could enhance S and Fe cycling as observed by Straub et al. (Straub and Schink, 2004). Additionally, enrichments with ferrihydrite as the sole electron acceptor resulted in high numbers of "C. sulfidicus" sequences in the 16S rRNA gene libraries.

Biogeochemical processes supporting white and orange microbial mat formation. Brine flow associated with mud volcanism is a common feature of Eastern Mediterranean sediments (Woodside, 2000, Woodside and Volgin, 1996). These brines often co-migrate with hydrocarbons and sulfides (De Lange and Brumsack, 1998, vanSantvoort and deLange, 1996). This is apparent in methane (2.4 mM) and sulfide (7.2 mM) concentrations previously measured in the brine pool at Chefren (Caprais, pers. Comm.).

The large variations in fluid flow (Fig. 4) through both mats on scales of centimeters to meters is typical for focused fluid flow, which can result in tremendous heterogeneity in fluid flow rates (Luff and Wallmann, 2003, Sahling, et al., 2002). We did not sample the black exposed sediments, from which the brine flowed (Fig. 2), but it is likely that sulfide was present within the brine, precipitating Fe(II). The brine flow across the white mat likely impeded the exchange with oxygenated water from the water column, providing a microaerophilic environment for sulfide oxidation.

Sulfide underneath the white mat was clearly provided by SR, rather than by upward transport with brine (Fig. 5). The distribution of DSS658-targeted cells matched the sulfide profile, as they displayed a maximum of 25% of the total cells between 0 - 2 cm (Table 2). Although our sampling resolution did not allow for the precise

determination of the limits of sulfide penetration, the rapid sulfide consumption at the fluidic top of the core was likely due to a combination of "C. sulfidicus" activity and Fe(II) precipitation. This environment is similar to high fluid flow environments (Sievert, et al., 2006, Taylor and Wirsen, 1997), where sulfide and oxygen overlap due to advective processes and is likely to be a niche for "C. sulfidicus" rather than for giant sulfide oxidizing bacteria.

Similar to the biogeochemistry of the white mat, SR rates under the orange mat were significantly higher than AOM rates (Fig. 5). SRB cells, most of which were not associated to ANME consortia, reached 8 - 15% of total cells under the orange mat. Maximum SR activity was located roughly at 4 - 10 cm, which corresponded to increased amounts of solid phase Fe and S (Fig. 5). Similar to the situation under the white mat the sulfide produced in this zone likely caused the precipitation of Fe and S complexes. No free sulfide was detected within this core, therefore it is likely that the entire sulfide production went into the reduction of Fe(III) and precipitation of Fe(II). The excess Fe(II) was transported upwards by fluid flow, and utilized by Fe(II)-oxidizing bacteria as energy source.

Bacterial community composition. Significant differences ($P < 1\%$) were identified between all bacterial 16S rRNA gene libraries obtained in this study. This was not surprising given the markedly differing biogeochemistry in these samples. The importance of SR was reflected by the high percentage of sequences (Table 4) belonging to members of the δ-proteobacteria in both sediment libraries (31- 43%, Table 4). As expected these sequences grouped with those from genera of known sulfate reducers such

as *Desulfobacter*, *Desulfosarcina*, *Desulfocapsa*, and *Desulfobulbus* (Fig. 7). Some members of these genera are also capable of iron reduction, which occurred within the orange mat and in the underlying sediment. Sequences from γ-proteobacteria, which represent oxidative metabolisms, such as Fe(II)-oxidation, sulfide-oxidation, and methane-oxidation, were very prevalent in the libraries (10 - 73%). Most grouped with aerobic type I methanotrophs, such as *M. marinu*s *C. polyspora* and *C. fusca* (Fig. 8), as well as with environmental sequences from methane rich sediments and symbionts in the gills of methanotrophic clams. Cultivated members of this group primarily oxidize methane with oxygen, but are also capable of oxidizing other C-1 compounds. As methane reached the top of both cores and was present in the water column, the sediment surface and especially the more oxidized orange mats represent potential niches for aerobic methanotrophy.

Most of the ε-proteobacterial sequences (Fig. 8) could not be identified, except for some S-oxidizing ("C. sulfidicus", *Sulfurimonas*) and S-reducing (*Sulfurospirillum*) microorganisms.

Archaeal community composition. Unlike the bacterial libraries, no statistical difference was found between archaeal libraries (P>5%). Sixty to seventy percent of the archaeal sequences (Table 4) recovered from sediments underlying the orange and white mats belonged to the ANME-2 and ANME-3 clusters (Fig. 9). Their distribution differed between the sediments underlying the mats (Tab 3). Most environments typically have a mix of ANME communities with a clear dominance of one community (Knittel, et al., 2005). The Chefren seep represents the second cold seep habitat characterized by a

relatively high abundance of ANME-3 cells (Niemann, et al., 2006). However, all of the ANME-3 cells that were detected were not associated with any bacterial partners. The remaining archaeal sequences comprised members of the marine benthic groups, (MBGB and MBGD) which are typical members of cold seep and subsurface communities (Inagaki, et al., 2006, Knittel, et al., 2005). However, no members of these two groups have been cultivated; therefore their roles in the sediments of Chefren and elsewhere remain unknown.

Comparison to other cold seep ecosystems. While fluid flow velocities and SR rates were similar to previously investigated cold seep systems, the associated AOM rates were comparatively low (Niemann, et al., 2006, Niemann, et al., 2006, Treude, et al., 2003, Treude, et al., 2005) (Omoregie, et al., in preparation). The sulfate reducing community apparently utilized compounds other than methane or organic detritus (Table 3) as has been postulated at other cold seeps (Joye, et al., 2004, Niemann, et al., 2006) (Omoregie et al., in preparation). C-2 and higher hydrocarbons have been detected within the pore waters of Chefren and in the overlying water column (Mastalerz, unpublished data). This was furthered by SR and AOM rates, which differed (> 28:1) from the known stoichiometry (1:1) of SR coupled to AOM. In addition, ANME-2 cells (Table 2) were 2 - 13%, and ANME-3 cells 6 - 27% of total cells within this zone. These cell numbers, as well as the total cell numbers (10^9 cells cm^{-3}) are lower than at other sites were AOM is the dominant biogeochemical process. Sites like Hydrate Ridge, the Black Sea and the Haakon Mosby mud volcano typically have ANME cell abundances of $>10^9$ cells cm^{-3} and contribute up to 90% of total cell numbers (Boetius, et al., 2000, Knittel, et al., 2003).

Conclusion. This study has elucidated some of the major processes and organisms involved in the formation of Fe(II)-oxidizing and sulfide-oxidizing mats at an active cold seep. Previously, these types of mats have only been described from hydrothermal vent settings, where sulfide and reduced iron was produced by seawater-rock interactions, and advected by venting. Our findings suggest that such mats could also be fueled by microbial sulfate reduction based on anaerobic hydrocarbon degradation, maintained by relatively high fluid flow. Several questions still remain, such as the actual substrates fueling sulfate reduction, the rates of microbial vs. chemical Fe(II) and sulfide oxidation, the spatial relationship between the organisms that carry out these processes, and the ultimate fate of the end products (i.e. elemental S and Fe(III)-(hydr)oxide). Clearly, the relationship between carbon, sulfur and iron cycling in advective systems, such as cold seeps and hydrothermal vents, as well as the responsible organisms are important subjects in geomicrobiological research, especially with regard to their implication for the evolution of life on Earth and the prehistory of element cycles.

Acknowledgements

We thank the crews of the RV L'Atalante and the submersible Nautile as well as the NAUTINIL scientific party for excellent support with work at sea. We thank Friederike Heinrich, Viola Beier and Tomas Wilkop for their initial processing of the samples, Claus Burkhardt for help with the electron microscope, Stefan Sievert for informing us about "*Candidatus* Arcobacter sulfidicus", Alban Ramette, Katrin Knittel for scientific suggestions and Casey Hubert for their helpful comments on this manuscript. The work

of E.O. and A.B. in the ESF EUROCORES EUROMARGIN project The work of A.K. was supported by an Emmy-Noether fellowship from the German Research Foundation (DFG). The work of E.O. and A.B. in the ESF EUROCORES MEDIFLUX was financially supported by ESF, DFG and the Max Planck Society.

References

1. **Aharon, P., and B. Fu.** 2000. Microbial sulphate reduction rates and sulfur and oxygen isotope fractionations at oil and gas seeps in deepwater Gulf of Mexico. Geochim. Cosmochim. Acta **64:**233-246.
2. **Aloisi, G., I. Bouloubassi, S. K. Heijs, R. D. Pancost, C. Pierre, J. S. S. Damste, J. C. Gottschal, L. J. Forney, and J. M. Rouchy.** 2002. CH4-consuming microorganisms and the formation of carbonate crusts at cold seeps. Earth Planet Sc Lett **203:**195-203.
3. **Amann, R. I., L. Krumholz, and D. A. Stahl.** 1990. Fluorescent-oligonucleotide probing of whole cells for determinative, phylogenetic and environmental studies in microbiology. J. Bacteriol. **172:**762-770.
4. **Bayon, G., L. Loncke, S. Dupré, J.-C. Caprais, E. Ducassou, S. Duperron, J.-P. Foucher, Y. Fouquet, S. Gontharet, G. M. Henderson, J. Etoubleau, I. Klaucke, J. Mascle, S. Migeon, H. Ondréas, C. Pierre, C. Huguen, A. Stadnitskaia, J. Woodside, and M. Sibuet.** 2007. In situ investigation of the Centre Nile margin: Linking fluid seepage and continental-slope instabilities. Deep-Sea Res. Part I Oceanogr. Res. Pap. **Submitted**.
5. **Boetius, A., and K. Lochte.** 1996. Effect of organic enrichments on hydrolytic potentials and growth of bacteria in deep-sea sediments. Mar. Ecol. Prog. Ser. **140:**239-250.
6. **Boetius, A., K. Ravenschlag, C. J. Schubert, D. Rickert, F. Widdel, A. Giesecke, R. Amann, B. B. Jørgensen, U. Witte, and O. Pfannkuche.** 2000. A marine microbial consortium apparently mediating anaerobic oxidation of methane. Nature **407:**623-626.
7. **Boetius, A., S. Scheibe, A. Tselepides, and H. Thiel.** 1996. Microbial biomass and activities in deep-sea sediments of the Eastern Mediterranean: trenches are benthic hotspots. Deep-Sea Res. Part I Oceanogr. Res. Pap. **43:**1439-1460.
8. **Burdige, D. J., and K. H. Nealson.** 1986. Chemical and Microbiological Studies of Sulfide-Mediated Manganese Reduction. Geomicrobiol. J. **4:**361-387.
9. **Campbell, B. J., A. S. Engel, M. L. Porter, and K. Takai.** 2006. The versatile epsilon-proteobacteria: key players in sulphidic habitats. Nat. Rev. Microbiol. **4:**458-468.
10. **Daims, H., A. Brühl, R. Amann, and K. H. Schleifer.** 1999. The domain-specific probe EUB338 is insufficient for the detection of all Bacteria: Development and evaluation of a more comprehensive probe set. Syst. Appl. Microbiol. **22:**434-444.
11. **De Lange, G. J., and H. Brumsack, J.** 1998. The occurrence of gas hydrates in Eastern Mediteranean mud dome structures as indicated by porewater composition. Geol. Soc. Spec. **137:**167-175.
12. **Devereux, R., M. D. Kane, J. Winfrey, and D. A. Stahl.** 1992. Genus- and group specific hybridization probes for determinative and environmental studies of sulfate-reducing bacteria. Syst. Appl. Microbiol. **15:**601-609.
13. **Dupré, S., J. M. Woodside, J.-P. Foucher, G. de Lange, J. Mascle, A. Boetius, V. Mastalerz, A. Stadnitskaia, H. Ondreas, C. Huguen, F. Harmégnies, S. Gontharet, L. Loncke, E. Deville, H. Niemann, E. Omoregie, K. Olu-Le Roy,**

A. Fiala-Médioni, A. Dählmann, J.-C. Caprais, A. Prinzhofer, M. Sibuet, C. Pierre, J. Sinninghe Damsté, and N. S. Party. 2007. Seafloor geological studies above active gas chimneys off Egypt (Central Nile Deep Sea Fan). Deep-Sea Res. Part I Oceanogr. Res. Pap. **In Press**.

14. **Eller, G., S. Stubner, and P. Frenzel.** 2001. Group-specific 16S rRNA targeted probes for the detection of type I and type II methanotrophs by fluorescence in situ hybridisation. FEMS Microbiol. Lett. **198:**91-97.
15. **Emerson, D., and C. L. Moyer.** 2002. Neutrophilic Fe-Oxidizing Bacteria Are Abundant at the Loihi Seamount Hydrothermal Vents and Play a Major Role in Fe Oxide Deposition. Appl. Environ. Microbiol. **68:**3085-3093.
16. **Emerson, D., and N. P. Revsbech.** 1994. Investigation of an Iron-Oxidizing Microbial Mat Community Located near Aarhus, Denmark - Laboratory Studies. Appl. Environ. Microbiol. **60:**4032-4038.
17. **Emerson, D., J. V. Weiss, and J. P. Megonigal.** 1999. Iron-Oxidizing Bacteria Are Associated with Ferric Hydroxide Precipitates (Fe-Plaque) on the Roots of Wetland Plants. Appl. Environ. Microbiol. **65:**2758-2761.
18. **Finster, K., W. Liesack, and B. Thamdrup.** 1998. Elemental sulfur and thiosulfate disproportionation by *Desulfocapsa sulfoexigens* sp. nov., a new anaerobic bacterium isolated from marine surface sediment. Appl. Environ. Microbiol. **64:**119-125.
19. **Grasshoff, K., M. Ehrhardt, and K. Kremling.** 1983. p. 419, Methods of seawater analysis. Verlag Chemie, Weinheim.
20. **Heijs, S. K., G. Aloisi, I. Bouloubassi, R. D. Pancost, C. Pierre, J. S. S. Damste, J. C. Gottschal, J. D. van Elsas, and L. J. Forney.** 2006. Microbial community structure in three deep-sea carbonate crusts. Microb. Ecol. **52:**451-462.
21. **Hinrichs, K.-U., and A. Boetius.** 2002. The anaerobic oxidation of methane: new insights in microbial ecology and biogeochemistry, p. 457-477. *In* G. Wefer, D. Billett, D. Hebbeln, B. B. Joergensen, M. Schlüter, and T. Van Weering (ed.), Ocean Margin Systems. Springer-Verlag, Berlin.
22. **Huguen, C., J. P. Foucher, J. Mascle, H. Ondreas, M. Thouement, S. Gonthat, A. Stadnitskaia, C. Pierre, G. Bayon, L. Loncke, A. Boetius, I. Bouloubassi, G. d. Lange, Y. Fouquet, J. Woodside, and N. S. Party.** In preparation. The Western Nile Margin Fluid seepages features: "in situ" observations of the Menes caldera (NAUTINIL Expedition, 2003).
23. **Inagaki, F., M. M. M. Kuypers, U. Tsunogai, J. Ishibashi, K. Nakamura, T. Treude, S. Ohkubo, M. Nakaseama, K. Gena, H. Chiba, H. Hirayama, T. Nunoura, K. Takai, B. B. Jorgensen, K. Horikoshi, and A. Boetius.** 2006. Microbial community in a sediment-hosted CO2 lake of the southern Okinawa Trough hydrothermal system. Proc. Natl. Acad. Sci. U. S. A. **103:**14164-14169.
24. **Ishii, K., M. Mussmann, B. J. MacGregor, and R. Amann.** 2004. An improved fluorescence in situ hybridization protocol for the identification of bacteria and archaea in marine sediments. FEMS Microbiol. Ecol. **50:**203-213.
25. **Iversen, N., and T. H. Blackburn.** 1981. Seasonal rates of methane oxidation in anoxic marine sediments. Appl. Environ. Microbiol. **41:**1295-1300.

26. **Iversen, N., and B. Jørgensen, B.** 1993. Diffusion Coefficients of Sulfate and Methane in Marine Sediments Influence of Porosity. Geochim. Cosmochim. Acta **57:**571-578.
27. **James, R. E., and F. G. Ferris.** 2004. Evidence for microbial-mediated iron oxidation at a neutrophilic groundwater spring. Chem. Geol. **212:**301.
28. **Jørgensen, B., B.** 1978. A comparison of methods for the quantification of bacterial sulfate reduction in coastal marine sediments. Measurement with radiotracer techniques. Geomicrobiol. J. **1:**11-27.
29. **Joye, S. B., A. Boetius, B. N. Orcutt, J. P. Montoya, H. N. Schulz, M. J. Erickson, and S. K. Logo.** 2004. The anaerobic oxidation of methane and sulfate reduction in sediments from Gulf of Mexico cold seeps. Chem. Geol. **205:**219-238.
30. **Kalanetra, K. M., S. B. Joye, N. R. Sunseri, and D. C. Nelson.** 2005. Novel vacuolate sulfur bacteria from the Gulf of Mexico reproduce by reductive division in three dimensions. Environ. Microbiol. **7:**1451-1460.
31. **Kallmeyer, J., T. G. Ferdelman, A. Weber, H. Fossing, and B. B. Jørgensen.** 2004. Evaluation of a cold chromium distillation procedure for recovering very small amounts of radiolabeled sulfide related to sulfate reduction measurements. Limnol. Oceanogr. Methods **2:**171-180.
32. **Kane, M. D., L. K. Poulsen, and D. A. Stahl.** 1993. Monitoring the enrichment and isolation of sulfate-reducing bacteria by using oligonucleotide hybridization probes designed from environmentally derived 16S rRNA sequences. Appl. Environ. Microbiol. **59:**682-686.
33. **Kasten, S., and B. Jørgensen, B.** 2000. Sulfate reduction in marine sediments, p. 263-281. *In* H. Schulze, D., and M. Zabel (ed.), Marine Geochemistry. Springer, Berlin.
34. **Kennedy, C. B., S. D. Scott, and F. G. Ferris.** 2003. Characterization of bacteriogenic iron oxide deposits from Axial Volcano, Juan de Fuca Ridge, northeast Pacific Ocean. Geomicrobiol. J. **20:**199-214.
35. **Kennedy, C. B., S. D. Scott, and F. G. Ferris.** 2003. Ultrastructure and potential sub-seafloor evidence of bacteriogenic iron oxides from axial volcano, Juan de Fuca Ridge, North-east Pacific Ocean. FEMS Microbiol. Ecol. **43:**247-254.
36. **Knittel, K., A. Boetius, A. Lemke, H. Eilers, K. Lochte, O. Pfannkuche, P. Linke, and R. Amann.** 2003. Activity, distribution, and diversity of sulfate reducers and other bacteria in sediments above gas hydrate (Cascadia margin, Oregon). Geomicrobiol. J. **20:**269-294.
37. **Knittel, K., T. Losekann, A. Boetius, R. Kort, and R. Amann.** 2005. Diversity and distribution of methanotrophic archaea at cold seeps. Appl. Environ. Microbiol. **71:**467-479.
38. **Krom, M. D., S. Brenner, L. Israilov, and B. Krumgalz.** 1991. Dissolved Nutrients, Preformed Nutrients and Calculated Elemental Ratios in the South-East Mediterranean-Sea. Oceanologica Acta **14:**189-194.
39. **Lane, D., B. Pace, G. Olsen, D. Stahl, M. Sogin, and N. Pace.** 1985. Rapid determination of 16S ribosomal RNA sequences for phylogenetic analyses. Proc. Natl. Acad. Sci. U. S. A. **82:**6955-6959.

40. **Loncke, L., V. Gaullier, J. Mascle, B. Vendeville, and L. Camera.** 2006. The Nile deep-sea fan: An example of interacting sedimentation, salt tectonics, and inherited subsalt paleotopographic features. Marine and Petroleum Geology **23:**297-315.
41. **Loncke, L., J. Mascle, F. S. Parties, and.** 2004. Mud volcanoes, gas chimneys, pockmarks and mounds in the Nile deep-sea fan (Eastern Mediterranean): geophysical evidences. Marine and Petroleum Geology **21:**669-689.
42. **Lösekann, T., K. Knittel, T. Nadalig, B. Fuchs, H. Niemann, A. Boetius, and R. Amann.** 2007. Diversity and Abundance of Aerobic and Anaerobic Methane Oxidizers at the Haakon Mosby Mud Volcano, Barents Sea. Applied and Environmental Microbiology. Appl. Environ. Microbiol. **73:**3348-3362.
43. **Lovley, D. R., E. J. P. Phillips, D. J. Lonergan, and P. K. Widman.** 1995. Fe(III) and S^0 Reduction by *Pelobacter carbinolicus*. Appl. Environ. Microbiol. **61:**2132-2138.
44. **Ludwig, W., O. Strunk, R. Westram, L. Richter, H. Meier, Yadhukumar, A. Buchner, T. Lai, S. Steppi, G. Jobb, W. Forster, I. Brettske, S. Gerber, A. W. Ginhart, O. Gross, S. Grumann, S. Hermann, R. Jost, A. Konig, T. Liss, R. Lussmann, M. May, B. Nonhoff, B. Reichel, R. Strehlow, A. Stamatakis, N. Stuckmann, A. Vilbig, M. Lenke, T. Ludwig, A. Bode, and K.-H. Schleifer.** 2004. ARB: a software environment for sequence data. Nucleic Acids Res. **32:**1363-1371.
45. **Luff, R., and K. Wallmann.** 2003. Fluid flow, methane fluxes, carbonate precipitation and biogeochemical turnover in gas hydrate-bearing sediments at Hydrate Ridge, Cascadia Margin: numerical modeling and mass balances. Geochim. Cosmochim. Acta **67:**3403-3421.
46. **Manz, W., R. Amann, W. Ludwig, M. Wagner, and K.-H. Schleifer.** 1992. Phylogenetic oligodeoxynucleotide probes for the major subclasses of proteobacteria: problems and solutions. Syst. Appl. Microbiol. **15:**593-600.
47. **Mascle, J., L. Loncke, and L. Camera.** 2005. Geophysical evidences of fluid seepages and mud volcanoes on the Egyptian continental margin (Eastern Mediterranean).127-134.
48. **Massana, R., A. E. Murray, C. M. Preston, and E. F. DeLong.** 1997. Vertical distribution and phylogenetic characterization of marine planktonic Archaea in the Santa Barbara channel. Appl. Environ. Microbiol. **63:**50-56.
49. **Mau, S., H. Sahling, G. Rehder, E. Suess, P. Linke, and E. Soeding.** 2006. Estimates of methane output from mud extrusions at the erosive convergent margin off Costa Rica. Mar Geol **225:**129-144.
50. **Michaelis, W., R. Seifert, K. Nauhaus, T. Treude, V. Thiel, M. Blumenberg, K. Knittel, A. Gieseke, K. Peterknecht, T. Pape, A. Boetius, A. Aman, B. B. Jørgensen, F. Widdel, J. Peckmann, N. V. Pimenov, and M. Gulin.** 2002. Microbial reefs in the Black Sea fueled by anaerobic oxidation of methane. Science **297:**1013-1015.
51. **Neef, A.** 1997. Anwendung der in situ-Einzelzell-Identifizierung von Bakterien zur Populations-Analyse in komplexen mikrobiellen Biozönosen. Technische Universität München, München.

52. **Nelson, D. C., C. O. Wirsen, and H. W. Jannasch.** 1989. Characterization of Large, Autotrophic Beggiatoa Spp Abundant at Hydrothermal Vents of the Guaymas Basin. Appl. Environ. Microbiol. **55:**2909-2917.
53. **Neubauer, S. C., D. Emerson, and J. P. Megonigal.** 2002. Life at the Energetic Edge: Kinetics of Circumneutral Iron Oxidation by Lithotrophic Iron-Oxidizing Bacteria Isolated from the Wetland-Plant Rhizosphere. Appl. Environ. Microbiol. **68:**3988-3995.
54. **Niemann, H., J. Duarte, C. Hensen, E. Omoregie, V. H. Magalhaes, M. Elvert, L. M. Pinheiro, A. Kopf, and A. Boetius.** 2006. Microbial methane turnover at mud volcanoes of the Gulf of Cadiz. Geochim. Cosmochim. Acta **70:**5336.
55. **Niemann, H., T. Losekann, D. de Beer, M. Elvert, T. Nadalig, K. Knittel, R. Amann, E. J. Sauter, M. Schluter, M. Klages, J. P. Foucher, and A. Boetius.** 2006. Novel microbial communities of the Haakon Mosby mud volcano and their role as a methane sink. Nature **443:**854.
56. **Nijenhuis, I., A., H. Bosch, J., J. Sinninghe Damsté, S., H. Brumsack, J., and G. De Lange, J.** 1999. Organic matter and trace element rich sapropels and black shales: a geochemical comparison. Earth Planet. Sc. Lett. **169:**277-290.
57. **Nikolaus, R., J. W. Ammerman, and I. R. MacDonald.** 2003. Distinct pigmentation and trophic modes in *Beggiatoa* from hydrocarbon seeps in the Gulf of Mexico. Aquat. Microb. Ecol. **32:**85-93.
58. **Olu-Le Roy, K., M. Sibuet, A. Fiala-Medioni, S. Gofas, C. Salas, A. Mariotti, J. P. Foucher, and J. Woodside.** 2004. Cold seep communities in the deep eastern Mediterranean Sea: composition, symbiosis and spatial distribution on mud volcanoes. Deep-Sea Res. Part I Oceanogr. Res. Pap. **51:**1915-1936.
59. **Pancost, R. D., J. S. S. Damste, S. de Lint, M. J. E. C. van der Maarel, J. C. Gottschal, and M. S. S. Party.** 2000. Biomarker evidence for widespread anaerobic methane oxidation in Mediterranean sediments by a consortium of methanogenic archaea and bacteria. Appl. Environ. Microbiol. **66:**1126-1132.
60. **Reitz, A., J. Thomson, G. J. de Lange, and C. Hensen.** 2006. Source and development of large manganese enrichments above eastern Mediterranean sapropel S1. Paleoceanography **21**.
61. **Robinson, C. A., J. M. Bernhard, L. A. Levin, G. F. Mendoza, and J. K. Blanks.** 2004. Surficial Hydrocarbon Seep Infauna from the Blake Ridge (Atlantic Ocean, 2150 m) and the Gulf of Mexico (690–2240 m). Mar. Ecol.Prog. Ser. **25:**313-336.
62. **Roden, E. E., and D. R. Lovley.** 1993. Dissimilatory Fe(Iii) Reduction by the Marine Microorganism Desulfuromonas-Acetoxidans. Appl. Environ. Microbiol. **59:**734-742.
63. **Sahling, H., D. Rickert, R. W. Lee, P. Linke, and E. Suess.** 2002. Macrofaunal community structure and sulfide flux at gas hydrate deposits from the Cascadia convergent margin, NE Pacific. Mar Ecol-Prog Ser **231:**121-138.
64. **Sassen, R., S. L. Losh, I. L. Cathles, H. H. Roberts, J. K. Whelan, A. V. Milkov, S. T. Sweet, and D. A. DeFreitas.** 2001. Massive vein-filling gas hydrate: relation to ongoing gas migration from the deep subsurface in the Gulf of Mexico. Marine and Petroleum Geology **18:**551.

65. **Sassen, R., H. H. Roberts, P. Aharon, J. Larkin, E. W. Chinn, and R. Carney.** 1993. Chemosynthetic bacterial mats at cold hydrocarbon seeps, Gulf of Mexico continental slope. Org. Geochem. **20:**77.
66. **Schloss, P. D., B. R. Larget, and J. Handelsman.** 2004. Integration of microbial ecology and statistics: a test to compare gene libraries. Appl. Environ. Microbiol. **70:**5485-5492.
67. **Sievert, S. M., E. B. A. Wieringa, C. O. Wirsen, and C. D. Taylor.** 2006. Growth and mechanism of filamentous-sulfur formation by *Candidatus* Arcobacter sulfidicus in opposing oxygen-sulfide gradients. Environ. Microbiol. **9:**271-276.
68. **Snaidr, J., R. Amann, I. Huber, W. Ludwig, and K. H. Schleifer.** 1997. Phylogenetic analysis and in situ identification of bacteria in activated sludge. Appl. Environ. Microbiol. **63:**2884-2896.
69. **Staudigel, H., S. R. Hart, A. Pile, B. E. Bailey, E. T. Baker, S. Brooke, D. P. Connelly, L. Haucke, C. R. German, I. Hudson, D. Jones, A. A. P. Koppers, J. Konter, R. Lee, T. W. Pietsch, B. M. Tebo, A. S. Templeton, R. Zierenberg, and C. M. Young.** 2006. Vailulu'u Seamount, Samoa: Life and death on an active submarine volcano. Proc. Natl. Acad. Sci. U. S. A. **103:**6448-6453.
70. **Stoecker, K., B. Bendinger, B. Schoning, P. H. Nielsen, J. L. Nielsen, C. Baranyi, E. R. Toenshoff, H. Daims, and M. Wagner.** 2006. Cohn's Crenothrix is a filamentous methane oxidizer with an unusual methane monooxygenase. P Natl Acad Sci USA **103:**2363-2367.
71. **Straub, K. L., and B. Schink.** 2004. Ferrihydrite-dependent growth of *Sulfurospirillum deleyianum* through electron transfer via sulfur cycling. Appl. Environ. Microbiol. **70:**5744-5749.
72. **Taylor, C. D., and C. O. Wirsen.** 1997. Microbiology and ecology of filamentous sulfur formation. Science **277:**1483-1485.
73. **Taylor, C. D., C. O. Wirsen, and F. Gaill.** 1999. Rapid microbial production of filamentous sulfur mats at hydrothermal vents. Appl. Environ. Microbiol. **65:**2253-2255.
74. **Taylor, S. W., C. R. Lange, and E. A. Lesold.** 1997. Biofouling of contaminated ground-water recovery wells: Characterization of microorganisms. Ground Water **35:**973-980.
75. **Thamdrup, B., H. Fossing, and B. Jørgensen, B.** 1994. Manganese, iron, and sulfur cycling in a coastal marine sediment, Aarhus Bay, Denmark. Geochim. Cosmochim. Acta **58:**5115-5129.
76. **Treude, T., A. Boetius, K. Knittel, K. Wallmann, and B. B. Jørgensen.** 2003. Anaerobic oxidation of methane above gas hydrates at Hydrate Ridge, NE Pacific Ocean. Mar. Ecol.Prog. Ser. **264:**1-14.
77. **Treude, T., K. Knittel, M. Blumenberg, R. Seifert, and A. Boetius.** 2005. Subsurface Microbial Methanotrophic Mats in the Black Sea. Appl. Environ. Microbiol. **71:**6375-6378.
78. **Treude, T., J. Niggemann, J. Kallmeyer, P. Wintersteller, C. J. Schubert, A. Boetius, and B. B. Jorgensen.** 2005. Anaerobic oxidation of methane and sulfate reduction along the Chilean continental margin. Geochim. Cosmochim. Acta **69:**2767-2779.

79. **van Veen, W., L., E. G. Mulder, and M. Deinema.** 1978. The *Spaerotilus-Leptothrix* Group of Bacteria. Microbiol. Rev. **42:**329-356.
80. **vanSantvoort, P. J. M., and G. J. deLange.** 1996. Messinian salt fluxes into the present-day eastern Mediterranean: Implications for budget calculations and stagnation. Mar Geol **132:**241-251.
81. **vanSantvoort, P. J. M., G. J. deLange, J. Thomson, H. Cussen, T. R. S. Wilson, M. D. Krom, and K. Strohle.** 1996. Active post-depositional oxidation of the most recent sapropel (S1) in sediments of the eastern Mediterranean Sea. Geochim. Cosmochim. Acta **60:**4007-4024.
82. **Vigliotta, G., E. Nutricati, E. Carata, S. M. Tredici, M. De Stefano, P. Pontieri, D. R. Massardo, M. V. Prati, L. De Bellis, and P. Alifano.** 2007. Clonothrix fusca Roze 1896, a Filamentous, Sheathed, Methanotrophic γ-Proteobacterium. Appl. Environ. Microbiol. **73:**3556-3565.
83. **Volker, H., R. Schweisfurth, and P. Hirsch.** 1977. Morphology and Ultrastructure of *Crenothrix Polyspora* Cohn. J. Bacteriol. **131:**306-313.
84. **Wallner, G., I. Steinmetz, D. Bitter-Suermann, and R. Amann.** 1996. Flow cytometric analysis of activated sludge with rRNA-targeted probes. Appl. Environ. Microbiol. **19:**569-576.
85. **Woodside, J., M.** 2000. Linking Mediterranean brine pools and mud volcanism. EOS Transactions of the American Geophysical Union **81**.
86. **Woodside, J. M., and A. V. Volgin.** 1996. Brine pools associated with Mediterranean Ridge mud diapirs: an interpretation of echo-free patches in deep tow sidescan sonar data. Mar Geol **132:**55-61.
87. **Zitter, T. A. C., C. Huguen, and J. M. Woodside.** 2005. Geology of mud volcanoes in the eastern Mediterranean from combined sidescan sonar and submersible surveys. Deep-Sea Res. Part I Oceanogr. Res. Pap. **52:**457-475.

Probe	Target Group	Taxon	Sequence (5' to 3')	Type	% Formamide	°C Hybrid/Wash	Reference
ARCH915	Most Archaea	Archaea	GTG CTC CCC CGC CAA TTC CT	CARD	35	46/48	(Amann, et al., 1990)
ANME-1-350	ANME-1	Euryarchaeota	GTG CTC CCC CGC CAA TTC CT	CARD	40	46/48	(Boetius, et al., 2000)
ANME-2-538	ANME-2	Euryarchaeota	GGC TAC CAC TCG GGC CGC	FISH	50	46/48	(Treude, et al., 2005)
ANME-3-1249	ANME-3	Euryarchaeota	TCG GAG TAG GGA CCC ATT	CARD	20	46/48	(Lösekann, et al., 2007)
EUB I	Most Bacteria	Bacteria	GCT GCC TCC CGT AGG AGT	CARD	35	46/48	(Amann, et al., 1990)
EUB II	Planctomycetales	Bacteria	GCA GCC ACC CGT AGG TGT	CARD	35	46/48	(Daims, et al., 1999)
EUB III	Verrucomicrobiales	Bacteria	GCT GCC ACC CGT AGG TGT	CARD	35	46/48	(Daims, et al., 1999)
Non338	negative hybridization probe	-	ACTCCTACGGGAGGCAGC	CARD/FISH	variable	46/48	(Wallner, et al., 1996)
Alf968	α-proteobacteria	α-proteobacteria	GGTAAGGTTCTGCGCGTT	FISH	35	46/48	(Neef, 1997)
Gam42	γ-proteobacteria	γ-proteobacteria	GCCTTCCCACATCGTTT	FISH	35	46/48	(Manz, et al., 1992)
Beta42a	β-proteobacteria	β-proteobacteria	GCCTTCCCACTTCGTTT	FISH	35	46/48	(Manz, et al., 1992)
DSS658	*Desulfosarcina/Desulfococcus*	δ-proteobacteria	TCCACTTCCCTCTCCCAT	CARD	50	46/48	(Manz, et al., 1992)
DBB660	*Desulfobulbus*	δ-proteobacteria	GAA TTC CAC TTT CCC CTC TG	CARD	60	46/48	(Devereux, et al., 1992)
Mγ705	Type I methanotrophs	γ-proteobacteria	CTG GTG TTC CTT CAG ATC	FISH	20	46/48	(Eller, et al., 2001)
Arc94	*Arcobacter*	ε-proteobacteria	TGC GCC ACT TAG CTG ACA	CARD	20	46/48	(Snaidr, et al., 1997)

Table 1. Oligonucleotide probes and hybridization conditions used in this study. EUB-I, II, III were mixed into a single solution.

			ARC915			ANME-2			ANME-3		
	Depth	Total cells $1x10^9$	Free cells $1x10^9$	Cells in Agg $1x10^9$	Percent Total cells	Free cells $1x10^9$	Cells in Agg $1x10^9$	Percent Total cells	Free cells 1x109	Cells in Agg 1x109	Percent Total cells
White	mat	1.00	0.03	<	3	<	<	<	<	<	nd
	0-2cm	0.90	0.14	<	16	<	<	<	<	<	nd
	2-4cm	1.20	0.18	0.19	31	<	0.12	10	<	<	nd
	4-6cm	1.17	0.18	0.17	30	<	0.16	13	0.14	<	12
	6-8cm	0.61	0.19	<	31	<	nd	<	0.17	<	27
	8-10cm	1.10	0.20	<	18	<	nd	<	0.07	<	6
	10-12cm	0.42	0.07	<	18	<	nd	<	<	<	nd
	12-14cm	0.20	0.02	<	12	<	nd	<	<	<	nd
	14-16cm	0.20	0.03	<	14	<	nd	<	<	<	nd
	16-18cm	0.24	nd	nd	nd	<	nd	<	<	<	nd
Orange	mat	0.80	0.02	<	3	<	nd	<	<	<	nd
	0-2cm	1.18	0.03	0.02	4	<	0.03	3	<	<	nd
	2-4cm	3.47	0.95	0.27	35	<	0.31	9	<	<	nd
	4-6cm	0.76	0.19	<	25	<	nd	<	<	<	nd
	6-8cm	1.15	0.25	<	22	<	nd	<	<	<	nd
	8-10cm	1.09	0.16	<	14	<	nd	<	0.08	<	7
	10-12cm	0.91	0.24	<	26	<	nd	<	0.06	<	7
	12-14cm	1.60	0.24	<	15	<	nd	<	<	<	nd
	14-16cm	0.97	0.15	<	16	<	nd	<	<	<	nd
	16-18cm	0.62	0.09	<	14	<	nd	<	<	<	nd

			EUBI-III			DSS658			ARC94			My705		
	Depth	Total cells $1x10^9$	Free cells $1x10^9$	Cells in Agg $1x10^9$	Percent Total cells	Free cells $1x10^9$	Cells in Agg $1x10^9$	Percent Total cells	Free cells $1x10^9$	Cells in Agg $1x10^9$	Percent Total cells	Free cells $1x10^9$	Cells in Agg $1x10^9$	Percent Total cells
White	mat	1.00	0.67	<	67	<	<	nd	0.24	<	24	0.003	<	<
	0-2cm	0.90	0.47	<	52	0.21	<	23	0.20	<	22	<	<	nd
	2-4cm	1.20	0.49	0.09	48	0.17	0.05	18	0.10	<	8	<	<	nd
	4-6cm	1.17	0.29	0.08	32	0.07	0.04	9	0.01	<	1	<	<	nd
	6-8cm	0.61	0.15	<	25	0.03	<	5	<	<	nd	<	<	nd
	8-10cm	1.10	0.41	<	37	<	<	nd	<	<	nd	<	<	nd
	10-12cm	0.42	0.13	<	30	<	<	nd	<	<	nd	<	<	nd
	12-14cm	0.20	0.12	<	60	<	<	nd	<	<	nd	<	<	nd
	14-16cm	0.20	0.02	<	11	<	<	nd	<	<	nd	<	<	nd
	16-18cm	0.24	nd	<	nd	<	<	nd	<	<	nd	<	<	nd
Orange	mat	0.80	0.54	<	67	0.08	<	10	0.03	<	4	0.06	<	8
	0-2cm	1.18	0.78	0.01	67	0.17	0.01	15	0.04	<	nd	0.03	<	2
	2-4cm	3.47	1.09	0.13	35	0.32	0.30	9	0.03	<	nd	<	<	nd
	4-6cm	0.76	0.27	<	36	0.06	<	8	<	<	nd	<	<	nd
	6-8cm	1.15	0.30	<	26	0.14	<	12	<	<	nd	<	<	nd
	8-10cm	1.09	0.38	<	35	0.03	<	3	<	<	nd	<	<	nd
	10-12cm	0.91	0.16	<	17	0.09	<	10	<	<	nd	<	<	nd
	12-14cm	1.60	0.65	<	41	0.16	<	10	<	<	nd	<	<	nd
	14-16cm	0.97	0.39	<	40	0.11	<	12	<	<	nd	<	<	nd
	16-18cm	0.62	0.15	<	24	nd	<	nd	<	<	nd	<	<	nd

Table. 2 Fluorescence in Situ Hybridization counts for the white and orange mats as well the underlying sediment. "Total cells" indicate cell numbers obtained with AODC. Counts for ANME-1 and DBB660 were both below 1% of the total cells in all samples. "<" indicates numbers were less than 0.1% of the total cells. "nd" indicates not determined.

White Mat Depth (cm)	Corg (% w/w)	Cl (mM)	Na (mM)	Fe (%)	S (%)
Bottom water	-	863	704	-	
0-2 cm	-	1487	1240	13.6	11.35
2-4 cm	0.70	1545	1209	17.14	15.54
4-6 cm	0.44	1657	1282	5.10	2.10
6-8 cm	0.77	1627	1317	13.87	12.47
8-10 cm	0.24	1602	1317	3.50	-0.16
10-12 cm	0.23	1571	1293	5.00	0.24
12-14 cm	0.22	1567	1244	4.85	-0.14
14-16 cm	0.21	1573	1332	5.23	-0.19
16-18 cm	0.18	-	1380	2.51	0.22
18-20 cm	0.21	-	1301	2.17	-0.08

Orange Mat Depth (cm)	Corg (% w/w)	Cl (mM)	Na (mM)	Fe (%)	S (%)
Bottom water	-	657	565	-	
mat	-	-	-	11.62	3.51
0.75 cm	0.60	824	737	5.08	2.37
1-3 cm	0.53	1020	913	4.34	1.80
3-5 cm	0.44	1151	1011	4.32	1.45
5-7 cm	0.61	1239	1099	7.77	1.19
7-9 cm	0.56	1031	871	4.88	2.03
9-11 cm	0.57	1370	1187	5.06	2.46
11-13 cm	0.58	1375	1235	5.19	2.50
13 - 15 cm	0.56	1388	1242	4.84	2.04
15 - 17 cm	-	-	1153	-	-

Table 3. Pore water and solid phase geochemical profiles of the white and orange mats as well as the underlying sediment.

Phylogenetic group	White mat	White mat (Sediment)	Organge mat	Orange mat (sediment)
Total number of bacterial clones	**91**	**83**	**120**	**88**
% α-proteobacteria	**1**	**0**	**3**	**1**
% γ-proteobacteria	**2**	**8**	**74**	**34**
Type I methanotrophs	0	2	42	7
% δ-proteobacteria	**32**	**42**	**7**	**31**
Desulfobacteraceae (*Desulfosarcina variabilis*)	2(0)	30(23)	1(0)	16(10)
Desulfobulbaceae (*Desulfocapsa sulfexigens*)	20(20)	8(6)	6(0)	10(1)
Desulfuromonadaceae	9	0	0	1
% ε-proteobacteria	**36**	**0**	**12**	**7**
"Candidatus Arcobacter Sulfidicus"	2	0	1	0
Sulfurospirillum arcachonense	2	0	0	0
Sulfurimonas autotrophica	30	0	0	0
% Other bacteria	**29**	**42**	**5**	**22**
% Unidentified bacteria	**0**	**7**	**0**	**6**
Total number of archaeal clones		**71**		**66**
% Euryarcheaota		**96**		**98**
Nitrate reducing-ANME		0		3
ANME-2A		18		52
ANME-2C		1		3
ANME-3		55		0
MBG-D		15		36
% Crenarcheaota		**4**		**2**
MBG-B		4		2
MBG-1		0		0

Table 4. Breakdown of 16S rRNA gene sequences, in percentages obtained from the white and orange mats as well as the top 4 cm of sediment.

Figure Legends

Figure 1. (A) Bathymetric map of the Nile Deep Sea Fan (NDSF), kindly provided by Jean Mascle, Geosciences Azur. Circle indicates the Menes Caldera. (B) Bathymetric map of the Menes Caldera. (C) Bathymetric map of the Chefren mud volcano. "X" indicates the location on Chefren characterized by orange and white mats, the circle indicates the location of brine samples obtained during *Nautile* Dive18 (data not shown). Both maps were obtained during METEOR expedition BIONIL M70/2 in 2006 using the EM120 multibeam.

Figure 2. The microbial mat system of the brine-impacted seep at the rim of the Chefren mud volcano. (A) Photograph taken by the submersible *Nautile*, at the recovery site of the orange and white mats. On the right side, the sediments are populated by sessile worms (arrows) forming mud tubes. Scale bar is 3 m. (B) Close up of the mat system. Brine flowed downward (arrow) from the steep rim of the Chefren mud volcano across the white mats, and upward through the mats. Scale bar is 1 m. (C) A crab dwelling the worm-infested sediments associated with mats. Scale bar is 20 cm. (D) Photograph of a core from the white mat. The white mat was composed of white sulfur-like granules overlying black fluidic sediments. Scale bar is 3 cm. Inset: small motile polychaetes associated with white mat and the black sediment layer. The red color of the polychaetes indicates elevated hemoglobin levels, a typical adaptation to reduced sediments. Scale bar is 0.5 cm. (E) Photograph of a core from the orange mat. Arrow indicates a sessile worm. The orange fluff and flakes overlay grayish sediments. Scale bar is 3 cm. (F) Orange precipitates on sediments at the border of a brine lake in the MV center. Scale bar is 20

cm. (G) Muddy brine outflow from the top of the Chefren mud volcano. Scale bar is 3 m (H) Mushroom-like dense white mats floating on top of the large brine lake filling the center of the Chefren mud volcano. Scale bar is 20 cm.

Figure 3. (A) S granule from the white mat. (B) Phase contrast image of S filaments from the white mat. (C) High resolution SEM image of filaments and associated cells from the white mat. (D) FISH image showing ARC94 targeted cells (green). (E) Image of Fe-oxide flakes from the orange mat. (F) Light microscope image from an orange flake. (G) High resolution SEM image of damaged sheaths from a flake. Arrows indicate two distinct types of sheathed bacteria (bacteria are not visible, just their sheaths). (H) FISH image showing Mγ705 targeted sheaths. Arrows indicate two distinct types of sheathed bacteria similar to *Clonothrix fusca* (1) and *Crenothrix polyspora* (2). Scale bars for B-D and F-H indicate 10 µm.

Figure 4. Cl^- profiles from fluid flow models. (A) Measured Cl^- profile from underneath the white mats (circles), modeled Cl^- profile at a constant flow of 15 $m*a^{-1}$ (straight line) and modeled Cl^- profile after 10 h zero fluid flow velocity (dashed line). (B) Measured Cl profile from underneath the orange mats (circles), modeled Cl^- profile at a constant flow of 0.6 $m*a^{-1}$ (straight line) and modeled Cl^- profile after 10 h at zero fluid flow velocity (dashed line).

Figure 5. (A) Replicate sulfate reduction rate measurements and sulfate measurements (uninterrupted line) underneath the white mats. (B) Replicate rates of methane oxidation

and methane measurements (uninterrupted line) from underneath the white mats. (C) Fe(II) (white circles) and HS^- (black circles) concentrations from underneath the white mats. (D) Sedimentological description of the sediment underneath the white mats. (E) Replicate sulfate reduction rate measurements and sulfate measurements (uninterrupted line) from underneath the orange mats. (F) Replicate methane oxidation rates and methane measurements (uninterrupted line) from underneath the orange mats. (G) Fe(II) (white circles) and HS^- (black circles) concentrations from underneath the orange mats. (H) Sedimentological description of the sediment underneath the orange mats.

Figure 6. (A) Double hybridization using FISH probes ANME2-538 (red) and DSS658 (green). (B) ANME3-1249 targeted cells. (C) DSS658 targeted cells. (D) Mγ705 targeted single cells. All bars indicate 10 μm.

Figure 7. Neighbor-joining tree of 16S rRNA gene sequences from δ-proteobacteria obtained in this study, as well as from the GENBANK database. Sequences from this study are indicated in bold, and the numbers in brackets indicate the number of sequences within 98% identity to the relevant sequence from the white mat, underlying sediment, the orange mat and its underlying sediment. Only selected sequences are displayed in the tree. Sequences that are targeted by the DSS658 and the DBB660 probes are indicated.

Figure 8. Neighbor-joining tree of 16S rRNA gene sequences from γ-, β-, and ε-proteobacteria, and unidentified sequences obtained in this study, as well as from the GENBANK database. Sequences from this study are indicated in bold, and the numbers

in brackets indicate the number of sequences within 98% identity to the relevant sequence from the white mat, underlying sediment, the orange mat and its underlying sediment. Only selected sequences are displayed in the tree. Sequences that are targeted Arc94 and Mγ705 are indicated.

Figure 9. Neighbor-joining tree of 16S rRNA gene sequences from archaea obtained in this study, as well as from the GENBANK database. Sequences from this study are indicated in bold, and the numbers in brackets indicate the number of sequences within 98% identity to the relevant sequence from the white mat, underlying sediment, the orange mat and its underlying sediment. Only selected sequences are displayed in the tree. Sequences that are targeted by ANME-1-350, ANME-2-538 and ANME-3-1249 are indicated.

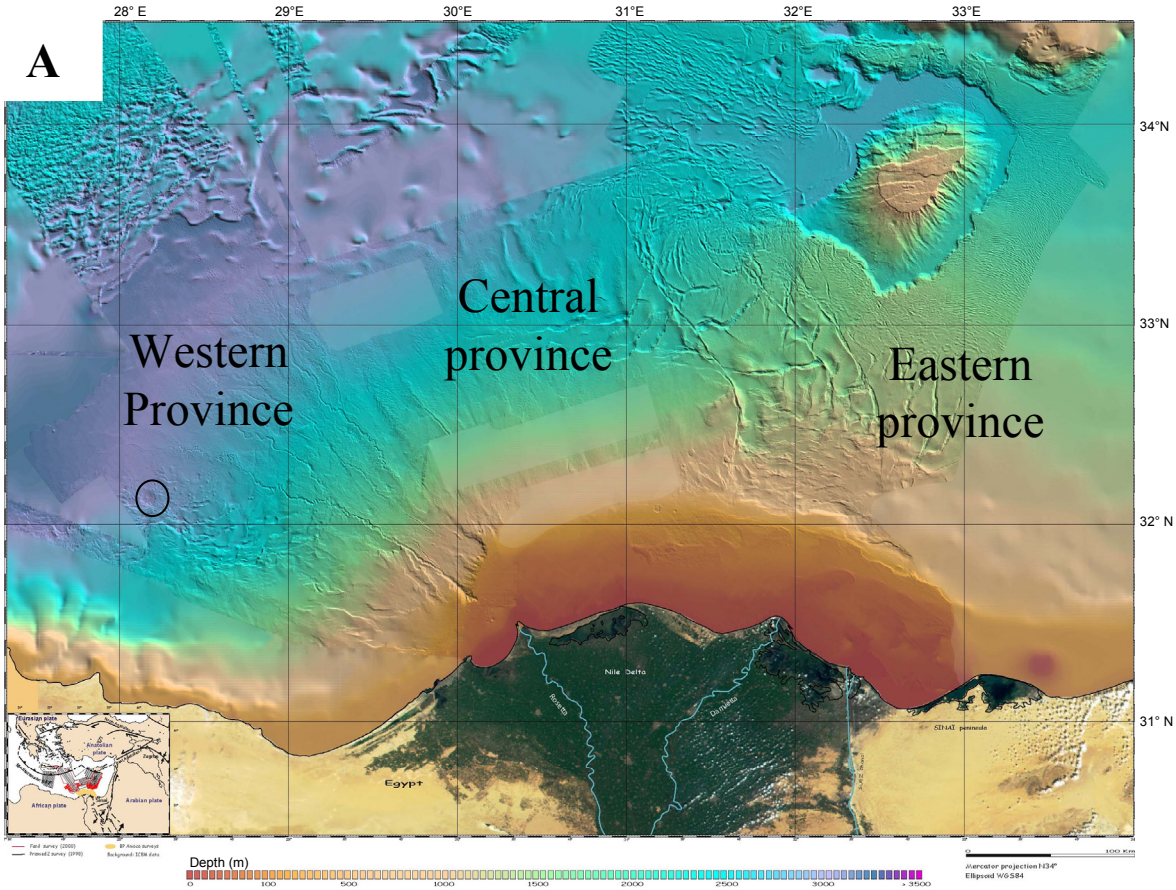
A
28° E
29°E
30°E
31°E
32°E
33°E
34°N
33°N
32° N
31° N
Western Province
Central province
Eastern province
Nile Delta
Egypt
Depth (m)
0
100
500
1000
1500
2000
2500
3000
> 3500

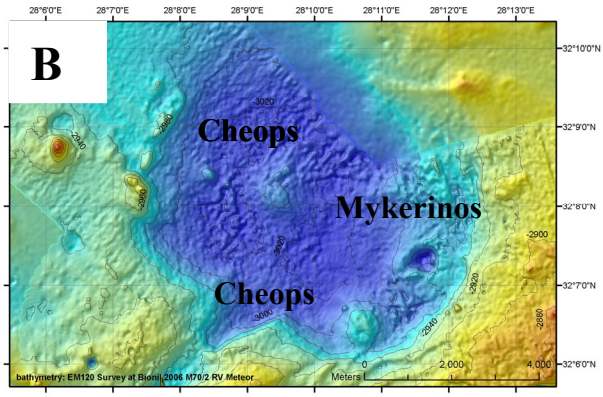
B
Cheops
Mykerinos
Cheops
bathymetry: EM120 Survey at Bionil 2006 M70/2 RV Meteor
Meters
0
2,000
4,000

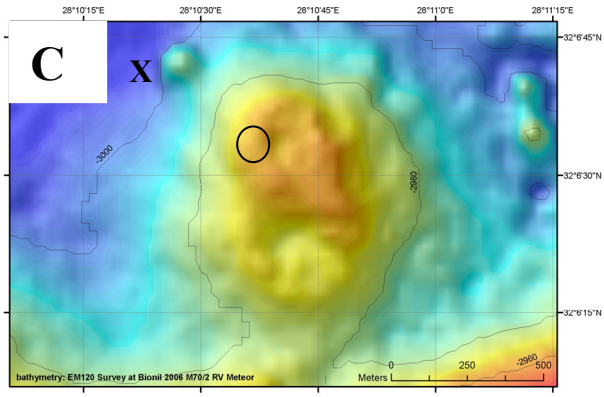
C
x
bathymetry: EM120 Survey at Bionil 2006 M70/2 RV Meteor
Meters
0
250
500

Figure 1

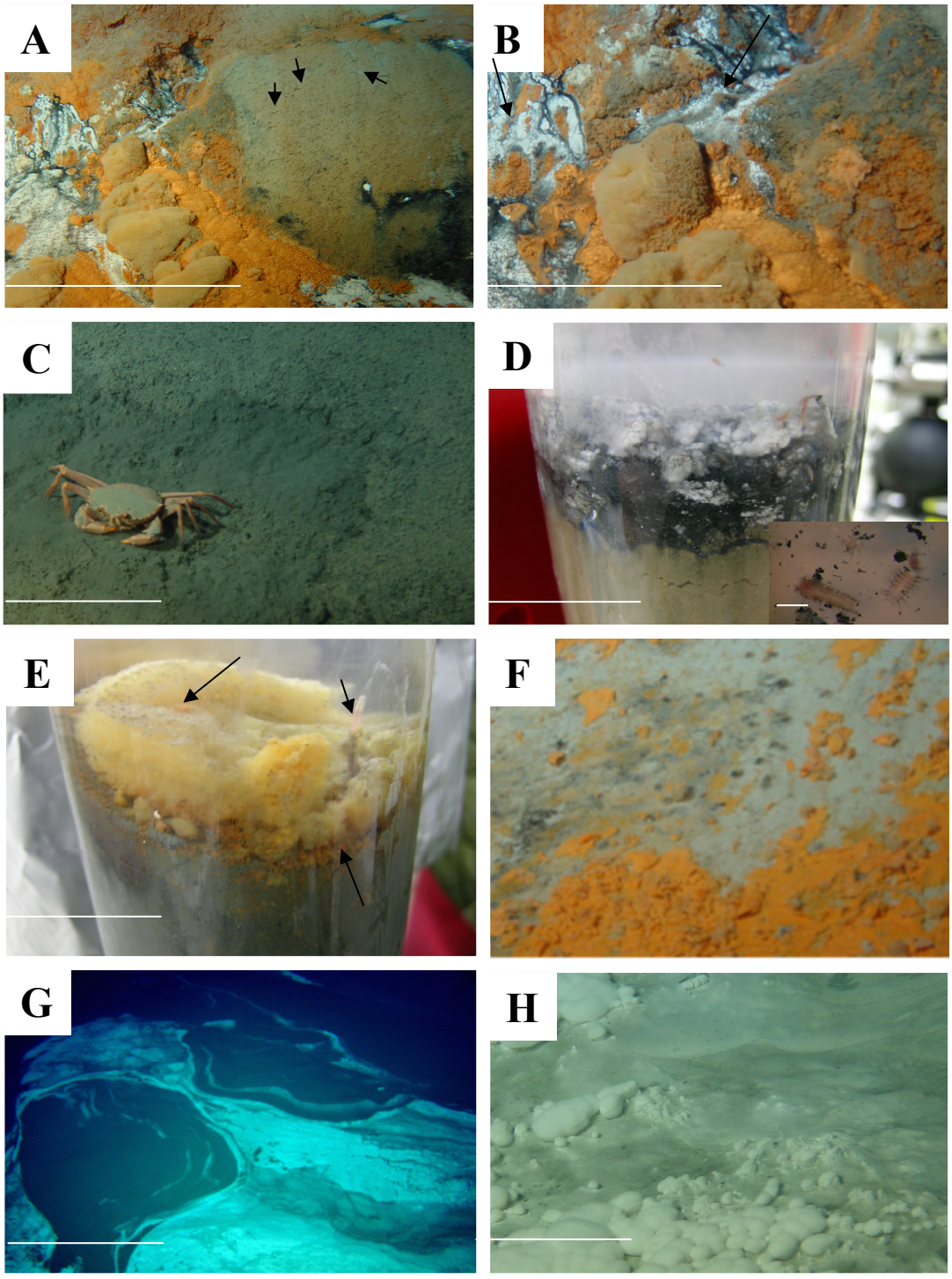

Figure 2

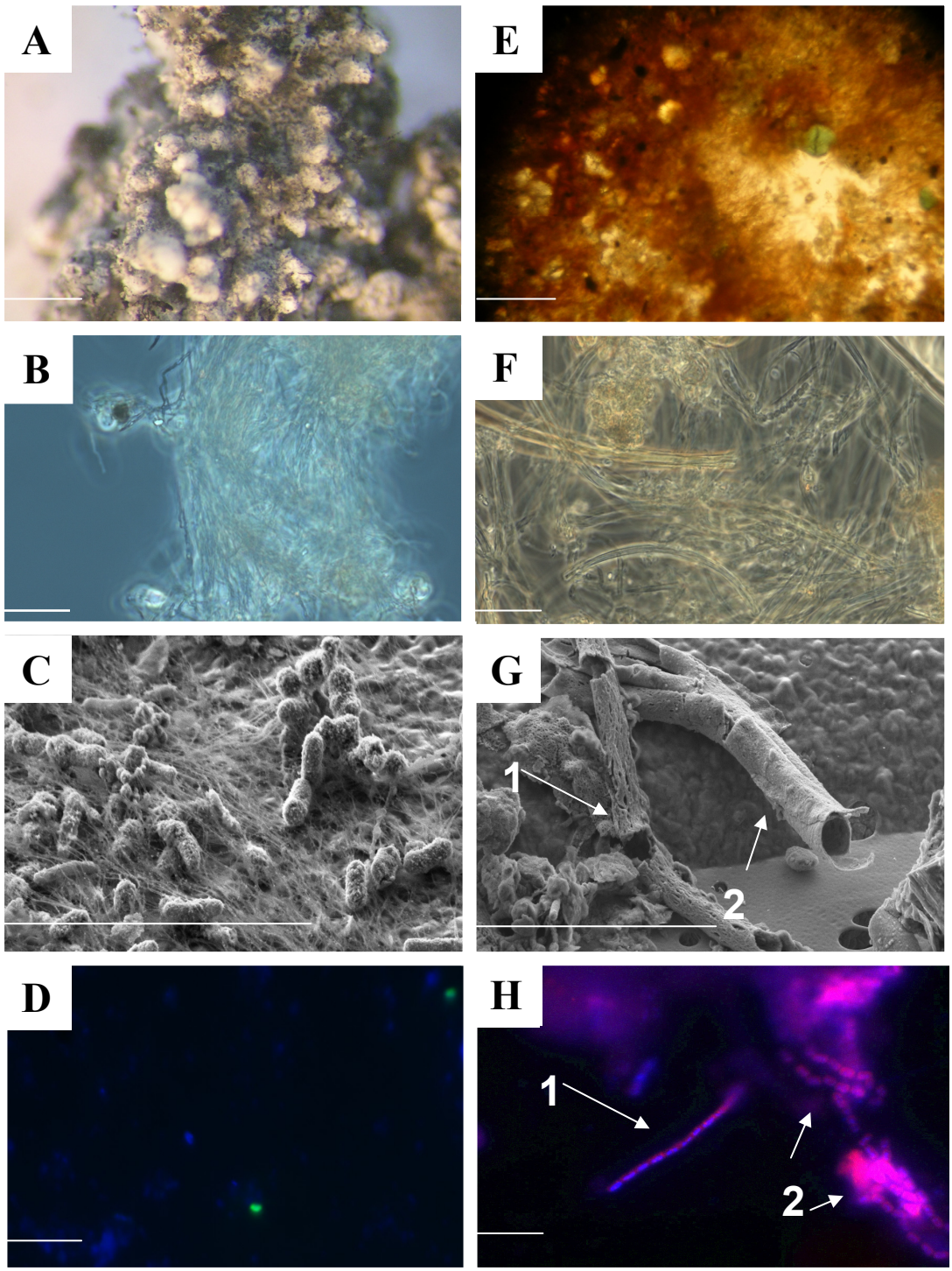

Figure 3

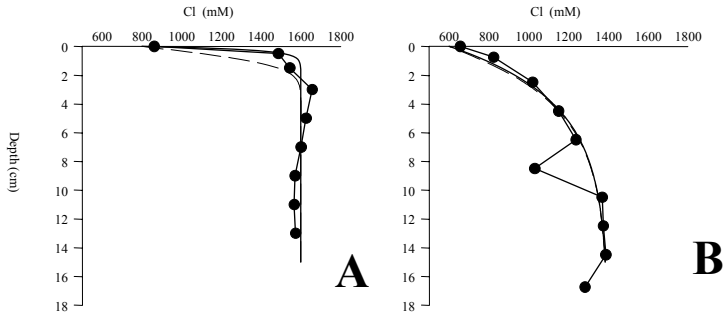
Cl (mM)
600 800 1000 1200 1400 1600 1800
0 2 4 6 8 10 12 14 16 18
Depth (cm)
A
Cl (mM)
600 800 1000 1200 1400 1600 1800
0 2 4 6 8 10 12 14 16 18
B

Figure 4

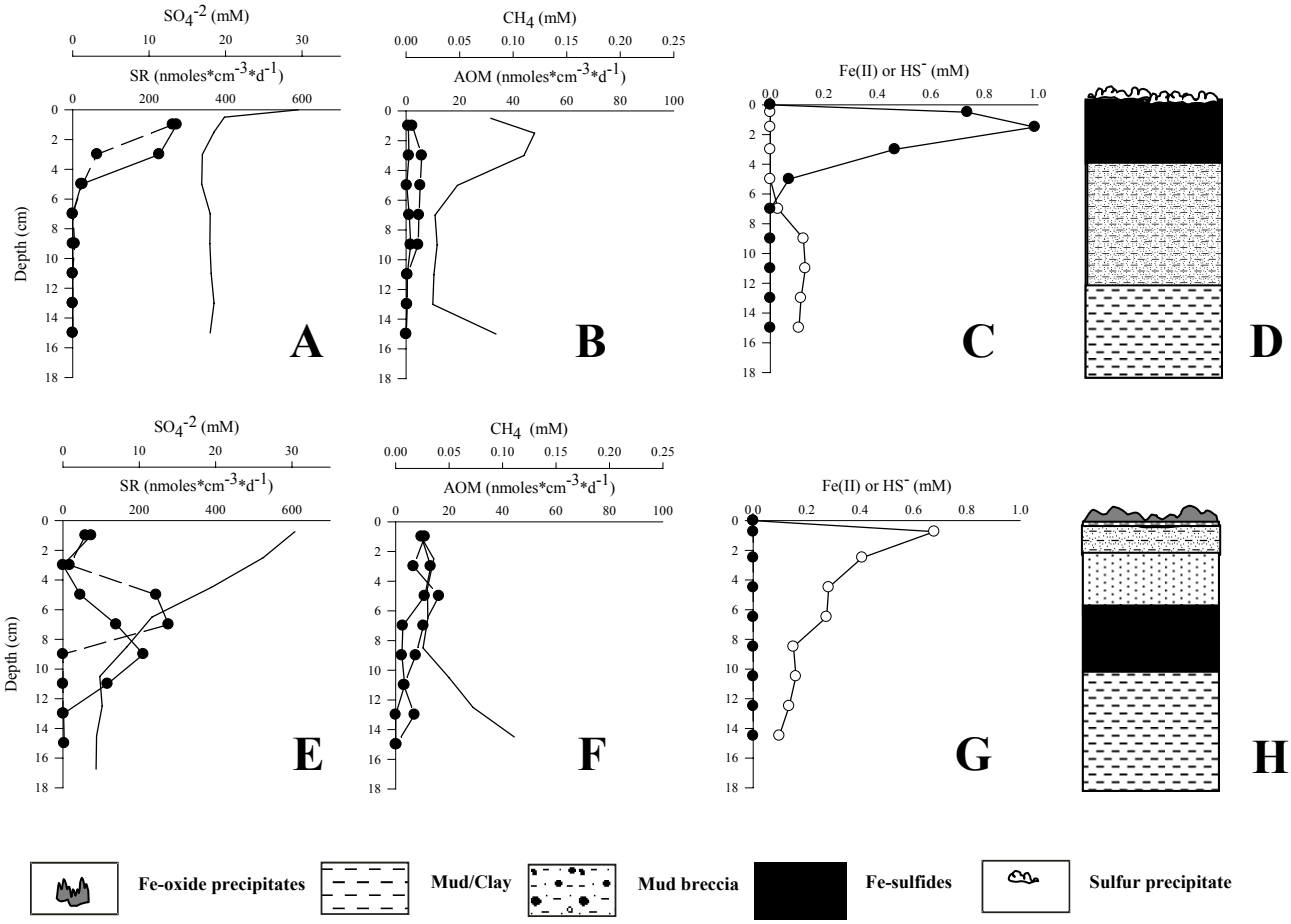
SO_4^{-2} (mM)
SR (nmoles*cm^{-3}*d^{-1})
Depth (cm)
A
CH_4 (mM)
AOM (nmoles*cm^{-3}*d^{-1})
B
Fe(II) or HS$^-$ (mM)
C
D
E
F
G
H
Fe-oxide precipitates
Mud/Clay
Mud breccia
Fe-sulfides
Sulfur precipitate

Figure 5

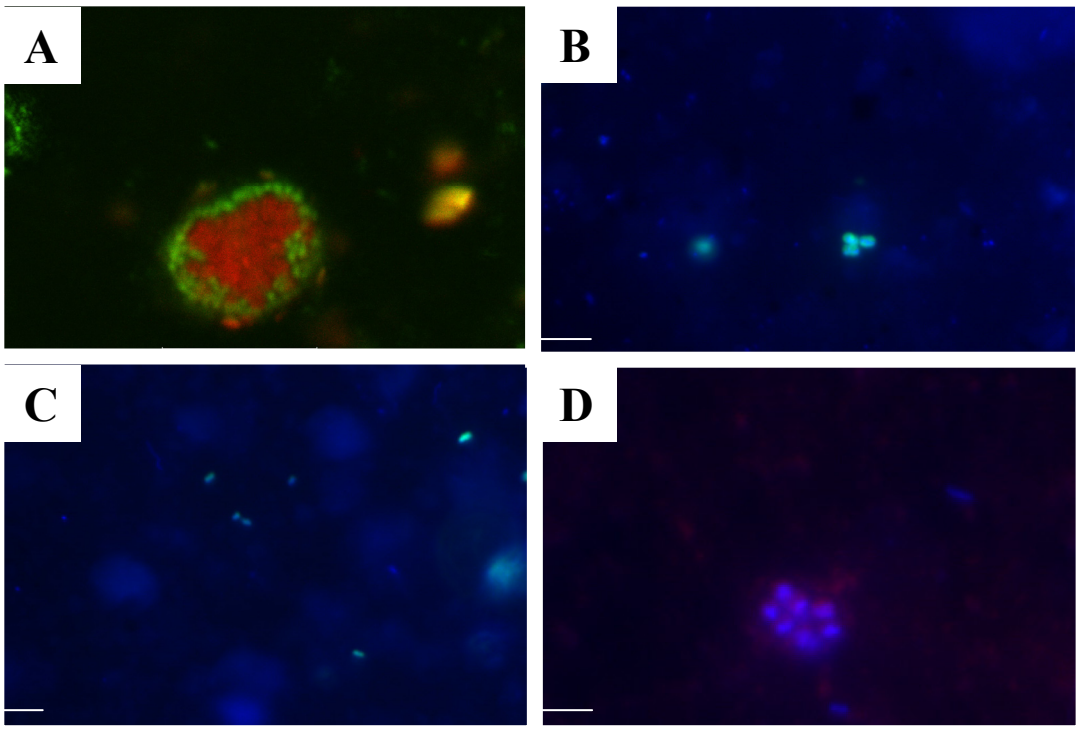

Figure 6

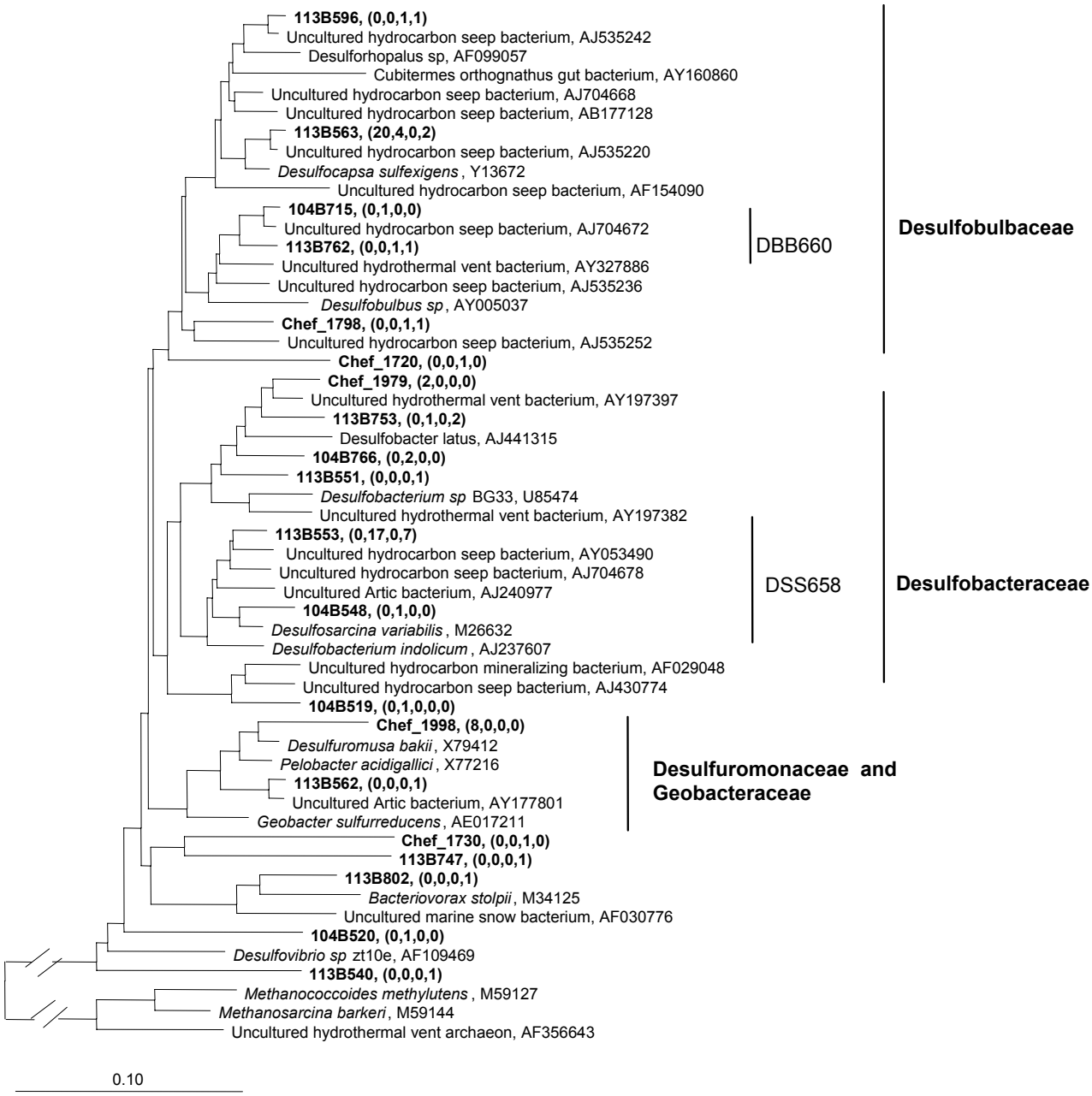
113B596, (0,0,1,1)
Uncultured hydrocarbon seep bacterium, AJ535242
Desulforhopalus sp, AF099057
Cubitermes orthognathus gut bacterium, AY160860
Uncultured hydrocarbon seep bacterium, AJ704668
Uncultured hydrocarbon seep bacterium, AB177128
113B563, (20,4,0,2)
Uncultured hydrocarbon seep bacterium, AJ535220
Desulfocapsa sulfexigens, Y13672
Uncultured hydrocarbon seep bacterium, AF154090
104B715, (0,1,0,0)
Uncultured hydrocarbon seep bacterium, AJ704672
113B762, (0,0,1,1)
Uncultured hydrothermal vent bacterium, AY327886
Uncultured hydrocarbon seep bacterium, AJ535236
Desulfobulbus sp, AY005037
Chef_1798, (0,0,1,1)
Uncultured hydrocarbon seep bacterium, AJ535252
Chef_1720, (0,0,1,0)
DBB660
Desulfobulbaceae
Chef_1979, (2,0,0,0)
Uncultured hydrothermal vent bacterium, AY197397
113B753, (0,1,0,2)
Desulfobacter latus, AJ441315
104B766, (0,2,0,0)
113B551, (0,0,0,1)
Desulfobacterium sp BG33, U85474
Uncultured hydrothermal vent bacterium, AY197382
113B553, (0,17,0,7)
Uncultured hydrocarbon seep bacterium, AY053490
Uncultured hydrocarbon seep bacterium, AJ704678
Uncultured Artic bacterium, AJ240977
104B548, (0,1,0,0)
Desulfosarcina variabilis, M26632
Desulfobacterium indolicum, AJ237607
DSS658
Desulfobacteraceae
Uncultured hydrocarbon mineralizing bacterium, AF029048
Uncultured hydrocarbon seep bacterium, AJ430774
104B519, (0,1,0,0,0)
Chef_1998, (8,0,0,0)
Desulfuromusa bakii, X79412
Pelobacter acidigallici, X77216
113B562, (0,0,0,1)
Uncultured Artic bacterium, AY177801
Geobacter sulfurreducens, AE017211
Desulfuromonaceae and Geobacteraceae
Chef_1730, (0,0,1,0)
113B747, (0,0,0,1)
113B802, (0,0,0,1)
Bacteriovorax stolpii, M34125
Uncultured marine snow bacterium, AF030776
104B520, (0,1,0,0)
Desulfovibrio sp zt10e, AF109469
113B540, (0,0,0,1)
Methanococcoides methylutens, M59127
Methanosarcina barkeri, M59144
Uncultured hydrothermal vent archaeon, AF356643
0.10

Figure 7

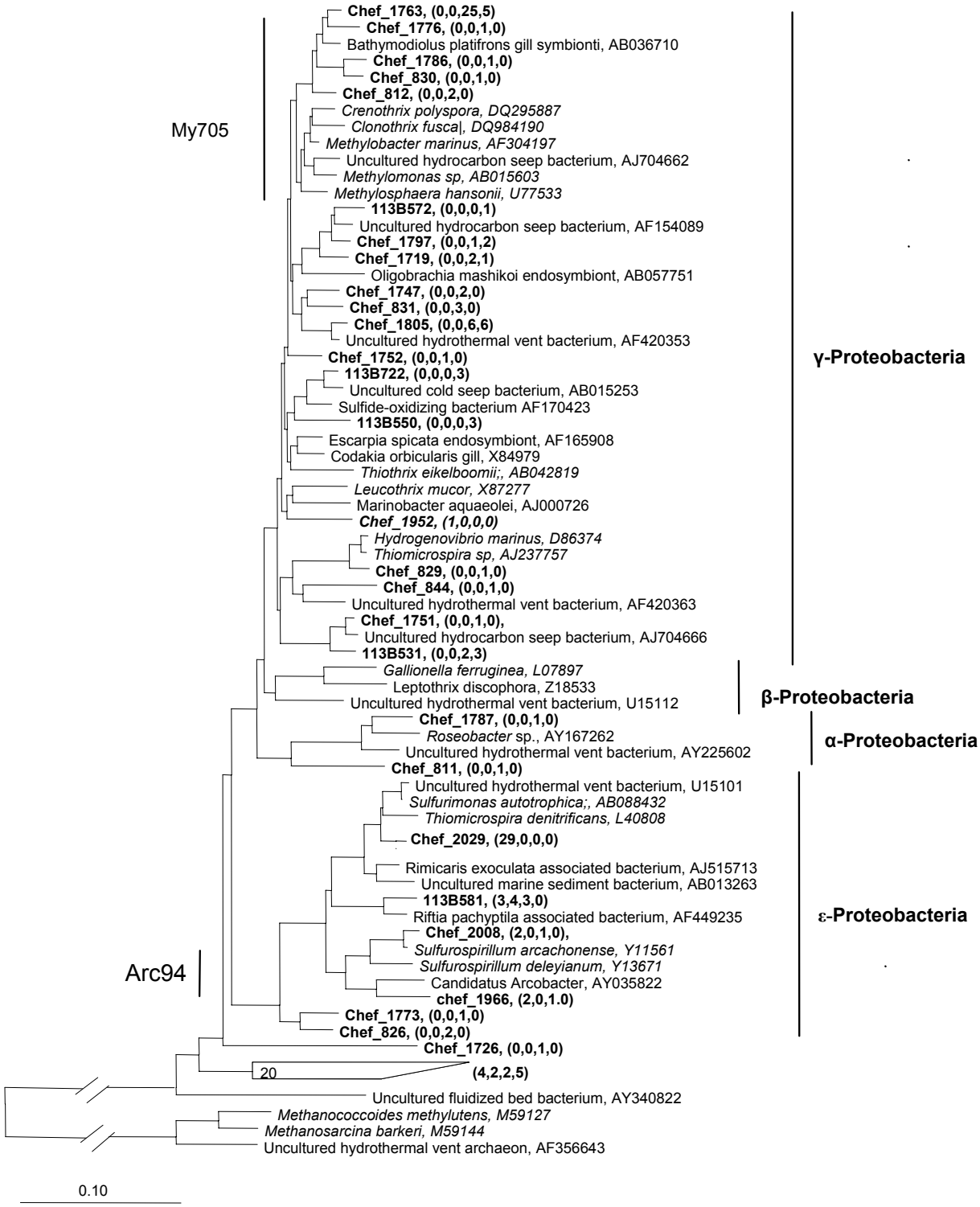
Chef_1763, (0,0,25,5)
Chef_1776, (0,0,1,0)
Bathymodiolus platifrons gill symbionti, AB036710
Chef_1786, (0,0,1,0)
Chef_830, (0,0,1,0)
Chef_812, (0,0,2,0)
Crenothrix polyspora, DQ295887
Clonothrix fusca|, DQ984190
Methylobacter marinus, AF304197
Uncultured hydrocarbon seep bacterium, AJ704662
Methylomonas sp, AB015603
Methylosphaera hansonii, U77533
My705
113B572, (0,0,0,1)
Uncultured hydrocarbon seep bacterium, AF154089
Chef_1797, (0,0,1,2)
Chef_1719, (0,0,2,1)
Oligobrachia mashikoi endosymbiont, AB057751
Chef_1747, (0,0,2,0)
Chef_831, (0,0,3,0)
Chef_1805, (0,0,6,6)
Uncultured hydrothermal vent bacterium, AF420353
Chef_1752, (0,0,1,0)
113B722, (0,0,0,3)
Uncultured cold seep bacterium, AB015253
Sulfide-oxidizing bacterium AF170423
113B550, (0,0,0,3)
Escarpia spicata endosymbiont, AF165908
Codakia orbicularis gill, X84979
Thiothrix eikelboomii;, AB042819
Leucothrix mucor, X87277
Marinobacter aquaeolei, AJ000726
Chef_1952, (1,0,0,0)
Hydrogenovibrio marinus, D86374
Thiomicrospira sp, AJ237757
Chef_829, (0,0,1,0)
Chef_844, (0,0,1,0)
Uncultured hydrothermal vent bacterium, AF420363
Chef_1751, (0,0,1,0),
Uncultured hydrocarbon seep bacterium, AJ704666
113B531, (0,0,2,3)
γ-Proteobacteria
Gallionella ferruginea, L07897
Leptothrix discophora, Z18533
Uncultured hydrothermal vent bacterium, U15112
β-Proteobacteria
Chef_1787, (0,0,1,0)
Roseobacter sp., AY167262
Uncultured hydrothermal vent bacterium, AY225602
α-Proteobacteria
Chef_811, (0,0,1,0)
Uncultured hydrothermal vent bacterium, U15101
Sulfurimonas autotrophica;, AB088432
Thiomicrospira denitrificans, L40808
Chef_2029, (29,0,0,0)
Rimicaris exoculata associated bacterium, AJ515713
Uncultured marine sediment bacterium, AB013263
113B581, (3,4,3,0)
Riftia pachyptila associated bacterium, AF449235
ε-Proteobacteria
Chef_2008, (2,0,1,0),
Sulfurospirillum arcachonense, Y11561
Sulfurospirillum deleyianum, Y13671
Arc94
Candidatus Arcobacter, AY035822
chef_1966, (2,0,1.0)
Chef_1773, (0,0,1,0)
Chef_826, (0,0,2,0)
Chef_1726, (0,0,1,0)
20
(4,2,2,5)
Uncultured fluidized bed bacterium, AY340822
Methanococcoides methylutens, M59127
Methanosarcina barkeri, M59144
Uncultured hydrothermal vent archaeon, AF356643
0.10

Figure 8

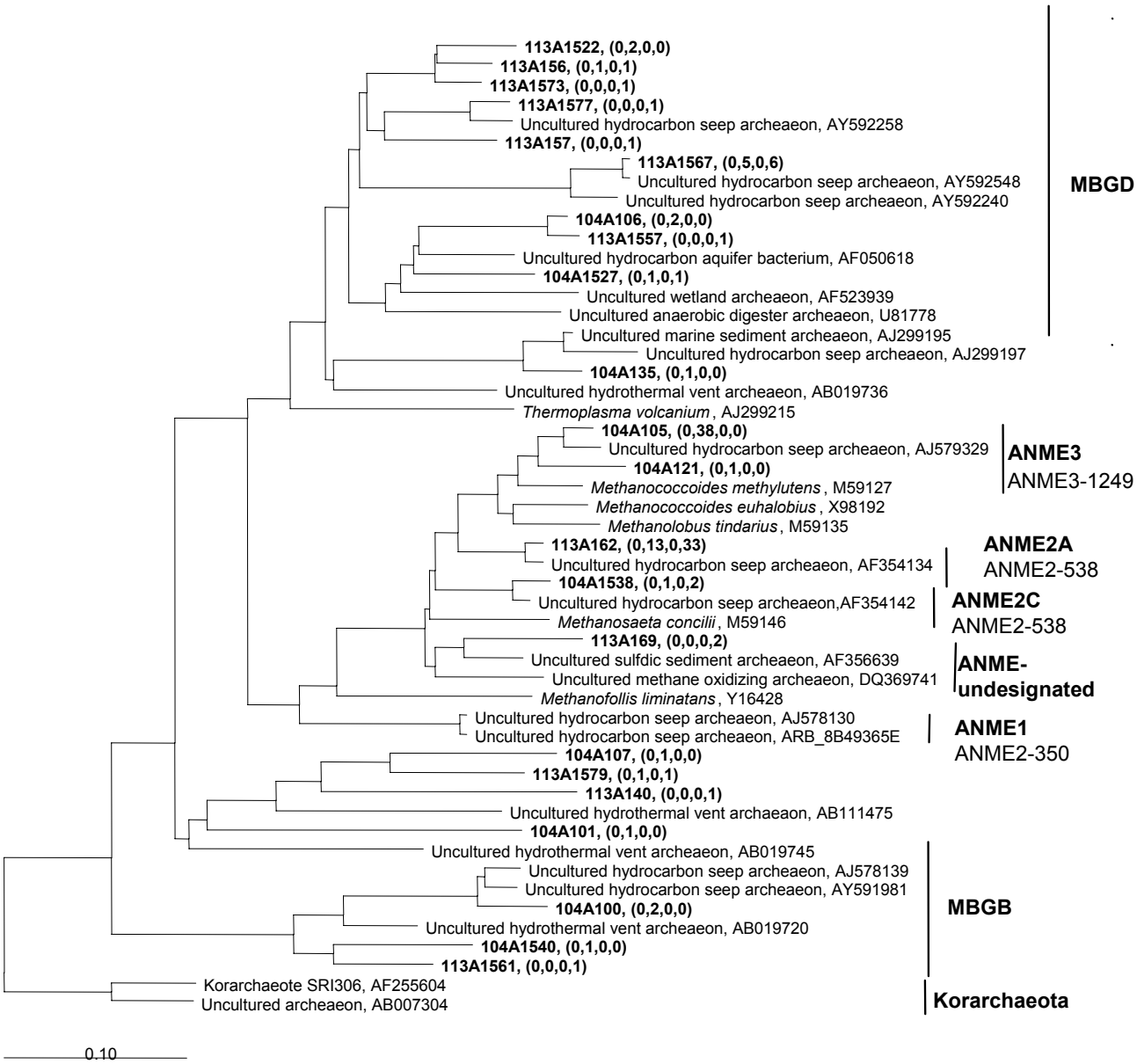
113A1522, (0,2,0,0)
113A156, (0,1,0,1)
113A1573, (0,0,0,1)
113A1577, (0,0,0,1)
Uncultured hydrocarbon seep archeaeon, AY592258
113A157, (0,0,0,1)
113A1567, (0,5,0,6)
Uncultured hydrocarbon seep archeaeon, AY592548
Uncultured hydrocarbon seep archeaeon, AY592240
104A106, (0,2,0,0)
113A1557, (0,0,0,1)
Uncultured hydrocarbon aquifer bacterium, AF050618
104A1527, (0,1,0,1)
Uncultured wetland archeaeon, AF523939
Uncultured anaerobic digester archeaeon, U81778
Uncultured marine sediment archeaeon, AJ299195
Uncultured hydrocarbon seep archeaeon, AJ299197
104A135, (0,1,0,0)
Uncultured hydrothermal vent archeaeon, AB019736
Thermoplasma volcanium, AJ299215
104A105, (0,38,0,0)
Uncultured hydrocarbon seep archeaeon, AJ579329
104A121, (0,1,0,0)
Methanococcoides methylutens, M59127
Methanococcoides euhalobius, X98192
Methanolobus tindarius, M59135
113A162, (0,13,0,33)
Uncultured hydrocarbon seep archeaeon, AF354134
104A1538, (0,1,0,2)
Uncultured hydrocarbon seep archeaeon,AF354142
Methanosaeta concilii, M59146
113A169, (0,0,0,2)
Uncultured sulfdic sediment archeaeon, AF356639
Uncultured methane oxidizing archeaeon, DQ369741
Methanofollis liminatans, Y16428
Uncultured hydrocarbon seep archeaeon, AJ578130
Uncultured hydrocarbon seep archeaeon, ARB_8B49365E
104A107, (0,1,0,0)
113A1579, (0,1,0,1)
113A140, (0,0,0,1)
Uncultured hydrothermal vent archaeaon, AB111475
104A101, (0,1,0,0)
Uncultured hydrothermal vent archeaeon, AB019745
Uncultured hydrocarbon seep archeaeon, AJ578139
Uncultured hydrocarbon seep archeaeon, AY591981
104A100, (0,2,0,0)
Uncultured hydrothermal vent archeaeon, AB019720
104A1540, (0,1,0,0)
113A1561, (0,0,0,1)
Korarchaeote SRI306, AF255604
Uncultured archeaeon, AB007304
0.10
MBGD
ANME3
ANME3-1249
ANME2A
ANME2-538
ANME2C
ANME2-538
ANME-
undesignated
ANME1
ANME2-350
MBGB
Korarchaeota

Figure 9

Chapter VI: General conclusions

During my dissertation, I examined the activities of archaea and bacteria in microbial mats and sediment communities, i.e., those that were part of cyanobacterial mat from La Salada de Chiprana, sediment communities from cold seeps in the Gulf of Cadiz, sulfide- and iron-oxidizing mats and sediment communities from cold seeps in the Eastern Mediterranean. These studies focused on revealing the diversity and functioning of key microbes and their interaction with the environment.

Within the cyanobacterial mats, cyanobacteria and Chloroflexus-like bacteria (CLB) were found to be key members of the microbial communities. The importance of cyanobacteria with respect to C-fixation and oxygen production has long been recognized, and was exemplified by the measured oxygen concentrations. CLB were very abundant as well as diverse within the investigated mat, their potential importance was revealed by the decrease in respiration rates upon infrared illumination. This indicated that CLB can have a tremendous affect on C and O dynamics in a microbial mat system. The treatment within this study was under artificial light conditions, and thus future studies will have to take into affect natural light conditions. Additionally, several questions remain, among them are the co-substrate(s) utilized with oxygen, amount of carbon fixed by CLB and the identity and physiology of the different CLB phylotypes.

The cold seep sediment communities within the Gulf of Cadiz and the Eastern Mediterranean were diverse, but methane oxidizing and sulfate reducing bacteria were the dominate microorganisms at these settings. Their distribution and abundance matched the peaks in methane oxidation and sulfate reduction. The activity of these microbes largely differed between these systems with higher rates of activity seen at the cold seeps within the Eastern Mediterranean. Despite these differences, the microbial communities within the Gulf of Cadiz were able to halt the methane flux to the bottom ocean unlike the communities observed within the Eastern Mediterranean. However, the long term and short variability of this activity, the substrates fueling the microbial communities, and the physiology of the unidentified phylotypes, need to be further investigated. An especially interesting result of my investigation was the low activity in the sulfate- and methane-rich sediments of the Eastern Mediterranean, pointing to an unknown control of anaerobic methanotrophic activity in these sediments.

I was able to identify the key organisms and processes leading to the formation of novel types of microbial mats at cold seeps. The sediment communities underlying the sulfide- and

iron-oxidizing mats at Chefren mud volcano were in part responsible for the formation of these mats. The sulfate-reducing bacteria provided the free sulfide, which reacted with sedimentary iron, and iron-reducing microbial populations to provide free Fe(II). The sulfide was oxidized by "*Candidatus* Arcobacter sulfidicus", which was responsible for the extensive sulfur precipitation at the brine seep. Iron precipitates were produced by iron-oxidizing bacteria which formed abundant sheath structures. Many questions still remain for this mat system, such as the substrates fueling iron and sulfate reduction, the contribution of biotic iron-oxidation to the system, identity of the iron oxidizers, and physiology of many of the phylotypes identified in this study.

These studies endeavored to understand the activities of microbes within the sediment communities and mats. In these environments, we were able to identify key species, as well as the processes they mediate. In all cases, follow up studies will be needed to further elucidate the roles of these species, as well as others within these environments. Time scale studies will be needed to evaluate reactions of microbial communities to the long- and short-term changes in the highly variable seep systems. Future work on unknown and uncultivable microorganisms, which form mats or dominate sediment communities should couple the use of classical techniques, such as cultivation and genomic studies to investigate the physiology of organisms of interest, NANO-SIMS (secondary ion mass spectrometry) to investigate nanoscale interactions between microbes, and microsensor measurements to characterize the microbial habitats in situ.

Publications List

Omoregie, E., Mastalerz, V., de Lange, G., Straub, K.L., Kappler, A., Roey, H., Stadnitskaia , A., Foucher, J.P., Boetius, A., Biogeochemistry of sulfide-oxidizing and iron-oxidizing bacterial mats at the Chefren mud volcano. In preparation for submission to Applied and Environmental Microbiology.

Omoregie, E., Niemann, H., de Lange, G., Mastalerz, V., Stadnitskaia , A., Boetius A., Foucher, J.P., Anaerobic oxidation of methane and sulfate reduction at cold seeps in the Eastern Mediterranean sea. In preparation for submission to Marine Geology.

Bachar, A., Omoregie, E., Jonkers, H., Biogeography of *Chloroflexus*-like bacteria in a hypersaline microbial mat. In Preparation.

Stadnitskaia, A., Omoregie, E., Boetius, A., Sinninghe Damsté, J.S., A novel association of methanotrophic archaea and bacteria in a cold seepage location: significance of aerobic methane utilization. In Preparation

Stadnitskaia, A., Omoregie, E., Boetius, A., Sinninghe Damsté, J.S., Lipid composition reveals methanotrophic diversity in different fluid venting environments of the Nile deep-sea fan, Eastern Mediterranean. In Preparation

Bachar, A., Omoregie, E.,de Wit, R., Jonkers, H., Diversity and function of *Chloroflexus*-like bacteria in a hypersaline microbial mat: phylogenetic characterization and impact on aerobic respiration. Applied and Environmental Microbiology. 73 (2007): 3975-3983

Dupré, S., Woodside, J., Foucher, J.P., de Lange, G., Mascle, J., Boetius, A., Mastalerz, V., Stadnitskaia, A., Ondréas, H., Huguen, C., Harmégnies, H., Gontharet, S., Loncke, L., Deville, E., Niemann, H., Omoregie, E., Olu-Le Roy, K., Fiala-Medioni, A., Dählmann, A., Caprais, J.C., Prinzhofer, A., Sibuet, M., Pierre, C., Damsté, J., and the NAUTINIL Scientific Party. Seafloor geological studies of active gas chimneys offshore Egypt (central Nile Fan). Deep Sea Reasearch Part I. 54 (2007): 1146-1172

Niemann, H, Duarte, J, Hensen, C, Omoregie, E., Elvert, M, Magalhães , V. , Boetius, A. , Pinheiro, L. M., 2006. Microbial methane turnover at mud volcanoes of the Gulf of Cadiz. Geochimica et Cosmochimica Acta. 70, 5336-5355.

Presentation List (underlined is the presenting author)

Stadnitskaia A., Omoregie E., Boetius A., Sinninghe Damsté J.S., 2007. A novel association of methanotrophic archaea and bacteria in a cold seepage location: significance of aerobic methane utilization. European Geophysical Union. Vienna, Austria

Omoregie, E., Niemann, H., Stadnitskaia A., de Lange G., Mastalerz, V., Straub, K., Kappler, A., Foucher, J.P., Boetius, A., 2006. Biogeochemistry and community analysis of sulfide-oxidizing and iron-oxidizing bacterial mats at the Chefren mud volcano. International Society for Microbial Ecology, Vienna, Austria

Stadnitskaia, A., Omoregie, E., Boetius, A., Sinninghe Damsté , J.S., 2006. Lipid composition and methanotrophic diversity in different fluid venting environments of the Nile deep-sea fan, Eastern Mediterranean. European Geophysical Union. Vienna, Austria

Omoregie, E., Niemann, H., Treude, T., Boetius, A., 2005. Molecular Diversity and Processes of Microbial Communities Overlying Methane Seeps. Joint International Symposia for Subsurface Microbiology (ISSM 2005) and Environmental Biogeochemistry. Jackson Hole, USA

Omoregie, E, Niemann, H., Boetius, A., 2005. Anaerobic oxidation of Methane and Sulfate reduction in the Nile Deep Sea Fan. European Geophysical Union. Vienna, Austria

Niemann, H., Duarte, J., Hensen, C., Omoregie, E., Elvert, M., Magalhães , V. , Boetius, A. , Pinheiro, L. M., 2005. Diverse Microbial Communities Mediate Anaerobic Oxidation of Methane at Mud Volcanoes in the Gulf of Cadiz. European Geophysical Union. Vienna, Austria

Bachar, A, E. Omoregie, D. de Beer and H. M. Jonkers, 2005. Role of *Chloroflexus*-like bacteria in a hypersaline microbial mat. European Geophysical Union. Vienna, Austria

Omoregie, E., 2004, MEDIFLUX participants. First geommicrobial results from the MEDIFLUX campaign: Microbial processes fueled by seepage. ESF EUROMARGINS meeting, Barcelona, Spain

Omoregie, E., 2004, MEDIFLUX participants. Looking for the Anaerobic Oxidation of Methane in the Nile deep see fan. ESF EUROMARGINS meeting, Aveiro, Portugal

List of activities in the MARMIC program

MARMIC tutor for biogeochemistry, microbiology and general oceanography

Marmic Molecular biology lab course: Assistant

Marmic Lab rotation supervisor: Chibola Chikwililwa

Special courses in Leadership, Presentation strategies and Time management

Marmic Class of 2006 speaker